

**SISSA**

Scuola  
Internazionale  
Superiore di  
Studi Avanzati

Physics Area - PhD course in  
Theoretical Particle Physics

# New Physics Hints from Flavour

Candidate:  
Valerio Gherardi

Advisors:  
Prof. Andrea Romanino  
Dr. David Marzocca

Academic Year 2020-21



arXiv:2111.00285v1 [hep-ph] 30 Oct 2021

# New Physics Hints from Flavour

ABSTRACT. This Thesis presents my personal contributions to two distinct fields, namely the recent experimental anomalies in  $B$ -meson decays, and the longstanding quest for a theoretical explanation of lepton masses and mixings, under a unifying umbrella: Flavour Physics. The modern view of the Standard Model as an effective theory is motivated, and the dual role of flavour, as a probe of New Physics effects on one side, and as a piece of the puzzle itself on the other, is emphasized. By jointly discussing two physics cases of different nature, I attempt to offer a broader perspective on the current status of Beyond Standard Model searches.

The discussion begins with a preliminary review of Standard Model Effective Field Theories, in which some utility results in theory matching are presented. The focus then moves to  $B$ -meson decay anomalies: after introducing Lepton Flavour Universality, we discuss the phenomenology of a specific Standard Model extension by scalar leptoquarks, and also present the Effective Field Theory framework of Rank-One Flavor Violation, providing a less detailed but broader picture for the case of neutral-current anomalies. Finally, we tackle the Standard Model flavour puzzle, describing an attempt to address charged lepton mass hierarchies in the framework of supersymmetric modular invariant models of lepton flavour.

# Contents

Introduction	6
<b>Part 1. The Standard Model Effective Field Theory</b>	<b>9</b>
Chapter 1. The Standard Model Effective Field Theory	10
1.1. The Standard Model as an Effective Field Theory	10
1.2. Computing with EFTs: theory matching	15
1.3. Advanced matching methods	16
Chapter 2. A case study: the $S_1 + S_3$ Leptoquark model	18
2.1. The $S_1 + S_3$ model	18
2.2. One-loop matching	20
2.3. One-loop matching example	21
2.4. A SMEFT dimension-six Green's basis	23
2.5. Appendix: $S_1 + S_3$ scalar potential	28
<b>Part 2. New Physics signals from flavour: the <math>B</math>-anomalies</b>	<b>29</b>
Chapter 3. Introduction	30
3.1. Low-energy implications of SM flavour	30
3.2. The $B$ -meson decay anomalies	33
Chapter 4. $S_1 + S_3$ model's phenomenology	36
4.1. Methodology	37
4.2. Observables	38
4.3. Scenarios and results	41
4.4. Prospects	54
4.5. Light generations	56
4.6. Conclusions	56
Chapter 5. Rank One Flavor Violation	59
5.1. The ROFV framework	60
5.2. General correlations in $V - A$ solutions	64
5.3. SMEFT and simplified mediators	65
5.4. ROFV and flavour symmetries	71
5.5. Prospects	74
5.6. Conclusions	76
<b>Part 3. Explaining the SM flavour structure</b>	<b>78</b>



Chapter 6. The SM flavour puzzle	79
6.1. Pieces of the puzzle	79
6.2. Theoretical ideas	83
Chapter 7. Are lepton masses modular forms?	86
7.1. Modular invariant models	87
7.2. Residual symmetry near $\tau = i$	90
7.3. Models	91
7.4. Conclusions	102
7.5. Appendix: Kähler potential quadratic in $Y^{(2)}$	103
Bibliography	106

## Introduction

The Standard Model (SM) of Particle Physics [1–3] is arguably one of the greatest intellectual achievements of modern science. It synthesizes a whole century of theoretical breakthroughs, from quantum mechanics and Lorentz invariance to gauge invariance and spontaneous symmetry breaking through renormalizable field theory, which were paralleled by a remarkable history of experimental discoveries that climaxed in 2012, with the detection of the scalar boson [4,5] conjectured about fifty years before by P. Higgs [6], R. Brout and F. Englert [7], and G. Guralnik, C. R. Hagen and T. Kibble [8]. The discovery of the Higgs boson, which was the last angular stone of the theory waiting for experimental validation, completes a beautiful picture of the sub-atomic world, which is by far the best available, and to which the physicist cannot help but look with amazement.

If, on the one hand, the impressive agreement of SM predictions with experimental data [9] represents a tremendous scientific success, the same precise feature might also be perceived by some as a source of uneasiness [10]. In fact, along with its lengthy record of triumphs, time has brought to surface a great many pieces of evidence indicating that the SM is, from a strict point of view, just a phenomenological effective theory - the most incontrovertible of which is perhaps the existence of unexplained Dark Matter (see *e.g.* [11]). From a Naturalness [12,13] standpoint, the fact that the Higgs discovery would take place in a total absence of signals of physics Beyond the SM (BSM) was somewhat disappointing, for it opened the doors to an alternative, rather depressing but logically conceivable interpretation: that BSM phenomena might be energetically inaccessible by particle accelerators available at present or foreseeable in a next future.

While there is no substantial reason suggesting this worst-case scenario to be the actual case, it is fair to say that direct indications from data pointing to a concrete BSM threshold energy are still very limited. In this groping one's way to New Physics (NP), *flavour* plays the dual role of a glow in the dark on one side, and a long-standing sphynx on the other. In this Thesis, I discuss both these aspects through the lens of the topics I have been primarily involved in during the last three years: the  $B$ -meson decay anomalies, and the origins of lepton flavour.

The term “flavour” has a long history in Particle Physics, and its meaning has undergone a certain distortion across the years. Here and in what follows, the expression refers to all those features of the SM fermionic matter content (*i.e.* quarks and leptons) which are not univocally fixed by gauge invariance or other structural requirements: these include the quark and lepton representations under the SM gauge group, the number of families, and the mass and mixing patterns of the two sectors. The dual nature of flavour mentioned above can now be clarified: the SM flavour structure represents a powerful probe of NP effects and, at the same time, cries for a theoretical explanation regarding its

origins. The first aspect is what gives rise to the so-called SM flavour problem, whereas the second one is what we refer to the SM flavour puzzle [14].

Let us briefly introduce the two concrete physics cases addressed in the present work. The  $B$ -meson decay anomalies ( $B$ -anomalies for short) are a set of discrepancies between SM predictions and experimental data on semileptonic decays of  $B$ -mesons, which have by now persisted altogether for more than seven years. The deviations were initially reported for  $\bar{B} \rightarrow D^{(*)}\ell^-\nu_\ell$  decay [15–25], which according to the SM are mediated by a tree-level  $W^\pm$  exchange, and subsequently followed by comparable deviations in  $B \rightarrow K^{(*)}\ell^+\ell^-$  decays [26–36], which is instead a one-loop suppressed flavour-changing neutral-current process in the SM. The current measurements continue to exhibit a tension with the SM, with a combined statistical significance of  $\approx 3$  standard deviations for the data on charged-current decays, whereas the global statistical significance of  $b \rightarrow s\ell^+\ell^-$  anomalies has been recently estimated to be  $3.9\sigma$  [37].

Although still in need of experimental confirmation (which, if ever, might require several years [38]), these experimental results definitely fuel the hope that NP might be discovered close to the TeV scale, in partial rescue of the Naturalness argument. In fact, the masses of candidate NP mediators for the anomalies can be roughly estimated from the size of the experimental deviations, and turn out to be generically in the  $1 \div 100$  TeV range [39], although values could go down to  $\mathcal{O}(10)$  GeV in  $Z'$  models [40], or  $\mathcal{O}(100)$  GeV in one-loop models. Moreover, and quite in alignment with the main topic of the present Thesis, the  $B$ -anomalies challenge in a notably coherent way a very special feature of the SM flavour structure: Lepton Flavour Universality (LFU) [38], which we will describe in full detail along this work. Indeed, the most important observables involved in  $B$ -anomalies are the so-called LFU ratios, for which SM predictions are especially clean thanks to LFU.

Precisely concerning lepton flavour structure, from a phenomenological point of view, this is defined by lepton (charged lepton and neutrino) masses and mixing parameters. Charged lepton masses are known with very high precision [9] and, coherently with their quark counterparts, exhibit magnitude hierarchies between the three SM replicas (electron, muon and tau), spanning three orders of magnitude in the MeV  $\div$  GeV range. Neutrino oscillation experiments have measured two independent neutrino squared mass differences and three mixing angles with an accuracy approaching the percent-level, and a (Dirac) CP violating phase with  $\mathcal{O}(10\%)$  accuracy [41]. Squared mass differences lie in the  $10^{-3} \div 10^{-5} \text{ eV}^2$  range, and also exhibit a (mild) relative hierarchy; two out of the three mixing angles,  $\theta_{12}$  and  $\theta_{23}$ , are of order unity, while  $\theta_{13}$  is comparable in size to the CKM Cabibbo angle; the Dirac phase  $\delta$  is also  $\mathcal{O}(1)$ . Furthermore, data from both cosmology [9] and nuclear physics [42] bounds the absolute scale of neutrino masses, roughly below the eV scale. Assuming a framework with three light active neutrinos, which is coherent with current experimental data, remaining unknowns are the relative mass ordering (normal or inverted), the two Majorana CP violating phases of the PMNS matrix and, of course, the absolute values of neutrino masses.

Lepton flavour is, of course, a BSM issue *per se*, as the mechanism behind the generation of neutrino masses is not part of the SM (at least according to its usual definition). From the point of view of the flavour puzzle, the features which most distinctly call for a theoretical explanation are the hierarchies in the charged lepton mass spectrum, the

smallness of neutrino masses and the origin of the PMNS mixing patterns (in the minimal three-neutrino framework). Addressing all these points in a natural and predictive framework, and which could hopefully be extended to also describe the quark sector, represents a challenging open problem. In this Thesis, I describe some results in this direction, from the recently proposed approach to the lepton flavour puzzle based on modular invariant supersymmetric models [43].

This Thesis is composed of three parts. *Part I*, which has a somewhat preliminary function with respect to the remaining material, centers on the so-called SM Effective Field Theory: a non-renormalizable theory whose renormalizable limit coincides with the familiar SM. After briefly reviewing the basic formalism and the systematics of theory matching, I present a personal contribution [44], in which the complete one-loop matching of a phenomenologically motivated SM extension is performed. In *Part II*, I discuss  $B$ -anomalies and my work on the subject [45, 46]; the results of Ref. [46] leverage on the matching performed in [44], described in the previous Part. Finally, *Part III*, whose flavour is more theoretical<sup>1</sup>, tackles the SM flavour puzzle and describes an attempt to address charged lepton mass hierarchies within the framework of modular invariant models [47].

---

<sup>1</sup>No pun intended.

## Part 1

# The Standard Model Effective Field Theory

## CHAPTER 1

# The Standard Model Effective Field Theory

Effective Field Theory and Renormalization play an essential role in our current understanding and speculations about Particle Physics. By taking a bottom-up approach, the Standard Model itself can be fruitfully characterized within this framework, in which the guiding theoretical principles of Symmetry and Symmetry Breaking are naturally implemented. On the other hand, from a top-down perspective, Effective Field Theories provide a powerful computational tool for studying Standard Model high-energy extensions.

This Chapter provides an introduction to the Standard Model Effective Field Theory and sets up the notation to be employed in the subsequent Chapters of this thesis. Section 1.1 introduces the notations used throughout this work and present the Effective Field Theory formulation of the Standard Model; Section 1.2 provides a brief review of the general theory matching procedure; finally, Section 1.3 discusses some advanced matching methods.

### 1.1. The Standard Model as an Effective Field Theory

The Standard Model (SM) can be succinctly described as the most general renormalizable theory of quarks, leptons and the Higgs field, invariant under the electroweak gauge group:

$$G_{\text{SM}} = \text{SU}(3)_c \times \text{SU}(2)_L \times \text{U}(1)_Y. \quad (1.1.1)$$

Renormalizability implies scale-independent self-consistency, in the sense that, from a purely theoretical point of view, the validity of the SM can be extended up to arbitrarily high energy scales<sup>1</sup>. On the other hand, as discussed in the Introduction, there are irrefutable reasons to believe that the SM is not the ultimate theory of Nature, which in turn makes renormalizability a dispensable, if not unmotivated, feature for a realistic theory. Dropping the renormalizability requirement leads from the ultraviolet complete SM theory to an Effective Field Theory (EFT) known as Standard Model Effective Field Theory (SMEFT) [51, 52].

Any quantum field theory with the same light degrees of freedom as the SM, plus some extra heavy degree of freedom, is correctly described by SMEFT at sufficiently low energies (that is, below the EFT cut-off, which is usually of order of the lightest new

---

<sup>1</sup>This is admittedly an oversimplification, for our discussion ignores both the problems of vacuum stability [48] and of potential Landau poles [49, 50] in the renormalization group flow of SM couplings. While, from a purely theoretical point of view, both these issues should be considered seriously, the involved energy scales are usually several order of magnitudes higher than effective cut-offs coming from the explicit introduction of a non-renormalizable interaction in the theory.

Field	Lorentz	SU(3) <sub>c</sub>	SU(2) <sub>L</sub>	U(1) <sub>Y</sub>
$G^\mu$	$(\frac{1}{2}, \frac{1}{2})$	8	1	0
$W^\mu$	$(\frac{1}{2}, \frac{1}{2})$	1	3	0
$B^\mu$	$(\frac{1}{2}, \frac{1}{2})$	1	1	0
$q_i \equiv \begin{pmatrix} u_i & d_i \end{pmatrix}^T$	$(0, \frac{1}{2})$	3	2	$+\frac{1}{6}$
$u_i$	$(\frac{1}{2}, 0)$	3	1	$+\frac{2}{3}$
$d_i$	$(\frac{1}{2}, 0)$	3	1	$-\frac{1}{3}$
$\ell_\alpha \equiv \begin{pmatrix} \nu_\alpha & e_\alpha \end{pmatrix}^T$	$(0, \frac{1}{2})$	1	2	$-\frac{1}{2}$
$e_\alpha$	$(\frac{1}{2}, 0)$	1	1	$+1$
$H$	$(0, 0)$	1	2	$+\frac{1}{2}$

TABLE 1. Standard Model fields. All fermionic fields are four-component Dirac-Weyl fields and family indexes  $i$  or  $\alpha$  run from 1 to 3

particle mass). Although this case does not cover all conceivable generalizations of the SM<sup>2</sup>, it definitely includes a large majority of phenomenological theories which attempt to address one or more SM shortcomings.

In what follows we review the standard SMEFT construction [51, 52] and set our SMEFT notations. The quantum numbers of SM fields under  $G_{\text{SM}}$  are collected in Table 1, together with their Lorentz representations. From Table 1, we can immediately construct the SM lagrangian density (or, simply, “lagrangian”):

$$\mathcal{L}_{\text{SM}} = \mathcal{L}_{\text{SM}}^{\text{gauge}} + \mathcal{L}_{\text{SM}}^{\text{yuk}} - \mathcal{V}_{\text{SM}} \quad (1.1.2)$$

$$\mathcal{L}_{\text{SM}}^{\text{gauge}} = -\frac{1}{4}G_{\mu\nu}^A G^{A\mu\nu} - \frac{1}{4}W_{\mu\nu}^I W^{\mu\nu I} - \frac{1}{4}B_{\mu\nu} B^{\mu\nu} + \quad (1.1.3)$$

$$+ \bar{q}_i \not{D} q + \bar{u}_i \not{D} u + \bar{d}_i \not{D} d + \bar{\ell}_i \not{D} \ell + \bar{e}_i \not{D} e +$$

$$+ (D_\mu H)^\dagger (D^\mu H) +$$

$$+ \frac{\theta g_s^2}{64\pi^2} \delta_{AB} \epsilon^{\mu\nu\rho\sigma} G_{\mu\nu}^A G_{\rho\sigma}^B,$$

$$\mathcal{L}_{\text{SM}}^{\text{yuk}} = -(y_U)_{ij} \bar{q}_i \tilde{H} u_j - (y_D)_{ij} \bar{q}_i H d_j - (y_E)_{\alpha\beta} \bar{\ell}_\alpha H e_\beta + \text{h.c.}, \quad (1.1.4)$$

$$\mathcal{V}_{\text{SM}} = \frac{1}{2} \lambda (H^\dagger H)^2 - m^2 H^\dagger H. \quad (1.1.5)$$

In the equations above,  $\tilde{H}$  denotes the conjugate Higgs field  $\tilde{H} = i\sigma_2 H^*$ , and  $D_\mu$  is the gauge covariant derivative, defined by:

$$D_\mu = \partial_\mu + ig_s G_\mu^A T_A^{(3)} + ig W_\mu^I T_I^{(2)} + ig' B_\mu Y, \quad (1.1.6)$$

<sup>2</sup>For instance, theories which extend the SM with light, feebly coupled degrees of freedom, such as axions or light singlet neutrinos, cannot be directly described by SMEFT.

where the generators  $T^{(3,2)}$  and  $Y$  are given in the relevant representations; we will also occasionally employ the notation  $\phi_1 \overleftrightarrow{D}_\mu \phi_2 = \phi_1 D_\mu \phi_2 - (D_\mu \phi_1) \phi_2$ . All constants appearing in Eqs. (1.1.3)-(1.1.5) have been experimentally measured [9] (except for the QCD  $\theta$  angle, for which only an upper bound exists [53]).

A key ingredient in postulating the SM lagrangian (1.1.2) is renormalizability, which is simply implemented by the requirement that all SM operators have mass dimension at most four (the space-time dimension). Together with gauge invariance, it fully determines the (finite) list of operators which can appear on the right-hand side of Eq. (1.1.2). On the other hand, if renormalizability is not required, it does still make sense to consider Eq. (1.1.2) as the leading order expansion of a non-renormalizable lagrangian, the SMEFT lagrangian, whose higher dimensional operator coefficients are unknown. Concretely, we take:

$$\mathcal{L}_{\text{SMEFT}} = \mathcal{L}_{\text{SM}} + \sum_{d_{\mathcal{O}} > 4} \frac{c_{\mathcal{O}}}{\Lambda_{\mathcal{O}}^{d_{\mathcal{O}}-4}} \mathcal{O}. \quad (1.1.7)$$

In the previous equation, the sum extends over all gauge-invariant operators  $\mathcal{O}$  with mass dimension  $d_{\mathcal{O}} > 4$  which can be built out of the SM fields;  $\Lambda_{\mathcal{O}}$  is an energy scale specific to the operator  $\mathcal{O}$  and  $c_{\mathcal{O}}$  is a dimensionless coefficient of  $\mathcal{O}((4\pi)^{-\ell})$ , where  $\ell$  is the loop-order at which the operator is generated; the combination  $C_{\mathcal{O}} = c_{\mathcal{O}} \Lambda_{\mathcal{O}}^{4-d_{\mathcal{O}}}$  defines the so-called Wilson coefficient of the operator  $\mathcal{O}$ . The effects of  $\mathcal{O}$  at experimental energies  $E$  are suppressed by a factor of  $C_{\mathcal{O}} E^{d_{\mathcal{O}}-4} = c_{\mathcal{O}} (E/\Lambda_{\mathcal{O}})^{d_{\mathcal{O}}-4}$ , which could explain why conclusive evidence of deviations from the SM is still lacking. The non-renormalizable theory defined by (1.1.7) has an implicit energy cut-off  $\Lambda_{\text{SMEFT}}$ , which restricts its validity to energies  $E \leq \Lambda_{\text{SMEFT}}$ , and is expected to be of the same order of the smallest operator scales  $\Lambda_{\mathcal{O}}$ .

In practice, only operators with mass dimension up to a maximal value are included in Eq. (1.1.7). Truncating the sum at dimension five, the only extra non-renormalizable operator is the well known Weinberg operator [54]:

$$(\mathcal{O}_{\nu\nu})_{\alpha\beta} = (\tilde{H}^\dagger \ell_\alpha)^T \mathcal{C} (\tilde{H}^\dagger \ell_\beta), \quad (1.1.8)$$

together with its hermitian conjugate (here  $\mathcal{C}$  denotes the Dirac charge conjugation matrix). At dimension six, the list of effective operators is much richer and consists of 59 independent operators, which we report in Tables 2 to 5 in the so-called Warsaw basis [52].



$X^3$		$X^2 H^2$		$H^4 D^2$	
$\mathcal{O}_{3G}$	$f^{ABC} G_\mu^{A\nu} G_\nu^{B\rho} G_\rho^{C\mu}$	$\mathcal{O}_{HG}$	$G_{\mu\nu}^A G^{A\mu\nu} (H^\dagger H)$	$\mathcal{O}_{H\Box}$	$(H^\dagger H) \Box (H^\dagger H)$
$\mathcal{O}_{3\tilde{G}}$	$f^{ABC} \tilde{G}_\mu^{A\nu} G_\nu^{B\rho} G_\rho^{C\mu}$	$\mathcal{O}_{H\tilde{G}}$	$\tilde{G}_{\mu\nu}^A G^{A\mu\nu} (H^\dagger H)$	$\mathcal{O}_{HD}$	$(H^\dagger D^\mu H)^\dagger (H^\dagger D_\mu H)$
$\mathcal{O}_{3W}$	$\epsilon^{IJK} W_\mu^{I\nu} W_\nu^{J\rho} W_\rho^{K\mu}$	$\mathcal{O}_{HW}$	$W_{\mu\nu}^I W^{I\mu\nu} (H^\dagger H)$	$H^6$	
$\mathcal{O}_{3\tilde{W}}$	$\epsilon^{IJK} \tilde{W}_\mu^{I\nu} W_\nu^{J\rho} W_\rho^{K\mu}$	$\mathcal{O}_{H\tilde{W}}$	$\tilde{W}_{\mu\nu}^I W^{I\mu\nu} (H^\dagger H)$	$\mathcal{O}_H$	$(H^\dagger H)^3$
		$\mathcal{O}_{HB}$	$B_{\mu\nu} B^{\mu\nu} (H^\dagger H)$		
		$\mathcal{O}_{H\tilde{B}}$	$\tilde{B}_{\mu\nu} B^{\mu\nu} (H^\dagger H)$		
		$\mathcal{O}_{HWB}$	$W_{\mu\nu}^I B^{\mu\nu} (H^\dagger \tau^I H)$		
		$\mathcal{O}_{H\tilde{W}B}$	$\tilde{W}_{\mu\nu}^I B^{\mu\nu} (H^\dagger \tau^I H)$		

TABLE 2. SMEFT bosonic operators.

$\psi^2 X H + \text{h.c.}$		$\psi^2 H^3 + \text{h.c.}$		$\psi^2 D H^2$	
$\mathcal{O}_{uG}$	$(\bar{q} T^A \sigma^{\mu\nu} u) \tilde{H} G_{\mu\nu}^A$	$\mathcal{O}_{uH}$	$(H^\dagger H) \bar{q} \tilde{H} u$	$\mathcal{O}_{Hq}^{(1)}$	$(\bar{q} \gamma^\mu q) (H^\dagger i \overleftrightarrow{D}_\mu H)$
$\mathcal{O}_{uW}$	$(\bar{q} \sigma^{\mu\nu} u) \tau^I \tilde{H} W_{\mu\nu}^I$	$\mathcal{O}_{dH}$	$(H^\dagger H) \bar{q} H d$	$\mathcal{O}_{Hq}^{(3)}$	$(\bar{q} \tau^I \gamma^\mu q) (H^\dagger i \overleftrightarrow{D}_\mu^I H)$
$\mathcal{O}_{uB}$	$(\bar{q} \sigma^{\mu\nu} u) \tilde{H} B_{\mu\nu}$	$\mathcal{O}_{eH}$	$(H^\dagger H) \bar{\ell} H e$	$\mathcal{O}_{Hu}$	$(\bar{u} \gamma^\mu u) (H^\dagger i \overleftrightarrow{D}_\mu H)$
$\mathcal{O}_{dG}$	$(\bar{q} T^A \sigma^{\mu\nu} d) H G_{\mu\nu}^A$			$\mathcal{O}_{Hd}$	$(\bar{d} \gamma^\mu d) (H^\dagger i \overleftrightarrow{D}_\mu H)$
$\mathcal{O}_{dW}$	$(\bar{q} \sigma^{\mu\nu} d) \tau^I H W_{\mu\nu}^I$			$\mathcal{O}_{Hud}$	$(\bar{u} \gamma^\mu d) (\tilde{H}^\dagger i D_\mu H)$
$\mathcal{O}_{dB}$	$(\bar{q} \sigma^{\mu\nu} d) H B_{\mu\nu}$			$\mathcal{O}_{H\ell}^{(1)}$	$(\bar{\ell} \gamma^\mu \ell) (H^\dagger i \overleftrightarrow{D}_\mu H)$
$\mathcal{O}_{eW}$	$(\bar{\ell} \sigma^{\mu\nu} e) \tau^I H W_{\mu\nu}^I$			$\mathcal{O}_{H\ell}^{(3)}$	$(\bar{\ell} \tau^I \gamma^\mu \ell) (H^\dagger i \overleftrightarrow{D}_\mu^I H)$
$\mathcal{O}_{eB}$	$(\bar{\ell} \sigma^{\mu\nu} e) H B_{\mu\nu}$			$\mathcal{O}_{He}$	$(\bar{e} \gamma^\mu e) (H^\dagger i \overleftrightarrow{D}_\mu H)$

TABLE 3. SMEFT two-fermion operators. Fermion family indices are omitted.

Four quark		Four lepton		Semileptonic	
$\mathcal{O}_{qq}^{(1)}$	$(\bar{q}\gamma^\mu q)(\bar{q}\gamma_\mu q)$	$\mathcal{O}_{\ell\ell}$	$(\bar{\ell}\gamma^\mu \ell)(\bar{\ell}\gamma_\mu \ell)$	$\mathcal{O}_{\ell q}^{(1)}$	$(\bar{\ell}\gamma^\mu \ell)(\bar{q}\gamma_\mu q)$
$\mathcal{O}_{qq}^{(3)}$	$(\bar{q}\gamma^\mu \sigma^I q)(\bar{q}\gamma_\mu \sigma^I q)$	$\mathcal{O}_{ee}$	$(\bar{e}\gamma^\mu e)(\bar{e}\gamma_\mu e)$	$\mathcal{O}_{\ell q}^{(3)}$	$(\bar{\ell}\gamma^\mu \sigma^I \ell)(\bar{q}\gamma_\mu \sigma^I q)$
$\mathcal{O}_{uu}$	$(\bar{u}\gamma^\mu u)(\bar{u}\gamma_\mu u)$	$\mathcal{O}_{\ell e}$	$(\bar{\ell}\gamma^\mu \ell)(\bar{e}\gamma_\mu e)$	$\mathcal{O}_{eu}$	$(\bar{e}\gamma^\mu e)(\bar{u}\gamma_\mu u)$
$\mathcal{O}_{dd}$	$(\bar{d}\gamma^\mu d)(\bar{d}\gamma_\mu d)$			$\mathcal{O}_{ed}$	$(\bar{e}\gamma^\mu e)(\bar{d}\gamma_\mu d)$
$\mathcal{O}_{ud}^{(1)}$	$(\bar{u}\gamma^\mu u)(\bar{d}\gamma_\mu d)$			$\mathcal{O}_{qe}$	$(\bar{q}\gamma^\mu q)(\bar{e}\gamma_\mu e)$
$\mathcal{O}_{ud}^{(8)}$	$(\bar{u}\gamma^\mu T^A u)(\bar{d}\gamma_\mu T^A d)$			$\mathcal{O}_{lu}$	$(\bar{\ell}\gamma^\mu \ell)(\bar{u}\gamma_\mu u)$
$\mathcal{O}_{qu}^{(1)}$	$(\bar{q}\gamma^\mu q)(\bar{u}\gamma_\mu u)$			$\mathcal{O}_{ld}$	$(\bar{\ell}\gamma^\mu \ell)(\bar{d}\gamma_\mu d)$
$\mathcal{O}_{qu}^{(8)}$	$(\bar{q}\gamma^\mu T^A q)(\bar{u}\gamma_\mu T^A u)$			$\mathcal{O}_{ledq}$	$(\bar{\ell}e)(\bar{d}q)$
$\mathcal{O}_{qd}^{(1)}$	$(\bar{q}\gamma^\mu q)(\bar{d}\gamma_\mu d)$			$\mathcal{O}_{lequ}^{(1)}$	$(\bar{\ell}^r e)_{rs}(\bar{q}^s u)$
$\mathcal{O}_{qd}^{(8)}$	$(\bar{q}\gamma^\mu T^A q)(\bar{d}\gamma_\mu T^A d)$			$\mathcal{O}_{lequ}^{(3)}$	$(\bar{\ell}^r \sigma^{\mu\nu} e)_{rs}(\bar{q}^s \sigma_{\mu\nu} u)$
$\mathcal{O}_{quqd}^{(1)}$	$(\bar{q}^r u)_{rs}(\bar{q}^s d)$				
$\mathcal{O}_{quqd}^{(8)}$	$(\bar{q}^r T^A u)_{rs}(\bar{q}^s T^A d)$				

TABLE 4. SMEFT four-fermion baryon number conserving operators. Fermion family indices are omitted.

$B$ and $L$ violating	
$\mathcal{O}_{duq}$	$\varepsilon_{\alpha\beta\gamma}\epsilon_{rs} [(d^\alpha)^T \mathcal{C} u^\beta] [(q^{\gamma r})^T \mathcal{C} \ell^s]$
$\mathcal{O}_{qqu}$	$\varepsilon_{\alpha\beta\gamma}\epsilon_{rs} [(q^{\alpha r})^T \mathcal{C} q^{\beta s}] [(u^\gamma)^T \mathcal{C} e]$
$\mathcal{O}_{qqq}$	$\varepsilon_{\alpha\beta\gamma}\epsilon_{rs}\epsilon_{pt} [(q^{\alpha r})^T \mathcal{C} q^{\beta s}] [(q^{\gamma p})^T \mathcal{C} \ell^t]$
$\mathcal{O}_{duu}$	$\varepsilon_{\alpha\beta\gamma} [(d^\alpha)^T \mathcal{C} u^\beta] [(u^\gamma)^T \mathcal{C} e]$

TABLE 5. SMEFT four-fermion baryon number violating operators. Fermion family indices are omitted. Greek and latin indices denote color and weak isospin, respectively.

The precise sense in which Warsaw basis operators are independent is the following: none of the operators in Tables 2-5 can be obtained from the remaining ones by taking linear combinations, adding a total divergence, or applying smooth field redefinitions (as its name suggests, the Warsaw basis is also complete, in the sense that any dimension six operator can be obtained from Warsaw basis operators by means of these three operations). The last requirement follows from a well known theorem [55, 56] which states that for any smooth transformation  $\phi \mapsto F(\phi)$  of the coordinate fields  $\phi$ , the two quantum lagrangians  $\mathcal{L}$  and  $\mathcal{L}' = \mathcal{L} \circ F$  give rise to the same physical  $S$  matrix.

To conclude this Section, we observe that the SMEFT formalism we have just described allows one to obtain low energy parametrizations of, virtually, any SM extension

by heavy new fields. The procedure by which one can pass from a high-energy ultraviolet complete model to the low-energy SMEFT description is called *matching*, and is the object of the next Section.

## 1.2. Computing with EFTs: theory matching

The standard matching of EFTs enforces the physical equivalence between an high-energy theory and an effective theory with a reduced number of light degrees of freedom, by requiring equality between the Green's functions<sup>3</sup> of light fields computed in the two theories at a fixed renormalization scale  $\mu$ . The latter is typically chosen to be close to the typical mass scale  $M$  of the fields being integrated out<sup>4</sup>, to ensure that the matching conditions can be computed perturbatively, as  $l$ -loop diagrams can contribute to the matching equations with terms proportional to  $(4\pi)^{-l} \ln(\mu/M)^{l-i}$  for  $i = 0, 1, \dots, l$  [57].

In practice, it is sufficient to enforce matching for the so-called 1-Light-Particle Irreducible (1LPI) Green's functions of the light fields, which are defined as sums of connected Feynman graphs which do not have a single line cut corresponding to an internal light field exchange. At a fixed maximal power  $M^{-k}$  in the EFT expansion, only a finite number of 1LPI Green's function receive contributions from integrating out the heavy fields in the high-energy theory, and each of these gives rise to an independent matching equation for the Wilson coefficients of EFT operators of dimension  $d \leq 4+k$ . Concretely, a sample computation would go as follows [57, 58]:

- (1) Compute the 1LPI Green's function in the high-energy theory, expanding in powers of  $\frac{1}{M}$  up to the desired order.
- (2) Compute the same function in the EFT, including the contributions from effective operators with unknown (as yet) Wilson coefficients.
- (3) Equate the two results.

It goes without mention that steps 1 and 2 above can usually be carried out only in a perturbative fashion, *i.e.* expanding the corresponding Green's function to a fixed loop order (which should be the same in the high-energy and effective theories). The output of this procedure is the full list of EFT Wilson coefficients at the given loop accuracy, which are usually reported in a standard basis, such as the Warsaw basis for SMEFT dimension-six operators.

Adopting a standard operator basis is useful for communicating the final results of an EFT calculation in a compact and unambiguous manner. That said, the diagrammatic

---

<sup>3</sup>This is actually stronger than requiring the equality of (physical)  $S$ -matrix elements, but does not imply a loss in generality. In fact, given a theory with lagrangian  $\mathcal{L}(\phi, \Phi)$ , where  $\phi$  and  $\Phi$  denote the set of light and heavy fields respectively, we can always define a low-energy theory by the lagrangian:

$$\mathcal{L}_{\text{EFT}}(\phi) = \log \left\{ \int \mathcal{D}\Phi \exp [\mathcal{L}(\phi, \Phi)] \right\}.$$

By construction,  $\mathcal{L}_{\text{EFT}}$  and  $\mathcal{L}$  give rise to the same  $\phi$  Green's functions, and the scale separation between  $\phi$  and  $\Phi$  fields ensures that  $\mathcal{L}_{\text{EFT}}$  can be expanded in a series of local operators.

<sup>4</sup>We assume here that there exists only one such scale. In the presence of several scales  $M_1 \ll M_2 \ll \dots \ll M_n$  with sizable separations, the matching is usually performed in a sequential fashion, connecting the various scales  $M_i$  and  $M_{i+1}$  using the renormalization group flow of the intermediate EFTs resulting from the procedure.

matching calculations described above are most naturally performed using a larger effective operator basis, which I will refer to as the *Green's basis*, following the terminology of Ref. [59]. In defining Green's basis operators, we drop the requirement of independence under field redefinitions; the Green's basis is the correct operator menu to be used in the second step of the matching procedure described above, since there exists a bijective linear correspondence between dimension- $d$  Green's operators and Green's *functions*.

### 1.3. Advanced matching methods

Simplifying EFT calculations can provide great help to BSM phenomenologists, by accelerating the process of model building and evaluation. There are two main possible sources of simplification, namely: mathematical methods and automation.

On the mathematical side, the problem of SMEFT tree-level matching up to dimension-six terms was completely solved in Ref. [60], which provided the complete dictionary of SMEFT contributions for all possible tree-level mediators. The key observation behind this work is that, for any fixed maximal effective operator dimension, the number of extra fields and couplings which can give rise to SMEFT operators at low energies is finite, so that the program of Ref. [60] can, at least in principle, be carried out up to any effective operator dimension.

Unfortunately, such a simplification no longer occurs for  $\ell \geq 1$ -loop contributions, in which case more general methods are required. In particular, functional methods (focusing on Green's function generating functionals) have provided significant advances in the context of one-loop computations, the latest approaches being based on the so-called Universal One-Loop Effective Action (UOLEA) [61], which generalises methods based on the Covariant Derivative Expansion (CDE) [62], but whose formalism is still incomplete (see Ref. [61] and references therein for a recent discussion, and for an application of the UOLEA formalism).

Concerning automated methods, many general tools aimed at simplifying EFT calculations are already available (for a comprehensive review, see [63] and references therein). For the specific task of EFT matching, however, the tool-set is still for a large part under development. We cite here the software packages mentioned in Ref. [63]:

- **MatchingTools** [64], a Python library providing support for tree-level matching of generic field theories (*i.e.* not restricted by the SM gauge group and field content). This package was used, in particular, for an extensive check of the analytic results provided by Ref. [60] mentioned earlier.
- **CoDEx** [65], a Mathematica package devoted to SMEFT matching at one-loop and up to dimension-six operators. CoDEx is based on the Covariant Derivative Expansions, and the latest release (v1.0.0) by the time of this writing can correctly handle only one-loop diagrams not involving light internal particles in the loop.
- **MatchMaker** [63], a work-in-progress Python package whose primary purpose is, again, the complete SMEFT one-loop matching (with the grand goal of extending the tool-set to arbitrary field theories). Unfortunately, by the time of this writing, no further update on the progress status of MatchMaker is available.

To conclude, both mathematical and computer-based methods for EFT calculations still offer large room for improvement, and progress in this area could definitely provide precious help in our meandering search for BSM signals.

## CHAPTER 2

### A case study: the $S_1 + S_3$ Leptoquark model

This Chapter discusses my contribution [44], in collaboration with D. Marzocca and E. Venturini, in which we performed the complete SMEFT one-loop matching for the  $S_1 + S_3$  leptoquark model, up to dimension-six (leading order) in the EFT expansion.

This model has received attention from the phenomenology community during recent years, as one of the most promising candidates for the solution of so-called (neutral- and charged-current)  $B$ -anomalies, which will be the central subject of Part II of this Thesis. As was recently realized, the model can also (simultaneously) provide a good fit to the long-standing muon  $(g - 2)_\mu$  discrepancy [44], while giving rise to additional further predictions (for *e.g.* Lepton Flavor Violating observables) which are compatible with current bounds, but in the ball-park of future prospects. All in all, the  $S_1 + S_3$  model offers a particularly intriguing New Physics scenario, which is fully amenable to the EFT analysis discussed in the previous Chapter.

Beyond its phenomenological interest, Ref. [44] provides one of the very few examples of complete SMEFT one-loop matchings, performed in the standard diagrammatic way, available in the literature. In [66, 67] the one-loop matching for bosonic SMEFT operators from integrating out sfermions in the MSSM is derived, Refs. [59, 61] perform the complete one-loop matching for a singlet scalar (see also [68]), and [69] considers the SM with an additional light sterile neutrino and heavy fermions and a scalar singlet. The model considered in Ref. [44], with two coloured and weakly-charged states coupled to all SM particles with non-trivial flavour structures, represents a very rich example of such a matching. In hindsight, results of this kind will be of value as important cross-checks for more advanced matching techniques, including functional- and even computer-based approaches (some ongoing work in this direction was mentioned in Sec. 1.3). Indeed, given the relevance of the subject to model building, automating (or, at least, simplifying) EFT calculations has a great potential for streamlining the work of many phenomenologists, and establishing a set of (reasonably complex) test cases is an unavoidable step in the process of building these more sophisticated tools.

The complete one-loop matching presented in this Chapter allows for in-depth phenomenological analyses of the leptoquark model. In Part II, Chapter 4, we will describe in detail the phenomenology of the  $S_1 + S_3$  model, as a potential combined solution of the  $B$ -decay anomalies and the muon  $(g - 2)_\mu$  discrepancy.

#### 2.1. The $S_1 + S_3$ model

The UV model under consideration is defined by the SM gauge group and field content, with the addition of two colored scalar *leptoquarks*:

$$S_1 \sim (\bar{\mathbf{3}}, \mathbf{1})_{1/3}, \quad S_3 \sim (\bar{\mathbf{3}}, \mathbf{3})_{1/3}, \quad (2.1.1)$$

where in parenthesis we indicate the  $S_{1,3}$  representations under  $(\text{SU}(3)_c, \text{SU}(2)_L)_{\text{U}(1)_Y}$ . At the renormalizable level, the two additional scalars directly couple to SM fermions through the Yukawa terms:

$$((\lambda^{1L})_{i\alpha} \bar{q}_i^c \epsilon \ell_\alpha + (\lambda^{1R})_{i\alpha} \bar{u}_i^c e_\alpha) S_1 + (\lambda^{3L})_{i\alpha} \bar{q}_i^c \sigma^I \epsilon \ell_\alpha S_3^I, \quad (2.1.2)$$

(hence the name “leptoquarks”). The couplings in Eq. (2.1.2) by themselves do not imply a violation of baryon or lepton number conservation, as can be seen by the  $S_{1/3}$  lepton and baryon number assignments:

$$(L_S, B_S) = \left(-1, +\frac{1}{3}\right). \quad (2.1.3)$$

On the other hand, the following additional “diquark” operators are also allowed by gauge invariance:

$$\bar{u}_i d_j^c S_1, \quad \bar{q}_i q_j^c S_1, \quad \bar{q}_i \epsilon \sigma^I q_j^c S_3^I, \quad (2.1.4)$$

which violate baryon number conservation according to Eq. (2.1.3), and may lead, *e.g.*, to proton decay. As a consequence, since the phenomenological motivations mentioned above require the introduction of relatively low-scale NP degrees of freedom (of order  $\mathcal{O}(\text{TeV})$ , say), baryon and lepton number conservation is actually postulated *a priori*<sup>1</sup>, along with Eq. (2.1.3), which allows the leptoquark couplings (2.1.2) but forbids the diquark ones, Eq. (2.1.4). Finally, the addition of  $S_{1/3}$  also gives rise to a scalar potential:

$$\mathcal{V}_S = M_1^2 |S_1|^2 + M_3^2 |S_3|^2 + \Delta \mathcal{V}_S(S_1, S_3, H), \quad (2.1.5)$$

where  $\Delta \mathcal{V}_S$  denotes trilinear and tetralinear terms in the  $S_{1/3}$  and Higgs fields, which we omit here for brevity (the full expression is reported in Sec. 2.5).

The leptoquark couplings in Eq. (2.1.2), as well as the omitted potential couplings in Eq. (2.1.5)) are assumed to be in the perturbative regime<sup>2</sup>, so that theory quantities such as Green’s functions admit a sensible perturbative expansion, which, following standard arguments [72], is equivalent to a loop-wise expansion in Feynman graph calculations. Assuming the leptoquark masses  $M_1^2$  and  $M_3^2$  to be of similar order of magnitude (and, of course, large with respect to the electroweak scale), it is easy<sup>3</sup> to obtain the tree-level,

<sup>1</sup>See Ref. [70] for an extended gauge model involving  $S_1$  and  $S_3$ , in which lepton and baryon number are accidental symmetries, as in the SM.

<sup>2</sup>See Ref. [71] for an analysis of perturbativity bounds from unitarity principles.

<sup>3</sup>These can be easily obtained by replacing  $S_1$  and  $S_3$  in the leptoquark model’s lagrangian with the corresponding solutions (in terms of SM fields) of the classical Equations Of Motion (EOM). In doing this, one should take into account the following simplifications, which reduce the problem at hand to linear algebra:

- (1) Terms in the scalar potential (2.1.5) which are not quadratic in  $S_{1/3}$  do not contribute to tree-level matching at leading dimension, and can be safely omitted from the EOM.
- (2) Covariant derivative terms (*i.e.*  $|D_\mu S_{1,3}|^2$ ) from the kinetic lagrangian also give rise to higher ( $\geq 8$ ) dimensional operators, and can be disregarded for the purpose of tree-level matching.

dimension-six SMEFT matching conditions for the (lepton-baryon number conserving)  $S_1 + S_3$  model:

$$\left[ C_{\ell q}^{(1)}(\mu) \right]_{\alpha\beta ij}^{(0)} = \frac{\lambda_{i\alpha}^{1L*} \lambda_{j\beta}^{1L}}{4M_1^2} + 3 \frac{\lambda_{i\alpha}^{3L*} \lambda_{j\beta}^{3L}}{4M_3^2}, \quad (2.1.6)$$

$$\left[ C_{\ell q}^{(3)}(\mu) \right]_{\alpha\beta ij}^{(0)} = -\frac{\lambda_{i\alpha}^{1L*} \lambda_{j\beta}^{1L}}{4M_1^2} + \frac{\lambda_{i\alpha}^{3L*} \lambda_{j\beta}^{3L}}{4M_3^2}, \quad (2.1.7)$$

$$\left[ C_{\ell equ}^{(1)}(\mu) \right]_{\alpha\beta ij}^{(0)} = \frac{\lambda_{i\alpha}^{1L*} \lambda_{j\beta}^{1R}}{2M_1^2}, \quad (2.1.8)$$

$$\left[ C_{\ell equ}^{(3)}(\mu) \right]_{\alpha\beta ij}^{(0)} = -\frac{\lambda_{i\alpha}^{1L*} \lambda_{j\beta}^{1R}}{8M_1^2}, \quad (2.1.9)$$

$$\left[ C_{eu}^{(1)}(\mu) \right]_{\alpha\beta ij}^{(0)} = \frac{\lambda_{i\alpha}^{1R*} \lambda_{j\beta}^{1R}}{2M_1^2}. \quad (2.1.10)$$

The Wilson coefficient notation refers to the Warsaw basis (Tables 2-5). The suffixes <sup>(0)</sup> indicate the accuracy (in terms of loop orders, here zero) of Eqs. (2.1.6)-(2.1.10), and the RG sliding scale  $\mu$  is assumed to be close in magnitude to  $M_{1,3}^2$  (the running UV couplings in the right-hand sides of Eqs. (2.1.6)-(2.1.10) are understood to be evaluated at the same scale).

## 2.2. One-loop matching

In general, taking perturbativity as given, Wilson coefficients admit a loop-wise expansion of the form:

$$C_{\mathcal{O}}(\mu) = C_{\mathcal{O}}(\mu)^{(0)} + \frac{1}{(4\pi)^2} C_{\mathcal{O}}(\mu)^{(1)} + \frac{1}{(4\pi)^4} C_{\mathcal{O}}(\mu)^{(2)} + \dots \quad (2.2.1)$$

Going beyond the tree-level matching, apart from the (obviously) increased computational complexity, a few other technicalities need to be taken into account:

- (1) Loop computations require the introduction of a renormalization scheme, which must be entirely specified along with the final (renormalized) results. We employ the  $\overline{\text{MS}}$  scheme with the Naive Dimensional Regularization (NDR) prescription for analytically extending Dirac matrices to arbitrary real dimensions  $d = 4 - 2\epsilon$ . Furthermore, all computations are performed in a generic  $R_\xi$  gauge, in order to check for the expected elision of  $\xi$ -dependencies in the Wilson coefficients of gauge invariant operators.
- (2) A further scheme-dependence can (and does, in our case) arise from the prescriptions adopted for evanescent operators [73], which are Dirac operators that vanish in four dimension, but may be non-vanishing in  $d = 4 - 2\epsilon^4$ . We follow the

---

<sup>4</sup>An instructive example is given by the two Dirac tensors:

$$\begin{aligned} \mathcal{E}_1 &= P_L \gamma^\mu \gamma^\nu P_L \otimes P_L \gamma_\mu \gamma_\nu P_L - 4P_L \otimes P_L + P_L \sigma^{\mu\nu} P_L \otimes P_L \sigma_{\mu\nu} P_L, \\ \mathcal{E}_2 &= P_L \gamma^\mu \gamma^\nu P_L \otimes P_R \gamma_\mu \gamma_\nu P_R - 4P_L \otimes P_R. \end{aligned}$$

Following the NDR prescription for the Dirac algebra in dimension  $d = 4 - 2\epsilon$ :

$$\{\gamma^\mu, \gamma^\nu\} = 2\eta^{\mu\nu}, \quad \{\gamma^\mu, \gamma^5\} = 0, \quad \text{Tr}(\eta) = 4 - 2\epsilon,$$



conventions of Ref. [74], keeping the scheme-defining coefficients  $\{a_{\text{ev}}, b_{\text{ev}}, \dots\}$  arbitrary in our computations (in practice, the only coefficient entering one-loop computations is  $a_{\text{ev}}$ ).

- (3) As discussed in Sec. 1.2, diagrammatic matching computations are naturally performed in the Green's basis. An important result of Ref. [44] was thus (i) to classify all SMEFT dimension-six Green's basis operators, and (ii) to provide a set of (linear) reduction equations which allow to pass from the Green's basis to the standard Warsaw basis, after field redefinition redundancy is properly taken into account.
- (4) Integrating out the leptoquarks at one loop also generates contributions to SM renormalizable operators and, in particular, fermion kinetic terms. Such modifications can be undone by suitable field and SM coupling redefinitions, which however also introduce additional contributions to tree-level generated WCs<sup>5</sup>. In our case only fermion kinetic terms (i.e. wave-functions renormalizations) are relevant, as the tree-level WCs in Eqs. (2.1.6)-(2.1.10) do not depend on any SM coupling. The one-loop formulas below include the contributions due to fermion field renormalization.

In what follows we illustrate the diagrammatic matching steps with a fully detailed example, and subsequently review the procedures used in Ref. [44] to obtain a dimension-six SMEFT Green's basis and the corresponding equations for reduction onto the Warsaw basis. For additional details, including the final complete results for the SMEFT Wilson coefficients of the  $S_1 + S_3$  model, we address the reader to the original reference [44].

### 2.3. One-loop matching example

In this Section we discuss in some details the matching of a specific Green's function, in order to illustrate some of the most relevant aspects of our computation.

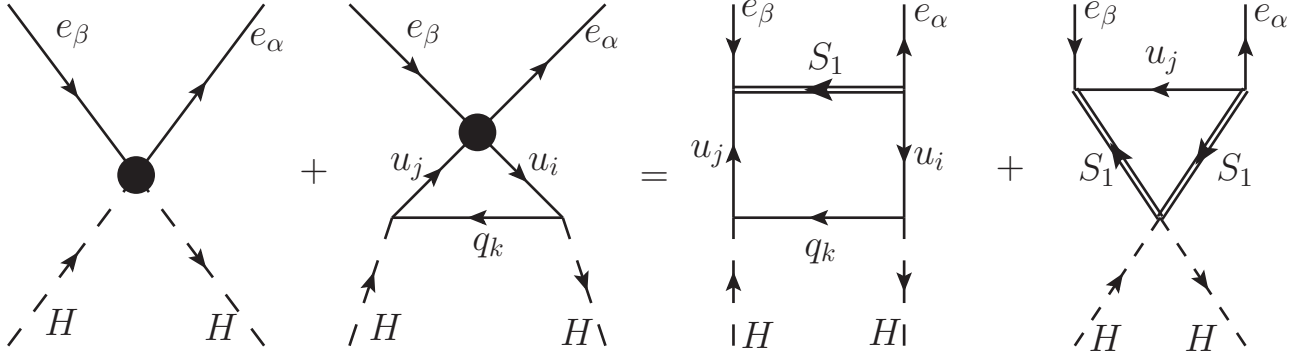
---

one can easily work out the result  $\mathcal{E}_1 = -2\epsilon P_L \otimes P_L$ . However, the operator  $\mathcal{E}_2$  is not univocally fixed by the NDR rules, and  $\mathcal{E}_2$  is usually expressed in terms of canonical Dirac tensors as follows [74]:

$$\mathcal{E}_2 = 4a_{\text{ev}}\epsilon P_L \otimes P_R + E_{LR}^{(2)}(a_{\text{ev}}),$$

where the actual form of  $E_{LR}^{(2)}(a_{\text{ev}})$  in the right-hand side depends on the value of  $a_{\text{ev}}$ , which is completely arbitrary and should be regarded as part of the regularization scheme (for  $a_{\text{ev}} = -\frac{1}{2}$  one gets  $E_{LR}^{(2)}(a_{\text{ev}}) = P_L \sigma^{\mu\nu} P_L \otimes P_R \sigma_{\mu\nu} P_R$ , cf. Ref. [74]).

<sup>5</sup>Since field redefinitions arise at one loop in our model, only tree-level WCs are affected. In general, any tree-level shift in SM couplings and wave-function renormalizations that could influence loop-generated coefficients should be taken into account, see e.g. [59].

FIGURE 2.3.1. Diagrams of the matching of the  $\langle e\bar{e}HH^\dagger \rangle$  Green's function.

Let us consider the off-shell Green's function  $\mathcal{G} \equiv \langle e_\beta(p_1)\bar{e}_\alpha(p_2)H_b(q_1)H_a^\dagger(q_2) \rangle$ , where all momenta are incoming and  $a, b$  are  $SU(2)_L$  indices. The matching conditions for this correlator are depicted diagrammatically in Fig. 2.3.1, where the left and right hand-side show the EFT and UV contributions, respectively. We briefly comment on the various steps of this computation.

We begin by listing the various contributions to  $\mathcal{G}$ , both in the SMEFT and the leptoquark model. The SMEFT operators which contribute at tree level to  $\mathcal{G}$  are (cf. Table 2 for the notation):

$$[\mathcal{O}_{He}]_{\alpha\beta} = (\bar{e}_\alpha \gamma^\mu e_\beta)(H^\dagger i \overleftrightarrow{D}_\mu H), \quad (2.3.1)$$

$$[\mathcal{O}'_{He}]_{\alpha\beta} = (\bar{e}_\alpha i \gamma_\mu \overleftrightarrow{D}^\mu e_\beta)(H^\dagger H), \quad (2.3.2)$$

$$[\mathcal{O}''_{He}]_{\alpha\beta} = (\bar{e}_\alpha \gamma^\mu e_\beta) \partial_\mu (H^\dagger H) \quad (2.3.3)$$

Moreover, we must take into account a one-loop contribution from  $\mathcal{O}_{eu}$ , which is generated at the tree-level in our model according to Eq. (2.1.10). Since this tree-level WC is fixed, the matching of  $\mathcal{G}$  allows us to fix the coefficients of the operators in Eqs. (2.3.1)-(2.3.3), see the left-hand side of Fig. 2.3.1. In the leptoquark model there are two diagrams contributing to  $\mathcal{G}$ , both mediated by  $S_1$ , shown on the right-hand side of Fig. 2.3.1: a box diagram proportional to (schematically)  $y_U y_U^\dagger \lambda^{1R} \lambda^{1R\dagger}$ , and a triangle diagram proportional to  $\lambda_{H1} \lambda^{1R\dagger} \lambda^{1R}$  (the coupling  $\lambda_{H1}$  is defined in Eq. (2.5.1)).

By total momentum conservation, only three out of the four momenta  $p_1, p_2, q_1, q_2$  are independent. Writing  $(p_1, p_2, q_1, q_2) = (p - r, -p - r, q + r, -q + r)$ , the tree-level contributions from the operators in Eqs. (2.3.1)-(2.3.3) read:

$$[\mathcal{G}_{\text{EFT}}^{\text{tree}}(\mu_M)]_{\alpha\beta} = 2\not{q}[G_{He}(\mu_M)]_{\alpha\beta} + 2\not{p}[G'_{He}(\mu_M)]_{\alpha\beta} - 2i\not{r}[G''_{He}(\mu_M)]_{\alpha\beta} \quad (2.3.4)$$

where we drop here and below a global  $\delta_{ab}$  factor, and we denote Green's basis WCs by  $G_i$ . The UV and EFT one-loop contributions are more easily computed when only one

of the independent momenta  $p, q, r$  is non-vanishing, and yield respectively:

$$\left[\mathcal{G}_{\text{UV}}^{1\text{-loop}}(\mu_M)\right]_{\alpha\beta}^{q=r=0} = -\not{p} \frac{N_c(\lambda^{1R\dagger} y_U^T y_U^* \lambda^{1R})_{\alpha\beta}}{(4\pi)^2 2M_1^2} + \not{p} \frac{N_c \lambda_{H1}(\lambda^{1R\dagger} \lambda^{1R})_{\alpha\beta}}{(4\pi)^2 2M_1^2}, \quad (2.3.5)$$

$$\left[\mathcal{G}_{\text{UV}}^{1\text{-loop}}(\mu_M)\right]_{\alpha\beta}^{p=r=0} = -\not{q} \frac{N_c(\lambda^{1R\dagger} y_U^T y_U^* \lambda^{1R})_{\alpha\beta}}{(4\pi)^2 M_1^2} \log \frac{-q^2}{M_1^2}, \quad (2.3.6)$$

$$\left[\mathcal{G}_{\text{UV}}^{1\text{-loop}}(\mu_M)\right]_{\alpha\beta}^{p=q=0} = 0 \quad (2.3.7)$$

and

$$\left[\mathcal{G}_{\text{EFT}}^{1\text{-loop}}(\mu_M)\right]_{\alpha\beta}^{q=r=0} = 0 \quad (2.3.8)$$

$$\left[\mathcal{G}_{\text{EFT}}^{1\text{-loop}}(\mu_M)\right]_{\alpha\beta}^{p=r=0} = \not{q} \frac{N_c(\lambda^{1R\dagger} y_U^T y_U^* \lambda^{1R})_{\alpha\beta}}{(4\pi)^2 M_1^2} \left(1 + \log \frac{\mu_M^2}{-q^2}\right) \quad (2.3.9)$$

$$\left[\mathcal{G}_{\text{EFT}}^{1\text{-loop}}(\mu_M)\right]_{\alpha\beta}^{p=q=0} = 0, \quad (2.3.10)$$

where we employed the tree-level value of  $[C_{eu}]_{\alpha\beta}^{(0)}$  given in Eq. (2.1.10). Notice that the EFT computation presents an ultraviolet divergence, which we regulate in the  $\overline{\text{MS}}$  scheme at renormalization scale  $\mu_M$ . On the other hand, on the basis of renormalizability, the UV contribution must be (and is) finite. Finally, both EFT and UV diagrams present an infrared divergence, corresponding to the  $\log(-q^2)$  terms in Eqs. (2.3.6) and (2.3.9). The agreement of these two terms, which is guaranteed by the EFT construction, provides a further check of validity of the computation.

Requiring  $\mathcal{G}_{\text{EFT}}(\mu_M) = \mathcal{G}_{\text{UV}}(\mu_M)$ , we finally obtain the matching conditions:

$$\begin{aligned} [G_{He}(\mu_M)]_{\alpha\beta} &= -\frac{N_c(\lambda^{1R\dagger} y_U^T y_U^* \lambda^{1R})_{\alpha\beta}}{32\pi^2 M_1^2} \left(1 + \log \frac{\mu_M^2}{M_1^2}\right) \\ [G'_{He}(\mu_M)]_{\alpha\beta} &= -\frac{N_c(\lambda^{1R\dagger} y_U^T y_U^* \lambda^{1R})_{\alpha\beta}}{64\pi^2 M_1^2} + \frac{N_c \lambda_{H1}(\lambda^{1R\dagger} \lambda^{1R})_{\alpha\beta}}{64\pi^2 M_1^2} \\ [G''_{He}(\mu_M)]_{\alpha\beta} &= 0 \end{aligned}$$

As a cross-check, we observe that the  $\mu_M$  dependence of  $[G_{He}(\mu_M)]_{\alpha\beta}$  corresponds to the SMEFT RG running of  $C_{He}$  due to  $C_{eu}$  [75]

$$(4\pi)^2 \mu \frac{d[C_{He}]_{\alpha\beta}}{d\mu} = -2N_c[C_{eu}]_{\alpha\beta ij} (y_U^T y_U^*)_{ij},$$

once Eq. (2.1.10) is taken into account.

## 2.4. A SMEFT dimension-six Green's basis

As discussed in Sec. 1.2, a Green's basis of fixed dimension  $d$  consists of a maximal set of  $d$ -dimensional operators independent by linear combinations and addition of total divergences. The strategy used in Ref. [44] for obtaining a SMEFT dimension-six Green's basis is mainly a re-adaptation of the line of reasoning of Ref. [52] (to which we refer the reader for further clarification), with the important exception that field redefinitions are not allowed for removing operator redundancies. We simply examine all possible

Lorentz-invariant combinations of gauge field strengths, covariant derivatives, Standard Model fermions and the Higgs field, denoted  $X$ ,  $D$ ,  $\psi$  and  $H$  respectively. Tables 1-4 list the operators of a dimension-six SMEFT Green's basis obtained in this way, defined in such a way that the Warsaw basis forms a proper subset of it.

$X^3$		$X^2 H^2$		$H^2 D^4$	
$\mathcal{O}_{3G}$	$f^{ABC} G_\mu^{A\nu} G_\nu^{B\rho} G_\rho^{C\mu}$	$\mathcal{O}_{HG}$	$G_{\mu\nu}^A G^{A\mu\nu} (H^\dagger H)$	$\mathcal{O}_{DH}$	$(D_\mu D^\mu H)^\dagger (D_\nu D^\nu H)$
$\mathcal{O}_{3\tilde{G}}$	$f^{ABC} \tilde{G}_\mu^{A\nu} G_\nu^{B\rho} G_\rho^{C\mu}$	$\mathcal{O}_{H\tilde{G}}$	$\tilde{G}_{\mu\nu}^A G^{A\mu\nu} (H^\dagger H)$	$H^4 D^2$	
$\mathcal{O}_{3W}$	$\epsilon^{IJK} W_\mu^{I\nu} W_\nu^{J\rho} W_\rho^{K\mu}$	$\mathcal{O}_{HW}$	$W_{\mu\nu}^I W^{I\mu\nu} (H^\dagger H)$	$\mathcal{O}_{H\Box}$	$(H^\dagger H) \Box (H^\dagger H)$
$\mathcal{O}_{3\widetilde{W}}$	$\epsilon^{IJK} \widetilde{W}_\mu^{I\nu} W_\nu^{J\rho} W_\rho^{K\mu}$	$\mathcal{O}_{H\widetilde{W}}$	$\widetilde{W}_{\mu\nu}^I W^{I\mu\nu} (H^\dagger H)$	$\mathcal{O}_{HD}$	$(H^\dagger D^\mu H)^\dagger (H^\dagger D_\mu H)$
$X^2 D^2$		$\mathcal{O}_{HB}$	$B_{\mu\nu} B^{\mu\nu} (H^\dagger H)$	$\mathcal{O}'_{HD}$	$(H^\dagger H) (D_\mu H)^\dagger (D^\mu H)$
$\mathcal{O}_{2G}$	$-\frac{1}{2} (D_\mu G^{A\mu\nu}) (D^\rho G_{\rho\nu}^A)$	$\mathcal{O}_{H\tilde{B}}$	$\tilde{B}_{\mu\nu} B^{\mu\nu} (H^\dagger H)$	$\mathcal{O}''_{HD}$	$(H^\dagger H) D_\mu (H^\dagger \overleftrightarrow{D}^\mu H)$
$\mathcal{O}_{2W}$	$-\frac{1}{2} (D_\mu W^{I\mu\nu}) (D^\rho W_{\rho\nu}^I)$	$\mathcal{O}_{HWB}$	$W_{\mu\nu}^I B^{\mu\nu} (H^\dagger \tau^I H)$	$H^6$	
$\mathcal{O}_{2B}$	$-\frac{1}{2} (\partial_\mu B^{\mu\nu}) (\partial^\rho B_{\rho\nu})$	$\mathcal{O}_{H\widetilde{W}B}$	$\widetilde{W}_{\mu\nu}^I B^{\mu\nu} (H^\dagger \tau^I H)$	$\mathcal{O}_H$	$(H^\dagger H)^3$
		$H^2 X D^2$			
		$\mathcal{O}_{WDH}$	$D_\nu W^{I\mu\nu} (H^\dagger i \overleftrightarrow{D}_\mu^I H)$		
		$\mathcal{O}_{BDH}$	$\partial_\nu B^{\mu\nu} (H^\dagger i \overleftrightarrow{D}_\mu H)$		

TABLE 1. Bosonic Green's basis operators. Operators colored in blue are also included in the Warsaw basis.

$\psi^2 D^3$		$\psi^2 XD$		$\psi^2 DH^2$	
$\mathcal{O}_{qD}$	$\frac{i}{2}\bar{q}\{D_\mu D^\mu, \not{D}\}q$	$\mathcal{O}_{Gq}$	$(\bar{q}T^A\gamma^\mu q)D^\nu G_{\mu\nu}^A$	$\mathcal{O}_{Hq}^{(1)}$	$(\bar{q}\gamma^\mu q)(H^\dagger i\overleftrightarrow{D}_\mu H)$
$\mathcal{O}_{uD}$	$\frac{i}{2}\bar{u}\{D_\mu D^\mu, \not{D}\}u$	$\mathcal{O}'_{Gq}$	$\frac{1}{2}(\bar{q}T^A\gamma^\mu i\overleftrightarrow{D}^\nu q)G_{\mu\nu}^A$	$\mathcal{O}_{Hq}'^{(1)}$	$(\bar{q}i\overleftrightarrow{D}^\nu q)(H^\dagger H)$
$\mathcal{O}_{dD}$	$\frac{i}{2}\bar{d}\{D_\mu D^\mu, \not{D}\}d$	$\mathcal{O}'_{\tilde{G}q}$	$\frac{1}{2}(\bar{q}T^A\gamma^\mu i\overleftrightarrow{D}^\nu q)\tilde{G}_{\mu\nu}^A$	$\mathcal{O}_{Hq}''^{(1)}$	$(\bar{q}\gamma^\mu q)\partial_\mu(H^\dagger H)$
$\mathcal{O}_{\ell D}$	$\frac{i}{2}\bar{\ell}\{D_\mu D^\mu, \not{D}\}\ell$	$\mathcal{O}_{Wq}$	$(\bar{q}\tau^I\gamma^\mu q)D^\nu W_{\mu\nu}^I$	$\mathcal{O}_{Hq}^{(3)}$	$(\bar{q}\tau^I\gamma^\mu q)(H^\dagger i\overleftrightarrow{D}_\mu^I H)$
$\mathcal{O}_{eD}$	$\frac{i}{2}\bar{e}\{D_\mu D^\mu, \not{D}\}e$	$\mathcal{O}'_{Wq}$	$\frac{1}{2}(\bar{q}\tau^I\gamma^\mu i\overleftrightarrow{D}^\nu q)W_{\mu\nu}^I$	$\mathcal{O}_{Hq}'^{(3)}$	$(\bar{q}i\overleftrightarrow{D}^I q)(H^\dagger \tau^I H)$
$\psi^2 HD^2 + \text{h.c.}$		$\mathcal{O}'_{\tilde{W}q}$	$\frac{1}{2}(\bar{q}\tau^I\gamma^\mu i\overleftrightarrow{D}^\nu q)\tilde{W}_{\mu\nu}^I$	$\mathcal{O}_{Hq}''^{(3)}$	$(\bar{q}\tau^I\gamma^\mu q)D_\mu(H^\dagger \tau^I H)$
$\mathcal{O}_{uHD1}$	$(\bar{q}u)D_\mu D^\mu \tilde{H}$	$\mathcal{O}_{Bq}$	$(\bar{q}\gamma^\mu q)\partial^\nu B_{\mu\nu}$	$\mathcal{O}_{Hu}$	$(\bar{u}\gamma^\mu u)(H^\dagger i\overleftrightarrow{D}_\mu H)$
$\mathcal{O}_{uHD2}$	$(\bar{q}i\sigma_{\mu\nu}D^\mu u)D^\nu \tilde{H}$	$\mathcal{O}'_{Bq}$	$\frac{1}{2}(\bar{q}\gamma^\mu i\overleftrightarrow{D}^\nu q)B_{\mu\nu}$	$\mathcal{O}'_{Hu}$	$(\bar{u}i\overleftrightarrow{D}^\nu u)(H^\dagger H)$
$\mathcal{O}_{uHD3}$	$(\bar{q}D_\mu D^\mu u)\tilde{H}$	$\mathcal{O}'_{\tilde{B}q}$	$\frac{1}{2}(\bar{q}\gamma^\mu i\overleftrightarrow{D}^\nu q)\tilde{B}_{\mu\nu}$	$\mathcal{O}_{Hu}''$	$(\bar{u}\gamma^\mu u)\partial_\mu(H^\dagger H)$
$\mathcal{O}_{uHD4}$	$(\bar{q}D_\mu u)D^\mu \tilde{H}$	$\mathcal{O}_{Gu}$	$(\bar{u}T^A\gamma^\mu u)D^\nu G_{\mu\nu}^A$	$\mathcal{O}_{Hd}$	$(\bar{d}\gamma^\mu d)(H^\dagger i\overleftrightarrow{D}_\mu H)$
$\mathcal{O}_{dHD1}$	$(\bar{q}d)D_\mu D^\mu H$	$\mathcal{O}'_{Gu}$	$\frac{1}{2}(\bar{u}T^A\gamma^\mu i\overleftrightarrow{D}^\nu u)G_{\mu\nu}^A$	$\mathcal{O}'_{Hd}$	$(\bar{d}i\overleftrightarrow{D}^\nu d)(H^\dagger H)$
$\mathcal{O}_{dHD2}$	$(\bar{q}i\sigma_{\mu\nu}D^\mu d)D^\nu H$	$\mathcal{O}'_{\tilde{G}u}$	$\frac{1}{2}(\bar{u}T^A\gamma^\mu i\overleftrightarrow{D}^\nu u)\tilde{G}_{\mu\nu}^A$	$\mathcal{O}_{Hd}''$	$(\bar{d}\gamma^\mu d)\partial_\mu(H^\dagger H)$
$\mathcal{O}_{dHD3}$	$(\bar{q}D_\mu D^\mu d)H$	$\mathcal{O}_{Bu}$	$(\bar{u}\gamma^\mu u)\partial^\nu B_{\mu\nu}$	$\mathcal{O}_{Hud}$	$(\bar{u}\gamma^\mu d)(\tilde{H}^\dagger iD_\mu H)$
$\mathcal{O}_{dHD4}$	$(\bar{q}D_\mu d)D^\mu H$	$\mathcal{O}'_{Bu}$	$\frac{1}{2}(\bar{u}\gamma^\mu i\overleftrightarrow{D}^\nu u)B_{\mu\nu}$	$\mathcal{O}_{H\ell}^{(1)}$	$(\bar{\ell}\gamma^\mu \ell)(H^\dagger i\overleftrightarrow{D}_\mu H)$
$\mathcal{O}_{eHD1}$	$(\bar{\ell}e)D_\mu D^\mu H$	$\mathcal{O}'_{\tilde{B}u}$	$\frac{1}{2}(\bar{u}\gamma^\mu i\overleftrightarrow{D}^\nu u)\tilde{B}_{\mu\nu}$	$\mathcal{O}_{H\ell}'^{(1)}$	$(\bar{\ell}i\overleftrightarrow{D}^\nu \ell)(H^\dagger H)$
$\mathcal{O}_{eHD2}$	$(\bar{\ell}i\sigma_{\mu\nu}D^\mu e)D^\nu H$	$\mathcal{O}_{Gd}$	$(\bar{d}T^A\gamma^\mu d)D^\nu G_{\mu\nu}^A$	$\mathcal{O}_{H\ell}''^{(1)}$	$(\bar{\ell}\gamma^\mu \ell)\partial_\mu(H^\dagger H)$
$\mathcal{O}_{eHD3}$	$(\bar{\ell}D_\mu D^\mu e)H$	$\mathcal{O}'_{Gd}$	$\frac{1}{2}(\bar{d}T^A\gamma^\mu i\overleftrightarrow{D}^\nu d)G_{\mu\nu}^A$	$\mathcal{O}_{H\ell}^{(3)}$	$(\bar{\ell}\tau^I\gamma^\mu \ell)(H^\dagger i\overleftrightarrow{D}_\mu^I H)$
$\mathcal{O}_{eHD4}$	$(\bar{\ell}D_\mu e)D^\mu H$	$\mathcal{O}'_{\tilde{G}d}$	$\frac{1}{2}(\bar{d}T^A\gamma^\mu i\overleftrightarrow{D}^\nu d)\tilde{G}_{\mu\nu}^A$	$\mathcal{O}_{H\ell}'^{(3)}$	$(\bar{\ell}i\overleftrightarrow{D}^I \ell)(H^\dagger \tau^I H)$
$\psi^2 XH + \text{h.c.}$		$\mathcal{O}_{Bd}$	$(\bar{d}\gamma^\mu d)\partial^\nu B_{\mu\nu}$	$\mathcal{O}_{H\ell}''^{(3)}$	$(\bar{\ell}\tau^I\gamma^\mu \ell)\partial_\mu(H^\dagger H)$
$\mathcal{O}_{uG}$	$(\bar{q}T^A\sigma^{\mu\nu}u)\tilde{H}G_{\mu\nu}^A$	$\mathcal{O}'_{Bd}$	$\frac{1}{2}(\bar{d}\gamma^\mu i\overleftrightarrow{D}^\nu d)B_{\mu\nu}$	$\mathcal{O}_{He}$	$(\bar{e}\gamma^\mu e)(H^\dagger i\overleftrightarrow{D}_\mu H)$
$\mathcal{O}_{uW}$	$(\bar{q}\sigma^{\mu\nu}u)\tau^I \tilde{H}W_{\mu\nu}^I$	$\mathcal{O}'_{\tilde{B}d}$	$\frac{1}{2}(\bar{d}\gamma^\mu i\overleftrightarrow{D}^\nu d)\tilde{B}_{\mu\nu}$	$\mathcal{O}'_{He}$	$(\bar{e}i\overleftrightarrow{D}^\nu e)(H^\dagger H)$
$\mathcal{O}_{uB}$	$(\bar{q}\sigma^{\mu\nu}u)\tilde{H}B_{\mu\nu}$	$\mathcal{O}_{W\ell}$	$(\bar{\ell}\tau^I\gamma^\mu \ell)D^\nu W_{\mu\nu}^I$	$\mathcal{O}_{He}''$	$(\bar{e}\gamma^\mu e)\partial_\mu(H^\dagger H)$
$\mathcal{O}_{dG}$	$(\bar{q}T^A\sigma^{\mu\nu}d)HG_{\mu\nu}^A$	$\mathcal{O}'_{W\ell}$	$\frac{1}{2}(\bar{\ell}\tau^I\gamma^\mu i\overleftrightarrow{D}^\nu \ell)W_{\mu\nu}^I$	$\psi^2 H^3 + \text{h.c.}$	
$\mathcal{O}_{dW}$	$(\bar{q}\sigma^{\mu\nu}d)\tau^I HW_{\mu\nu}^I$	$\mathcal{O}'_{\tilde{W}\ell}$	$\frac{1}{2}(\bar{\ell}\tau^I\gamma^\mu i\overleftrightarrow{D}^\nu \ell)\tilde{W}_{\mu\nu}^I$	$\mathcal{O}_{uH}$	$(H^\dagger H)\bar{q}\tilde{H}u$
$\mathcal{O}_{dB}$	$(\bar{q}\sigma^{\mu\nu}d)HB_{\mu\nu}$	$\mathcal{O}_{B\ell}$	$(\bar{\ell}\gamma^\mu \ell)\partial^\nu B_{\mu\nu}$	$\mathcal{O}_{dH}$	$(H^\dagger H)\bar{q}Hd$
$\mathcal{O}_{eW}$	$(\bar{\ell}\sigma^{\mu\nu}e)\tau^I HW_{\mu\nu}^I$	$\mathcal{O}'_{B\ell}$	$\frac{1}{2}(\bar{\ell}\gamma^\mu i\overleftrightarrow{D}^\nu \ell)B_{\mu\nu}$	$\mathcal{O}_{eH}$	$(H^\dagger H)\bar{\ell}He$
$\mathcal{O}_{eB}$	$(\bar{\ell}\sigma^{\mu\nu}e)HB_{\mu\nu}$	$\mathcal{O}'_{\tilde{B}\ell}$	$\frac{1}{2}(\bar{\ell}\gamma^\mu i\overleftrightarrow{D}^\nu \ell)\tilde{B}_{\mu\nu}$		
		$\mathcal{O}_{Be}$	$(\bar{e}\gamma^\mu e)\partial^\nu B_{\mu\nu}$		
		$\mathcal{O}'_{Be}$	$\frac{1}{2}(\bar{e}\gamma^\mu i\overleftrightarrow{D}^\nu e)B_{\mu\nu}$		
		$\mathcal{O}'_{\tilde{B}e}$	$\frac{1}{2}(\bar{e}\gamma^\mu i\overleftrightarrow{D}^\nu e)\tilde{B}_{\mu\nu}$		

TABLE 2. Two-fermion Green's basis operators. Operators colored in blue are also included in the Warsaw basis. Fermion family indices are omitted.



Four quark		Four lepton		Semileptonic	
$\mathcal{O}_{qq}^{(1)}$	$(\bar{q}\gamma^\mu q)(\bar{q}\gamma_\mu q)$	$\mathcal{O}_{\ell\ell}$	$(\bar{\ell}\gamma^\mu \ell)(\bar{\ell}\gamma_\mu \ell)$	$\mathcal{O}_{\ell q}^{(1)}$	$(\bar{\ell}\gamma^\mu \ell)(\bar{q}\gamma_\mu q)$
$\mathcal{O}_{qq}^{(3)}$	$(\bar{q}\gamma^\mu \sigma^I q)(\bar{q}\gamma_\mu \sigma^I q)$	$\mathcal{O}_{ee}$	$(\bar{e}\gamma^\mu e)(\bar{e}\gamma_\mu e)$	$\mathcal{O}_{\ell q}^{(3)}$	$(\bar{\ell}\gamma^\mu \sigma^I \ell)(\bar{q}\gamma_\mu \sigma^I q)$
$\mathcal{O}_{uu}$	$(\bar{u}\gamma^\mu u)(\bar{u}\gamma_\mu u)$	$\mathcal{O}_{\ell e}$	$(\bar{\ell}\gamma^\mu \ell)(\bar{e}\gamma_\mu e)$	$\mathcal{O}_{eu}$	$(\bar{e}\gamma^\mu e)(\bar{u}\gamma_\mu u)$
$\mathcal{O}_{dd}$	$(\bar{d}\gamma^\mu d)(\bar{d}\gamma_\mu d)$			$\mathcal{O}_{ed}$	$(\bar{e}\gamma^\mu e)(\bar{d}\gamma_\mu d)$
$\mathcal{O}_{ud}^{(1)}$	$(\bar{u}\gamma^\mu u)(\bar{d}\gamma_\mu d)$			$\mathcal{O}_{qe}$	$(\bar{q}\gamma^\mu q)(\bar{e}\gamma_\mu e)$
$\mathcal{O}_{ud}^{(8)}$	$(\bar{u}\gamma^\mu T^A u)(\bar{d}\gamma_\mu T^A d)$			$\mathcal{O}_{\ell u}$	$(\bar{\ell}\gamma^\mu \ell)(\bar{u}\gamma_\mu u)$
$\mathcal{O}_{qu}^{(1)}$	$(\bar{q}\gamma^\mu q)(\bar{u}\gamma_\mu u)$			$\mathcal{O}_{\ell d}$	$(\bar{\ell}\gamma^\mu \ell)(\bar{d}\gamma_\mu d)$
$\mathcal{O}_{qu}^{(8)}$	$(\bar{q}\gamma^\mu T^A q)(\bar{u}\gamma_\mu T^A u)$			$\mathcal{O}_{\ell edq}$	$(\bar{\ell}e)(\bar{d}q)$
$\mathcal{O}_{qd}^{(1)}$	$(\bar{q}\gamma^\mu q)(\bar{d}\gamma_\mu d)$			$\mathcal{O}_{\ell equ}^{(1)}$	$(\bar{\ell}^T e)\epsilon_{rs}(\bar{q}^s u)$
$\mathcal{O}_{qd}^{(8)}$	$(\bar{q}\gamma^\mu T^A q)(\bar{d}\gamma_\mu T^A d)$			$\mathcal{O}_{\ell equ}^{(3)}$	$(\bar{\ell}^T \sigma^{\mu\nu} e)\epsilon_{rs}(\bar{q}^s \sigma_{\mu\nu} u)$
$\mathcal{O}_{quqd}^{(1)}$	$(\bar{q}^r u)\epsilon_{rs}(\bar{q}^s d)$				
$\mathcal{O}_{quqd}^{(8)}$	$(\bar{q}^r T^A u)\epsilon_{rs}(\bar{q}^s T^A d)$				

TABLE 3. Baryon and lepton number conserving four-fermion Green's basis operators. All operators are included in the Warsaw basis. Fermion family indices are omitted. Indices  $r, s, p, t, \dots$  denote the  $SU(2)_L$  fundamental representations.

$B$ and $L$ violating	
$\mathcal{O}_{duq}$	$\varepsilon_{\alpha\beta\gamma}\epsilon_{rs} [(d^\alpha)^T \mathcal{C} u^\beta] [(q^\gamma)^T \mathcal{C} \ell^s]$
$\mathcal{O}_{qqu}$	$\varepsilon_{\alpha\beta\gamma}\epsilon_{rs} [(q^{\alpha r})^T \mathcal{C} q^{\beta s}] [(u^\gamma)^T \mathcal{C} e]$
$\mathcal{O}_{qqq}$	$\varepsilon_{\alpha\beta\gamma}\epsilon_{rs}\epsilon_{pt} [(q^{\alpha r})^T \mathcal{C} q^{\beta s}] [(q^{\gamma p})^T \mathcal{C} \ell^t]$
$\mathcal{O}_{duu}$	$\varepsilon_{\alpha\beta\gamma} [(d^\alpha)^T \mathcal{C} u^\beta] [(u^\gamma)^T \mathcal{C} e]$

TABLE 4. Baryon and lepton number violating four-fermion Green's basis operators. All operators are included in the Warsaw basis. Fermion family indices are omitted. Indices  $r, s, p, t, \dots$  and  $a, b, c, \dots$  denote the  $SU(2)_L$  and  $SU(3)_c$  fundamental representations, respectively.  $\mathcal{C}$  is the Dirac charge conjugation matrix.

In order to obtain the reduction equations from the Green's to the Warsaw basis, one must apply the SM equations of motion [52] to the additional (not marked in blue) Green's operators in Tables 1-4, which results in a set of linear equations in the form  $C_i = \sum_j a_{ij} G_j$ , where  $C_i$  and  $G_j$  are the Warsaw and Green's basis Wilson coefficients, respectively, and the  $a_{ij}$  are functions of SM couplings. The full set of  $a_{ij}$  coefficients is available from our original reference [44].

### 2.5. Appendix: $S_1 + S_3$ scalar potential

We report here, for completeness, the expression of the  $S_1 + S_3$  scalar potential used in Ref. [44]:

$$\begin{aligned}
 V = & M_1^2 |S_1|^2 + M_3^2 |S_3|^2 + \\
 & + \lambda_{H1} |H|^2 |S_1|^2 + \lambda_{H3} |H|^2 |S_3|^2 + \left( \lambda_{H13} (H^\dagger \sigma^I H) S_3^{I\dagger} S_1 + \text{h.c.} \right) + \\
 & + \lambda_{\epsilon H3} i \epsilon^{IJK} (H^\dagger \sigma^I H) S_3^{J\dagger} S_3^K + \\
 & + \frac{c_1}{2} (S_1^\dagger S_1)^2 + c_{13}^{(1)} (S_1^\dagger S_1) (S_3^\dagger S_3) + c_{13}^{(8)} (S_1^\dagger T^A S_1) (S_3^\dagger T^A S_3) + \\
 & + \frac{c_3^{(1)}}{2} (S_3^\dagger S_3) (S_3^\dagger S_3) + \frac{c_3^{(3)}}{2} (S_3^{I\dagger} \epsilon^{IJK} S_3^J) (S_3^{L\dagger} \epsilon^{LMK} S_3^M) + \\
 & + \frac{c_3^{(5)}}{2} \left[ \frac{(S_3^{I\dagger} S_3^J) (S_3^{I\dagger} S_3^J) + (S_3^{I\dagger} S_3^J) (S_3^{J\dagger} S_3^I)}{2} - \frac{1}{3} (S_3^\dagger S_3) (S_3^\dagger S_3) \right]
 \end{aligned} \tag{2.5.1}$$



## Part 2

# New Physics signals from flavour: the *B*-anomalies

## CHAPTER 3

### Introduction

The rich variety of phenomena predicted by the SM is due, to a large extent, to its non-trivial flavour structure. The particular flavour patterns in physical observables predicted by the SM can be turned into a powerful probe of NP interactions, which are a priori restricted by no means to follow the same SM patterns. In this Chapter, we discuss a set of experimental results, collectively known as *B*-anomalies, which put into question SM predictions precisely from this point of view.

#### 3.1. Low-energy implications of SM flavour

The phenomenological peculiarities of SM quarks and leptons originate from the Yukawa part of the SM lagrangian (cf. Eq. (1.1.2)):

$$\mathcal{L}_{\text{SM}}^{\text{yuk}} = -(y_U)_{ij} \bar{q}_i \tilde{H} u_j - (y_D)_{ij} \bar{q}_i H d_j - (y_E)_{\alpha\beta} \bar{\ell}_\alpha H e_\beta + \text{h.c.} \quad (3.1.1)$$

In the absence of these terms the whole SM would be symmetric under a global flavour symmetry group:

$$G_F = \text{U}(3)^5 \equiv \text{U}(3)_q \times \text{U}(3)_u \times \text{U}(3)_d \times \text{U}(3)_\ell \times \text{U}(3)_e, \quad (3.1.2)$$

which acts by independent unitary transformations of the SM electroweak multiplets:

$$\psi_n \xrightarrow{G_F} (U^\psi)_n^m \psi_m \quad (\psi = q, u, d, \ell, e). \quad (3.1.3)$$

It is the breaking of  $G_F$  induced by  $\mathcal{L}_{\text{SM}}^{\text{yuk}}$  which gives rise to the actual properties of quarks and leptons which we observe in low-energy experiments. For convenience, we will discuss separately the breakings of the quark  $\text{U}(3)_Q^3 \equiv \text{U}(3)_q \times \text{U}(3)_u \times \text{U}(3)_d$  and lepton  $\text{U}(3)_L^2 \equiv \text{U}(3)_\ell \times \text{U}(3)_e$  part of  $G_F$ .

Concerning the quark sector, we can assume without loss of generality that the Yukawa matrices  $y_{U,D}$  take the following forms<sup>1</sup>:

$$y_D = \text{diag}(y_d, y_s, y_b), \quad y_U = V^\dagger \text{diag}(y_u, y_c, y_t), \quad (3.1.4)$$

where  $V$  can be identified with the Cabibbo-Kobayashi-Maskawa (CKM) matrix, and the singular values  $y_\bullet$  are proportional to quark masses. The minimal residual symmetry group resulting from Eqs. (3.1.4) is a  $\text{U}(1)_B$  group, whose corresponding conserved charge is the total baryon number  $B$ , and this is what is actually realized in Nature: since all quark masses are different, and  $V$  is experimentally known to be non-trivial (*i.e.* not

---

<sup>1</sup>The special forms in Eq. (3.1.4) can always be achieved through an appropriate redefinition of the basic quark fields  $q, u, d$  (this is sometimes referred to in the literature as the “down-quark basis”). The field redefinition can be made to employ  $G_F$  transformations only, which, by definition of  $G_F$  itself, leave the rest of the SM lagrangian invariant.

equivalent to the identity matrix), the only subgroup of  $G_F$  which leaves  $y_D$  and  $y_U$  simultaneously invariant consists of  $U(1)$  transformations of the form:

$$q \rightarrow e^{i\alpha}q, \quad u \rightarrow e^{i\alpha}u, \quad d \rightarrow e^{i\alpha}d. \quad (3.1.5)$$

Quark masses  $m_\bullet \propto y_\bullet$  and mixing parameters contained in the CKM matrix  $V$  give rise to the different phenomenological properties of the six (up and down) quarks.

A corresponding discussion for the lepton sector is unavoidably made somewhat fuzzier by our limited knowledge regarding the mechanism generating neutrino masses. The charged lepton Yukawa matrix in Eq. (3.1.1) can, again without loss of generality, be taken to be diagonal:

$$y_E = \text{diag}(y_e, y_\mu, y_\tau), \quad (3.1.6)$$

and the resulting minimal residual symmetry group is  $U(1)_e \times U(1)_\mu \times U(1)_\tau$ , whose corresponding conserved charges are the total numbers of electrons, muons and taus. Here, the only source of breaking of the original  $U(3)_L^2$  are the differences in lepton masses  $m_{e,\mu,\tau} \propto y_{e,\mu,\tau}$ . This description is, of course, incomplete, for it does not take into account neutrino masses and mixings, whose well-established measurements [76] provide conclusive evidence for the violation of individual (flavour specific) lepton numbers, and arguably also hint to total lepton number violation [54]. However, the extra (external to the SM) sources of this further breaking are expected to be feebly coupled to the SM, either because of heavy mediators or small couplings, as suggested by the extreme smallness of neutrino masses. As a consequence, in many experimental settings, the SM description with massless neutrinos is sufficient for all practical purposes.

An important SM prediction concerning leptonic flavour observables is Lepton Flavor Universality (LFU), which is the mere observation that the full leptonic  $U(3)_L^2$  symmetry is restored in the limit of vanishing lepton masses<sup>2</sup>. Such a symmetry manifests itself in actual experiments as a degeneracy in physical processes involving different charged leptons and/or neutrinos in their final state. As a relevant example, consider the differential branching fractions:

$$\frac{d}{dq^2} \text{Br}(B \rightarrow K \ell^+ \ell^-), \quad (\ell = e, \mu), \quad (3.1.7)$$

where  $q^2$  denotes the invariant mass of the charged lepton pair. This process is at the core of neutral current  $B$ -anomalies, which we discuss below. For sufficiently large  $q^2$ , say  $q^2 \geq (1 \text{ GeV})^2$ , the final state lepton masses are practically negligible, and it turns out that:

$$\frac{d}{dq^2} \text{Br}(B \rightarrow K e^+ e^-) \approx \frac{d}{dq^2} \text{Br}(B \rightarrow K \mu^+ \mu^-) \quad (3.1.8)$$

(we will formalize the approximate equalities in Eq. (3.1.8) in the following Section).

**3.1.1. Flavor from symmetries.** We make a small digression to discuss some prominent ideas connected with the SM flavour structure, and with the quark sector in particular. Explaining the SM flavour structure is the main topic of Chapter 6, but the ideas presented here also play an important role in model building for SM deviations.

---

<sup>2</sup>The same observation is, of course, valid for quark flavour observables. For example, the SM decay widths  $\Gamma(Z \rightarrow q\bar{q})$  are essentially equal for all light down quarks  $q = d, s, b$ , an instance of “Down Quark Flavor Universality”.

The SM breaking pattern  $U(3)_Q^3 \rightarrow U(1)_B$ , parametrized by quark masses and the CKM matrix, works remarkably well from the phenomenological point of view, perhaps beyond reasonable expectations, if one takes the view that there exists NP lying not too far from the TeV scale, *and* whose quark flavour structure is completely unrelated to the SM one. A patent example of this fact is provided by the bounds on NP Wilson coefficients coming from  $\Delta F = 2$  neutral meson mixing processes [77, 78]: if one assumes arbitrary NP flavour structures, these bounds constrain the  $\Delta F = 2$  effective operator scales to orders of magnitude such as  $10^3 \div 10^5$  TeV, compared to the  $1 \div 10^2$  TeV scales which are affordable for an SM-like flavour structure. The conclusion is that flavour precision observables (such as  $\Delta F = 2$  amplitudes) naturally require low-scale SM extensions to align, to some extent, to the SM flavour structure.

A theoretically robust way of obtaining such an alignment makes use of *flavour symmetries*: one postulates that some subgroup of  $U(3)_Q^3$  is an actual high-energy, spontaneously broken symmetry group, and tries to correlate the SM and NP flavour structures by assuming that both these arise from a shared, limited set of fields with symmetry breaking expectation values, called flavons. An example is provided by the Minimal Flavor Violation (MFV) framework [79], in which the symmetry group is the whole  $U(3)_Q^3$ , and the flavons are the two SM Yukawa matrices themselves, which carry the following representations:

$$y_U \sim \mathbf{3}_q \otimes \bar{\mathbf{3}}_u, \quad y_D \sim \mathbf{3}_q \otimes \bar{\mathbf{3}}_d, \quad (U(3)_Q^3) \quad (3.1.9)$$

In MFV,  $y_U$  and  $y_D$  are assumed to be the only sources of  $U(3)_Q^3$  breaking for the SM *and* for NP, which provides the desired alignment in, *e.g.*,  $\Delta F = 2$  amplitudes. A less stringent example is provided by  $U(2)_Q^3$  symmetry [80], which only acts on light generation fermions. One can again decompose the Yukawa matrices in terms of  $U(2)_Q^3$  representations:

$$y_U \sim \mathbf{1} \oplus \mathbf{2}_q \oplus \mathbf{2}_u \oplus \mathbf{2}_q \otimes \mathbf{2}_u, \quad y_D \sim \mathbf{1} \oplus \mathbf{2}_q \oplus \mathbf{2}_d \oplus \mathbf{2}_q \otimes \mathbf{2}_d \quad (U(2)_Q^3). \quad (3.1.10)$$

Actually, in the minimal  $U(2)_Q^3$  setup [81], we can restrict ourselves to the following set of flavons:

$$\Delta_{u(d)} \sim \mathbf{2}_q \otimes \mathbf{2}_{u(d)}, \quad \mathbf{V}_q \sim \mathbf{2}_q, \quad (3.1.11)$$

in terms of which the Yukawa matrices are given by:

$$y_U = y_t \begin{pmatrix} \Delta_u & c_U \mathbf{V}_q \\ 0 & 1 \end{pmatrix}, \quad y_D = y_b \begin{pmatrix} \Delta_d & c_D \mathbf{V}_q \\ 0 & 1 \end{pmatrix}. \quad (3.1.12)$$

NP couplings involving quarks must also be expressed in terms of  $\Delta_{u,d}$  and  $\mathbf{V}_q$ , which again yields correlations between the SM and NP flavour structure. In fact, for instance,  $\mathbf{V}_q$  in Eq. (3.1.12) can be shown to be approximately proportional to  $(V_{td}^*, V_{ts}^*)^T$  in the down quark mass basis [81].

The above discussion can be extended as a whole (including the MFV and  $U(2)$  symmetry examples) to the leptonic sector, in which case, however, correlations tend to be looser than in the quark case, the main source of uncertainty being again the unknown neutrino mass generation mechanism.

### 3.2. The $B$ -meson decay anomalies

The SM provides an excellent description of physical phenomena in a wide range of energies and scales. Despite no direct evidence for new physics emerged in direct searches at the LHC, for several years now some low energy measurements continue to show significant deviations from the respective SM predictions, which fuel the hope that some New Physics (NP) might be lurking somewhere at the TeV scale. In this Chapter, we discuss a set of measurements in  $B$ -meson decays, which exhibit a very explicit tension with SM predictions and, in particular, with LFU.

Specifically, important deviations from the SM have been observed within the following three set of observables:

- The neutral current LFU ratios [26, 27, 31, 33, 34, 36]:

$$R(K^{(*)}) = \frac{\text{Br}(B \rightarrow K^{(*)}\mu^+\mu^-)}{\text{Br}(B \rightarrow K^{(*)}e^+e^-)} \Big|_{q^2 \in [1.1, 6] \text{ GeV}^2}. \quad (3.2.1)$$

Here  $q^2$  denotes the invariant mass of the dilepton pairs in the final states (more on this below).

- The differential angular distribution in  $B \rightarrow K^*\mu^+\mu^-$ , as well as several branching fractions of  $b \rightarrow s\mu^+\mu^-$  processes [28–30, 32, 35].
- The charged current LFU ratios [15–25]:

$$R(D^{(*)}) = \frac{\text{Br}(B \rightarrow D^{(*)}\tau\nu)}{\text{Br}(B \rightarrow D^{(*)}l\nu)} \quad (l = \mu, e). \quad (3.2.2)$$

While the muon specific observables of the second point provide an important piece of information for disentangling NP effects in  $b \rightarrow s\mu^+\mu^-$  and  $b \rightarrow se^+e^-$  in the  $R(K^{(*)})$  observables (which, as we will shortly see, both exhibit a deficiency with respect to SM predictions), for the present discussion I will mainly focus on the LFU ratios (3.2.1) and (3.2.2). For these observables, the SM predictions are particularly clean, since the theoretical uncertainties coming from the hadronic  $B \rightarrow D^{(*)}$  and  $B \rightarrow K^{(*)}$  integrated form factors cancel out in large part in the  $R(K^{(*)})$  and  $R(D^{(*)})$  ratios, respectively.

Let us first consider the theoretical predictions for Eqs. (3.2.1) and (3.2.2). The SM predictions for  $R(K^{(*)})$  are particularly simple:

$$R(K^{(*)})_{\text{SM}} = 1 \quad (3.2.3)$$

where the theoretical relative uncertainties, due to neglected electromagnetic corrections, are of order  $\mathcal{O}(1\%)$  [82] and can be safely ignored for phenomenological purposes. This simple result can be understood from the viewpoint of LFU: given the considered energy range (cf. Eq. (3.2.1)), both the final state electrons and muons can be effectively taken to be massless; therefore, due to LFU, electrons or muons are both kinematically and dynamically equivalent in the decay, and the rates for the two different leptonic channels are equal. As a side note, we observe that the  $q^2$  bin in Eq. (3.2.1) is chosen in such a way that both the  $\rho$  ( $m_\rho^2 \sim 0.6 \text{ GeV}^2$ ) and  $J/\psi$  ( $m_{J/\psi}^2 \sim 9 \text{ GeV}^2$ ) resonances lie far away from the  $q^2$  range; this ensures that the  $B \rightarrow K^{(*)}\ell^+\ell^-$  SM decays are dominated by short distance (*i.e.* electroweak) interactions, whose contributions can be computed with relatively good accuracy.

The story is slightly more complicated for  $R(D^{(*)})$ . The SM predictions read [83]:

$$R(D) = 0.299, \quad (3.2.4)$$

$$R(D^*) = 0.258, \quad (3.2.5)$$

where we again neglected theoretical uncertainties, which are of order a few percents. In this case lepton masses are definitely relevant, since the final states with  $\tau$  or  $\mu/e$  leptons have very different configuration spaces, and the cancellation between the hadronic  $B \rightarrow D^{(*)}$  form factors between the numerators and denominators of  $R(D^{(*)})$  is only partial. In spite of this, the hadronic form factors can be computed with good accuracy in the SM [83], and moreover the calculation is in this case free of complications from long-distance effects.

We now compare the theoretical predictions (3.2.3), (3.2.4) and (3.2.5) with the corresponding experimental results, which are collected in Table 1. We observe in the first place that all experimental relative uncertainties range between 5% and 10%, justifying our neglect of theoretical uncertainties. The experimental results for  $R(K^{(*)})$  both show a deficit with respect to the SM prediction: if combined with the  $b \rightarrow s\mu^+\mu^-$  data previously mentioned, the global significance of the deviation is of about 3.9 standard deviations [37]<sup>3</sup>. The measurements of  $R(D^{(*)})$  show, instead, an enhancement with respect to the SM, with a combined significance of  $\approx 3$  standard deviations.

One thing to notice is that the quark level transitions underlying  $R(D^{(*)})$  (*i.e.*  $b \rightarrow c\ell\nu$ ) and  $R(K^{(*)})$  (*i.e.*  $b \rightarrow s\ell\ell$ ) are a tree-level and a one-loop process in the SM, respectively. Since, on the other hand, all experimental deviations are roughly of the same relative order, this implies that in order to provide a *combined* NP explanation of both anomalies, one of the two following conditions must hold:

- The NP mediators giving rise to the deviation in  $R(D^{(*)})$  must be lighter (roughly by a factor of ten) than those contributing to  $R(K^{(*)})$ , or
- The NP effective couplings affecting the  $b \rightarrow c\ell\nu$  transition must be enhanced with respect to those affecting  $b \rightarrow s\ell\ell$ .

The second scenario is clearly more appealing, if one assumes that  $R(D^{(*)})$  and  $R(K^{(*)})$  do not have independent origins, and can in principle be naturally realized, for instance under the framework of flavour symmetries [81]; a different possibility, which we also include under the second scenario, is that  $R(D^{(*)})$  is modified at the tree-level, whereas  $R(K^{(*)})$  is contributed only at one-loop, see e.g. Refs. [88] [89] for some relevant work in this direction.

The experimental discrepancies discussed in this Chapter have been for many years object of great interest from both the phenomenological and experimental communities. The upcoming years will be critical in revealing the true nature of the anomalies, which may either be recognized as genuine New Physics or turn out to be mere statistical fluctuations and/or to result from uncontrolled systematics. Even though the precise evolution of statistical significances critically depends on central values, it is highly likely

---

<sup>3</sup>Such an estimate differs from (and is more robust than) the SM pulls found by previous fits (see *e.g.* Refs. [84–87], and the additional references in [37]), which would seem to report higher significances, in that it does not assume any special direction in NP Wilson Coefficient space - *i.e.* it does not enforce a priori any NP alternative hypothesis using the bias from the  $B$ -anomalies data.

Observable	Experimental value	Ref.
$R(K)$	$0.846^{+0.044}_{-0.041}$	[ <b>36</b> ]
$R(K^*)$	$0.69^{+0.12}_{-0.09}$	[ <b>31, 34</b> ]
$R(D)$	$0.340 \pm 0.030$	[ <b>83</b> ]
$R(D^*)$	$0.295 \pm 0.014$	[ <b>83</b> ]

TABLE 1. Experimental results for LFU ratios.

that the next five/ten years, with upcoming data from LHCb, Belle II, ATLAS and CMS, should provide definitive answers in these respects.

## CHAPTER 4

### $S_1 + S_3$ model's phenomenology

We now come back to the leptoquark theory discussed in Sec. 2. As we already commented there, this model provides one of the most promising candidate solutions to  $B$ -anomalies, as well as to the longstanding  $(g - 2)_\mu$  anomaly [90–92]. This Chapter presents results from my work [46], in collaboration with D. Marzocca and E. Venturini, in which we performed a detailed phenomenological study of the  $S_1 + S_3$  model, including all one-loop contributions to a selected list of observables. The study leverages on our previous work [44], described in Chap. 2, in which the full one-loop matching of the model onto the SMEFT was performed (see Chap. 2 for more details).

The logic behind the  $S_1 + S_3$  model is quite simple: it was early observed that the leptoquarks  $S_1$  and  $S_3$  separately provided a solution to the  $R(D^{(*)})$  and  $R(K^{(*)})$  anomalies, respectively, and one might naively think that a model featuring both of them would provide a combined solution for both anomalies. The primary purpose of our work was to validate such intuition, through a global fit which included all observables which could provide relevant phenomenological constraints.

The goal of Ref. [46] was to find interesting scenarios, within the  $S_1 + S_3$  setup, capable of addressing one or more of the anomalies listed above, find the preferred region in parameter space, and discuss the most important experimental constraints in each case. Specifically, we first aimed to quantify how well single leptoquark models are able to address the various anomalies, then we discussed combined explanations with both leptoquarks. Thanks to the complete one-loop matching, we also discussed limits on leptoquark couplings to the SM Higgs boson, arising from electroweak precision data and Higgs measurements.

We found that models involving only the  $S_1$  leptoquark can consistently address  $R(D^{(*)})$  and  $(g - 2)_\mu$  anomalies, while a fully-satisfactory solution for  $b \rightarrow s\ell\ell$  anomalies is prevented by the combination of constraints from  $B_s$ -mixing and LFU in  $\tau$  decays. Conversely, the  $S_3$  leptoquark when taken alone can only address neutral-current  $B$ -meson anomalies. A model with both  $S_1$  and  $S_3$ , and only left-handed couplings for  $S_1$ , can address both  $B$ -anomalies but not the muon magnetic moment. Finally, allowing for right handed  $S_1$  couplings makes it possible to fit also  $(g - 2)_\mu$ . Ref. [46] also examined the prospects for both the LF conserving branching fraction  $\text{Br}(B \rightarrow K\tau\tau)$  and the LFV one  $\text{Br}(B \rightarrow K\tau\mu)$ , which are found to be in the ballpark of the future expected sensitivity of Belle-II and LHCb.

The  $S_1 + S_3$  model discussed in this Chapter was defined in Sec. 2.1. In the following Sections, we describe the fit methodology of Ref. [46], the observables considered in the fit, and the detailed results (including future prospects) for the various scenarios considered in our work.



### 4.1. Methodology

Our goal is to study the phenomenology of the  $S_1 + S_3$  model described in the Sec. 2.1, expressing the low-energy observables as functions of the UV parameters at one-loop level. Given the separation of scales between the LQ masses, assumed to be at the TeV scale, and the typical energy scales of the observables considered, the EFT approach is particularly suited for this goal. In fact, it allows to separate the complete procedure in a sequence of steps, which can be generalised to be applicable also to other UV scenarios. Going from the ultraviolet to the infrared, the matching procedure allows to pass physical thresholds, i.e. to integrate out heavy fields while defining a new EFT for that energy range, while the renormalization group evolution (RGE) allows to change the scale within an EFT approach.

In our specific case, we have the following steps:

- The one-loop matching for the  $S_1 + S_3$  model onto the SMEFT, up to dimension-six operators, resulting by integrating out the two scalar leptoquarks at a scale of the order of their masses  $\mu_M \sim M_1, M_3$ . The complete set of matching conditions, obtained with  $\overline{\text{MS}}$  renormalization scheme, has been discussed in Chap. 2.
- The RGE of the SMEFT Wilson coefficients from the UV matching scale  $\mu_M$  down to the electroweak scale [75, 93, 94].
- The one-loop matching between the SMEFT and the EFT valid below the electroweak scale, known as Low Energy EFT (LEFT). This results from integrating out the Higgs, the massive electroweak gauge bosons and the top quark and has been done in [74].
- The RGE of the LEFT Wilson coefficients [95] from the electroweak scale to the relevant scales of the processes;
- The expression of the low-energy observables and pseudo-observables in terms of the LEFT Wilson coefficients, taking into account contributions that arise at one-loop level within the LEFT, from the operators generated already at the tree-level.<sup>1</sup>

By combining everything, we obtain expressions for the observables as a function of the parameters of the scalar leptoquark model at the TeV scale; in such a way, experimental bounds on low-energy data can be used to set constraints on the  $S_{1,3}$  couplings. On the other hand, the intermediate steps provide model-independent expressions for observables in terms of EFT Wilson coefficients, which might be exploited in other NP scenarios.

For a generic EFT coefficient we can separate a contribution arising at the tree-level from one arising at one-loop  $C_i = C_i^{(0)} + (4\pi)^{-2}C_i^{(1)}$ . Working at one-loop accuracy, the RGE, one-loop matching between SMEFT and LEFT, and the one-loop matrix elements to the observables, should only be considered for tree-level generated coefficients,  $C_i^{(0)}$  (in our case, those in Eqs. (2.1.6)-(2.1.10)). For the loop-generated coefficients,  $C_i^{(1)}$ , only the tree-level matching conditions from SMEFT to LEFT, and tree-level matrix elements

---

<sup>1</sup>In case of observables at the electroweak scale, such as the measurements of  $Z$  couplings, the observables can be expressed directly in terms of SMEFT Wilson coefficients at the electroweak scales, so that the last three steps do not need to be considered.

Observable	SM prediction	Experimental bounds
$b \rightarrow s\ell\ell$ observables		
$\Delta\mathcal{C}_9^{sb\mu\mu}$	0	$-0.43 \pm 0.09$ [96]
$\mathcal{C}_9^{\text{univ}}$	0	$-0.48 \pm 0.24$ [96]
$b \rightarrow c\tau(\ell)\nu$ observables		
$R_D$	$0.299 \pm 0.003$ [83]	$0.34 \pm 0.027 \pm 0.013$ [83]
$R_D^*$	$0.258 \pm 0.005$ [83]	$0.295 \pm 0.011 \pm 0.008$ [83]
$P_\tau^{D^*}$	$-0.488 \pm 0.018$ [97]	$-0.38 \pm 0.51 \pm 0.2 \pm 0.018$ [21]
$F_L$	$0.470 \pm 0.012$ [97]	$0.60 \pm 0.08 \pm 0.038 \pm 0.012$ [98]
$\text{Br}(B_c^+ \rightarrow \tau^+\nu)$	2.3%	$< 10\%$ (95% CL) [99]
$R_D^{\mu/e}$	1	$0.978 \pm 0.035$ [100, 101]
$D$ leptonic decay		
$\text{Br}(D_s \rightarrow \tau\nu)$	$(5.169 \pm 0.004) \times 10^{-2}$ [102]	$(5.48 \pm 0.23) \times 10^{-2}$ [103]
$b \rightarrow s\nu\nu$ and $s \rightarrow d\nu\nu$		
$R_K^\nu$	1 [104]	$< 4.65$ [105]
$R_{K^*}^\nu$	1 [104]	$< 3.22$ [105]
$\text{Br}(K^+ \rightarrow \pi^+\nu\nu)$	$8.64 \times 10^{-11}$ [58]	$(11.0 \pm 4.0) \times 10^{-11}$ [106]
$\text{Br}(K_L \rightarrow \pi^0\nu\nu)$	$3.4 \times 10^{-11}$ [58]	$< 3.57 \times 10^{-9}$ [107]
$B$ LFV decays		
$\text{Br}(B_d \rightarrow \tau^\pm\mu^\mp)$	0	$< 1.4 \times 10^{-5}$ [108]
$\text{Br}(B_s \rightarrow \tau^\pm\mu^\mp)$	0	$< 4.2 \times 10^{-5}$ [108]
$\text{Br}(B^+ \rightarrow K^+\tau^-\mu^+)$	0	$< 5.4 \times 10^{-5}$ [109]
$\text{Br}(B^+ \rightarrow K^+\tau^+\mu^-)$	0	$< 3.3 \times 10^{-5}$ [109]
		$< 4.5 \times 10^{-5}$ [110]

TABLE 1. Low-energy *semileptonic* observables with their SM predictions and experimental bounds. Upper limits correspond to 95%CL.

should be included, the other contributions giving terms which are formally of two-loop order and that could be of the same order as neglected two-loop matching conditions.

The exception to this is in the RGE due to QCD from the TeV to the GeV scale, for example in four-quark operators contributing to  $\Delta F = 2$  observables. In this case the RGE contribution is well known to be important, also due to the large separation of scales, which gives to this effect a parametric enhancement with respect to the neglected two-loop corrections even if four-quark operators are generated at one-loop.

## 4.2. Observables

One of our main goals is to provide, with the  $S_1 + S_3$  model, a combined explanation for the hints of LFU violation in the neutral and charged current semileptonic  $B$ -meson decays, namely to account for the experimental measurements of  $R(K^{(*)})$  and  $R(D^{(*)})$ , and of the deviation in the muon anomalous magnetic moment  $(g-2)_\mu$ . The leptoquark couplings involved in these observable enter also in the other low-energy observables (or pseudo observables), both at tree-level or one-loop level. Therefore, to quantify how the

$S_1 + S_3$  model can consistently explain the observed anomalies, one should take into account a set of low-energy data as complete as possible. In Tables 1, 2 and 3 we show the list of low-energy observables that we analyze, together with their SM predictions and experimental bounds.

The detailed computations for each observables are contained in the Appendix of the original reference [46]; here we limit ourselves to quote the relevant results for the global fit. In our numerical analysis, the full set of one-loop corrections to each observable was

Observable	SM prediction	Experimental bounds
$\Delta F = 2$ processes		
$B^0 - \bar{B}^0:  C_{B_d}^1 $	0	$< 9.11 \times 10^{-7} \text{ TeV}^{-2}$ [77, 111]
$B_s^0 - \bar{B}_s^0:  C_{B_s}^1 $	0	$< 2.01 \times 10^{-5} \text{ TeV}^{-2}$ [77, 111]
$K^0 - \bar{K}^0: \text{Re}[C_K^1]$	0	$< 8.04 \times 10^{-7} \text{ TeV}^{-2}$ [77, 111]
$K^0 - \bar{K}^0: \text{Im}[C_K^1]$	0	$< 2.95 \times 10^{-9} \text{ TeV}^{-2}$ [77, 111]
$D^0 - \bar{D}^0: \text{Re}[C_D^1]$	0	$< 3.57 \times 10^{-7} \text{ TeV}^{-2}$ [77, 111]
$D^0 - \bar{D}^0: \text{Im}[C_D^1]$	0	$< 2.23 \times 10^{-8} \text{ TeV}^{-2}$ [77, 111]
$D^0 - \bar{D}^0: \text{Re}[C_D^4]$	0	$< 3.22 \times 10^{-8} \text{ TeV}^{-2}$ [77, 111]
$D^0 - \bar{D}^0: \text{Im}[C_D^4]$	0	$< 1.17 \times 10^{-9} \text{ TeV}^{-2}$ [77, 111]
$D^0 - \bar{D}^0: \text{Re}[C_D^5]$	0	$< 2.65 \times 10^{-7} \text{ TeV}^{-2}$ [77, 111]
$D^0 - \bar{D}^0: \text{Im}[C_D^5]$	0	$< 1.11 \times 10^{-8} \text{ TeV}^{-2}$ [77, 111]
LFU in $\tau$ decays		
$ g_\mu/g_e ^2$	1	$1.0036 \pm 0.0028$ [112]
$ g_\tau/g_\mu ^2$	1	$1.0022 \pm 0.0030$ [112]
$ g_\tau/g_e ^2$	1	$1.0058 \pm 0.0030$ [112]
LFV observables		
$\text{Br}(\tau \rightarrow \mu\phi)$	0	$< 1.00 \times 10^{-7}$ [113]
$\text{Br}(\tau \rightarrow 3\mu)$	0	$< 2.5 \times 10^{-8}$ [114]
$\text{Br}(\mu \rightarrow e\gamma)$	0	$< 5.00 \times 10^{-13}$ [115]
$\text{Br}(\tau \rightarrow \mu\gamma)$	0	$< 5.24 \times 10^{-8}$ [116]
$\text{Br}(\tau \rightarrow e\gamma)$	0	$< 3.93 \times 10^{-8}$ [116]
EDMs		
$d_e$	$< 10^{-44} \text{ e cm}$ [117, 118]	$< 1.1 \times 10^{-29} \text{ e cm}$ [119]
$d_\mu$	$< 10^{-42} \text{ e cm}$ [118]	$< 1.9 \times 10^{-19} \text{ e cm}$ [120]
$d_\tau$	$< 10^{-41} \text{ e cm}$ [118]	$(1.15 \pm 1.70) \times 10^{-17} \text{ e cm}$ [121]
Anomalous Magnetic Moments		
$a_e - a_e^{SM}$	$\pm 2.3 \times 10^{-13}$ [122, 123]	$(-8.9 \pm 3.6) \times 10^{-13}$ [124]
$a_\mu - a_\mu^{SM}$	$\pm 43 \times 10^{-11}$ [92]	$(279 \pm 76) \times 10^{-11}$ [92, 125]
$a_\tau - a_\tau^{SM}$	$\pm 3.9 \times 10^{-8}$ [122]	$(-2.1 \pm 1.7) \times 10^{-7}$ [126]

TABLE 2. Meson-mixing and leptonic observables, with their SM predictions and experimental bounds. Upper limits correspond to 95%CL.

Observable	Experimental bounds
<i>Z</i> boson couplings	
$\delta g_{\mu_L}^Z$	$(0.3 \pm 1.1)10^{-3}$ [127]
$\delta g_{\mu_R}^Z$	$(0.2 \pm 1.3)10^{-3}$ [127]
$\delta g_{\tau_L}^Z$	$(-0.11 \pm 0.61)10^{-3}$ [127]
$\delta g_{\tau_R}^Z$	$(0.66 \pm 0.65)10^{-3}$ [127]
$\delta g_{b_L}^Z$	$(2.9 \pm 1.6)10^{-3}$ [127]
$\delta g_{c_R}^Z$	$(-3.3 \pm 5.1)10^{-3}$ [127]
$N_\nu$	$2.9963 \pm 0.0074$ [128]

TABLE 3. Limits on the deviations in *Z* boson couplings to fermions from LEP I.

considered. Some observables vanish or are flavour-suppressed at tree-level, for example meson-mixing  $\Delta F = 2$  processes,  $\tau \rightarrow 3\mu$  and  $\tau \rightarrow \mu\gamma$  LFV interactions or  $\tau \rightarrow \mu\phi(\eta, \eta')$  decay; in such cases the inclusion of one-loop contributions is relevant and might bring non negligible changes in a global fit of the low-energy data.

From the observables listed above, and their expression in terms of the parameters of the model, LQ couplings and masses, we build a global likelihood as:

$$-2 \log \mathcal{L} \equiv \chi^2(\lambda_x, M_x) = \sum_i \frac{(\mathcal{O}_i(\lambda_x, M_x) - \mu_i)^2}{\sigma_i^2}, \quad (4.2.1)$$

where  $\mathcal{O}_i(\lambda_x, M_x)$  is the expression of the observable as function of the model parameters,  $\mu_i$  its experimental central value, and  $\sigma_i$  the uncertainty. From the  $\chi^2$  built in this way, in each scenario considered we obtain the maximum likelihood point by minimizing the  $\chi^2$ , which we use to compute the  $\Delta\chi^2 \equiv \chi^2 - \chi_{\min}^2$ . This allows us to obtain the 68, 95, and 99 % CL regions. In the Standard Model limit we get a  $\chi_{\text{SM}}^2 = 101.0$ , for 50 observables.

For each scenario we get the CL regions in the plane of two real couplings, by profiling the likelihood over all the other couplings. We are often also interested in the values of some observables corresponding to these CL regions. To obtain this, we perform a numerical scan over all the parameter space<sup>2</sup> and select only the points with a  $\Delta\chi^2$  less than the one corresponding to 68 and 95 % CL. The points obtained in this way also reproduce the CL regions in parameter space obtained by profiling. With this set of parameter-space points we can then plot any observable evaluated on them.

**4.2.1. Collider constraints.** Leptoquarks are also actively searched for at high-energy colliders. Their most important signatures can be classified in three categories: *i*) pair production, *ii*) resonant single-production, and *iii*) off-shell *t*-channel exchange in Drell-Yan processes,  $pp \rightarrow \ell^+\ell^-$  or  $\ell\nu$ . See e.g. Refs. [129, 130] for reviews.

<sup>2</sup>For each numerical scan we collected  $O(10^4)$  benchmark points. For our more complex models (*i.e.* with up to ten parameters), this is quite demanding from the computational point of view; in order to efficiently scan the high-dimensional parameter spaces, we employ a Markov Chain Monte Carlo algorithm (Hastings-Metropolis) for the generation of trial points.

The pair production cross section is mostly independent on the LQ couplings to fermions, unless some are very large, and thus provides limits which depend only on the LQ mass and the branching ratios in the relevant search channels. We refer to Refs. [130–133] for reviews of such searches. Once the branching ratios are taken into account, the most recent ATLAS and CMS searches using an integrated luminosity of  $\sim 36\text{fb}^{-1}$  put a lower bound on the  $S_1$  and  $S_3$  masses at  $\approx 1\text{TeV}$  or less. At present, limits from single production are not competitive with those from pair production and Drell-Yan [130].

Leptoquarks can also be exchanged off-shell in the  $t$ -channel in Drell-Yan processes. The final states most relevant to our setup are  $\tau\bar{\tau}$ ,  $\tau\bar{\nu}$ , and  $\mu\bar{\mu}$ . The limits on LQ couplings as a function of their mass from neutral-current processes can be taken directly from [130, 132, 134] (see also [135–138] for other studies of dilepton tails in relation with  $B$ -anomalies) while the mono-tau channel in relation to the  $B$ -anomalies has been studied in [139–144] and at present it doesn't exclude the region of interest. Using the results from [132] we get the following 95% CL upper limits on the couplings relevant to our model for  $M_{1,3} = 1\text{TeV}$ , taken one at a time:

$$\lambda_{c\tau}^{1R} < 1.62, \quad (4.2.2)$$

$$\lambda_{c\mu}^{1R} < 0.90, \quad (4.2.3)$$

$$\lambda_{s\tau}^{1L} < 1.66, \quad (4.2.4)$$

$$\lambda_{s\mu}^{1L} < 0.91, \quad (4.2.5)$$

$$\lambda_{b\tau}^{3L} < 1.40, \quad (4.2.6)$$

$$\lambda_{s\tau}^{3L} < 0.97, \quad (4.2.7)$$

$$\lambda_{b\mu}^{3L} < 0.77, \quad (4.2.8)$$

$$\lambda_{s\mu}^{3L} < 0.56 \quad (4.2.9)$$

### 4.3. Scenarios and results

In this Section we discuss several minimal models within the  $S_1 + S_3$  setup, and how well (or bad) each of them is able to address the charged and/or neutral current anomalies, while remaining compatible with all the other experimental constraints. We denote the leptoquark couplings to fermions by:

$$\lambda^{1R} = \begin{pmatrix} \lambda_{ue}^{1R} & \lambda_{u\mu}^{1R} & \lambda_{u\tau}^{1R} \\ \lambda_{ce}^{1R} & \lambda_{c\mu}^{1R} & \lambda_{c\tau}^{1R} \\ \lambda_{te}^{1R} & \lambda_{t\mu}^{1R} & \lambda_{t\tau}^{1R} \end{pmatrix}, \quad \lambda^{1L} = \begin{pmatrix} \lambda_{de}^{1L} & \lambda_{d\mu}^{1L} & \lambda_{d\tau}^{1L} \\ \lambda_{se}^{1L} & \lambda_{s\mu}^{1L} & \lambda_{s\tau}^{1L} \\ \lambda_{be}^{1L} & \lambda_{b\mu}^{1L} & \lambda_{b\tau}^{1L} \end{pmatrix}, \quad \lambda^{3L} = \begin{pmatrix} \lambda_{de}^{3L} & \lambda_{d\mu}^{3L} & \lambda_{d\tau}^{3L} \\ \lambda_{se}^{3L} & \lambda_{s\mu}^{3L} & \lambda_{s\tau}^{3L} \\ \lambda_{be}^{3L} & \lambda_{b\mu}^{3L} & \lambda_{b\tau}^{3L} \end{pmatrix}. \quad (4.3.1)$$

The main experimental anomalies driving the fit can be split in three categories:

- $CC$ : deviations in  $b \rightarrow c\tau\nu$  transitions;
- $NC$ : deviations in  $b \rightarrow s\mu\mu$  transitions;
- $(g-2)_\mu$ : deviation in the muon magnetic moment.

While our setup allows to keep all the above couplings in a completely general analysis, given the large number of parameters this would preclude a clear understanding of

Model	Couplings	CC	NC	$(g-2)_\mu$
$S_1^{(CC)}$	$\lambda_{c\tau}^{1R}, \lambda_{b\tau}^{1L}$	✓	✗	✗
$S_1^{(a_\mu)}$	$\lambda_{t\mu}^{1R}, \lambda_{b\mu}^{1L}$	✗	✗	✓
$S_3^{(CC+NC)}$	$\lambda_{b\tau}^{3L}, \lambda_{s\tau}^{3L}, \lambda_{b\mu}^{3L}, \lambda_{s\mu}^{3L}$	✗	✓	✗
$S_1 + S_3^{(LH)}$	$\lambda_{b\tau}^{1L}, \lambda_{s\tau}^{1L}, \lambda_{b\tau}^{3L}, \lambda_{s\tau}^{3L}, \lambda_{b\mu}^{3L}, \lambda_{s\mu}^{3L}$	✓	✓	✗
$S_1 + S_3^{(all)}$	$\lambda_{b\tau}^{1L}, \lambda_{s\tau}^{1L}, \lambda_{b\mu}^{1L}, \lambda_{t\tau}^{1R}, \lambda_{c\tau}^{1R}, \lambda_{t\mu}^{1R}, \lambda_{b\tau}^{3L}, \lambda_{s\tau}^{3L}, \lambda_{b\mu}^{3L}, \lambda_{s\mu}^{3L}$	✓	✓	✓
$S_1 + S_3^{(pot)}$	$\lambda_{H1}, \lambda_{H3}, \lambda_{H13}, \lambda_{eH3}$	—	—	—

TABLE 4. Summary of leptoquark models considered in this Chapter. The third column lists the couplings we allow to be different from zero in our global fit. The last three columns indicate whether the models provide a satisfying fit of each set of anomalies, respectively.

the physics underlying the fit. Furthermore, it can be interesting to consider only one leptoquark or to focus on one specific experimental anomaly. For these reasons we take a step-by-step approach by starting with single-leptoquark scenarios and switching on the couplings needed to fit a given set of anomalies. In all cases, we keep the complete likelihood described in the previous Section, with all the observables. For instance, if the couplings to muons are set to zero, neutral-current  $B$ -anomalies and the muon anomalous magnetic moment are automatically *frozen* to the corresponding Standard Model values and do not impact the final fit.

The models are thus defined by the leptoquark content and the set of active couplings, which, for simplicity, we assume to be real. We have considered the models detailed in Table 4, for each of which we allow the couplings listed in the third column of the table to be non-vanishing in our global fit. We first analyze single mediator models and study their potential to address as many anomalies as possible. In each case we point out the main tensions which prevent a combined explanation of all anomalies. Then, we move on to study models involving both leptoquarks. In the first we only allow left-handed couplings,  $\lambda^{1L}$  and  $\lambda^{3L}$ , as this possibility has better chances to find motivation in a scenario in which the flavour structure is determined by a flavour symmetry, see e.g. [81, 131]. In the second we switch on also some of the  $S_1$  couplings to right-handed fermions, and aim to provide a combined explanation for all three anomalies. Finally, we study the limits on the leptoquark potential couplings to the Higgs, which is an analysis largely independent on the couplings to fermions and requires to consider different observables than those studied in the main fit, see also [145].

In any given model there is, of course, no particular reason to expect the exact flavour structures implied by Table 4. For instance, the couplings we set to zero will be radiatively generated. In our bottom-up approach we assume them to be small enough

at the matching scale that the observables in the fit are not impacted in a sizeable way. In a more top-down approach one might have expectations on the size of these terms based on the UV picture, such as due to the presence of approximate flavour symmetries or other flavour-protection mechanisms [146] (see Subsec. 4.5).

In the numerical analysis we fix for concreteness values of leptoquark masses equal to  $M_1 = M_3 = 1 \text{ TeV}$ . While this is borderline with the exclusion limits from pair production, discussed previously, the results do not change qualitatively by increasing slightly the masses. Since most of the observables driving the fits scale as  $\lambda^2/M^2$ , with a good approximation this scaling can be used to adapt our fits to slightly larger masses.<sup>3</sup> We note that the future limits on LQ masses from HL-LHC are expected to not go much above 1.5 TeV [131].

Concerning our specific benchmarks, the choice of active couplings in each case is guided by some simple phenomenological observations (more details on each concrete model can be found in the relevant Subsections below):

- (1) Since the observed deviations in  $B$ -decays involve LQ couplings to second and third generation, and given the strong constraints on  $s \leftrightarrow d$  quark flavour transitions, couplings to first generation of down quarks can only play a minor role in the fit of  $B$ -anomalies and are thus set to zero (see however Sec. 4.5; note that even in our case, due to the CKM matrix, effects in up-quark observables are present, for instance  $D$ -meson mixing).
- (2) Hints to LFU violation in rare  $B$ -decays, combined with the deviations observed in  $B \rightarrow K^* \mu^+ \mu^-$ , suggest that the LQ couplings to muons should be larger than those to electrons. We consider, for simplicity the case in which  $b \rightarrow s \ell \ell$  anomalies are entirely explained by muon couplings and set to zero the couplings to electrons.
- (3) The  $S_1$  couplings to  $\mu_R$  and  $c_R$  or  $t_R$  do not contribute to  $b \rightarrow s \ell \ell$ , nor to  $b \rightarrow c(\tau/\ell)\nu$ , however are relevant for fitting the observed anomaly in the muon anomalous magnetic moment, which gets the main contribution from the couplings to  $b_L \mu_L$  and  $t_R \mu_R$ , as shown in the original reference [46].

Details for all models are given in the following Subsections.

#### 4.3.1. Single-leptoquark $S_1$ .

4.3.1.1. *Addressing  $CC$  anomalies.* This LQ can address the deviations in  $R(D)$  and  $R(D^*)$  with only two couplings:  $\lambda_{b\tau}^{1L}$  and  $\lambda_{c\tau}^{1R}$ . They generate at tree-level a contribution to the semileptonic scalar and tensor operators  $C_{lequ}^{(1,3)}$  at the UV matching scale, Eqs. (2.1.8) and (2.1.9), which then run down to the GeV scale. The best fit region is entirely determined by the following few observables:  $R(D)$ ,  $R(D^*)$ ,  $\text{Br}(B_c^+ \rightarrow \tau^+ \nu)$ ,  $|g_\tau/g_\mu|$ , and the constraints from  $pp \rightarrow \tau^+ \tau^-$ .

The results from the fit, assuming real couplings and  $M_1 = 1 \text{ TeV}$ , can be seen in Fig. 4.3.1. Since all the relevant low-energy observables scale with  $\lambda/M$ , the fit can be easily adapted to other masses. The left panel shows confidence level regions for the two

<sup>3</sup>The exception to this scaling are  $\Delta F = 2$  observables, which scale as  $\lambda^4/M^4$ , but are relevant only for the fits of Sec. 4.3.2 and 4.3.3.

couplings. The dashed lines are 95% CL constraints from single observables, and help illustrate the role of each observable within the global fit.

In the right panel we show how the 68% and 95% CL region from the global fit of the left panel maps in the  $R(D^{(*)})$  plane. This is almost degenerate, due to the approximate linear relationship between these two observables in the present model. We overlay as gray lines the CL ellipses (for 2 degrees of freedom) from the HFLAV global fit of the two observables [83] (specifically, the Spring 2019 update).

The model is successful in fitting the deviation in  $R(D^{(*)})$  within the 68%CL level, with smaller values of  $R(D^*)$  (or larger  $R(D)$ ) preferred by the fit. Improved measurements of  $R(D^{(*)})$  can test this setup due to the precise linear relationship among the two modes predicted by the model, as well as improved Drell-Yan constraints.

The best-fit point, for  $M_1 = 1$  TeV, is found for  $\lambda_{b\tau}^{1L} \approx 0.24$ ,  $\lambda_{c\tau}^{1R} \approx -1.00$ .

4.3.1.2. *Addressing NC anomalies.* One may attempt to fit neutral-current anomalies in  $b \rightarrow s\ell\ell$  from the one-loop contributions from  $S_1$ . This scenario has been considered for the first time in [147]. Significant contributions to  $\Delta C_9^\mu$  may only come from the two muon couplings  $\lambda_{b\mu}^{1L}$  and  $\lambda_{s\mu}^{1L}$ , whereas the universal contribution is always negligible ( $C_9^u \approx 0$ ).

$B_s$ -mixing and  $B \rightarrow K^{(*)}\nu\nu$  put strong constraints on the product of the two couplings [46]. Thanks to the different scaling of these observables and  $\Delta C_9^\mu$  on the leptoquark couplings, the limits can be avoided by a suitably large leptoquark mass, as can be seen in Fig. 4.3.2 (left). For  $M_1 \gtrsim 3$  TeV it is possible to avoid these limits while having couplings still in the perturbative range (see also [148, 149]). Nevertheless, even while

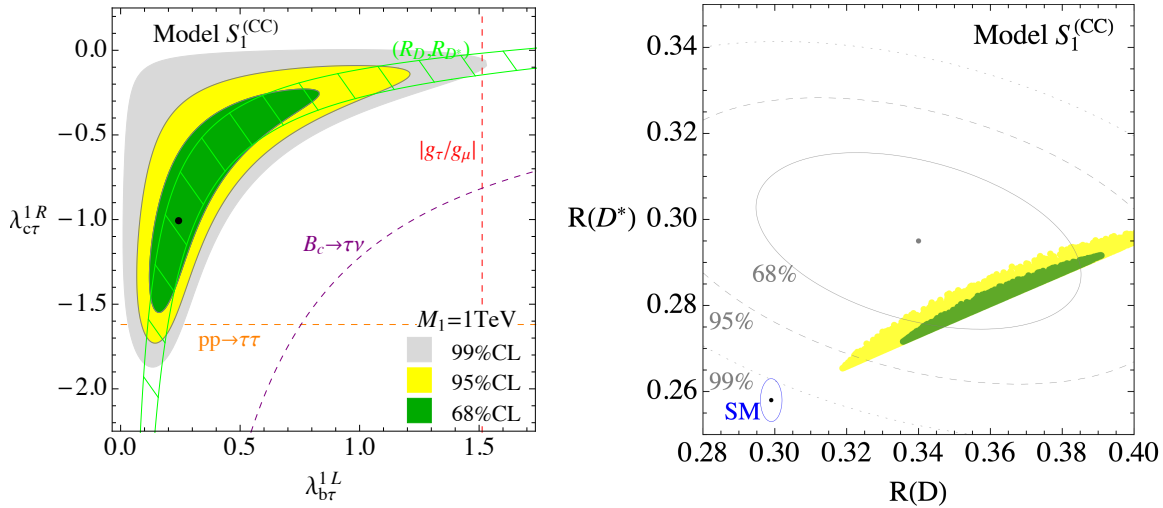


FIGURE 4.3.1. Result from a fit in the two  $S_1$  couplings  $\lambda_{b\tau}^{1L}$  and  $\lambda_{c\tau}^{1R}$ , for a leptoquark of 1 TeV. In the left panel we show the preferred regions in the plane of the two couplings, and the individual  $2\sigma$  limits from the most relevant observables (except for  $(R(D), R(D^*))$ , for which we show the 68%CL region). The black dot corresponds to the best-fit point. In the right panel we show where this preferred region is mapped in the plane of  $R(D) - R(D^*)$ , together with the experimental combination from HFLAV [83].



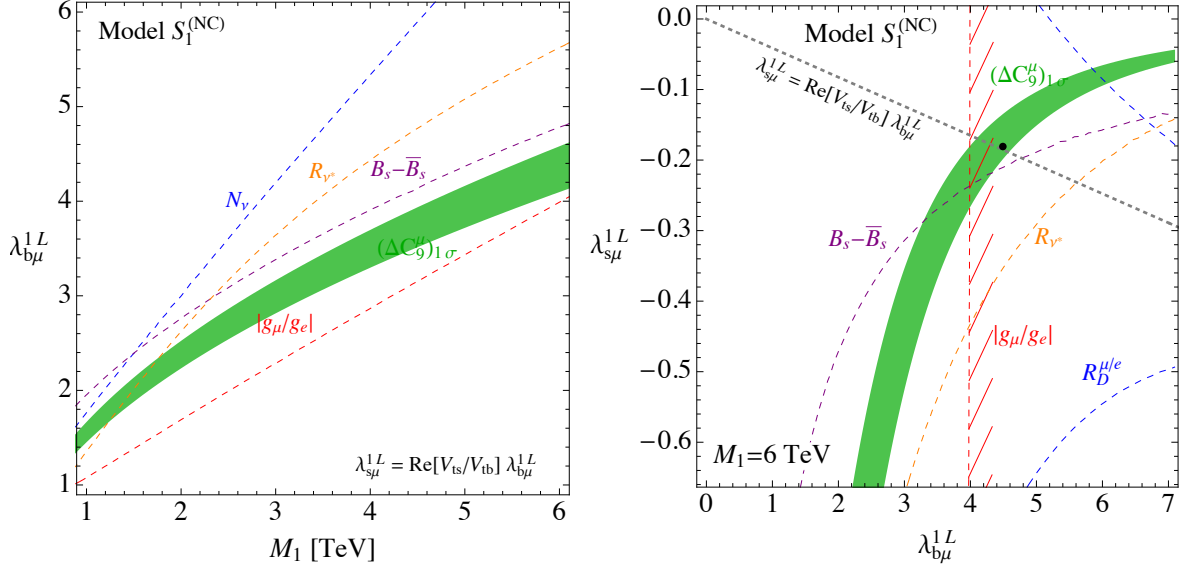


FIGURE 4.3.2. Left: 95% CL limits in the plane of  $\lambda_{b\mu}^{1L} - M_1$ , for  $\lambda_{s\mu}^{1L} = -\Re[V_{cb}/V_{cs}]\lambda_{b\mu}^{1L}$ . Right: 95% CL limits from individual observables in the plane of  $\lambda_{b\mu}^{1L} - \lambda_{s\mu}^{1L}$ , fixing  $M_1 = 6$  TeV. In both plots the green region is the  $1\sigma$  favourite one from  $\Delta C_9^\mu$ .

marginally evading the  $B_s$ -mixing constraint, the  $\Delta C_9^\mu$  deviation remains in  $\approx 2\sigma$  tension with the bound on  $\lambda_{b\mu}^{1L}$  arising from the LFU limit from  $\tau$  decays,  $|g_\mu/g_e|$ . The situation is illustrated in the right panel of Fig. 4.3.2. This is slightly exacerbated by a  $\sim 1\sigma$  deviation in the opposite direction measured in  $|g_\mu/g_e|$ .

We thus conclude that the  $S_1$  leptoquark is not able to fit neutral-current anomalies while remaining completely consistent with all other constraints. The situation regarding NC anomalies is not modified significantly by letting also the other couplings vary in the fit. This issue could be avoided by allowing a mild cancellation by tuning a further contribution to this observable, possibly arising from some other state. Fixing  $M_1 = 6$  TeV we find the best-fit point for:  $\lambda_{b\mu}^{1L} \approx 4.5$ ,  $\lambda_{s\mu}^{1L} \approx -0.18$ .

4.3.1.3. *Addressing  $(g - 2)_{\mu,e}$ .*  $S_1$  is also a good candidate to address the observed deviation in the muon anomalous magnetic moment. Ref. [46] finds that the leading contribution is given numerically by:

$$\Delta a_\mu \approx 8.23 \times 10^{-7} \frac{\lambda_{b\mu}^{1L} \lambda_{t\mu}^{1R}}{M_1^2 / (1 \text{ TeV})^2} (1 + 0.53 \log \frac{M_1^2}{(1 \text{ TeV})^2}) \quad (4.3.2)$$

The observed deviation can thus be addressed for small couplings, and no other observable is influenced significantly. Analogously, it is possible to address the (smaller and less significant) deviation in the electron magnetic moment, see Table 2.

A combined explanations of both deviations with a single mediator was thought not to be viable, due to the very strong constraint from  $\mu \rightarrow e\gamma$ , see e.g. Refs. [150]. More recently, in the updated versions of [151, 152] it was realized that a possible way out is to align the  $S_1$  leptoquark-muon couplings to the top quark, while the leptoquark-electron

ones to the charm<sup>4</sup>. In our formalism this can be achieved aligning the  $S_1$  couplings as  $\lambda_{ie}^{1L} = V_{ci}\lambda_e^{1L}$  and  $\lambda_{i\mu}^{1L} = V_{ti}\lambda_\mu^{1L}$ . In this way one finds [46]:

$$\Delta a_e \approx 1.9 \times 10^{-10} \frac{\lambda_e^{1L} \lambda_{ce}^{1R}}{M_1^2/(1 \text{ TeV})^2} (1 + 0.09 \log \frac{M_1^2}{(1 \text{ TeV})^2}), \quad (4.3.3)$$

$$\Delta a_\mu \approx 8.23 \times 10^{-7} \frac{\lambda_\mu^{1L} \lambda_{t\mu}^{1R}}{M_1^2/(1 \text{ TeV})^2} (1 + 0.53 \log \frac{M_1^2}{(1 \text{ TeV})^2}), \quad (4.3.4)$$

$$\text{Br}(\mu \rightarrow e\gamma) = 0. \quad (4.3.5)$$

On the one hand, the strong limit from  $\mu \rightarrow e\gamma$  implies that the alignment described above must be held with high accuracy. On the other hand, radiative corrections to leptoquark couplings from SM Yukawas are expected to induce deviations from it. For this reason we will not investigate this direction further.

---

<sup>4</sup>We thank the authors of [151] and [152] for pointing this out to us.

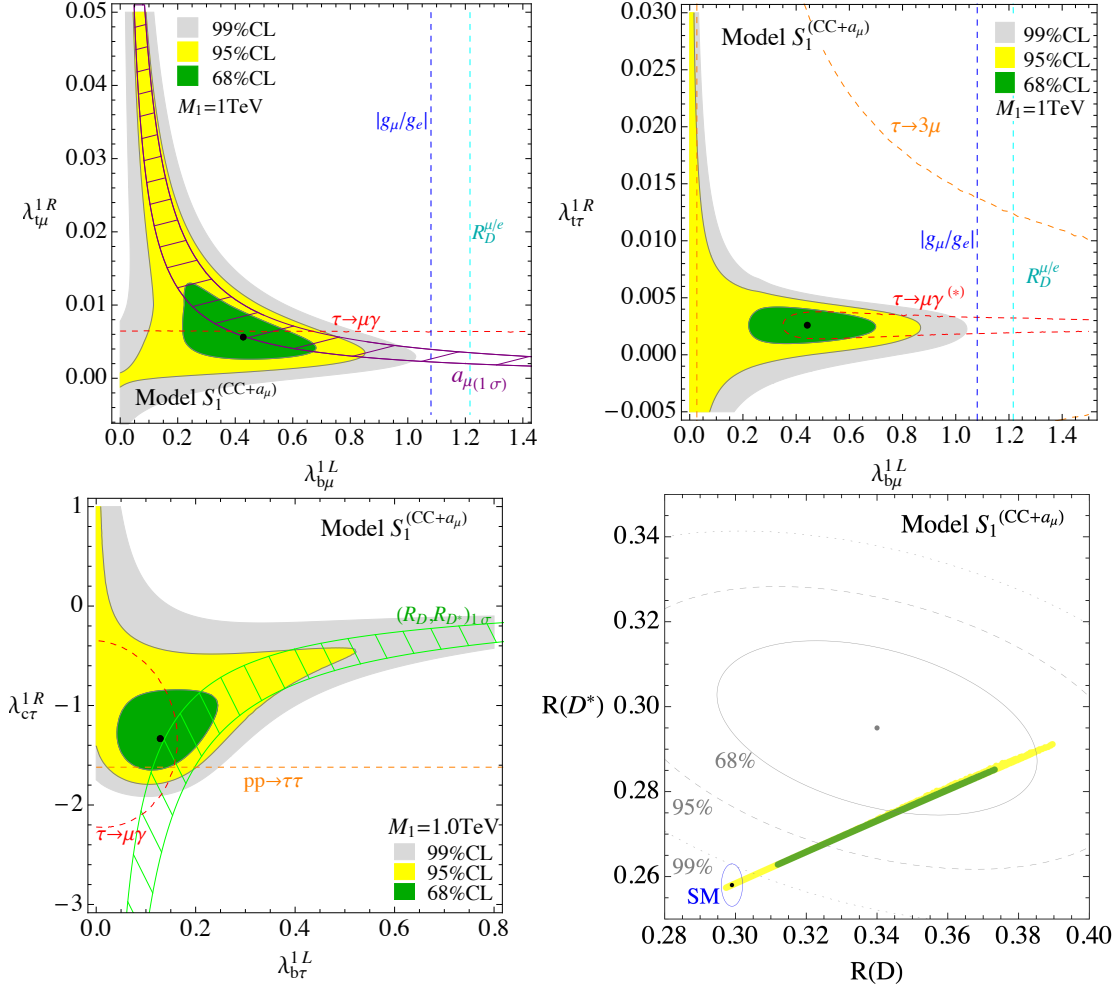


FIGURE 4.3.3. Result from the fit in the  $S_1$  model aimed to addressing the CC and  $(g - 2)_\mu$  anomalies. We show the preferred regions in the planes of two couplings, where those not shown are profiled over. The dashed lines show, for illustrative purposes,  $2\sigma$  limits from individual observables where the other couplings are fixed at the best-fit point (black dot). In the lower-right panel we show where the preferred region is mapped in the plane of  $R(D) - R(D^*)$ .

4.3.1.4. *Addressing CC and  $(g - 2)_\mu$ .* Following the previous Subsections, the next natural step is to attempt to fit both  $R(D^{(*)})$  and  $a_\mu$  anomalies with  $S_1$ . The relevant couplings are  $\lambda_{b\tau}^{1L}$ ,  $\lambda_{b\mu}^{1L}$ ,  $\lambda_{t\tau}^{1R}$ ,  $\lambda_{c\tau}^{1R}$ ,  $\lambda_{t\mu}^{1R}$ .

This setup is not simply the combination of those discussed previously. Indeed, due to the  $\lambda_{b\tau}^{1L}$  and  $\lambda_{c\tau}^{1R}$  couplings on the one hand (required to fit the charged-current  $B$ -anomaly), and  $\lambda_{t\mu}^{1R}$ ,  $\lambda_{b\mu}^{1L}$  on the other hand (necessary to fit  $a_\mu$ ), sizeable contributions to  $\tau \rightarrow \mu\gamma$  are generated at one-loop. The values of  $\lambda_{b\tau, b\mu}^{1L}$  and  $\lambda_{c\tau, t\mu}^{1R}$  required to fit  $R(D^{(*)})$  and  $(g - 2)_\mu$  would induce a too large contribution to this LFV decay. However, we find that the large contribution to  $\tau \rightarrow \mu\gamma$  arising from the product of  $\lambda_{b\mu}^{1L}\lambda_{c\tau}^{1R}$  can be mostly cancelled by the  $\lambda_{b\mu}^{1L}\lambda_{t\tau}^{1R}$  term with  $\lambda_{t\tau}^{1R} \sim O(10^{-3})$  (requiring a mild fine-tuning

of roughly one part in five). Such a small value does not affect any other observable in our fit. It should be noted that the only effect of this coupling is to tune this observable.

We show the preferred region in parameters space, obtained from our fit, in Fig. 4.3.3. In the upper two panels we show the fit in the  $(\lambda_{b\mu}^{1L}, \lambda_{t\mu}^{1R})$  and  $(\lambda_{b\mu}^{1L}, \lambda_{t\tau}^{1R})$  planes, including the preferred region from the global fit as well as the individual 95% CL limits from single observables, to help illustrating the physics behind the analysis. It can be noted that the observed value of the muon magnetic moment can be reproduced, and that  $\tau \rightarrow \mu\gamma$  requires a non-zero value of  $\lambda_{t\tau}^{1R}$ , as discussed above. Regarding the top-right panel, the single-observable constraint from  $\tau \rightarrow \mu\gamma$  (red dashed line) is shown by imposing that  $a_\mu$  is fixed to the value we get at the best-fit point. In the lower-left panel we show the fit in the couplings contributing to  $R(D^{(*)})$ ,  $(\lambda_{b\tau}^{1L}, \lambda_{c\tau}^{1R})$ , and how this preferred region is mapped in the plane of  $R(D) - R(D^*)$  (lower-right panel). Comparing to the allowed region in the same plane in the model studied in Fig. 4.3.1, we see that  $\tau \rightarrow \mu\gamma$  strongly reduced the allowed region, while still not preventing a good fit of the charged-current  $B$ -anomalies. Due to this reduction of the allowed  $(\lambda_{b\tau}^{1L}, \lambda_{c\tau}^{1R})$  parameter space, specifically with smaller values of  $\lambda_{b\tau}^{1L}$ , the points in the  $R(D^*) - R(D)$  plane line up more closely in a line than what is observed in Fig. 4.3.1.

We conclude that the  $R(D^{(*)})$  and  $(g - 2)_\mu$  anomalies can be addressed by the  $S_1$  leptoquark, for perturbative couplings and TeV-scale mass. We find the best-fit point, with  $M_1 = 1$  TeV, for  $\lambda_{b\tau}^{1L} \approx 0.13$ ,  $\lambda_{b\mu}^{1L} \approx 0.44$ ,  $\lambda_{t\tau}^{1R} \approx 0.0026$ ,  $\lambda_{c\tau}^{1R} \approx -1.33$ ,  $\lambda_{t\mu}^{1R} \approx 0.0051$ .

**4.3.2. Single-leptoquark  $S_3$ .** We move on to examine  $S_3$ , and we attempt directly a combined explanation of charged and neutral current anomalies. It is well known that  $S_3$  provides a simple and good explanation for the deviations observed in  $b \rightarrow s\ell\ell$ , thanks to its tree-level contribution to the partonic process. The couplings required are  $\lambda_{b\mu}^{3L} - \lambda_{s\mu}^{3L}$ , with small enough values that other observables do not pose relevant constraints. The leading contribution to both  $R(D^{(*)})$  and  $C_9^u$ , instead, arises via the  $\lambda_{b\tau}^{3L} - \lambda_{s\tau}^{3L}$  couplings. For concreteness we fix  $M_3 = 1$  TeV, but the fit would be very similar for a slightly larger mass.

Our results can be seen in Fig. 4.3.4. As expected, the model is successful in fitting  $\Delta C_9^\mu$ . The couplings to the tau allow to also fit  $C_9^u$ , while charged-current anomalies cannot be reproduced. The main limiting observables are  $B_s$ -mixing and  $B \rightarrow K^{(*)}\nu\nu$ , as can be seen from the top-right panel.

The best-fit point, for  $M_3 = 1$  TeV, is found for  $\lambda_{b\tau}^{3L} \approx 0.36$ ,  $\lambda_{s\tau}^{3L} \approx -0.13$ ,  $\lambda_{b\mu}^{3L} \approx 0.050$ ,  $\lambda_{s\mu}^{3L} \approx 0.015$ .

**4.3.3.  $S_1 + S_3$  with LH couplings only.** Models involving  $S_1$  and  $S_3$  with left-handed couplings have been first considered in [81, 131, 153]. In particular, in [81, 131] it was shown how this setup could fit both charged- and neutral-current anomalies with couplings compatible with a minimally broken  $U(2)^5$  flavour symmetry, albeit with a tension between  $R(D^{(*)})$  and the  $B_s$ -mixing constraint. Since then, new experimental updates on  $R(D^{(*)})$  pushed the preferred region closer to the SM, thus also alleviating the tension with meson mixing. Here, we update the fit for this scenario, without assuming a priori a specific flavour structure for the relevant couplings.

The relevant couplings are  $\lambda_{[bs]\tau}^{1L}$ ,  $\lambda_{[bs]\mu}^{3L}$ , and  $\lambda_{[bs]\tau}^{3L}$ . A first qualitative understanding of the model can be obtained by noticing the main roles of the various couplings with regard to the anomalies:

$$\lambda_{[b,s]\mu}^{3L} \rightarrow \Delta C_9^\mu, \quad \lambda_{[b,s]\tau}^{3L} \rightarrow C_9^u, \quad (\lambda_{[b,s]\tau}^{1L}, \lambda_{[b,s]\tau}^{3L}) \rightarrow R(D^{(*)})$$

In this model, the relative deviation in  $R(D)$  and  $R(D^*)$  from the respective SM values is predicted to be exactly the same, since it is only due to the same left-handed vector-vector operator generated in the SM.

The most salient features of the fit are summarized in Fig. 4.3.5. In the top two panels we show the preferred regions in the  $\lambda_{b\tau}^{1L} - \lambda_{s\tau}^{1L}$  and  $\lambda_{b\tau}^{3L} - \lambda_{s\tau}^{3L}$  planes, together

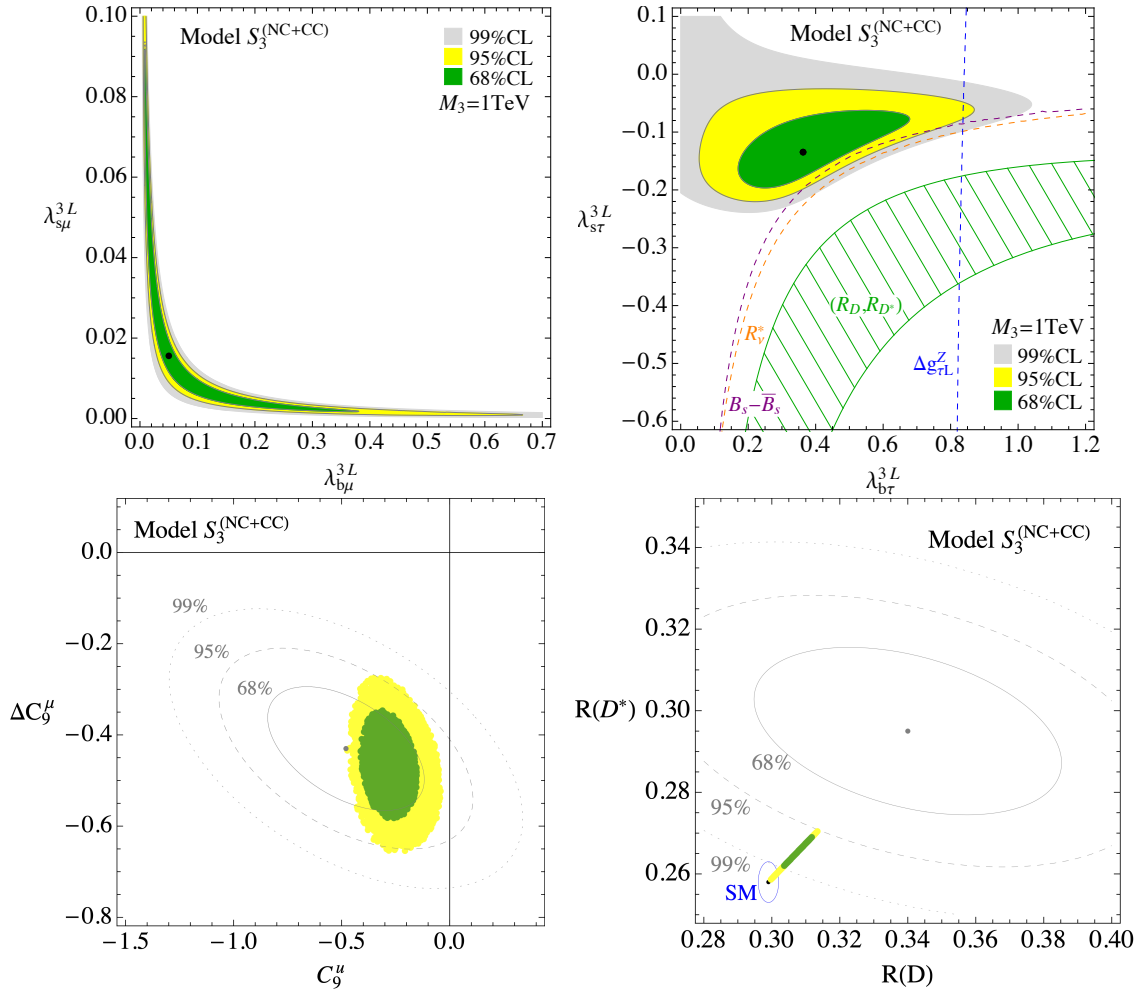


FIGURE 4.3.4. Result from the fit in the  $S_3$  model. In the upper panels we show the preferred regions in the planes of two couplings, where the two not shown are profiled over. The dashed lines show, for illustrative purposes,  $2\sigma$  limits from individual observables where the other couplings are fixed at the best-fit point (black dot). In the lower panels we show where the preferred region is mapped in the planes of the neutral and charged-current anomalies.

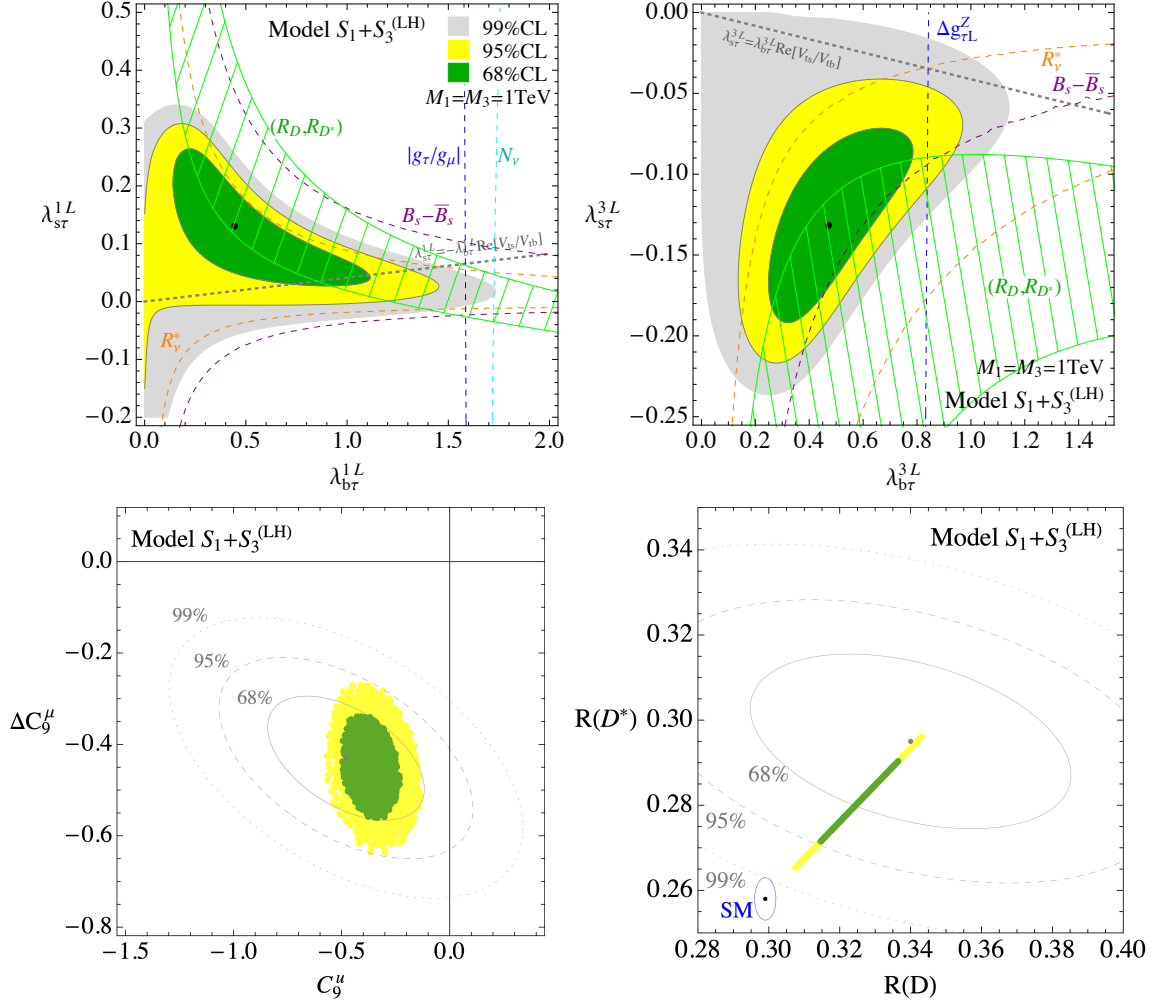


FIGURE 4.3.5. Result from the fit in the  $S_1 + S_3^{(LH)}$  model, with only left-handed couplings. In the upper panels we show the preferred regions in the planes of two couplings, where the two not shown are profiled over. The dashed lines show, for illustrative purposes,  $2\sigma$  limits from individual observables where the other couplings are fixed at the best-fit point (black dot). In the lower panels we show where the preferred region is mapped in the planes of the neutral and charged-current anomalies.

with the single-observable  $2\sigma$  limits obtained fixing the other couplings to the global best-fit value. The favoured region in the  $\lambda_{b\mu}^{3L} - \lambda_{s\mu}^{3L}$  plane is very similar to the one of model  $S_3^{(CC+NC)}$  (Fig. 4.3.4 top-left), thus we do not show it again. The constraint from  $B \rightarrow K^{(*)}\nu\nu$  is avoided thanks to a slight cancellation between the tree-level contributions of the two leptoquarks [81]. There is a (small) leftover tension in the  $R(D^{(*)})$  fit, due to constraints from  $B_s$ -mixing. It should be noted that this tension grows with larger LQ masses (thus larger required couplings) since the deviation in  $R(D^{(*)})$  scales as  $\lambda^2/M^2$  while the contribution to meson mixing goes as  $\lambda^4/M^2$ .

We also point out that the parameter-region preferred by the fit is compatible with the relations between couplings predicted by a minimally-broken  $U(2)^5$  flavour symmetry,  $\lambda_{s\alpha} = c_{U(2)} V_{ts} \lambda_{b\alpha}$ , with  $c_{U(2)}$  an  $\mathcal{O}(1)$  complex parameter, see e.g. [81] and references therein. The case with  $|c_{U(2)}| = 1$  is shown with grey dashed lines in the upper panels.

In the lower two panels we show how the preferred regions in parameter space maps into the anomalous  $B$ -decay observables. As can be seen, it is possible to reproduce them within  $1\sigma$ . The best-fit point, for  $M_1 = M_3 = 1$  TeV, is found for  $\lambda_{b\tau}^{3L} \approx 0.47$ ,  $\lambda_{s\tau}^{3L} \approx -0.13$ ,  $\lambda_{b\mu}^{3L} \approx 0.056$ ,  $\lambda_{s\mu}^{3L} \approx 0.014$ ,  $\lambda_{b\tau}^{1L} \approx 0.45$ ,  $\lambda_{s\tau}^{1L} \approx 0.13$ .

**4.3.4.  $S_1 + S_3$  addressing CC, NC, and  $(g-2)_\mu$ .** From the previous Sections it is clear that in order to address all anomalies, both  $S_1$  and  $S_3$  leptoquarks are required. NC anomalies are addressed only by  $S_3$ , the muon anomalous magnetic moment only by  $S_1$ , while  $R(D^{(*)})$  receives sizeable contributions from both. For our most general analysis we keep ten active couplings:  $\lambda_{[b,s]\tau}^{3L}$ ,  $\lambda_{[b,s]\mu}^{3L}$ ,  $\lambda_{[b,s]\tau}^{1L}$ ,  $\lambda_{b\mu}^{1L}$ ,  $\lambda_{[t,c]\tau}^{1R}$ ,  $\lambda_{t\mu}^{1R}$ . The results of our fit are shown in Fig. 4.3.6.

In the first row of Fig. 4.3.6 we show the preferred regions for the couplings relevant for the  $a_\mu$  fit. The situation is very similar to what already discussed for model  $S_1^{(CC+a_\mu)}$ , Sec. 4.3.1.4.

The couplings relevant for the  $R(D^{(*)})$  fit are shown in the second row. They show a behavior very similar to the one already seen in the models  $S_1^{(CC+a_\mu)}$  and  $S_1 + S_3^{(LH)}$ . The main contribution is due to the scalar+tensor operators generated via the  $\lambda_{c\tau}^{1R} \lambda_{b\tau}^{1L}$  couplings, but a sizeable contribution, which helps to improve the fit with respect to model  $S_1^{(CC)}$ , is induced via the left-handed couplings  $\lambda_{[b,s]\tau}^{1L}$  and  $\lambda_{[b,s]\tau}^{3L}$ , analogously to what we saw in model  $S_1 + S_3^{(LH)}$ . Contrary to that case, however, here the preferred region avoids any tension with both  $B_s$ -mixing and  $B \rightarrow K^{(*)} \nu \nu$ .

We do not show in Fig. 4.3.6 the preferred values for  $\lambda_{[s,b]\mu}^{3L}$ , which are necessary to fit  $\Delta C_9^\mu$ , since they are analogous to what we saw for model  $S_3^{(CC+NC)}$  (see Fig. 4.3.4 top-left).

We conclude that all the anomalies in  $R(D^{(*)})$ ,  $b \rightarrow s\mu\mu$ , and  $(g-2)_\mu$ , can be completely addressed in this model, for perturbative couplings and TeV-scale leptoquark masses. The best-fit point, for  $M_1 = M_3 = 1$  TeV, is found for  $\lambda_{b\tau}^{3L} \approx 0.40$ ,  $\lambda_{s\tau}^{3L} \approx -0.11$ ,  $\lambda_{b\mu}^{3L} \approx 0.31$ ,  $\lambda_{s\mu}^{3L} \approx 0.0024$ ,  $\lambda_{b\tau}^{1L} \approx 0.11$ ,  $\lambda_{s\tau}^{1L} \approx 0.082$ ,  $\lambda_{b\mu}^{1L} \approx 0.55$ ,  $\lambda_{t\tau}^{1R} \approx 0.0029$ ,  $\lambda_{c\tau}^{1R} \approx -1.26$ ,  $\lambda_{t\mu}^{1R} \approx 0.0052$ .

**4.3.5. Leptoquark potential couplings.** In this Section we study available constraints for the potential couplings of leptoquark with the Higgs boson from the leptoquark potential, Eq. (2.5.1). There are four such couplings:  $\lambda_{H1}$ ,  $\lambda_{H3}$ ,  $\lambda_{\epsilon H3}$ , and  $\lambda_{H13}$ . All contribute only at one-loop level in the matching to SMEFT operators, therefore possible phenomenological effects are suppressed both by a loop factor and by the LQ mass scale. We focus on effects of these couplings which are independent on the LQ couplings to fermions. We thus need precisely measured quantities in the bosonic sector of the SM.

Obvious candidates are the gauge-boson oblique corrections measured at LEP [158]:  $\hat{S}$ ,  $\hat{T}$ ,  $Y$ ,  $W$ , as well as the analogous effect for QCD,  $Z$ . All these parameters are

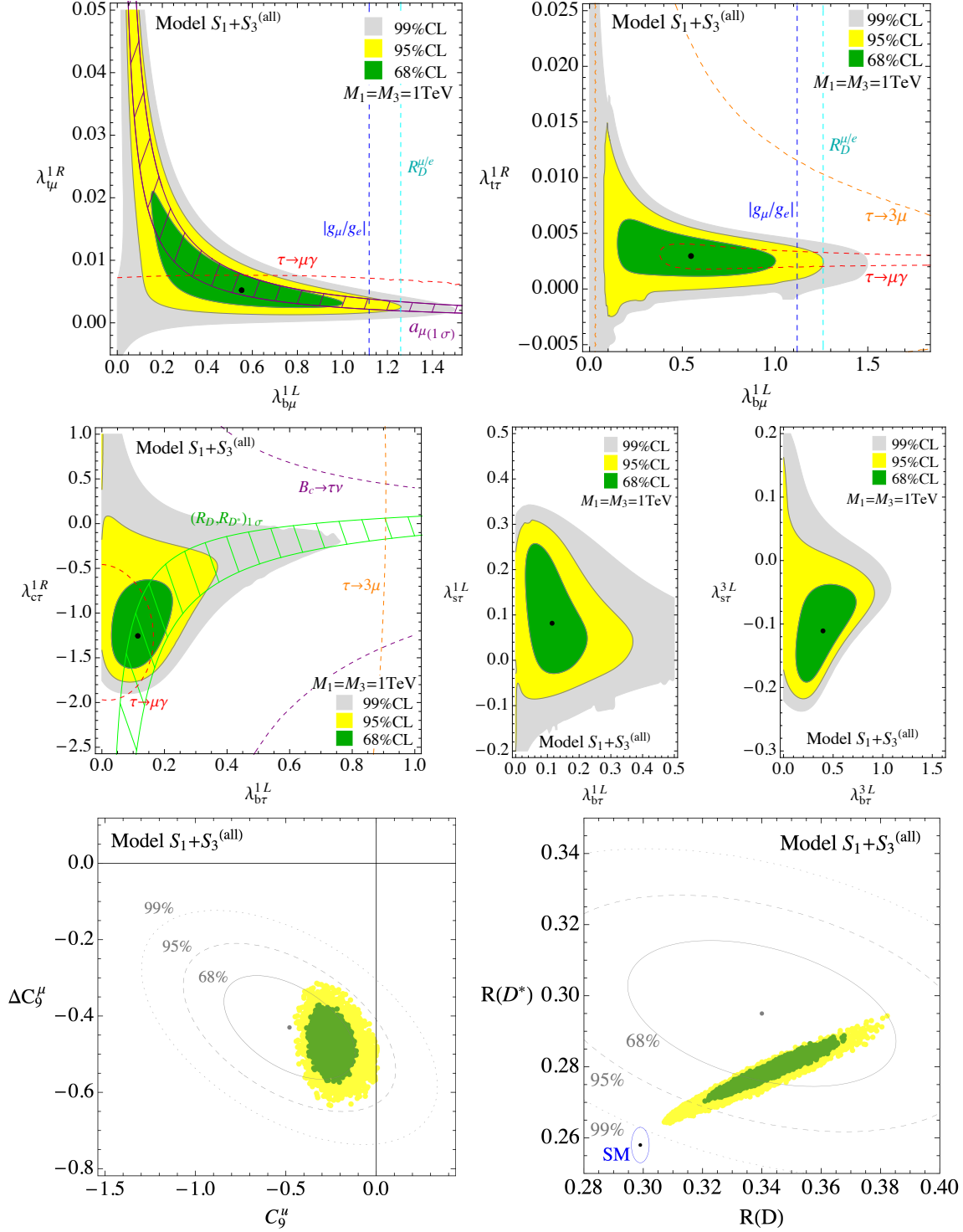


FIGURE 4.3.6. Result from the fit in the  $S_1 + S_3^{(\text{all})}$  model, aimed at addressing all anomalies (see description in the text).

measured at the per-mille level, and are able to constrain multi-TeV scale physics. Given



Observable	Measurement	Reference
$S$	$0.04 \pm 0.08$	[154]
$T$	$0.08 \pm 0.07$ ( $\rho_{S,T} = 0.92$ )	[154]
$\kappa_g$	$1.00 \pm 0.06$	[155]
$\kappa_\gamma$	$1.03 \pm 0.07$ ( $\rho_{\gamma,g} = -0.44$ )	[155]
$\sigma/\sigma_{\text{SM}}(Z\gamma)$	$2.0^{+1.0}_{-0.9}$ (ATLAS)	[156]
$\sigma/\sigma_{\text{SM}}(Z\gamma)$	$< 3.9$ @ 95% CL (CMS)	[157]

TABLE 5. Bosonic observables for the LQ potential couplings.

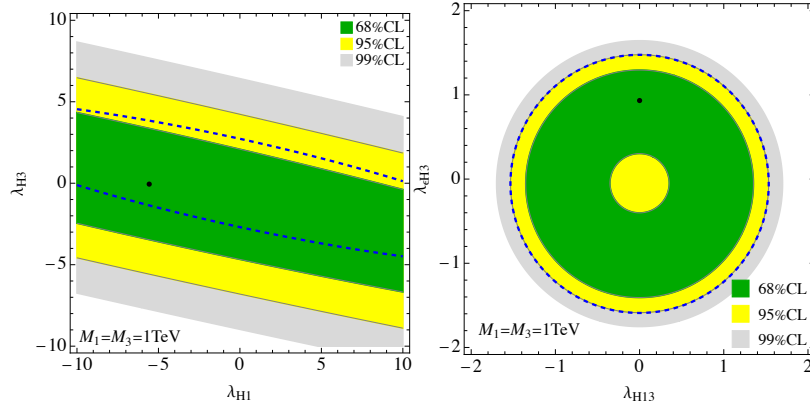


FIGURE 4.3.7. Limits on LQ potential couplings from oblique corrections and Higgs measurements. In each panel, the other two couplings have been marginalised. The black point represents the best-fit point while the dashed blue contours are the prospects for 95%CL limits after HL-LHC.

the expressions in the Warsaw basis of [159] and our one-loop matching of the SMEFT to the LQ model, we find:

$$\hat{S} = \frac{\alpha}{4s_W^2} S = -\frac{g^2 N_c v^2 Y_{S_3}}{48\pi^2} \frac{\lambda_{\epsilon H 3}}{M_3^2} \approx -5.4 \times 10^{-5} \frac{\lambda_{\epsilon H 3}}{m^2} \quad (4.3.6)$$

$$\begin{aligned} \hat{T} = \alpha T &= \frac{N_c v^2 \lambda_{\epsilon H 3}^2}{48\pi^2 M_3^2} + \frac{N_c v^2}{16\pi^2} |\lambda_{H 13}|^2 \frac{M_1^4 - M_3^4 - 2M_1^2 M_3^2 \log M_1^2/M_3^2}{(M_1^2 - M_3^2)^3} \\ &\approx 3.8 \times 10^{-4} \lambda_{\epsilon H 3}^2 / m^2 + 3.8 \times 10^{-4} |\lambda_{H 13}|^2 / m^2 \end{aligned} \quad (4.3.7)$$

where in the numerical expressions for simplicity we fixed  $M_1 = M_3 = m$  TeV. The contributions to  $Y$ ,  $W$ , and  $Z$  are instead at, or below, the  $10^{-6}$  level and thus completely negligible given the present experimental precision. The constraints on  $S$  and  $T$  from [154] are reported in Table 5. The contribution to the  $T$  parameter from the  $\lambda_{H 13}$  coupling has been also studied in [160], albeit not in the EFT approach. We checked that we agree once the EFT limit is taken into account.

The LQ couplings to the Higgs also generate at one-loop contributions to  $hgg$ ,  $h\gamma\gamma$ , and  $hZ\gamma$  couplings. Since these are also loop-generated in the SM, the percent-level precision presently available for the Higgs couplings to photons and gluons couplings allows to probe heavy new physics. Loop contributions to other couplings, which arise at

tree-level in the SM, are instead too small to have a sizeable impact. We thus consider the combined fit of Higgs couplings in the  $\kappa$ -framework where only  $\kappa_\gamma$  and  $\kappa_g$  are left free, and a constraint on  $\sigma/\sigma_{\text{SM}}(Z\gamma) = \kappa_g^2 \kappa_{Z\gamma}^2$ , which is however still not precisely measured, see Table 5. The approximate contributions to these parameters in our model are given by:

$$\kappa_g - 1 = -(3.51\lambda_{H3} + 1.17\lambda_{H1}) \times 10^{-2}/m^2, \quad (4.3.8)$$

$$\kappa_\gamma - 1 = -(2.32\lambda_{H3} + 0.66\lambda_{\epsilon H3} - 0.11\lambda_{H1}) \times 10^{-2}/m^2, \quad (4.3.9)$$

$$\kappa_{Z\gamma} - 1 = -(1.89\lambda_{H3} + 0.23\lambda_{\epsilon H3} - 0.033\lambda_{H1}) \times 10^{-2}/m^2. \quad (4.3.10)$$

Analogously to what presented above for flavour observables, we combine Higgs couplings and oblique constraints in a global likelihood. From this we find the maximum likelihood point and construct the 68, 95, and 99% CL regions in planes of two couplings, where the other two are marginalised. The results in the  $(\lambda_{H1}, \lambda_{H3})$  and  $(\lambda_{H13}, \lambda_{\epsilon H3})$  planes are shown in Fig. 4.3.7 for  $M_1 = M_3 = 1$  TeV. We observe that a limit of about 1.5 can be put on both  $\lambda_{H13}$  and  $\lambda_{\epsilon H3}$  (right panel). This comes mainly from the contribution to the  $\hat{T}$  parameter, which is quadratic in the two couplings and thus allows to constrain both at the same time. The  $\lambda_{H1}$  and  $\lambda_{H3}$  couplings, instead, are constrained mainly from their contribution to the  $h\gamma\gamma$  and  $hgg$  couplings, Eqs. (4.3.8) and (4.3.9). We see that with present experimental accuracy the limits are still rather weak, and there is an approximate flat direction which doesn't allow to put any relevant bound on  $\lambda_{H1}$ .

This situation will marginally improve with the more precise Higgs measurements from HL-LHC [161]. The future expected 95%CL contours are shown as dashed blue lines. This however has no appreciable effect on the limits shown in the right panel, since those are dominated by the constraint on the  $T$  parameter, which will instead improve substantially from measurements on the  $Z$  pole at FCC-ee. A more detailed analysis of FCC prospects are however beyond the scope of this paper.

#### 4.4. Prospects

In this Section, we discuss the implications of future Belle II measurements of

- LFV  $B$  decays induced at parton level by  $b \rightarrow s\tau\mu$ ;
- $B$  decays induced at parton level by  $b \rightarrow s\tau\tau$ .

These processes, in fact, are particularly interesting for leptoquark scenarios aiming at addressing both neutral and charged-current  $B$ -anomalies. Both are induced at tree-level by  $S_3$  and, by  $\text{SU}(2)_L$  relations, the  $b \rightarrow c\tau\nu_\tau$  transition, tree-level in the SM, is related to the FCNC transition  $b \rightarrow s\tau\tau$ . Also, LFV is a natural consequence of leptoquark couplings once also the coupling to muons is considered, as required by neutral-current anomalies. While the LFV  $B$ -meson decays are already included in the global fits described in the previous Sections, the current bounds on  $b \rightarrow s\tau\tau$  observables are of the order of  $\sim 10^{-3}$  and thus too weak to set constraints on the model parameters. However, Belle II, with  $50\text{ab}^{-1}$  of luminosity, will strongly improve the sensitivity, in particular for the branching fraction of the semileptonic decays. On the other hand, the Upgrade II of LHCb will set competitive bounds on the leptonic decay  $B_s \rightarrow \tau\tau$ . The relevant future expected limits at 95% C.L. for Belle II [162] and LHCb [163] are summarised in Table 6.

Observable	Present limit	Belle II (5)50ab <sup>-1</sup>	LHCb Up.-II
<i>b</i> → <i>s</i> τμ observables			
Br( <i>B</i> <sup>+</sup> → <i>K</i> <sup>+</sup> τ <sup>±</sup> μ <sup>∓</sup> )	< 3.3(5.4) × 10 <sup>-5</sup> [109, 110]	3.9 × 10 <sup>-6</sup>	$\mathcal{O}(10^{-6})$
Br( <i>B</i> <sub><i>s</i></sub> → τ <sup>±</sup> μ <sup>∓</sup> )	< 4.2 × 10 <sup>-5</sup> [108]	~ 4 × 10 <sup>-6</sup>	~ 1 × 10 <sup>-5</sup>
<i>b</i> → <i>s</i> ττ observables			
Br( <i>B</i> <sup>+</sup> → <i>K</i> <sup>+</sup> τ <sup>+</sup> τ <sup>-</sup> )	< 2.8 × 10 <sup>-3</sup> [164]	(7.7) 2.4 × 10 <sup>-5</sup>	-
Br( <i>B</i> <sub><i>s</i></sub> → τ <sup>+</sup> τ <sup>-</sup> )	< 6.8 × 10 <sup>-3</sup> [165]	(9.7) 3 × 10 <sup>-4</sup>	5 × 10 <sup>-4</sup>

TABLE 6. Future Belle II and LHCb sensitivities, at 95% C.L., for *b* → *s*τμ and *b* → *s*ττ observables.

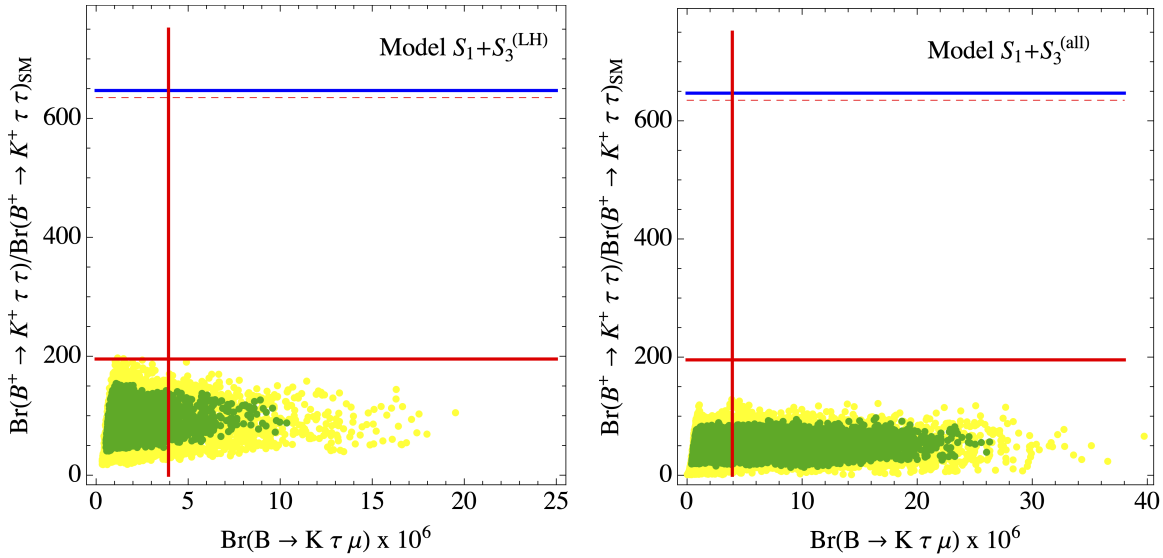


FIGURE 4.4.1. Results from the fit in the  $S_1 + S_3^{(LH)}$  model (left panel) and in the  $S_1 + S_3^{(all)}$  (right panel). The red solid (dashed) lines correspond to the 50ab<sup>-1</sup> (5ab<sup>-1</sup>) Belle II future bounds, at 95% C.L. . The blue solid line is the prospected bound for the LHCb Upgrade II, on  $\text{Br}(B_s \rightarrow \tau\tau)/\text{Br}(B_s \rightarrow \tau\tau)_{\text{SM}}$ .

In Fig. 4.4.1 we show how the preferred parameter-space regions for the models  $S_1 + S_3^{(LH)}$  (left) and  $S_1 + S_3^{(all)}$  (right) map in the plane of the branching fractions of the LFV decay  $B^+ \rightarrow K^+ \tau \mu$  and the decay  $B^+ \rightarrow K^+ \tau \tau$  (normalised to the SM value).<sup>5</sup> The red horizontal lines correspond to the Belle II future bounds at 95% C.L. on  $\text{Br}(B^+ \rightarrow K^+ \tau^+ \tau^-)$  at 5ab<sup>-1</sup> (dashed lines) and 50ab<sup>-1</sup> (solid lines), while the vertical ones represent the Belle II 50ab<sup>-1</sup> prospect for  $\text{Br}(B^+ \rightarrow K^+ \tau \mu)$ . One can see that, in both scenarios, the predictions for both the non-LFV and LFV semileptonic *B* decay into τ are in the ballpark of the future Belle II sensitivity at 50ab<sup>-1</sup>, while the expected bounds at 5ab<sup>-1</sup> are still too weak to set significant constraints on the models. Furthermore, one can notice that the future measurements of *b* → *s*ττ observables are

<sup>5</sup>It should be noted that at tree-level in our model this ratio is the same for all decays involving the *b* → *s*ττ transition, e.g.  $B_s \rightarrow \tau\tau$  (see Ref. [46]).

constraining more strongly the parameter space of the  $S_1 + S_3^{(\text{LH})}$  model than the one of the  $S_1 + S_3^{(\text{all})}$  model. For the leptonic decay  $B_s \rightarrow \tau^+ \tau^-$  at Belle II only the prospect at luminosity of  $5\text{ab}^{-1}$  is available; it is not shown in the plots since it is weaker with respect to the semileptonic decays and correspond to a horizontal line at  $\sim 1250$ . On the other hand, for the Upgrade II of LHCb, the prospected bound on  $\text{Br}(B_s \rightarrow \tau^+ \tau^-)$  (blue horizontal lines) is stronger and leads to constraints similar to the ones that we obtain from the  $B^+ \rightarrow K^+ \tau^+ \tau^-$  decay measured at  $5\text{ab}^{-1}$  Belle II. In order to evaluate the constraining power of future  $\text{Br}(B_s \rightarrow \tau \mu)$  measurements, in Fig. 4.4.1, one could keep in mind that in our model we have  $\text{Br}(B_s \rightarrow \tau \mu)/\text{Br}(B^+ \rightarrow K^+ \tau \mu) \approx 0.89$ , at tree-level [46].

### 4.5. Light generations

For the purpose of addressing  $B$ -anomalies and  $(g-2)_\mu$ ,  $S_1$  and  $S_3$  are only required to couple to second and third generation quarks and leptons, whereas couplings to first generation could in principle be very small. As already mentioned, the exact vanishing of first generation couplings assumed in Ref. [46] was a mere working hypothesis, whereas in more realistic models one would expect non-zero couplings, perhaps suppressed by some mechanism, *e.g.* flavour symmetry.

In Ref. [146], the authors consider the  $S_1 + S_3$  model with left-handed couplings only (cf. Subsec. 4.3.3) and with an assumed  $U(2)^5$  flavour symmetry, which dictates the magnitude of first generation couplings. As shown in the reference, the resulting constraints from Kaon observables prevent a fit of  $R(D^{(*)})$  beyond the  $2\sigma$  level, in contrast with our previous findings in Subsec. 4.3.3, where bounds from Kaon physics were neglected. Ref. [146] also studies generic predictions for Kaon observables such as  $\text{Br}(K_L \rightarrow \pi^0 \nu \nu)$  and  $\text{Br}(K_S \rightarrow \mu^+ \mu^-)$ , which could be potentially probed by KOTO stage-1 or LHCb are found to be allowed, and for electronic observables such as  $\mu \rightarrow e$  conversion in nuclei and  $\mu \rightarrow 3e$  decay, whose bounds are also expected to improve by several orders of magnitude in the near future [166–170].

We see thus that in the  $S_1 + S_3$  model there exist important correlations between Kaon observables, electron number violating observables, and the  $B$ -anomalies. These findings allow us to anticipate the *leitmotiv* of the next Chapter: if the  $B$ -anomalies are experimentally confirmed, a thorough understanding of how the anomalous  $b \rightarrow c \ell \nu$  and  $b \rightarrow s \ell \ell$  observables correlate with other observables will be crucial, both for model validation and for prospects.

### 4.6. Conclusions

In this Chapter we examined in detail and at one-loop accuracy the phenomenology of Standard Model extensions involving the two leptoquarks  $S_1$  and  $S_3$ , motivated by the experimental discrepancies observed in  $B$ -meson decays and in the muon anomalous magnetic moment  $(g-2)_\mu$ .

To this aim, we performed global fits for several benchmark models to a comprehensive list of flavor and electroweak precision observables, each computed at one-loop accuracy, leveraging on our previous work [44]. For each model, we identify best-fit regions and

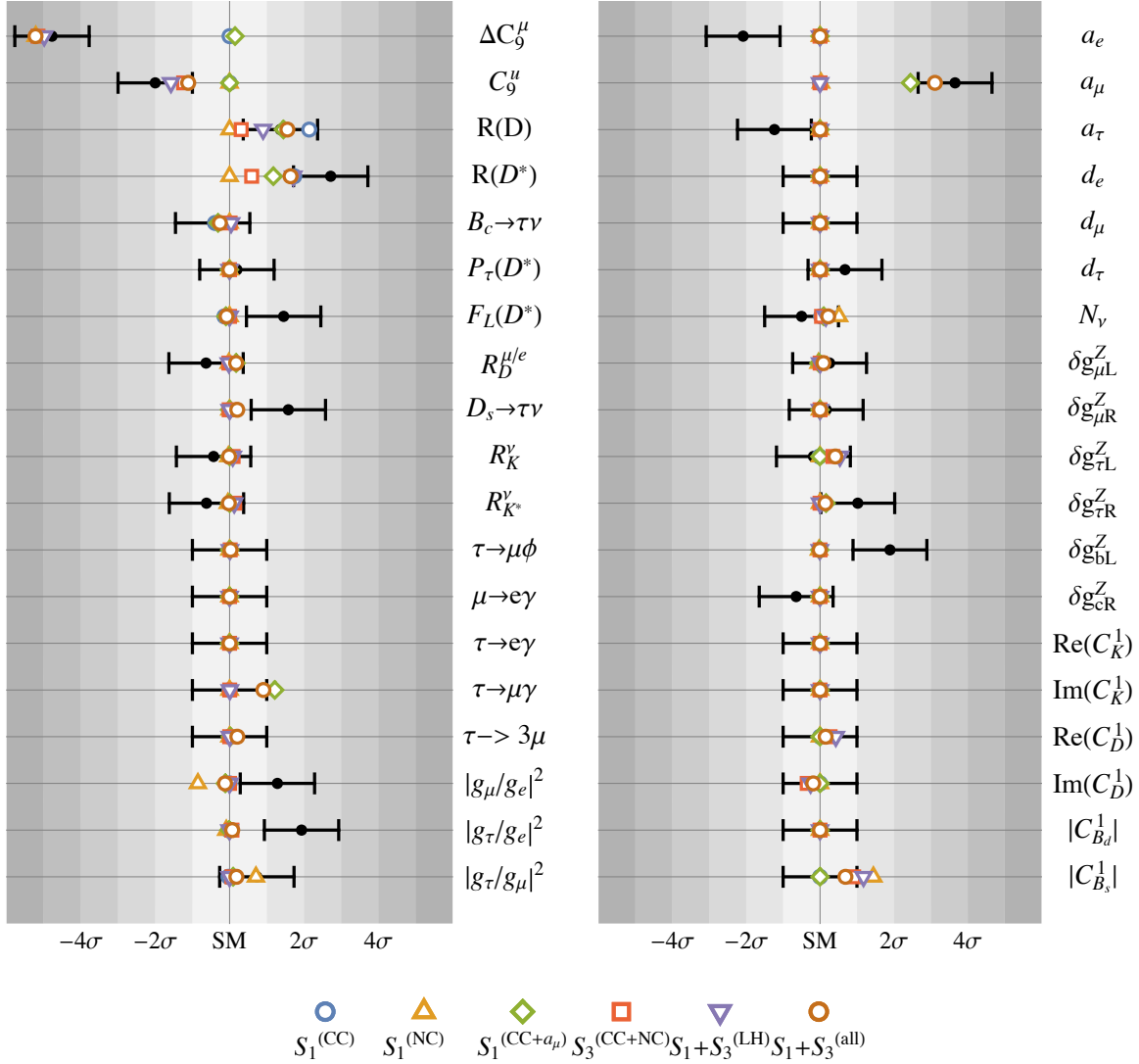


FIGURE 4.6.1. For the best-fit points in each model studied in this Chapter, we show the relative deviations from the Standard Model prediction in all observables, in terms of number of sigmas given by the experimental precision in that observable. The black intervals represent the experimental measurements

major sources of tension, when present, and also provide prospects for  $B$ -decays to  $\tau\tau$  and  $\tau\mu$ , in the experimental scope of Belle II and LHCb.

It is found that models involving only the  $S_1$  leptoquark can consistently address  $R(D^{(*)})$  and  $(g-2)_\mu$  anomalies, while a fully-satisfactory solution for  $b \rightarrow s\mu\mu$  anomalies is prevented by the combination of constraints from  $B_s$ -mixing and LFU in  $\tau$  decays. Conversely, the  $S_3$  leptoquark when taken alone can only address neutral-current  $B$ -meson anomalies. A model with both  $S_1$  and  $S_3$ , and only left-handed couplings for  $S_1$ , can address both  $B$ -anomalies but not the muon magnetic moment. Finally, allowing for right handed  $S_1$  couplings makes it possible to fit also  $(g-2)_\mu$ . Concerning the prospects for both the LF conserving branching fraction  $\text{Br}(B \rightarrow K\tau\tau)$  and the LFV one

$\text{Br}(B \rightarrow K\tau\mu)$ , they are found to be in the ballpark of the future expected sensitivity of Belle-II and LHCb.

A quick glance summary of the various models is provided by Fig. 4.6.1 where we show, for the best-fit point of each model, the deviations from the SM prediction of each of the most relevant observables studied in the global fit. The black dots and intervals represent the experimentally preferred values and uncertainties, and for each observable we normalize the  $x$ -axis to the corresponding uncertainty (i.e. we count the number of standard deviations). Detailed informations for each model can be found in Subsections 4.3.4-4.3.4. A separate analysis is provided in Sec. 4.3.5 for Higgs physics observables and electroweak oblique corrections, which put constraints on leptoquark-Higgs couplings.

To conclude, we find that the combination of  $S_1$  and  $S_3$  provides a good combined explanation of several experimental anomalies: charged and neutral-current  $B$ -meson anomalies as well as the muon magnetic moment. Their mass is necessarily close to the 1 TeV scale, particularly to address charged-current anomalies  $R(D^{(*)})$ , and is thus in the region that could still show some signals at HL-LHC, if they are light enough, but that will definitely be tested at future hadron colliders.

In the next few years, several experiments are expected to provide concluding answers as to the nature of all these puzzles. While at this time it is still very possible that some, or all, of these will turn out to be only statistical fluctuations and will be shown to be compatible with SM predictions, the possibility that even only one will instead be confirmed is real. Such an event would have profound and revolutionary implications for our understanding of Nature at the smallest scales. The scalar leptoquarks considered here are very good candidates for combined explanations and could thus be the heralds of a new physics sector lying at the TeV scale.

## CHAPTER 5

### Rank One Flavor Violation

The  $B$ -anomalies, if experimentally confirmed, could shed some light on the NP flavour structure, which can be probed by studying the correlations between the anomalies and other flavour observables. This type of information is, generically speaking, impossible to extract from few data such as the  $R(D^{(*)})$  or  $R(K^{(*)})$  discrepancies, and without any specific model in mind. However, under some generic flavour assumptions, one is sometimes able to draw model independent conclusions, which can be useful either to exclude the initial guess itself, or to make theoretically well-grounded predictions. This is the point of view taken in Ref. [45], a work in collaboration with D. Marzocca, M. Nardecchia and A. Romanino, which I describe in this Chapter.

In [45], we assume that the NP sector giving rise to the  $R(K^{(*)})$  anomalies couples only to muons and to a single direction in quark flavour space. In other words, the NP lagrangian takes the form<sup>12</sup>:

$$\mathcal{L}_{\text{NP}} = \mathcal{L}_{\text{NP}} [\hat{n}_i^* q^i, \ell_{2L}, \mu_R], \quad (5.0.1)$$

where  $\hat{n}$  is a unit complex vector. In this case, the Wilson coefficient matrices of the semileptonic operators contributing to  $R(K^{(*)})$ , which at the low-energy (*i.e.* GeV scale) level are:

$$O_{ij}^\chi = (\bar{d}_i \gamma_\rho P_L d_j) (\bar{\mu} \gamma^\rho P_\chi \mu) \quad (\chi = L, R) \quad (5.0.2)$$

are all of rank one and proportional:

$$C_{ij}^\chi = C^\chi \hat{n}_i \hat{n}_j^* \quad (\chi = L, R), \quad (5.0.3)$$

with  $C^\chi \in \mathbb{R}$ . An equation similar to (5.0.3) holds for the Wilson coefficients of SMEFT operators, as we will discuss in more details below.

We dub the scenario described above as Rank One Flavor Violation (ROFV). Although the ROFV assumption might appear quite ad-hoc, it is actually automatically realized in a handful of models addressing  $R(K^{(*)})$ : single leptoquark models, models in which the quark doublets mixes with a single generation of vector-like fermions, one-loop models of linear flavour violation [88], to give some examples. It is worth to notice that, as part of the ROFV hypothesis, it is assumed that the  $R(K^{(*)})$  deviations are entirely

---

<sup>1</sup>Semileptonic operators including right handed quarks do not contribute to  $R(K^{(*)})$  [171], and do not have any impact on the bounds studied in our work, so that the right handed quark fields  $d$  and  $u$  are not considered in Eq. (5.0.1) and what follows.

<sup>2</sup>In order to avoid confusions between SM and low-energy quark and lepton fields, in this Chapter we shall denote SM chiral fields by  $q_{iL}$ ,  $u_{iR}$ ,  $d_{iR}$ ,  $\ell_{\alpha L}$  and  $e_{\alpha R}$ , whereas the notation without any explicit chirality (such as  $\mu$ ,  $d$ ,  $u$ , etc.) refers to the Dirac (non-chiral) quark and lepton fields in the broken electroweak symmetry phase.

due to the muonic channel, *i.e.* the numerators in Eq. (3.2.1), which as we already commented is supported by data.

Under the ROFV assumption, one can establish correlations between  $R(K^{(*)})$  and other flavour observables, which mainly depend on the NP direction  $\hat{n}$ . For instance, in the low energy setting of Eqs. (5.0.2), once the unit vector  $\hat{n}$  and the ratios  $C^L : C^R$  are fixed, one can fit the overall energy scale of the Wilson coefficients in Eq. (5.0.3) to the  $R(K^{(*)})$  data; this, in turn, allows to compute NP contributions to all observables of the form  $d_i \rightarrow d_j \mu \mu$ . The latter information can be used in a two-fold way: either to constrain the possible NP directions  $\hat{n}$  using the bounds coming from  $d_i \rightarrow d_j \mu \mu$  processes (the main approach advocated in Ref. [45]), or to obtain predictions for these processes for a given (motivated, in some way) direction  $\hat{n}$ .

In our original work [45], we address only the neutral LFU ratio anomalies (*i.e.*  $R(K^{(*)})$ ), but it should be noted that even if an assumption analogous to Eq. (5.0.3) held within the  $b \rightarrow c \tau \nu_\tau$  sector, the corresponding unit vectors for neutral and charged current Wilson coefficients would, in general, be entirely uncorrelated.

Apart from identifying a set of relevant observables correlating with  $R(K^{(*)})$  under ROFV, the main conclusion of Ref. [45] is that, in models satisfying the rank-one condition, NP couplings must be closely aligned to the third family of quarks. Such an alignment can be naturally explained in the framework of flavour symmetries, in which case the quark  $U(2)_Q^3$  emerges as a promising candidate [45]. In the absence of flavour symmetries, the phenomenological constraints analysed in Ref. [45] call either for an alternative mechanism naturally providing the required alignment, or for a mere fine-tuning along the heavy quark family.

### 5.1. The ROFV framework

We start by listing the relevant effective operators for our analysis, both at the low-energy scale of  $B$ -anomalies, and at the high-energy scale of SMEFT, *i.e.* the GeV and TeV scales respectively. In what follows we consider only tree-level contributions to Wilson coefficients, so that the link between SMEFT and low-energy operators amounts to a simple projection.

Model-independent analyses of neutral-current anomalies hint towards NP coupling to quark and lepton vectorial currents [85, 96, 171–183]. As a matter of fact, the vast majority of NP explanations of the anomalies boils down, at low energy, to one of the following muonic operators:

$$\mathcal{O}_L = (\bar{s} \gamma_\rho P_L b) (\bar{\mu} \gamma^\rho P_L \mu), \quad \mathcal{O}_9 = (\bar{s} \gamma_\rho P_L b) (\bar{\mu} \gamma^\rho \mu), \quad (5.1.1)$$

although it has been pointed out that allowing for NP in both muons and electrons provides a slight improvement in the fits [184–186].

The two low-energy operators in Eq. (5.1.1) can be thought to be part of an effective lagrangian involving all the three quark families

$$\mathcal{L}_{\text{NP}}^{\text{EFT}} = C_L^{ij} (\bar{d}_i \gamma_\rho P_L d_j) (\bar{\mu} \gamma^\rho P_L \mu) + C_R^{ij} (\bar{d}_i \gamma_\rho P_L d_j) (\bar{\mu} \gamma^\rho P_R \mu), \quad (5.1.2)$$

where the coefficient of the  $\mathcal{O}_L$  operator is identified with  $C_L^{sb}$ , the coefficient of the  $\mathcal{O}_9$  operator with  $C_L^{sb} + C_R^{sb}$ , and we have focussed on muon processes on the leptonic side.



$R_K$ [1.1, 6] GeV <sup>2</sup>	$0.846 \pm 0.062$	LHCb [27, 187]
$R_{K^*}$ [0.045, 1.1] GeV <sup>2</sup>	$0.66 \pm 0.11$ $0.52^{+0.36}_{-0.26}$	LHCb [31] Belle [188]
$R_{K^*}$ [1.1, 6] GeV <sup>2</sup>	$0.69 \pm 0.12$ $0.96^{+0.45}_{-0.29}$	LHCb [31] Belle [188]
$R_{K^*}$ [15, 19] GeV <sup>2</sup>	$1.18^{+0.52}_{-0.32}$	Belle [188]
$\text{Br}(B_s^0 \rightarrow \mu\mu)$	$(3.0^{+0.67}_{-0.63}) \times 10^{-9}$ $(2.8^{+0.8}_{-0.7}) \times 10^{-9}$	LHCb [30] ATLAS [32]

TABLE 1. Clean observables sensitive to  $bs\mu\mu$  contact interactions.

From the SMEFT point of view, the operators that can contribute to (5.1.2) at the tree-level are collected in the following lagrangian:

$$\mathcal{L}_{\text{NP}}^{\text{SMEFT}} = C_S^{ij}(\overline{q_{iL}}\gamma_\rho q_{jL})(\overline{\ell_{2L}}\gamma^\rho \ell_{2L}) + C_T^{ij}(\overline{q_{iL}}\gamma_\rho \tau^a q_{jL})(\overline{\ell_{2L}}\gamma^\rho \tau^a \ell_{2L}) + C_R^{ij}(\overline{q_{iL}}\gamma_\rho q_{jL})(\overline{\mu_R}\gamma^\rho \mu_R) \quad (5.1.3)$$

with  $C_L^{ij} = C_S^{ij} + C_T^{ij}$ . In the previous equation,  $\ell_L^i = (\nu_L^i, e_L^i)^t$  and  $q_L^i = (V_{ji}^* u_L^j, d_L^i)^t$  are the lepton and quark doublets, in the charged-lepton and down quarks mass basis respectively, and  $V$  is the CKM matrix.

Our key assumption is that the NP sector responsible of the  $R_{K^{(*)}}$  signal couples to a single direction in the quark flavour space (as mentioned, we focus here on muon processes on the leptonic side), which requires the Wilson coefficient matrices  $C_{S,T,R}^{ij}$  in Eq. (5.1.3) (and consequently  $C_{L,R}^{ij}$  in (5.1.2)) to be rank-one and proportional:

$$C_{S,T,R,L}^{ij} = C_{S,T,R,L} \hat{n}_i \hat{n}_j^* \quad (5.1.4)$$

where  $C_{S,T,R,L} \in \mathbb{R}$ ,  $C_L = C_S + C_T$ , and  $\hat{n}_i$  is a unitary vector in  $U(3)_q$  flavour space. We dub this scenario *Rank-One Flavor Violation* (ROFV). Rather than being an assumption on the flavour symmetry and its breaking terms (such as Minimal Flavor Violation [79], for example), this is an assumption on the dynamics underlying these semileptonic operators. We refer to [189, 190] for similar approaches in different contexts.

It is perhaps worth emphasizing that our analysis does not rely upon any particular assumption concerning NP effects in the  $\tau$  sector, as far as observables with muons are concerned. Such effects could become relevant only when considering observables with neutrinos, whose flavour is not observed, or loop-generated ones such as  $\Delta F = 2$  processes in leptoquark models.<sup>3</sup> On the other hand, we do assume negligible NP effects in the electron sector. This is, by itself, a reasonable assumption since it is supported by data and it is also well motivated in scenarios where NP couplings to leptons follows the same hierarchy as SM Yukawas (such as  $SU(2)^5$  flavour symmetries or partial compositeness).

<sup>3</sup>Since experimental limits on semi-tauonic operators are much weaker than those on semi-muonic ones, couplings of new physics to tau leptons can be much larger than to muons, which is consistent with theoretical expectations from NP coupled preferentially to the third family, and for example allows combined explanations of both neutral and charged-current  $B$ -meson anomalies, see e.g. the analysis in [81].

The ROFV assumption is well motivated. For example, it is automatically realised in all single leptoquark models generating the operators in Eq. (5.1.1) at low energy<sup>4</sup> (see e.g. Ref. [132] for a recent comprehensive analysis). Furthermore, Eq. (5.1.4) is automatically satisfied in all cases where a single linear combination of SM quark doublets couples to NP. This condition is actually stronger than strictly required by ROFV, since not only semimuonic operators have rank-one coefficients, but all operators involving quark doublets. This scenario finds realization in several UV models, such as models with single vector-like fermion mediators, and one-loop models with linear flavour violation [88]. Contrary to the MFV or the minimally broken  $U(2)^5$  scenarios, which predict the flavour structure of all NP contributions, the ROFV assumption is specific to the set of semimuonic operators in Eq. (5.1.3). On the other hand, while those scenarios require strong assumptions on the flavour symmetry and its symmetry-breaking terms, ROFV can be accidentally realised from the underlying dynamics, see e.g. Refs. [191, 192].

From a theoretical point of view it might be natural to expect the direction of the unitary vector  $\hat{n}$  to be close to the third generation of SM quarks. This case is studied in more detail in Sec. 5.4. In the following, instead, we abandon any theory prejudice on  $\hat{n}$  and study what are the experimental constraints on its possible directions. We parametrize  $\hat{n}$  as

$$\hat{n} = \begin{pmatrix} \sin \theta \cos \phi e^{i\alpha_{bd}} \\ \sin \theta \sin \phi e^{i\alpha_{bs}} \\ \cos \theta \end{pmatrix}, \quad (5.1.5)$$

where the angles and phases can be chosen to lie in the following range:

$$\theta \in \left[0, \frac{\pi}{2}\right], \quad \phi \in [0, 2\pi), \quad \alpha_{bs, bd} \in \left[-\frac{\pi}{2}, +\frac{\pi}{2}\right] \quad (5.1.6)$$

The values of the angles and phases associated to specific directions in flavour space (up and down quarks) are collected in Table 2 and shown in the corresponding Figure.

The ROFV structure of the semileptonic operators, Eq. (5.1.4), implies the existence of correlations between the NP contributions to  $b \rightarrow s\mu\mu$  anomalous observables and to other observables. In the SMEFT, additional correlations follow from the  $SU(2)_L$  invariance of the lagrangian in (5.1.3). We can then take advantage of the experimental constraints on those additional observables to constrain the flavour directions  $\hat{n}$  accounting for the anomalies. In order to do that, we proceed as follows: for a given direction  $\hat{n}$ , we fix (some combination of) the overall coefficients in Eq. (5.1.4) by matching with the best-fit value of the  $C_L^{sb}$  (or  $C_9^{sb}$ ) coefficient obtained from global fits. Once this is done, we can compute NP contributions to other semileptonic processes as functions of  $\hat{n}$ , and compare with the corresponding experimental values/bounds. By this procedure, we are able to narrow down considerably the space of allowed flavour directions  $\hat{n}$ .<sup>5</sup>

We analyse the constraints on the direction  $\hat{n}$  under different assumptions. We begin in Sec. 5.2 by using the effective description in (5.1.2) and focussing on the case  $C_R = 0$ .

<sup>4</sup>To be precise, the correlations discussed in the present Chapter apply to all single leptoquark models in which the coupling to electrons is suppressed with respect to the one to muons.

<sup>5</sup>We checked explicitly that the results obtained in this way, i.e by fixing  $C_{L,9}^{bs}$  to its best-fit point, or by performing a global  $\chi^2$  analysis to get the 95%CL excluded region agree very well with each other.

quark	$\hat{n}$	$\phi$	$\theta$	$\alpha_{bd}$	$\alpha_{bs}$
down	(1, 0, 0)	0	$\pi/2$	0	0
strange	(0, 1, 0)	$\pi/2$	$\pi/2$	0	0
bottom	(0, 0, 1)	0	0	0	0
up	$e^{i \arg(V_{ub})}(V_{ud}^*, V_{us}^*, V_{ub}^*)$	0.23	1.57	-1.17	-1.17
charm	$e^{i \arg(V_{cb})}(V_{cd}^*, V_{cs}^*, V_{cb}^*)$	1.80	1.53	$-6.2 \times 10^{-4}$	$-3.3 \times 10^{-5}$
top	$e^{i \arg(V_{tb})}(V_{td}^*, V_{ts}^*, V_{tb}^*)$	4.92	0.042	-0.018	0.39

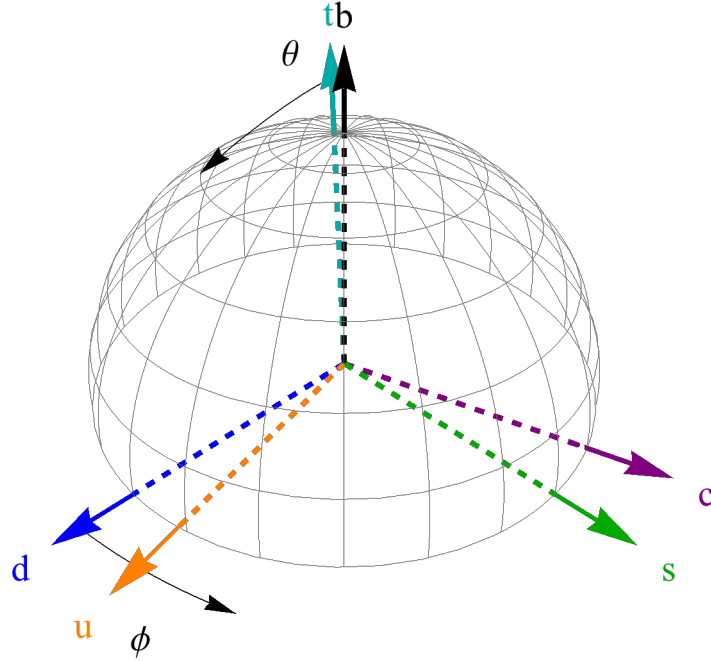


TABLE 2. SM quark directions of the unitary vector  $\hat{n}_i$ . The plot shows the corresponding directions in the semi-sphere described by the two angles  $(\theta, \phi)$ .

This allows us to derive general correlations with other  $d_i d_j \mu \mu$  observables. In Sec. 5.3 we extend the analysis to  $SU(2)_L \times U(1)_Y$  invariant operators, thus enabling us to consider also observables with up-quarks and/or muon neutrinos. Tab. 3 shows the dependencies of the various types of process upon the three coefficients  $C_{S,T,R}$ . In particular, we consider specific combinations of  $C_{S,T,R}$  obtained in some single-mediator simplified models:  $S_3$  and  $U_1^\mu$  leptoquarks, as well as of a  $Z'$  coupled to the vector-like combination of muon chiralities. In Sec. 5.4 we study the connection of our rank-one assumption with  $U(3)^5$  and  $U(2)^5$  flavour symmetries. A discussion on the impact of future measurements is presented in Sec. 5.5. The simplified fit of the  $R_K$  and  $R_{K^*}$  anomalies used below, as well as details on the flavour observables considered, are collected in the two Appendices of the original reference [45].

Channel	Coefficient dependencies
$d_i \rightarrow d_j \mu^+ \mu^-$	$C_S + C_T, C_R$
$u_i \rightarrow u_j \bar{\nu}_\mu \nu_\mu$	$C_S + C_T$
$u_i \rightarrow u_j \mu^+ \mu^-$	$C_S - C_T, C_R$
$d_i \rightarrow d_j \bar{\nu}_\mu \nu_\mu$	$C_S - C_T$
$u_i \rightarrow d_j \mu^+ \nu_\mu$	$C_T$

TABLE 3. Dependencies of various semileptonic processes on the three coefficients  $C_{S,T,R}$  (cf. Eq. (5.1.4)). Here and in the text, a given quark level process represents all processes obtained through a crossing symmetry from the shown one.

Observable	Experimental value/bound	SM prediction	References
$\text{Br}(B_d^0 \rightarrow \mu^+ \mu^-)$	$< 2.1 \times 10^{-10}$ (95% CL)	$(1.06 \pm 0.09) \times 10^{-10}$	[32, 193]
$\text{Br}(B^+ \rightarrow \pi^+ \mu^+ \mu^-)_{[1,6]}$	$(4.55^{+1.05}_{-1.00} \pm 0.15) \times 10^{-9}$	$(6.55 \pm 1.25) \times 10^{-9}$	[194–196]
$\text{Br}(K_S \rightarrow \mu^+ \mu^-)$	$< 1.0 \times 10^{-9}$ (95% CL)	$(5.0 \pm 1.5) \times 10^{-12}$	[197]
$\text{Br}(K_L \rightarrow \mu^+ \mu^-)_{\text{SD}}$	$< 2.5 \times 10^{-9}$	$\approx 0.9 \times 10^{-9}$	[198, 199]
$\text{Br}(K_L \rightarrow \pi^0 \mu^+ \mu^-)$	$< 3.8 \times 10^{-10}$ (90% CL)	$1.41^{+0.28}_{-0.26} (0.95^{+0.22}_{-0.21}) \times 10^{-11}$	[200–204]

TABLE 4. Observables with direct correlation with  $bs\mu\mu$ .

## 5.2. General correlations in $V - A$ solutions

In this Section, we study the correlations that follow directly from the rank-one condition, for all models in which NP couples only to left-handed fermions. We begin by using the effective description in (5.1.2). For  $C_R = 0$ , and for fixed  $\theta$  and  $\phi$  in the ranges specified by Eq. (5.1.6), the coefficient  $C_L = C_S + C_T$  and the phase  $\alpha_{bs}$  are univocally determined by the  $b \rightarrow s\mu^+\mu^-$  anomalies fit:

$$C_L \sin \theta \cos \theta \sin \phi e^{i\alpha_{bs}} = C_L^{bs} \equiv \frac{e^{i\alpha_{bs}}}{\Lambda_{bs}^2}. \quad (5.2.1)$$

From a fit of the observables listed in Table 1, we find that the phase  $\alpha_{bs}$  has an approximately flat direction in the range  $|\alpha_{bs}| \lesssim \pi/4$ . Since a non-zero phase necessarily implies a lower  $\Lambda_{bs}$  scale in order to fit the anomalies, to be conservative we fix  $\alpha_{bs} = 0$ . In this case the best-fit point for the NP scale is:

$$(\Lambda_{bs})_{\text{best-fit}} = 38.5 \text{ TeV} \quad (5.2.2)$$

We now constrain  $\hat{n}$  (or, more precisely,  $\theta$  and  $\phi$  for given  $\alpha_{bs}$ ) using the other observables correlated with  $R_K$  by the relation  $C_L^{ij} = C_L \hat{n}_i \hat{n}_j^*$ . Such observables are associated to the quark-level transitions

$$d_i \rightarrow d_j \mu^+ \mu^- \quad (5.2.3)$$

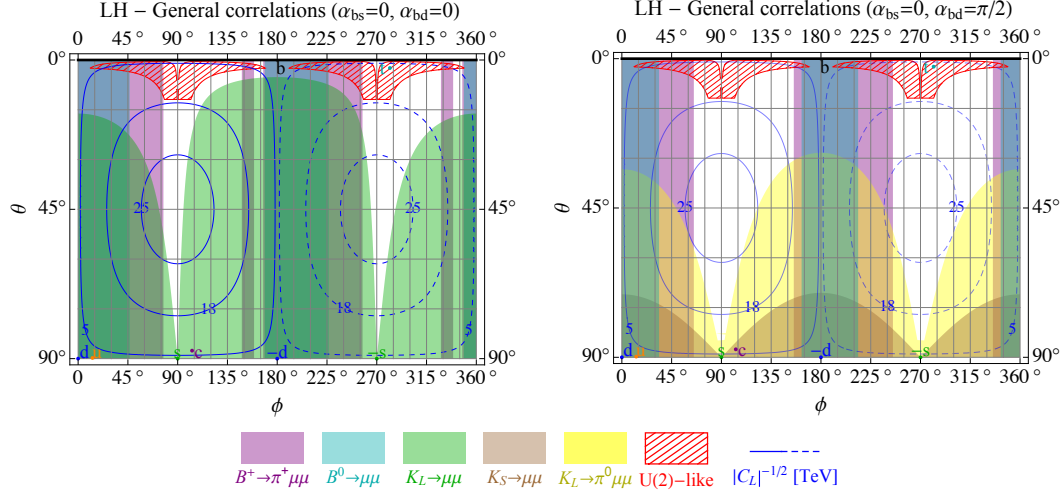


FIGURE 5.2.1. Limits in the plane  $(\phi, \theta)$  for two choices of the phases  $\alpha_{bs}$  and  $\alpha_{bd}$  from observables with direct correlation with  $R_{K^{(*)}}$ . The blue contours correspond to the value of  $|C_L|^{-1/2}$  in TeV, where solid (dashed) lines are for positive (negative)  $C_L$ . The meshed red region correspond to the one suggested by partial compositeness or  $SU(2)_q$ -like flavour symmetry, Eq. (5.4.5) with  $|a_{bd,bs}| \in [0.2 - 5]$ .

and cross-symmetric counterparts. The most relevant among those observables are listed in Tab. 4, and the corresponding allowed regions for  $\theta, \phi$  are shown in Fig. 5.2.1 in the two cases  $(\alpha_{bd}, \alpha_{bs}) = (0, 0)$  and  $(\alpha_{bd}, \alpha_{bs}) = (\pi/2, 0)$ . As can be seen from the plots, the most severe bounds arise from  $B^+ \rightarrow \pi^+ \mu^+ \mu^-$  (LHCb [194]) and  $K_L \rightarrow \mu^+ \mu^-$  (E871 [198, 199]). However, the latter observable does not yield any bound for  $\alpha_{bd} - \alpha_{bs} = \pi/2$ , i.e. for  $\text{Re} C_L^{ds} = 0$ . The imaginary part of that coefficient can instead be tested by  $K_S \rightarrow \mu^+ \mu^-$  (LHCb [205]) and  $K_L \rightarrow \pi^0 \mu^+ \mu^-$  (KTeV [200]). More details on the observables and their NP dependence can be found in Ref. [45].

As a final remark, let us stress that here and in the following we are ignoring possible NP contributions to (pseudo)scalar, tensor, or dipole operators. While these are known to be too constrained to give significant contributions to  $R_{K^{(*)}}$  (see e.g. [172]), they may nonetheless produce important effects in other observables, so that some of the bounds discussed here may be relaxed, if some degree of fine-tuning is allowed.

### 5.3. SMEFT and simplified mediators

Let us now assume that the effective operators in (5.1.2) originate from the SM-invariant ones in (5.1.3), as expected. The  $SU(2)_L$  invariance then relates  $d_i \rightarrow d_j \mu^+ \mu^-$  processes to processes involving up quarks and muon neutrinos listed in Tab. 3. Using the experimental constraints on those, we can impose further constraints on  $\hat{n}$ . These, though, are model dependent even in the  $C_R = 0$  case, as they depend on the relative size of the two operators in (5.1.3) contributing to  $C_L$ , i.e.  $C_S$  and  $C_T$ . The origin of the model dependence can be clarified taking advantage of a phenomenological observation. Our analysis (see below) shows that the the most relevant constraints come from the

Simplified model	Spin	SM irrep	$(c_S, c_T, c_R)$
$S_3$	0	$(\bar{3}, 3, 1/3)$	$(3/4, 1/4, 0)$
$U_1$	1	$(3, 1, 2/3)$	$(1/2, 1/2, 0)$
$U_3$	1	$(3, 3, 2/3)$	$(3/2, -1/2, 0)$
$V'$	1	$(1, 3, 0)$	$(0, 1, 0)$
$Z'$	1	$(1, 1, 0)$	$(1, 0, c_R)$

TABLE 5. Wilson coefficients ratios (cf. Eq. (5.3.4)) for some single-mediator simplified models.

processes

$$d_i \rightarrow d_j \mu^+ \mu^- \quad \text{and} \quad d_i \rightarrow d_j \bar{\nu}_\mu \nu_\mu . \quad (5.3.1)$$

As Table 3 shows, those two classes of processes are associated respectively to the two operators  $\mathcal{O}^\pm$  whose Wilson coefficients are  $C_\pm = C_S \pm C_T$  (note that  $C_+ \equiv C_L$ ), i.e.

$$\mathcal{O}_{ij}^+ = \frac{\mathcal{O}_{ij}^S + \mathcal{O}_{ij}^T}{2} = (\bar{q}_{iL} \gamma_\mu \ell_{2L}) (\bar{\ell}_L^2 \gamma^\mu q_L^j) \quad (5.3.2)$$

$$\mathcal{O}_{ij}^- = \frac{\mathcal{O}_{ij}^S - \mathcal{O}_{ij}^T}{2} = 2 (\bar{q}_{iL}^c \ell_{2L}) (\bar{\ell}_L^2 q_{jL}^c) . \quad (5.3.3)$$

The model-independent constraints shown in Fig. 5.2.1 only take into account the  $d_i \rightarrow d_j \mu^+ \mu^-$  processes and as such only depend on  $C_+$ , which is thus the only combination fixed by  $R_{K(*)}$ . On the other hand, the model-dependent weight of the  $d_i \rightarrow d_j \bar{\nu}_\mu \nu_\mu$  constraints depends on the relative size of  $C_-$ . In this context, the results in 5.2.1 correspond to a SMEFT with  $C_- = 0$ , i.e. to the  $U_1$  case in Tab. 5.

Note that the experimental constraints on the processes involving neutrinos do not distinguish among the three neutrino flavours. In order to get constraints on the muon neutrino operators we consider, one should then make an assumption on the relative size of the operators with different neutrino flavours. Below, we will conservatively assume that only the muon neutrino operators contribute to the neutrino processes.

In order to reduce the number of free parameters, we focus in this Section on single-mediator simplified models, which generate specific combinations of the three operators when integrated out at the tree-level. Some relevant benchmarks are shown in Table 5, where in the last column we list the ratios:

$$c_X \equiv \frac{C_X}{C_S + C_T} = \frac{C_X}{C_+} \quad (X = S, T, R) . \quad (5.3.4)$$

Notice that the exclusions shown in Fig. 5.2.1 hold in all models in Table 5, except for the  $Z'_V$  which has vector-like coupling to muons. We find that the most relevant bounds, beyond those already analyzed, arise from the FCNC observables  $\text{Br}(K^+ \rightarrow \pi^+ \nu_\mu \bar{\nu}_\mu)$  and  $\text{Br}(K_L \rightarrow \pi^0 \nu_\mu \bar{\nu}_\mu)$ , reported in 6. The connection of these observables with the  $B$ -meson anomalies has also been emphasised in Ref. [206]. The effect of constraints from rare kaon decays on LQ models addressing instead the  $\epsilon'/\epsilon$  anomaly have been studied in Ref. [207]. Some simplified models also allow to compute neutral meson mixing amplitudes, which we include in the analysis when appropriate.

Some comments are in order regarding the phenomenological relevance of the various processes listed in 3. Flavor observables of the type  $u_i \rightarrow u_j \bar{\nu}_\mu \nu_\mu$  or  $u_i \rightarrow u_j \mu^+ \mu^-$  are

Observable	Experimental value/bound	SM prediction	References
$\text{Br}(K^+ \rightarrow \pi^+ \nu_\mu \bar{\nu}_\mu)$	$(17.3^{+11.5}_{-10.5}) \times 10^{-11}$	$(8.4 \pm 1.0) \times 10^{-11}$	[208, 209]
$\text{Br}(K_L \rightarrow \pi^0 \nu_\mu \bar{\nu}_\mu)$	$< 3.0 \times 10^{-9}$ (90% CL)	$(3.4 \pm 0.6) \times 10^{-11}$	[107, 209]

TABLE 6.  $R_{K^{(*)}}$ -correlated observables for single-mediator models.

much less constrained than their  $d_i \rightarrow d_j$  counterparts, from the experimental point of view. On the other hand, the charged current processes  $u_i \rightarrow d_j \mu^+ \nu_\mu$  (which could in principle yield correlations between  $C_+$  and  $C_-$ ), being unsuppressed in the SM, receive only tiny corrections in the present framework. It turns out that all these observables lead to weaker bounds than those arising from other sectors, so that we omit them altogether from our analysis (as possibly relevant observables, we examined  $\text{Br}(J/\psi \rightarrow \text{invisible})$ ,  $\text{Br}(D^0 \rightarrow \mu^+ \mu^-)$  and  $\text{Br}(K^+(\pi^+) \rightarrow \mu^+ \nu_\mu)$ , for the three kind of quark level processes mentioned above, respectively.). Instead, for the purpose of comparison, we display in this Section the collider bounds arising from the high- $p_T$  tails of muonic Drell-Yan process measured at LHC [210], for which we follow the analysis of Ref. [135]. As it can be seen from the plots below, the collider bounds are outmatched by FCNC bounds in a large part of parameter space. The only region where LHC searches are the most relevant constraint is close to the bottom quark direction, i.e. for  $\theta \ll 1$ , as it can be seen directly in the top-left panel of Fig. 5.3.1 in the case of the  $S_3$  leptoquark.

In the rest of this Section we focus on the following models:

- (1) Scalar leptoquark  $S_3$ . This is the simplest *renormalizable* model explaining the  $R_{K^{(*)}}$  anomalies with NP in muons [172, 179, 191, 192, 211–213].
- (2) Vector leptoquark  $U_1$ . Besides having some theoretical motivation (from Pati-Salam SM extensions), this is the *only* single-mediator simplified model for which a combined explanation of  $R_{K^{(*)}}$  and  $R_{D^{(*)}}$  anomalies is possible [81, 214–223].
- (3) Vector singlet  $Z'$  with vector-like coupling to muons and a single vectorlike partner for quark doublets. Arguably the most compelling  $\mathcal{O}_9$ -type solution, it is relevant to some interesting proposals such as gauged  $L_\mu - L_\tau$  or  $B_3 - 3L_\mu$ , see for example Refs. [224–227].

**5.3.1. Scalar leptoquark  $S_3$ .** The relevant interaction of the  $S_3$  leptoquark with SM quarks and leptons can be described by the Lagrangian:

$$\mathcal{L}_{\text{NP}} \supset \beta_{i\mu} (\bar{q}_{iL}^c \epsilon \sigma^a \ell_{2L}) S_3^a + \text{h.c.} \quad (5.3.5)$$

where we focussed on the interaction with muons. Integrating out  $S_3$  at the tree-level, the effective operators in Eq. (5.1.3) are generated, with

$$C_S^{ij} = \frac{3}{4} \frac{\beta_{i\mu}^* \beta_{j\mu}}{M_{S_3}^2}, \quad C_T^{ij} = \frac{1}{4} \frac{\beta_{i\mu}^* \beta_{j\mu}}{M_{S_3}^2}, \quad C_R^{ij} = 0 \quad (5.3.6)$$

We can match to our parametrization by writing the coupling in (5.3.5) as  $\beta_{i\mu}^* \equiv \beta^* \hat{n}_i$ , giving  $C_+ = |\beta|^2/M_{S_3}^2 > 0$ ,  $c_S = 3/4$ ,  $c_T = 1/4$ , and  $c_R = 0$ . Since in this case  $C_+ = C_L > 0$  and the r.h.s. of Eq. (5.2.1) is also positive, the angle  $\phi$  is restricted to the range  $\phi \in [0, \pi]$ . The constraints on  $\phi$  and  $\theta$  we obtain are shown in Fig. 5.3.1.

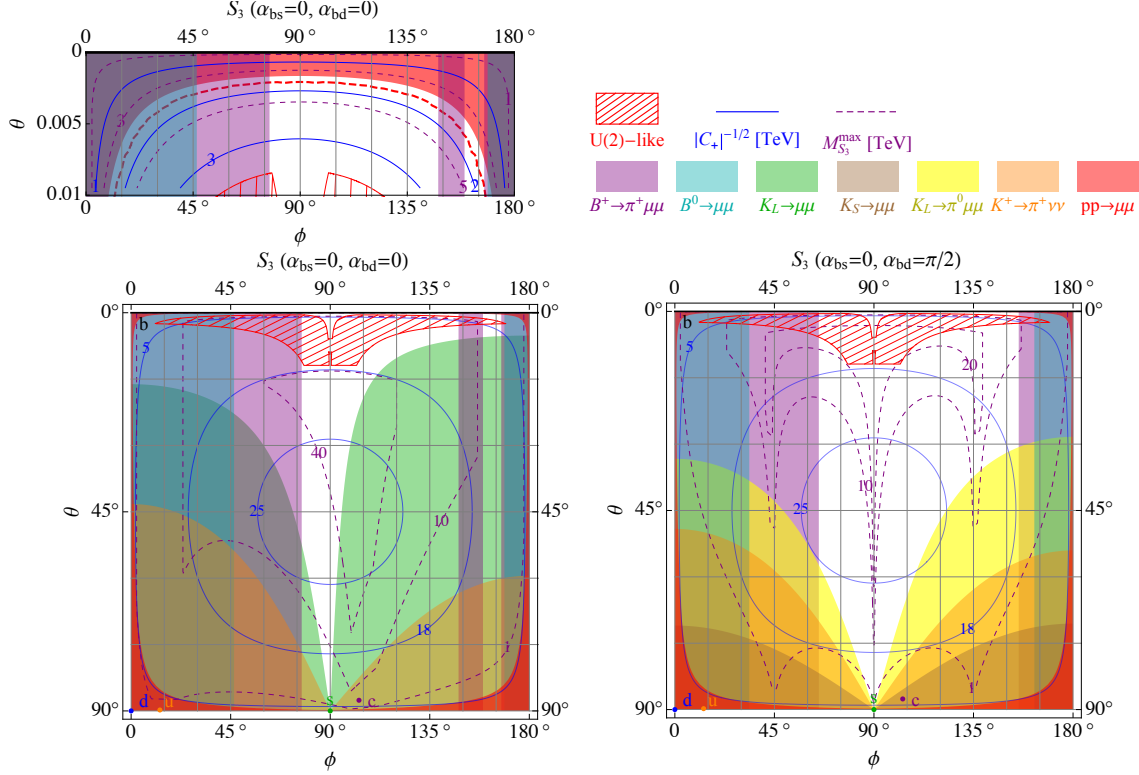


FIGURE 5.3.1. Limits in the plane  $(\phi, \theta)$  for the scalar leptoquark  $S_3$  and two choices of the phases  $\alpha_{bs}$  and  $\alpha_{bd}$ . In addition to the limits in Fig.1, the orange bound is from  $K \rightarrow \pi \nu \nu$  while the red one is from the high- $p_T$  tail of  $pp \rightarrow \mu^+ \mu^-$  at the LHC [135]. The top-left panel is a zoom of the region  $\theta \ll 10$  of the bottom-left one, which shows in more detail the region excluded by LHC dimuon searches. The dashed purple contour lines are the upper limits (in TeV) on the leptoquark mass from  $\Delta F = 2$  processes.

The scalar LQ  $S_3$  generates a contribution to  $\Delta F = 2$  processes at the one-loop level. The relevant diagrams are finite and the contribution from muonic loops is given by:

$$\Delta \mathcal{L}_{\Delta F=2} = -\frac{5}{128\pi^2} C_+^2 M_{S_3}^2 \left[ (\hat{n}_i \hat{n}_j^* \bar{d}_{iL} \gamma^\alpha d_{jL})^2 + (V_{ik} \hat{n}_k \hat{n}_l^* V_{jl}^* \bar{u}_{iL} \gamma^\alpha u_{jL})^2 \right] \quad (5.3.7)$$

Given a direction in quark space, i.e. a fixed  $\hat{n}$ , and fixing  $C_+$  to reproduce  $R_{K^{(*)}}$ , the experimental bounds on  $K - \bar{K}$ ,  $B_{d,s} - \bar{B}_{d,s}$ , and  $D_0 - \bar{D}_0$  mixing can be used to set an *upper limit* on the LQ mass, assuming the muonic contributions shown in Eq. (5.3.7) to be dominant compared to other possible NP terms. For the sake of clarity, it is worth remarking that loops involving  $\tau$  leptons could in general also give substantial contributions to Eq. (5.3.7), possibly making the bounds on  $M_{S_3}$  qualitatively stronger or weaker than those shown in Fig. 5.3.1, depending on the specific flavour structure of leptoquark couplings. Another upper limit on its mass, for a given value of  $C_+$ , can be set by requiring that the coupling  $\beta$  does not exceed the perturbative unitarity limit  $|\beta^{\max}|^2 = (8\pi)/(3\sqrt{3})$  [39]. The contours of the strongest of these two upper limits on  $M_{S_3}$  are shown as dashed purple lines (in TeV) in the plots of Fig. 5.3.1. The



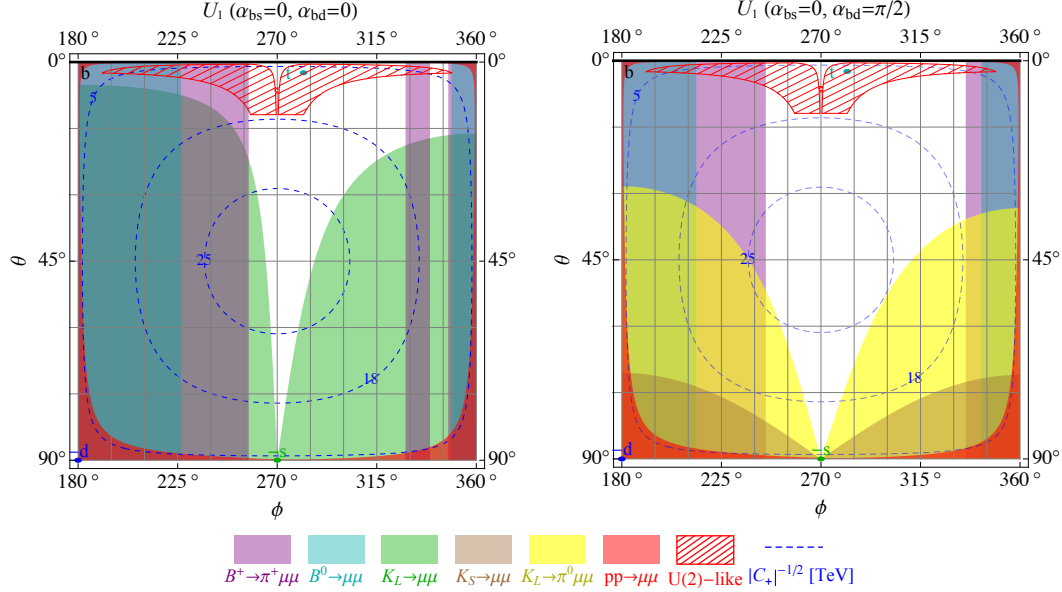


FIGURE 5.3.2. Limits in the plane  $(\phi, \theta)$  for the vector leptoquark  $U_1$  and two choices of the phases  $\alpha_{bs}$  and  $\alpha_{bd}$ . The red region is excluded by the high- $p_T$  tail of  $pp \rightarrow \mu^+ \mu^-$  at the LHC [135].

perturbativity limit is never stronger than the one from  $\Delta F = 2$  processes in this scenario. Direct searches at the LHC of pair-produced leptoquarks, on the other hand, set *lower limits* on its mass, which are now in the  $\sim 1$  TeV range.

**5.3.2. Vector leptoquark  $U_1$ .** The interaction lagrangian of the vector leptoquark  $U_1$  is

$$\mathcal{L}_{\text{NP}} \supset \gamma_{i\mu} (\bar{q}_{iL} \gamma_\alpha \ell_{2L}) U_1^\alpha + \text{h.c.} \quad (5.3.8)$$

The matching to the SMEFT operators generated by integrating out  $U_1$  at the tree-level is given by:

$$C_S^{ij} = C_T^{ij} = -\frac{1}{2} \frac{\gamma_{i\mu} \gamma_{j\mu}^*}{M_{U_1}^2}, \quad C_R = 0. \quad (5.3.9)$$

We can match to our parametrization by defining  $\gamma_{i\mu} \equiv \gamma \hat{n}_i$ , corresponding to  $C_+ = -|\gamma|^2/M_{U_1}^2 < 0$ ,  $c_S = 1/2$ ,  $c_T = 1/2$ , and  $c_R = 0$ . Contrary to the  $S_3$  model, the  $U_1$  LQ implies  $C_+ = C_L < 0$ . Therefore, Eq. (5.2.1), whose r.h.s. is positive, restricts the angle  $\phi$  to the range  $[\pi, 2\pi)$ . The constraints on  $\phi$  and  $\theta$  we obtain are shown in 5.3.2. As anticipated, they coincide with the constraints (in the  $\pi < \phi < 2\pi$  part) of 5.2.1.

Like  $S_3$ , also the  $U_1$  vector LQ contributes to meson anti-meson mixing at one-loop. Such a contribution is however UV-divergent and, in order to be calculable, requires a UV-completion of the simplified model. In general such UV completions contains other contributions to the same processes, which must also be taken into account [216–221, 223].

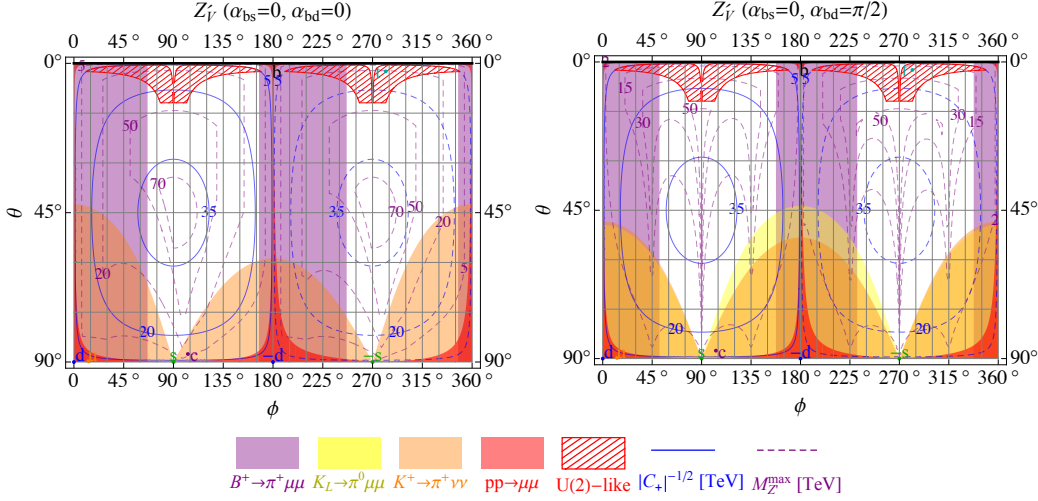


FIGURE 5.3.3. Limits in the plane  $(\phi, \theta)$  for the vector singlet  $Z'$  with vector-like couplings to muons and two choices of the phases  $\alpha_{bs}$  and  $\alpha_{bd}$ . The dashed purple contour lines are upper limits on the  $Z'$  mass [TeV] from  $\Delta F = 2$  processes using Eq. (5.3.15).

**5.3.3. Vector singlet  $Z'$  with vector-like couplings to muons.** Let us consider a heavy singlet vector  $Z'$  with couplings:

$$\mathcal{L}_{\text{NP}} \supset [g_q \hat{n}_i \hat{n}_j^* (\bar{q}_{iL} \gamma^\alpha q_{jL}) + g_\mu (\bar{\ell}_{2L} \gamma^\alpha \ell_{2L} + \bar{\mu}_R \gamma^\alpha \mu_R)] Z'_\alpha \quad (5.3.10)$$

Such a flavour structure of the  $Z'$  couplings to quarks could arise, for example, by assuming that they couple to  $Z'$  only via the mixing with a heavy vector-like quark doublet  $Q$  in the form

$$M_i \bar{Q} q_{iL} + \text{h.c.} \quad (5.3.11)$$

In such a case,  $\hat{n}_i \propto M_i^*$ . The matching with the SMEFT operators in this case is given by:

$$C_S^{ij} = C_R^{ij} = -\frac{g_q g_\mu}{M_{Z'}^2} \hat{n}_i \hat{n}_j^*, \quad C_T = 0, \quad (5.3.12)$$

corresponding to  $C_+ = -g_q g_\mu / (M_{Z'}^2)$ ,  $c_S = 1$ ,  $c_R = 1$ , and  $c_T = 0$ . The matching to the operators relevant for the  $b \rightarrow s \mu \mu$  anomalies is now

$$C_+ \sin \theta \cos \theta \sin \phi e^{i\alpha_{bs}} = \frac{G_F \alpha}{\sqrt{2} \pi} V_{tb} V_{ts}^* \Delta C_9^\mu. \quad (5.3.13)$$

Note that in this scenario the overall coefficient  $C_+$  can take any sign. It is worth noting that all purely leptonic meson decays such as  $K_{L,S}$  or  $B^0$  to  $\mu\mu$  vanish in this setup since the leptonic current is vector-like<sup>6</sup>. The only relevant limits then arise from  $B^+ \rightarrow \pi^+ \mu\mu$ ,  $K^+ \rightarrow \pi^+ \nu\nu$ , and from LHC dimuon searches, as shown in Fig. 5.3.3.

<sup>6</sup>The  $J = 0$  constraint forces the final muon pair to be in a state with  $C = +1$ , whereas the vectorial current  $\bar{\mu}\gamma\mu$  has negative  $C$ -parity.

This model also generates at the tree-level four quark operators which contribute to  $\Delta F = 2$  observables:

$$\Delta\mathcal{L}_{\Delta F=2} = -\frac{g_q^2}{2M_{Z'}^2} [(\hat{n}_i \hat{n}_j^* \bar{d}_{iL} \gamma^\alpha d_{jL})^2 + (V_{ik} \hat{n}_k \hat{n}_l^* V_{jl}^* \bar{u}_{iL} \gamma^\alpha u_{jL})^2] \quad (5.3.14)$$

For a fixed direction in quark space,  $\hat{n}$ , and a fixed value of  $R_{K(*)}$ , we can use  $\Delta F = 2$  constraints to put an upper limit on the ratio  $r_{q\mu} \equiv |g_q/g_\mu|$ . We can then assign a maximum value to  $g_\mu$  and derive an upper limit for the  $Z'$  mass:

$$M_{Z'}^{\text{lim}} = \min \left[ \sqrt{\frac{r_{q\mu}^{\text{lim}}}{|C_+|}} |g_\mu^{\text{max}}|, \sqrt{\frac{g_\mu^{\text{max}} g_q^{\text{max}}}{C_+}} \right] \quad (5.3.15)$$

where the first limit is from  $\Delta F = 2$  observables while the second is from perturbativity. For the maximum values of the couplings we use the limits from perturbative unitarity from Ref. [39],  $|g_\mu^{\text{max}}|^2 = 2\pi$  and  $|g_q^{\text{max}}|^2 = 2\pi/3$ .

#### 5.4. ROFV and flavour symmetries

In the previous Sections we have been agnostic about the structure of the rank one coefficients of the NP interactions, and parameterised it in terms of the unit vector  $\hat{n}$ . Here we would like to illustrate, with a flavour symmetry example, the possible theoretical expectations on the direction in flavour space at which  $\hat{n}$  points.

In the SM, the gauge lagrangian flavour group

$$\text{U}(3)^5 \equiv \text{U}(3)_q \times \text{U}(3)_\ell \times \text{U}(3)_u \times \text{U}(3)_d \times \text{U}(3)_e \quad (5.4.1)$$

is explicitly broken by the Yukawa couplings  $Y_{u,d,e}$ . Here, the unit vector  $\hat{n}$ , and the UV couplings from which it originates, represent an additional source of explicit breaking. In fact, we can formally assign the UV couplings introduced in the previous Section (and the SM Yukawa couplings) quantum numbers under  $\text{U}(3)^5$ :

$$\text{SM} : \begin{cases} Y_u \sim 3_q \otimes \bar{3}_u, \\ Y_d \sim 3_q \otimes \bar{3}_d, \\ Y_e \sim 3_\ell \otimes \bar{3}_e. \end{cases} \quad \hat{n}_i \propto \begin{cases} \beta_{i\mu} \sim \bar{3}_q \otimes \bar{3}_\ell & S_3, \\ \gamma_{i\mu} \sim \bar{3}_q \otimes 3_\ell & U_1^\mu, \\ M_i \sim 3_q & Z', V' \end{cases} \quad (5.4.2)$$

Therefore, different models can be characterised not only in terms of the SM quantum numbers of the messengers, but also in terms of the flavour quantum numbers of the couplings.

Correlations between the two sets of couplings in (5.4.2) can arise if they share a common origin. This may be the case, for example, if we assume a subgroup  $\mathcal{G} \subseteq \text{U}(3)^5$  to be an actual symmetry of the complete UV lagrangian, and the above couplings to originate from its spontaneous breaking by means of a common set of “flavon” fields.

Correlations cannot arise if  $\mathcal{G}$  coincides with the full  $\text{U}(3)^5$ . The quantum numbers of the relevant flavons coincide in this case with the transformation properties in (5.4.2). Therefore, the flavons entering the Yukawas and the NP couplings are in this case entirely independent. In particular, the ROFV assumption is not compatible with the Minimal Flavor Violation one [79]. We therefore need to consider proper subgroups of  $\text{U}(3)^5$ . Among the many possibilities, let us consider the  $\mathcal{G} = \text{U}(2)^5$  subgroup of transformations

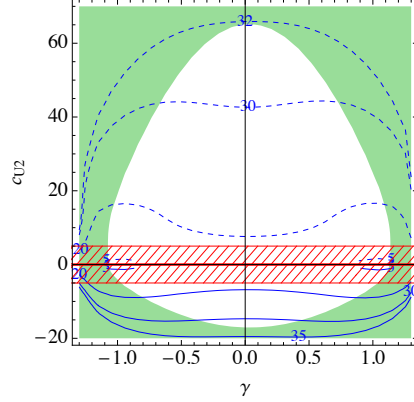


FIGURE 5.4.1. Region excluded at 95%CL in a global fit of  $bs\mu\mu$  clean observables and the other  $d_id_j\mu\mu$  ones listed in 4, assuming the structure of Eq. (5.4.3), in the plane  $(\gamma, c_{U2})$ . The relevant observable in the excluded region is  $K_L \rightarrow \mu^+\mu^-$ . The range  $|c_{U2}| \in [0.2 - 5]$  is highlighted as the meshed red region. Blue lines indicate the size of the overall coefficient  $|C_L|^{-1/2}$  (in TeV), as extracted from the fit. Solid (dashed) lines are for positive (negative) values of  $C_L$ .

on the first two fermion families. The latter extends the quark  $U(2)^3$  [80] to the leptons, relevant for two of the three NP couplings in (5.4.2). Some of the conclusions we will draw hold for a generic extension to  $U(2)^3 \times \mathcal{G}_l$ , where  $\mathcal{G}_l$  only acts on leptons.

The fact that correlations can arise in the  $U(2)$  case is not a surprise. In the unbroken limit, the versor  $\hat{n}$  and the SM Yukawas must leave the same  $U(2)_q$  subgroup invariant, and are therefore aligned (although no flavour violation would be generated in such a limit). In order to investigate them, we write all the  $\mathcal{G}$ -violating couplings as VEVs of flavons with irreducible  $\mathcal{G}$  quantum numbers, and assume the UV theory to contain at most one flavon of each type. The predictions that follow then depend on the structure of the flavon sector, as we now discuss.

Let us first consider the case, which we will refer to as “minimally broken”  $U(2)^5$ , in which no flavon is charged under both the quark  $U(2)^3$  and the lepton  $U(2)^2$ , or  $\mathcal{G}_l$ . In such a case one finds a precise correlation between the first two components of the unit vector  $\hat{n}$  and of the third line of the CKM matrix:  $\hat{n}_1/\hat{n}_2 = V_{td}^*/V_{ts}^*$ , up to corrections of order  $m_s/m_b$ . We then have

$$\hat{n}_{U2} \propto (c_{U2}e^{i\gamma}V_{td}^*, c_{U2}e^{i\gamma}V_{ts}^*, 1) \quad (5.4.3)$$

where  $c_{U2} \sim \mathcal{O}(1)$  and the normalisation is fixed by the condition  $|\hat{n}|^2 = 1$ . Comparing with the parametrization in Eq. (5.1.5), one gets:

$$\tan \phi = \frac{|V_{ts}|}{|V_{td}|}, \quad \tan \theta \approx c_{U2}|V_{ts}|, \quad \alpha_{bd} = -\arg(V_{td}) + \gamma, \quad \alpha_{bs} = -\arg(V_{ts}) + \gamma. \quad (5.4.4)$$

This prediction also applies in the case of  $Z'$  or  $V'$  messengers, independent on whether  $U(2)^5$  is minimally broken or not.

In the presence of flavons charged both under the quark and lepton part of the flavour group, or in the presence of more flavons with the same flavour quantum numbers, the above prediction does not need to hold. On the other hand, with reasonable assumptions on the size of the flavons, one obtains a generic correlation between the unit vector  $\hat{n}$  and the third line of the CKM matrix, which holds up to  $\mathcal{O}(1)$  factors:  $\hat{n} = (\mathcal{O}(V_{td}), \mathcal{O}(V_{ts}), \mathcal{O}(1))$ . We can parametrize such a scenario in full generality as

$$\hat{n} \propto (a_{bd}e^{i\alpha_{bd}}|V_{td}|, a_{bs}e^{i\alpha_{bs}}|V_{ts}|, 1) \quad (5.4.5)$$

where  $a_{bd}$  and  $a_{bs}$  are  $\mathcal{O}(1)$  real parameters. The area in the  $(\phi, \theta)$  plane corresponding to values  $|a_{bs, bd}| \in [0.2 - 5]$  is shown as a meshed-red one in the plots of Figs. 5.2.1, 5.3.1, 5.3.2.

The correlation in (5.4.5) is also found with different flavour groups, and in models with partial compositeness (and no flavour group). In the limit in which the top quark exchange dominates FCNC processes, the SM itself satisfies the ROFV condition, with  $\hat{n} = (V_{td}^*, V_{ts}^*, V_{tb}^*)$  also in the form above.

One comment is in order about the role of the lepton flavour sector. The latter can play a twofold role. On the one hand, it can affect the prediction for the direction of  $\hat{n}$ . This can be the case for  $S_3$  and  $U_1^\mu$  messengers, for which  $\hat{n}$  is associated to the muon row of the  $\beta$  and  $\gamma$  matrices in (5.4.2). On the other hand, the lepton flavour breaking can affect the overall size of the effect. The anomalies require in fact a breaking of  $\mu$ - $e$  lepton universality, whose size is associated to the size of  $U(2)_l$  breaking. A sizeable breaking is necessary in order to account for a NP effect as large as suggested by the  $B$ -meson anomalies. A detailed analysis of the implications of the anomalies for lepton flavour breaking and for processes involving other lepton families is outside the scope of this work.

We now focus on the case of minimally broken  $U(2)^5$ , (5.4.4). The 95%CL limit in the plane  $(\gamma, c_{U2})$ , from our global fit of  $bs\mu\mu$  clean observables and the other  $d_id_j\mu\mu$  ones (Tab. 4) is shown in Fig. 5.4.1-Left. The relevant observable in the excluded region is  $K_L \rightarrow \mu^+\mu^-$ . For positive (negative) values of  $C_+$  we obtain a limit  $c_{U2} \gtrsim -20$  ( $\lesssim 65$ ), which are well outside the natural region predicted by the flavour symmetry.

Another interesting point is that, within the parametrization (5.4.3), one has

$$R_K \approx R_\pi \quad (5.4.6)$$

up to  $\mathcal{O}(m_s/m_b)$  corrections, where:

$$R_H \equiv \frac{\text{Br}(B \rightarrow H\mu^+\mu^-)_{[1,6]}}{\text{Br}(B \rightarrow He^+e^-)_{[1,6]}} \quad (H = K, \pi) \quad (5.4.7)$$

so that a comparison between the two observables could in principle rule out, in this context, the  $V'$  and  $Z'$  cases, as well as minimally broken  $U(2)^5$ . Assuming no NP in the electron channels, we also have<sup>7</sup>:

$$R_\pi = \frac{\text{Br}(B \rightarrow \pi\mu^+\mu^-)_{[1,6]}}{\text{Br}(B \rightarrow \pi\mu^+\mu^-)_{[1,6]}^{\text{SM}}} \quad (5.4.8)$$

---

<sup>7</sup>Using the LFU ratios (5.4.7) is of course advisable from the theoretical point of view. Unfortunately, there are no measurements of  $\text{Br}(B \rightarrow \pi e^+e^-)$ , at present.

Observable	Expected sensitivity	Experiment	Reference
$R_K$	0.7 (1.7)%	LHCb 300 (50) fb <sup>-1</sup>	[163]
	3.6 (11)%	Belle II 50 (5) ab <sup>-1</sup>	[162]
$R_{K^*}$	0.8 (2.0)%	LHCb 300 (50) fb <sup>-1</sup>	[163]
	3.2 (10)%	Belle II 50 (5) ab <sup>-1</sup>	[162]
$R_\pi$	4.7 (11.7)%	LHCb 300 (50) fb <sup>-1</sup>	[163]
$\text{Br}(B_s^0 \rightarrow \mu^+ \mu^-)$	4.4 (8.2)%	LHCb 300 (23) fb <sup>-1</sup>	[163, 228]
	7 (12)%	CMS 3 (0.3) ab <sup>-1</sup>	[228]
$\text{Br}(B_d^0 \rightarrow \mu^+ \mu^-)$	9.4 (33)%	LHCb 300 (23) fb <sup>-1</sup>	[163, 228]
	16 (46)%	CMS 3 (0.3) ab <sup>-1</sup>	[228]
$\text{Br}(K_S \rightarrow \mu^+ \mu^-)$	$\sim 10^{-11}$	LHCb 300fb <sup>-1</sup>	[163, 228]
$\text{Br}(K_L \rightarrow \pi^0 \nu \nu)$	$\sim 1.8 \times 10^{-10}$	KOTO phase-I <sup>7</sup>	
	20%	KOTO phase-II <sup>7</sup>	
	20%	KLEVER	[229]
$\text{Br}(K^+ \rightarrow \pi^+ \nu \nu)$	10%	NA62 goal	[230]

TABLE 7. Future prospects for the precision reach in various flavour observables. The expected sensitivity in percent are quoted with respect to the Standard Model prediction.

The RHS of Eq. (5.4.8) is, experimentally, (cf. Table 4):

$$\frac{\text{Br}(B \rightarrow \pi \mu^+ \mu^-)_{[1,6]}^{\text{exp}}}{\text{Br}(B \rightarrow \pi \mu^+ \mu^-)_{[1,6]}^{\text{SM}}} = 0.70 \pm 0.30, \quad (5.4.9)$$

showing no tension neither with the SM prediction, nor with the  $\text{U}(2)^5$  prediction (5.4.6). Another prediction of this setup is for the branching ratio of  $B_d^0 \rightarrow \mu^+ \mu^-$  with respect to  $B_s \rightarrow \mu^+ \mu^-$ :

$$\frac{\text{Br}(B_s^0 \rightarrow \mu^+ \mu^-)}{\text{Br}(B_s^0 \rightarrow \mu^+ \mu^-)_{\text{SM}}} \approx \frac{\text{Br}(B_d^0 \rightarrow \mu^+ \mu^-)}{\text{Br}(B_d^0 \rightarrow \mu^+ \mu^-)_{\text{SM}}} \quad (5.4.10)$$

The two predictions (5.4.6) and (5.4.10) are independent on the specific chiral structure of the muon current. If the operators responsible for  $R_{K^{(*)}}$  are left-handed only, the two ratios in Eq. (5.4.10) are also predicted to be of the same size as  $R_K$  and  $R_\pi$ , up to  $\mathcal{O}(2\%)$  corrections. Such corrections are however negligible when compared to the expected precision in the measurements of these relations, which is at best of  $\approx 4\%$ , cf. 7. It is perhaps worth pointing out that the predictions in Eqs. (5.4.6, 5.4.10) are a consequence of the minimally broken  $\text{U}(2)^5$  flavour symmetry alone, independently of the ROFV assumption. This can be understood from the fact that the  $b-s$  and  $b-d$  transitions are related by  $\text{U}(2)^5$  symmetry as  $C_{S,T}^{bd}/C_{S,T}^{bs} = (V_q)^1/(V_q)^2 = V_{td}^*/V_{ts}^* = n_{U2}^1/n_{U2}^2$ , where  $V_q$  is the spurion doublet under  $\text{U}(2)_q$ .

## 5.5. Prospects

Future measurements by LHCb, Belle-II, and other experiments are expected to improve substantially the precision of most of the observables studied in the present Chapter. We collect in Table 7 the relevant prospects.

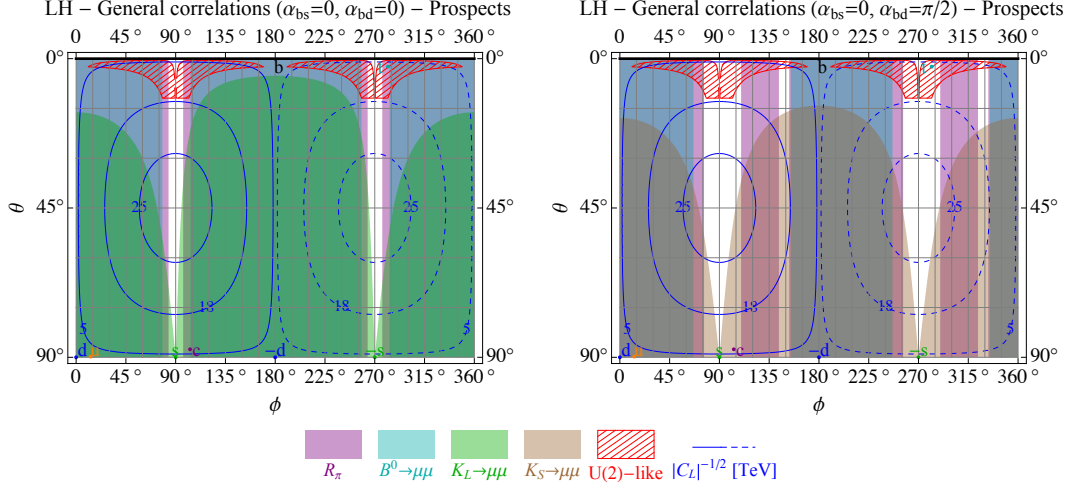


FIGURE 5.5.1. Future prospects for the exclusion limits in the plane  $(\phi, \theta)$  for two choices of the phases  $\alpha_{bs}$  and  $\alpha_{bd}$  from observables with direct correlation with  $R_{K^{(*)}}$ . For  $K_L \rightarrow \mu\mu$  we use the present bound.

First of all, the anomalous observables themselves,  $R_K$  and  $R_{K^*}$ , are expected to be tested with sub-percent accuracy by LHCb with  $300\text{fb}^{-1}$  of luminosity. Furthermore, a larger set of observables sensitive to the same partonic transition  $b \rightarrow s\mu^+\mu^-$  will be measured (such as  $R_\phi$ ,  $R_{pK}$  and  $Q_5$  for example [163]). This will allow to confirm or disprove the present anomalies and to pinpoint the size of the New Physics contribution with high accuracy.

The leptonic decays  $B_{(d,s)}^0 \rightarrow \mu^+\mu^-$  will be crucial for discriminating between the  $\mathcal{O}_9$  and  $\mathcal{O}_L$  scenarios. As to the  $B \rightarrow \pi\ell^+\ell^-$  channels, we note that the power of the muon-specific  $\text{Br}(B^+ \rightarrow \pi^+\mu^+\mu^-)$  as a probe of NP is, already at present, limited by theoretical uncertainties [196]. The situation improves substantially for the LFU ratio  $R_\pi$  (cf. Eq. (5.4.7)), for which, as already noted,  $U(2)^5$  flavour symmetry predicts  $R_\pi = R_K$  and for which LHCb is expected to reach a  $\sim 4.7\%$  sensitivity with  $300\text{fb}^{-1}$  of luminosity [163]. As can be seen in Fig. 5.5.1, these channels will be able to cover almost the complete parameter space of the setup studied here, particularly if the phase  $\alpha_{bd}$  is small.

In all cases where  $C_S \neq C_T$ , such as in the  $S_3$  and  $Z'$  models, other relevant channels which will improve substantially in sensitivity are  $\text{Br}(K^+ \rightarrow \pi^+\bar{\nu}\nu)$  and  $\text{Br}(K_L \rightarrow \pi^0\bar{\nu}\nu)$ . The former is expected to be measured with a 10% accuracy by NA62 [230] in the next few years, while, for the latter, the KOTO experiment at JPARC [107] should reach a single-event sensitivity at the level of the SM branching ratio, with a signal to background ratio  $\sim 1$ , which translates to a projected 95%CL limit of  $\sim 5.4$  times the SM value, i.e.  $\sim 1.8 \times 10^{-10}$ . A possible future upgrade of the whole KOTO experiment (stage-II)<sup>8</sup>, or the proposed KLEVER experiment at CERN SPS [229], could both reach a  $\sim 20\%$  sensitivity of the  $\text{Br}(K_L \rightarrow \pi^0\bar{\nu}\nu)$  SM value. An example for the prospects due to these

<sup>8</sup>From a CERN EP seminar given in February 2019 (slides at [https://indico.cern.ch/event/799787/attachments/1797668/2939627/EPSeminar\\_YuChen.pdf](https://indico.cern.ch/event/799787/attachments/1797668/2939627/EPSeminar_YuChen.pdf)) and of a talk presented at the Rencontres de Moriond 2019 (slides at [http://moriond.in2p3.fr/2019/EW/slides/1\\_Sunday/1\\_morning/5\\_Nanjo.pdf](http://moriond.in2p3.fr/2019/EW/slides/1_Sunday/1_morning/5_Nanjo.pdf)).

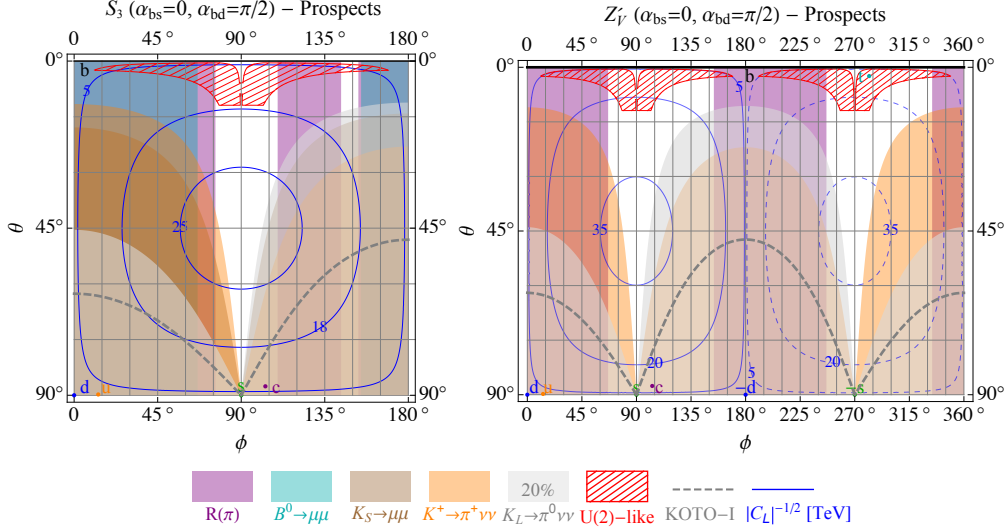


FIGURE 5.5.2. Future prospects for the exclusion limits in the  $(\phi, \theta)$  plane for the scalar leptoquark  $S_3$  (left) and the vector singlet  $Z'$  with vector-like couplings to muons (right), for a choice of phases. The orange and gray regions correspond to the future expected limits from  $K^+ \rightarrow \pi^+ \nu \nu$  (NA62 [230]) and  $K_L \rightarrow \pi^0 \nu \nu$  (KLEVER [229] or KOTO phase-II), respectively. The dashed gray line corresponds to the expected limit on  $K_L \rightarrow \pi^0 \nu \nu$  from KOTO phase-I.

observables for a particular choice of phases in the two simplified models are shown in Fig. 5.5.2.

## 5.6. Conclusions

If the flavor anomalies in  $b \rightarrow s \mu \mu$  transitions are experimentally confirmed, they will provide important information about the flavor structure of the underlying New Physics. The latter can be tested by studying possible correlations with other measurements in flavor physics. In this Chapter we assumed that the putative NP, responsible for the anomalous effects, couples to SM left-handed down quarks in such a way to generate a rank-one structure in the novel flavor-violating sector. We dub such a scenario *Rank-One Flavor Violation* (ROFV). Such a structure can result from a number of well motivated UV completions for the explanation of the flavor anomalies, in which a single linear combination of SM quark doublets couples to the relevant NP sector. This automatically includes all single-leptoquark models, and models where LH quarks mix with a single vector-like fermion partner. As these examples reveal, the ROFV condition might not originate from symmetry but rather as a feature of the UV dynamics.

Varying the direction associated to the NP ( $\hat{n}$ ) in  $U(3)_q$  flavor space, we identified the most important observables that can be correlated to the flavor anomalies. The more model-independent correlations are with  $d_i \rightarrow d_j \mu \mu$  transitions (and their crossed symmetric processes). A large part of the parameter space is probed by the measurement of the branching ratio of  $B^+ \rightarrow \pi^+ \mu \mu$ . While the sensitivity to NP effects in this channel is limited by the large hadronic uncertainty of the SM prediction, future measurements of



the theoretically clean ratio  $R_\pi$  are going to provide further information on  $b \rightarrow d$  flavor violations. Among the transitions involving the first two generations of quarks ( $s \rightarrow d$ ), the  $K_L \rightarrow \mu\mu$  decay rate has a major impact and it is particularly sensitive to the phases of our parametrization. Unfortunately, future prospects in this channel are limited by theory uncertainties in the SM prediction of the long-distance contribution to the decay. A sizeable improvement by LHCb is instead expected in the limit on the  $K_S \rightarrow \mu\mu$  decay rate.

While the former conclusions rely only on our rank-one hypothesis, more model dependent correlations can be established once the relevant effective operators are embedded into the SMEFT or in the presence of specific mediators. An example of such correlations is given by  $d_i \rightarrow d_j \nu\nu$  processes, and we have in fact shown that present data from  $K^+ \rightarrow \pi^+ \nu\nu$  are particularly relevant to the leptoquark  $S_3$  or vector  $Z'$  simplified models.

From a more theoretical point of view, we investigated whether the flavor violation associated to the NP can be connected to the one present in the SM Yukawa sector. A generic expectation is that the leading source of  $U(3)_q$  breaking in the NP couplings is provided by a direction in flavor space close to the one identified by the top quark. Indeed, we showed in a concrete example based on a flavor symmetry that the vector  $\hat{n}$  turns out to be correlated to the third line of the CKM matrix, as in Eq. (5.4.5). Remarkably, a large portion of the theoretically favoured region (red meshed lines region in our plots) survive the bounds from current flavor physics data. Our order of magnitude predictions can be narrowed down under further theoretical assumptions. For example a minimally broken  $U(2)^5$  flavor symmetry predicts  $R_K = R_\pi$  and the ratio  $\text{Br}(B_s \rightarrow \mu\mu)/\text{Br}(B_d \rightarrow \mu\mu)$  to be SM-like (up to small corrections of a few percent).

In our last section we explored future prospects for the exclusion limits in the ROFV framework. In the near future a series of experiments will be able to cover almost all of the parameter space identified by our ansatz. Indeed, in the next few years, significant information will be provided by the NA62 and KOTO experiments, thanks to precise measurements of the  $K^+ \rightarrow \pi^+ \nu\nu$  and  $K_L \rightarrow \pi^0 \nu\nu$  decays, while on a longer time scale results from LHCb and Belle II will almost completely cover our parameter space (and test the minimally broken  $U(2)^5$  model).

A confirmation of the  $B$ -meson anomalies would open a new era in high energy physics. In this enticing scenario, studying correlations of the anomalies to other observables would provide a powerful mean to investigate the flavor structure of New Physics.

## Part 3

# Explaining the SM flavour structure

## CHAPTER 6

### The SM flavour puzzle

Providing a theoretical explanation for the peculiarities observed in the SM fermion mass spectra and mixing patterns is arguably one of the greatest challenges of modern Particle Physics. What determines the mass hierarchies between the three families of charged fermions (quarks and charged leptons)? What is the nature of neutrino masses, and why are they so small? How do the quark and lepton mixing patterns, embodied by the CKM and PMNS matrices respectively, originate? These and many other questions constitute the so-called SM flavour puzzle. This introductory Chapter provides an overview of the various subproblems of which the SM flavour puzzle is composed.

#### 6.1. Pieces of the puzzle

The SM as it stands has a fairly high number of tunable inputs, both at the discrete and continuous levels. Although many of these are univocally fixed by experiment<sup>1</sup>, from a BSM perspective one has the hope that, at a sufficiently high scale, the relevant SM UV completion will provide theoretical explanations for at least some of the patterns observed at low energies. This kind of theoretical prejudice, when applied to the SM fermionic matter content, motivates what is known as the SM flavour puzzle [14].

At the discrete level, SM fermions are characterized by their representation under the SM gauge group, which is a direct sum of fifteen irreducible representations. Out of these, there are five inequivalent representations,  $q$ ,  $u$ ,  $d$ ,  $\ell$  and  $e$  (cf. Table 1), each of which is repeated exactly three times. For this reason, the SM fermionic matter content is usually depicted as being constituted by a certain number (which happens to be three) of repetitions of a single reducible representation, which is referred to as a “family”, or “generation”.

At the continuous level, flavour gets its shape from the Yukawa part of the SM lagrangian:

$$\mathcal{L}_{\text{SM}}^{\text{yuk}} = -(y_U)_{ij} \bar{q}_i \tilde{H} u_j - (y_D)_{ij} \bar{q}_i H d_j - (y_E)_{\alpha\beta} \bar{\ell}_\alpha H e_\beta + \text{h.c.}, \quad (6.1.1)$$

which gives rise to quark masses and mixings, and lepton masses (such a description is clearly insufficient for any phenomenological discussion of lepton flavour, as discussed below). The following two Subsections separately describe the flavour structures of the quark and lepton sectors.

**6.1.1. Quark sector.** Following the conventions of Sec. 3.1, without loss of generality, we can use the so-called “down-quark mass basis” of SM quark fields, in which (cf. Eq. (3.1.4)):

---

<sup>1</sup>A well recognized exception is the QCD  $\theta$  angle, for which only an upper bound exists [53].

$$y_D = \frac{1}{v} \text{diag}(m_d, m_s, m_b), \quad y_U = \frac{1}{v} V^\dagger \text{diag}(m_u, m_c, m_t). \quad (6.1.2)$$

Here  $m_\bullet$  are the quark running masses at the electroweak scale  $v$ , and  $V$  is the CKM matrix in the standard phase convention.

All quark masses but the top's one,  $m_t \sim v$ , are well below the electroweak scale. In terms of quark-Higgs couplings, we have  $y_t \sim \mathcal{O}(1)$ , whereas the remaining couplings are all suppressed by several orders of magnitudes. Some approximate values for  $m_\bullet/m_t$  (or equivalently  $y_\bullet/y_t$ ) are [9]:

$$\frac{1}{m_t} (m_d, m_s, m_b) \approx (2.9 \times 10^{-5}, 5.8 \times 10^{-4}, 2.6 \times 10^{-2}), \quad (6.1.3)$$

$$\frac{1}{m_t} (m_u, m_c, m_t) \approx (1.3 \times 10^{-5}, 7.8 \times 10^{-3}, 1). \quad (6.1.4)$$

Both down and up quark mass spectra are hierarchical, with a further overall suppression of third and second generation down quark masses relative to up quark ones.

Intriguing patterns are also observed in the quark mixing matrix  $V$ . These are most transparently illustrated in the Wolfenstein parametrization of the CKM matrix [9], *viz.*:

$$V = \begin{pmatrix} 1 - \frac{\lambda^2}{2} & \lambda & A\lambda^3(\rho - i\eta) \\ -\lambda & 1 - \frac{\lambda^2}{2} & A\lambda^2 \\ A\lambda^3(1 - \rho - i\eta) & -A\lambda^2 & 1 \end{pmatrix} + \mathcal{O}(\lambda^4), \quad (6.1.5)$$

where the Wolfenstein parameters are defined by:

$$\lambda \equiv \frac{|V_{us}|}{\sqrt{|V_{ud}|^2 + |V_{us}|^2}} \approx 0.22, \quad (6.1.6)$$

$$A \equiv \frac{|V_{cb}|}{\lambda |V_{us}|} \approx 0.83, \quad (6.1.7)$$

$$\rho + i\eta \equiv \frac{V_{ub}^*}{A\lambda^3} \approx 0.15 + 0.36i. \quad (6.1.8)$$

It is seen that non-diagonal entries, which govern the strength of  $u_i \rightarrow W^+ d_j$  and  $d_j \rightarrow W^- u_i$  transitions between different quark generations, are suppressed by powers of  $\lambda$  as follows:

$$1 \leftrightarrow 2 \sim \lambda, \quad 2 \leftrightarrow 3 \sim \lambda^2, \quad 3 \leftrightarrow 1 \sim \lambda^3. \quad (6.1.9)$$

Notice that  $\lambda$  can be identified with the Cabibbo sine, for which the well-known numerical relationship [231]:

$$\lambda \approx \sqrt{\frac{m_d}{m_s}}, \quad (6.1.10)$$

holds at the percent level.

To conclude, we remark that the quark flavour structure is (at least phenomenologically) fully accounted by the SM lagrangian (cf. Eq. (6.1.1)), and that quark running masses and CKM matrix elements can be either computed or experimentally determined with relatively high accuracy, so that the corresponding uncertainties often play little role in BSM discussions addressing the origins of quark flavour. We now turn to lepton

flavour, which presents important qualitative differences with respect to the quark case discussed so far.

**6.1.2. Lepton sector.** In contrast to quark flavour, lepton flavour is in large part a BSM issue. On the one hand, the SM can account, through its Yukawa couplings (6.1.1), for massive charged lepton and massless, left-handed neutrinos, whose mass and flavour eigenstates can be made to coincide. On the other one, it is an experimental fact that neutrinos have non-zero masses, and that their mass eigenstates are linear combinations of flavour eigenstates. Therefore, in order to discuss the experimental data on neutrino flavour, we need to move a step beyond the pure SM description and take a phenomenological approach.

Neutrino oscillation experiments measure neutrino squared mass (absolute) differences and mixing angles. Most of the experimental results can be coherently interpreted in the context of three light active neutrinos and CPT invariance [232], which we assume in what follows. Two standard independent mass differences are:

$$\delta m^2 = m_2^2 - m_1^2, \quad (6.1.11)$$

$$\Delta m^2 = m_3^2 - \frac{m_1^2 + m_2^2}{2}, \quad (6.1.12)$$

where  $m_{1-3}$  are neutrino masses in the usual labeling conventions [9]<sup>2</sup>; notice that  $\Delta m^2$  is positive (negative) for a mass spectrum with normal (inverted) ordering. The measured mixing angles can be explained in terms of a  $3 \times 3$  mixing matrix intervening in  $l_i^- W^+ \rightarrow \nu_j$ , the so called PMNS matrix  $U$ , defined by:

$$\mathcal{L}_{CC} = -\frac{g}{\sqrt{2}} W_\rho^+ (\bar{e}_L, \bar{\mu}_L, \bar{\tau}_L) \gamma^\rho U (\nu_1, \nu_2, \nu_3)^T. \quad (6.1.13)$$

The standard parametrization of  $U$ , *viz.*:

$$U = \begin{pmatrix} 1 & 0 & 0 \\ 0 & c_{23} & s_{23} \\ 0 & -s_{23} & c_{23} \end{pmatrix} \begin{pmatrix} c_{13} & 0 & s_{13}e^{-i\delta} \\ 0 & 1 & 0 \\ -s_{13}e^{i\delta} & -s_{23} & c_{13} \end{pmatrix} \begin{pmatrix} c_{12} & s_{12} & 0 \\ -s_{12} & c_{12} & 0 \\ 0 & 0 & 1 \end{pmatrix} \begin{pmatrix} e^{i\eta_1} & 0 & 0 \\ 0 & e^{i\eta_2} & 0 \\ 0 & 0 & 1 \end{pmatrix}, \quad (6.1.14)$$

is defined in terms of three mixing angles  $\theta_{12}$ ,  $\theta_{13}$  and  $\theta_{23}$ , a “Dirac” phase  $\delta$  and two “Majorana” phases  $\eta_{1,2}$ . Majorana phases are well-defined only if neutrinos are Majorana particles [9], since otherwise these phases can always be reabsorbed in the definition of the mass eigenstate fields; moreover, neutrino oscillation experiments are insensitive to  $\eta_{1,2}$  [233].

Currently, the mass differences  $\delta m^2$  and  $\Delta m^2$ , and the three mixing angles  $\theta_{12}$ ,  $\theta_{13}$  and  $\theta_{23}$  have been measured with percent-level accuracy, whereas there is still large ( $\mathcal{O}(10\% - 15\%)$ ) uncertainty on the Dirac phase  $\delta$ . We collect these observables in the lower part of Tab. 1 for the two ordering cases. The upper part of the Table reports

---

<sup>2</sup>In the standard convention,  $m_1$  and  $m_2$  are defined to be the mass eigenstates with smallest mass difference  $|m_2 - m_1|$ , with  $m_1 < m_2$ . Labeling the remaining eigenstate as  $m_3$ , there are two possibilities: either  $m_1 < m_2 < m_3$  or  $m_3 < m_1 < m_2$ , which correspond to a normal and inverted ordered mass spectrum, respectively.

Observable	Best-fit value with $1\sigma$ error	
$m_e/m_\mu$	$0.0048^{+0.0002}_{-0.0002}$	
$m_\mu/m_\tau$	$0.0565^{+0.0045}_{-0.0045}$	
	NO	IO
$\delta m^2 [10^{-5} \text{ eV}^2]$	$7.42^{+0.21}_{-0.20}$	
$\Delta m^2 [10^{-3} \text{ eV}^2]$	$2.480^{+0.026}_{-0.028}$	$-2.461^{+0.028}_{-0.028}$
$r \equiv \delta m^2 /  \Delta m^2 $	$0.0299^{+0.0009}_{-0.0009}$	$0.0301^{+0.0009}_{-0.0009}$
$\sin^2 \theta_{12}$	$0.304^{+0.012}_{-0.012}$	$0.304^{+0.013}_{-0.012}$
$\sin^2 \theta_{13}$	$0.02219^{+0.00062}_{-0.00063}$	$0.02238^{+0.00063}_{-0.00062}$
$\sin^2 \theta_{23}$	$0.573^{+0.016}_{-0.020}$	$0.575^{+0.016}_{-0.019}$
$\delta/\pi$	$1.09^{+0.15}_{-0.13}$	$1.57^{+0.14}_{-0.17}$

TABLE 1. Best-fit values of the charged lepton mass ratios and the neutrino oscillation parameters with the corresponding  $1\sigma$  errors. For the charged lepton mass ratios we have used the values given in ref. [234], averaged over  $\tan\beta$  as described in the text, whereas for the neutrino parameters we have used the results obtained in refs. [41, 76] (with Super-Kamiokande atmospheric data).

the ratios of running lepton masses at the GUT scale<sup>3</sup>. A number of lepton flavour observables is still unknown:

- The neutrino mass ordering (normal vs. inverted). A preference (currently at the level of about  $3\sigma$ ) for a normal mass ordering is starting to emerge from data [232], but is still far from conclusive evidence.
- The absolute scale of neutrino masses. Since neutrino oscillation experiments only measure squared mass differences, they give no direct information on the absolute values of neutrino masses. At present, the tightest upper bound on the sum of neutrino masses is the one from cosmology [9]:

$$\sum_i m_i < 0.12 \div 0.68 \text{ eV} \quad (6.1.15)$$

- The Majorana phases, if neutrinos are Majorana particles.

The picture which emerges from Tab. 1 is quite distinct from the one found in the quark sector. While charged lepton masses are hierarchical as the quark ones (and indeed comparable in size with those of down quarks), it is not clear whether the same holds for the neutrino spectrum, and, most importantly, neutrino masses are several order of magnitudes smaller than the ones of all other SM fermions. Also, the PMNS mixing matrix is radically different from its quark counterpart: while the CKM matrix is close to diagonal, with mixing angles  $\theta_{12}^{\text{CKM}}$ ,  $\theta_{23}^{\text{CKM}}$  and  $\theta_{13}^{\text{CKM}}$  suppressed by  $\lambda$ ,  $\lambda^2$  and  $\lambda^3$  respectively (cf. Eq. (6.1.5)), two of the three PMNS mixing angles are seen to be  $\mathcal{O}(1)$ . All these features strongly suggest that the mechanisms behind the generation

<sup>3</sup>We remark that such ratios have very weak scale dependencies, so that the precise scale is largely irrelevant for the purpose of our discussion. We follow Ref. [43] and employ the updated GUT scale determination [234] for these quantities.

of lepton and, in particular, neutrino masses and mixings are quite different from the corresponding ones underlying the quark sector.

To conclude (compare with the conclusions of Subsec. 6.1.1), we remark that our low-energy description of lepton flavour is necessarily of phenomenological kind, and the simple framework of three light active neutrinos with PMNS mixing provides a perfectly valid explanation of experimental data. Such a description has some important unknowns, most prominently the neutrino mass ordering, the absolute scale of neutrino masses and the two Majorana phases if neutrinos are Majorana particles.

## 6.2. Theoretical ideas

It is a widespread position that the special features of the SM fermionic spectrum discussed in the previous Section strongly suggests the existence of some non-trivial high-energy mechanism, or mechanisms, from which they would result in a natural way. This is, indeed, the essence of the SM flavour puzzle, which, according to our previous description, can be decomposed into a series of subproblems:

- (1) *Explaining the SM fermionic representation.* This includes the basic representation (*i.e.*  $q \oplus u \oplus d \oplus \ell \oplus e$ ) of a single SM family, and the actual number (three) of replicæ of this representation.
- (2) *Explaining quark masses and mixings.* What especially calls for a theoretical explanation are the hierarchies in down and up quark mass spectra, the overall down *vs.* up mass suppression, and the suppression and hierarchies in CKM matrix off-diagonal terms. Moreover, a natural question is whether (some of) these features are interconnected (see *e.g.* Eq. (6.1.10)).
- (3) *Explaining lepton masses and mixings.* Here, the most salient features are the hierarchies in the charged lepton mass spectrum, the huge suppression of neutrino masses and the structure of the PMNS matrix, with two large and one small mixing angles. There is also a possible hint to a hierarchy in the solar-to-atmospheric ratio  $r \equiv \delta m^2 / \Delta m^2 \approx 0.03$ <sup>4</sup>.

All these questions have inspired for a long time many theoretical investigations. Without any attempt at completeness (for a more comprehensive review, see *e.g.* [232] and references therein), let us cite some of the most prominent ideas which have been put forward on the various fronts.

**Grand Unification.** [235] One of the main appeals of Grand Unified Theories (GUTs) is their potential to explain the SM basic representation in terms of a few (ideally a single one) irreducible representations of the unification group. To cite a classical example, the SM basic representation can be embedded into a single spinorial representation of SO(10): the latter decomposes under the electroweak group into the five irreducible

---

<sup>4</sup>One should however realize that such a ratio is, in some sense, a small quantity by construction. For instance, performing the simple experiment of generating three neutrino masses uniformly at random in a fixed interval (say  $[0, 1]$ ), I find that  $\approx 25\%$  of the times  $r < 0.1$ ; with a positive gaussian and an exponential distribution, instead, the first quantiles of the  $r$  distribution are found for  $r \lesssim 0.07$  and  $r \lesssim 0.05$ , respectively. Clearly, these numbers indicate that the parameter space region producing a solar-to-atmospheric ratio as small as its actual value might not be small at all, depending on the particular measure adopted (cf. also the remarks at the end of the next Section).

representations of quarks and leptons, with an additional SM singlet, which can be identified with a singlet “sterile” neutrino. As the latter can in principle take part in the see-saw mechanism for generating neutrino masses (see below), this example also shows how the solutions of different parts of the flavour puzzle may well be interconnected.

**Flavour symmetries.** The theoretical reach of flavour symmetries spans from the explanation of the horizontal structure of the SM fermion content (*i.e.* the existence of three identical generations), to the prediction of mass and mixing hierarchies. For example, in the Froggatt-Nielsen mechanism [236], the hierarchies in quark masses and mixings originate from the soft spontaneous breaking of a  $U(1)_{\text{FN}}$  global symmetry, under which quark fields are charged. Also discrete flavour symmetries have been used extensively to address the SM flavour structures, in particular in the lepton sector, since the PMNS mixing structure is more straight-forwardly reproduced (or approximated) within this context [14].

**Accidental symmetries.** These class of symmetries is, conceptually, very different from the postulated flavour symmetries discussed in the previous point. Accidental symmetries are usually enforced by structural requirements such as gauge invariance and renormalizability. A particularly relevant example is provided by the  $U(1)_\ell$  global symmetry of the renormalizable SM, whose conserved charge is total lepton number. This symmetry implies, in particular, that SM neutrinos are massless at the renormalizable level, which is clearly a good leading order approximation; from a SMEFT point of view, neutrino mass generation is post-poned to dimension five, through the Weinberg operator (1.1.8), which can be originated at tree-level in models realizing one of the three types of See-Saw mechanisms [237]<sup>5</sup>. The general approach to fermion masses and mixings using accidental symmetries was originally proposed in Ref. [239].

**Special field theory frameworks.** Some of the features of the SM flavour structure might be enforced by a structural property of a class of SM extensions. For example, in (type II) Two Higgs Doublet Models (and, in particular, in the Supersymmetric SM), the large  $m_t/m_b$  ratio can be “explained” by a large  $v_u/v_d$  ratio (*i.e.* a large  $\tan\beta$ ), where  $v_{u,d}$  are the electroweak breaking expectation values of the up and down Higgses  $H_{u,d}$ , respectively. Even though at a first glance this might appear to be a vacuous explanation (after all, we exchange a large ratio,  $m_t/m_b$ , for a similarly large one,  $v_u/v_d$ ), notice that we have managed to transform the  $m_t/m_b$  problem into a dynamical one, since the Higgs expectation values are now controlled by the model’s scalar potential. Another special framework which can shed light on the  $m_t/m_b$  ratio is that of partial compositeness [240], if the  $t$ -quark has a significantly higher degree of compositeness than the other quarks.

---

<sup>5</sup>A simple minded SM extension with a (type I) See-Saw mechanism consists of the SM itself with the addition of three singlet right-handed fermions  $N_{1,2,3}$  with a large Majorana mass term  $M_{\alpha\beta}$ . The relevant terms in the model’s lagrangian are:

$$\mathcal{L} \supset -(y_N)_{\alpha\beta} \bar{\ell}_\alpha \tilde{H} N_\beta - \frac{M_{\alpha\beta}}{2} \bar{N}_\alpha^c N_\beta,$$

which, after integrating out the heavy singlets  $N$ , give rise to the Weinberg operator with Wilson coefficient  $C \sim \mathcal{O}(y_N^2 v^2/M)$ . If  $y_N$  has  $\mathcal{O}(1)$  singular values, the resulting neutrino masses turn out to be in the  $\text{meV} \div \text{eV}$  range if the  $M$  eigenvalues lie around the GUT scale. Unfortunately, the singlets’ Majorana mass term also has the side effect of destabilizing the electroweak scale, making the model incur in the (in)famous hierarchy problem [238].



**Anarchy.** Completely at odds with the approaches mentioned so far, one could argue that there is, in fact, no organizing principle underlying the SM flavour structure. This idea has been formalized in the context of neutrino mixing using a probabilistic/measure theoretic approach [241–245]. Even though such a position can be under many respects less appealing than the more theoretically driven approaches previously mentioned, one must concede that the lack of strong hierarchies in the PMNS mixing matrix (except perhaps for the small  $\theta_{13}$  angle) and, possibly, in the neutrino mass spectrum, provides a logical motivation for it (on the other hand, I find the same position hard to maintain when applied as a whole to the SM flavour puzzle).

The common denominator to all the frameworks mentioned in the previous Section (including, to a certain extent, also Anarchy) is *Naturalness*, in the sense that for the models in question there exists a reasonably large parameter space region for which the special (discrete or continuous) phenomenological features of SM flavour are realized. Furthermore, the examples also illustrate how the SM flavour puzzle is entangled with other theoretical enigmas surrounding the SM, gauge coupling unification and the Higgs mass hierarchy problem being just a few, to a degree which depends on the particular theoretical framework. A solution to the former might also shed light on some of these further fundamental questions.

## CHAPTER 7

### Are lepton masses modular forms?

Modular invariance has recently emerged in the context of neutrino physics [43]<sup>1</sup>, as a powerful generalization of discrete linear symmetry. In supersymmetric modular invariant models, the action is invariant under a non-linear realization of the  $SL(2, \mathbb{Z})$  group, which is inevitably broken by the vacuum expectation value of a superfield, the *modulus*  $\tau$ . The latter is acted on by the modular group by linear fractional transformations:

$$\tau \mapsto \frac{a\tau + b}{c\tau + d} \quad (a, b, c, d \in \mathbb{Z}, \quad ad - bc = 1), \quad (7.0.1)$$

and, by modular invariance, couplings of chiral fields (which transform non-linearly under  $SL(2, \mathbb{Z})$ ) must be functions of the modulus  $\tau$  with well-defined transformation properties under the modular group.

Specifically, supersymmetry forces the (holomorphic) superpotential couplings to be modular forms of  $SL(2, \mathbb{Z})$ , which, at a fixed level  $N$  of the principal congruence subgroup employed in the model's construction, form a linear space of finite dimension. This fact, combined with superpotential non-renormalization theorems [246], highly constrains the superpotential part of the supersymmetric action, which is bound to depend upon a reduced set of couplings, in addition to the complex expectation value of  $\tau$ . Such a strict determination significantly enhances the predictive power of this class of models, which goes without saying it is of the greatest importance for the task of explaining the SM flavour structure.

This Chapter presents results from my work [47] with F. Feruglio, A. Romanino and A. Titov, in which we attempt to address charged lepton mass hierarchies through modular invariance. We propose that the hierarchies might originate from a residual  $\mathbb{Z}_4$  symmetry subgroup of the full modular group, which is exact at the symmetric point  $\tau = i$ , and whose breaking is governed by the (assumed small) departure  $\tau - i$ . In fact, earlier model building attempts [43, 247–257] have shown that, for several modular invariant models of lepton flavour, a good agreement with experimental data is obtained in the neighbourhood of  $\tau \approx i$ , with deviation  $|\tau - i| \sim \mathcal{O}(10^{-2} \div 10^{-1})$ , and somewhat independently of the actual levels  $N$  and specific lepton field representations. This phenomenological observation led us to investigate in greater detail the structure of modular invariant theories in the symmetric limit, in which one of the two generators of the modular group, as well as the  $CP$  (charge-parity conjugation) generator, are not broken, and to point out some of its consequences for model building.

A second motivation for our work was to generalize the previous investigations by allowing for non-minimal terms in the model's Kähler potential: as a matter of fact, in most

---

<sup>1</sup>The title of this Chapter is a generalization to the question “Are neutrino masses modular forms?”, posed by the seminal paper [43].

of the literature a certain “minimal” form of Kähler potential is assumed without special mention; such a form arises, in fact, in certain string theory compactifications in the large volume limit, that is  $\text{Im}\tau \rightarrow \infty$  (see, e.g. [258, 259] and references therein), which however contradicts the findings of explicit model building attempts discussed so far. For  $\tau \approx i$ , the minimal Kähler potential can in principle receive large non-perturbative corrections, so that the original assumption appears to be somewhat unjustified. This is actually very relevant also from a low-energy point of view, since, in contrast to the superpotential, the Kähler potential does not have any holomorphicity or no-renormalization constraint, and it is in fact easy to show that modular invariance alone allows for an infinite number of functionally independent contributions to the Kähler metric of any chiral field.

If the Kähler potential is regarded to as completely arbitrary, much of the predictive power mentioned previously gets apparently lost. On the other hand, as we illustrate in Ref. [47] through explicit models, some *qualitative* predictions of the minimal models continue to be valid also in the presence of Kähler corrections, as long as the latters are at most  $\mathcal{O}(1)$  modifications of the minimal potential. In our special case, we are particularly concerned with charged lepton mass hierarchies, whose size turns out to be essentially governed by the soft breaking of  $\mathbb{Z}_4$  symmetry in the neighbourhood of  $\tau \approx i$ .

### 7.1. Modular invariant models

In the simplest case, modular invariance arises from the compactification of a higher dimensional theory on a torus or an orbifold. Size and shape of the compact space are parametrised by a modulus  $\tau$  living in the upper-half complex plane, up to modular transformations. These can be interpreted as discrete gauge transformations, related to the redundancy of the description. The low-energy effective theory, relevant to the known particle species, has to obey modular invariance and Yukawa couplings become functions of  $\tau$ . In this section we shortly review the formalism of supersymmetric modular invariant theories [260, 261] applied to flavour physics [43].

The theory depends on a set of chiral supermultiplets  $\varphi$  comprising the dimensionless modulus  $\tau \equiv \varphi_0/\Lambda$  ( $\text{Im } \tau > 0$ ) and other superfields  $\varphi_i$  ( $i \geq 1$ ). Here  $\Lambda$  represents the cut-off of our effective theory, and can be interpreted as the relevant mass scale of an underlying fundamental theory. In the case of rigid supersymmetry, the Lagrangian  $\mathcal{L}$ <sup>2</sup> is fully specified by the Kähler potential  $K(\varphi, \bar{\varphi})$ , a real gauge-invariant function of the chiral multiplets and their conjugates, by the superpotential  $W(\varphi)$ , a holomorphic gauge-invariant function of the chiral multiplets, and by the gauge kinetic function  $f(\varphi)$ , a dimensionless holomorphic gauge-invariant function of the chiral superfields. Neglecting gauge interactions, we have:

$$\mathcal{L} = \int d^2\theta d^2\bar{\theta} K(\varphi, \bar{\varphi}) + \int d^2\theta W(\varphi) + \int d^2\bar{\theta} \bar{W}(\bar{\varphi}).$$

---

<sup>2</sup>Up to terms with at most two derivatives in the bosonic fields.

The Lagrangian is invariant under transformations  $\gamma$  of the homogeneous modular group  $\Gamma = \text{SL}(2, Z)$ :

$$\tau \rightarrow \frac{a\tau + b}{c\tau + d}, \quad \varphi_i \rightarrow (c\tau + d)^{-k_i} \rho(\tilde{\gamma})_{ij} \varphi_j \quad (i, j \geq 1) \quad (7.1.1)$$

where  $a, b, c, d$  are integers obeying  $ad - bc = 1$ . Such transformations are generated by the two elements of  $\Gamma$ :

$$S = \begin{pmatrix} 0 & 1 \\ -1 & 0 \end{pmatrix} \quad \text{and} \quad T = \begin{pmatrix} 1 & 1 \\ 0 & 1 \end{pmatrix}. \quad (7.1.2)$$

The matrix  $\rho(\tilde{\gamma})$  is a unitary representation of the group  $\Gamma_N = \Gamma/\Gamma(N)$ , obtained as a quotient between the group  $\Gamma$  and a principal congruence subgroup  $\Gamma(N)$ , the positive integer  $N$  being the level of the representation. The level  $N$  is kept fixed in the construction, and  $\tilde{\gamma}$  represents the equivalence class of  $\gamma$  in  $\Gamma_N$ . In general  $\rho(\tilde{\gamma})$  is a reducible representation and all superfields belonging to the same irreducible component should have the same weight  $k_i$ , here assumed to be integer<sup>3</sup>. In the following, we denote by  $(\varphi_i, \psi_i)$  the spin-(0, 1/2) components of the chiral superfields  $\varphi_i$  ( $i \geq 1$ )<sup>4</sup>. The terms bilinear in the fermion fields read [264]:

$$\mathcal{L}_F = \mathcal{L}_{F,K} + \mathcal{L}_{F,2}, \quad (7.1.3)$$

with <sup>5</sup>:

$$\mathcal{L}_{F,K} = i K_i^j \bar{\psi}_j \bar{\sigma}^\mu D_\mu \psi^i, \quad \mathcal{L}_{F,2} = -\frac{1}{2} [W_{ij} - W_l (K^{-1})_m^l K_{ij}^m] \psi^i \psi^j + \text{h.c.}, \quad (7.1.4)$$

where lower (upper) indices in  $K$  and  $W$  stand for derivatives with respect to holomorphic (anti-holomorphic) fields. When the scalar fields in eq. (7.1.4) take their VEVs, we can move to the basis where matter fields are canonically normalised, through a transformation:

$$\psi_i \rightarrow (z^{-1/2})_{ij} \psi_j, \quad (7.1.5)$$

where the matrix  $(z^{1/2})_{ij}$  satisfies:  $K_i^j = [(z^{1/2})^\dagger]^{jl} (z^{1/2})_{li}$ <sup>6</sup>. We can identify the fermion mass matrix as:

$$m_{kn} = [W_{ij} - W_l (K^{-1})_m^l K_{ij}^m] (z^{-1/2})_{ik} (z^{-1/2})_{jn} \quad (7.1.6)$$

where VEVs are understood. In the previous equation, the second term in the square bracket vanishes when supersymmetry is unbroken and the VEV of  $W_l$  is zero. When we turn on supersymmetry breaking effects, the first term is expected to dominate over the second one, provided there is a sufficient gap between the sfermion masses  $m_{\text{SUSY}}$  and the messenger/cutoff scale  $M$ . This holds both for vector-like and for chiral fermions. Indeed, up to loop factors or other accidental factors, the VEVs of  $W_l$ ,  $W_{ij}$  and  $K_{ij}^m$  are of the order of  $m_{\text{SUSY}} M$ ,  $M$  and  $1/M$ , respectively, when fermions are vector-like. When chiral fermions are considered,  $W_{ij}$  and  $K_{ij}^m$  are both depleted by  $v/M$  with respect to the

<sup>3</sup>We restrict to integer modular weights. Fractional weights are in general allowed, but require a suitable multiplier system [262, 263].

<sup>4</sup>The distinction between superfields and their scalar components should be clear from the context.

<sup>5</sup>The covariant derivative is  $D_\mu \psi^i = \partial_\mu \psi^i + (K^{-1})_m^i K_{kl}^m \partial_\mu \varphi^k \psi^l$ .

<sup>6</sup>Notice that this transformation mixes holomorphic and anti-holomorphic indices, and there is no more fundamental distinction between upper and lower components of the matrix  $(z^{1/2})$ .

vector-like case,  $v$  denoting the gauge symmetry breaking scale. Thus we have a relative suppression between the two contributions of order  $m_{\text{SUSY}}/M$ , which can be made tiny (cf. ref. [248]). If we work under this assumption, the mass matrix is well approximated by:

$$m_{kn} = W_{ij} (z^{-1/2})_{ik} (z^{-1/2})_{jn}. \quad (7.1.7)$$

The supersymmetry breaking terms neglected here can be useful to give masses to light fermions, which otherwise would remain massless in the exact supersymmetry limit. We will come back to this point when discussing concrete models, in Section 7.3. Due to the conservation of the electric charge, the equality of eq. (7.1.7) holds separately in any charge sector. By focusing on the lepton sector ( $E^c, L$ ) and by assuming that the neutrino masses arise from the Weinberg operator, we have:

$$W = -E_i^c \mathcal{Y}_{ij}^e(\tau) L_j H_d - \frac{1}{2\Lambda_L} L_i \mathcal{C}_{ij}^\nu(\tau) L_j H_u H_u, \quad (7.1.8)$$

where  $H_{u,d}$  are the Higgs chiral multiplets and  $\Lambda_L$  is the scale where lepton number is broken. The general relation (7.1.7) specialises into:

$$m_e = (z_{E^c}^{-1/2})^T \mathcal{Y}^e(\tau) (z_L^{-1/2}) v_d, \quad m_\nu = (z_L^{-1/2})^T \mathcal{C}^\nu(\tau) (z_L^{-1/2}) v_u^2 / \Lambda_L, \quad (7.1.9)$$

where we have absorbed the renormalisation factors for  $H_{u,d}$  in the definition of their VEVs. In Section 7.3, we will also comment on the special limit where  $z_{E^c, L}^{-1/2}$  are universal, i.e. proportional to the unit matrix. The mass matrices obtained in this case will be referred to as “bare” matrices and denoted by  $m_{e,\nu}^{(0)}$ . An important consequence of modular invariance is the special functional dependence of  $\mathcal{Y}^e(\tau)$  and  $\mathcal{C}^\nu(\tau)$  on the modulus  $\tau$ . Under a transformation of  $\Gamma$ , the chiral multiplets ( $E_i^c, L_i, H_{u,d}$ ) transform as in eq. (7.1.1), with weights ( $k_{E_i^c}, k_{L_i}, k_{H_{u,d}}$ ) and representations ( $\rho_{E^c}(\tilde{\gamma}), \rho_L(\tilde{\gamma}), \mathbf{1}$ ). For the superpotential  $W$  to be modular invariant,  $\mathcal{Y}^e(\tau)$  and  $\mathcal{C}^\nu(\tau)$  should obey:

$$\mathcal{Y}^e(\gamma\tau) = (c\tau + d)^{k_e} \rho_{E^c}^*(\tilde{\gamma}) \mathcal{Y}^e(\tau) \rho_L^\dagger(\tilde{\gamma}), \quad \mathcal{C}^\nu(\gamma\tau) = (c\tau + d)^{k_\nu} \rho_L^*(\tilde{\gamma}) \mathcal{C}^\nu(\tau) \rho_L^\dagger(\tilde{\gamma}),$$

where the weights  $k_{e,\nu}$  are matrices satisfying:  $(k_e)_{ij} = k_{E_i^c} + k_{L_j} + k_{H_d}$  and  $(k_\nu)_{ij} = k_{L_i} + k_{L_j} + 2k_{H_u}$ . Thus  $\mathcal{Y}^e(\tau)$  and  $\mathcal{C}^\nu(\tau)$  are modular forms of given level and weight. Since the linear space of such modular forms is finite dimensional, the choices for  $\mathcal{Y}^e(\tau)$  and  $\mathcal{C}^\nu(\tau)$  are limited. If neutrino masses originate from a type I seesaw mechanism, Eqs. (7.1.8) and (7.1.7) hold with the identification:

$$\frac{\mathcal{C}^\nu(\tau)}{\Lambda_L} = -(\mathcal{Y}^\nu(\tau))^T \mathcal{M}(\tau)^{-1} \mathcal{Y}^\nu(\tau), \quad (7.1.10)$$

where  $\mathcal{Y}^\nu(\tau)$  and  $\mathcal{M}(\tau)$  denote the matrix of neutrino Yukawa couplings and the mass matrix of the heavy electroweak singlets  $N^c$ , respectively. Notice that there is no dependence on the renormalisation factor ( $z_{N^c}^{-1/2}$ ) of the heavy modes. In some cases  $\mathcal{Y}^e(\tau)$  and/or  $\mathcal{C}^\nu(\tau)$  are completely determined as a function of  $\tau$  up to an overall constant, thus providing a strong potential constraint on the mass spectrum, Eq. (7.1.7).

Unfortunately, such property does not extend to the Kähler potential  $K$  and to the renormalisation factors ( $z_{E^c, L}^{-1/2}$ ). Minimal choices of  $K$ , appropriate for a perturbative regime, can receive large non-perturbative corrections in the region of the moduli space we will consider. Without a control over the non-perturbative dynamics, in a generic point

of the moduli space the factors  $(z_{E^c,L}^{-1/2})$  remain unknown. If we allowed for completely arbitrary  $(z_{E^c,L}^{-1/2})$ , under mild conditions any mass matrix could be predicted. From eq. (7.1.7) we see that, given  $\mathcal{Y}^e(\tau)$  and  $(z_L^{-1/2})$ , we could reproduce any desired matrix  $m_e$ , by selecting a particular  $(z_{E^c}^{-1/2})^T$ :

$$(z_{E^c}^{-1/2})^T = m_e (\mathcal{Y}^e(\tau) v_d (z^{-1/2}))^{-1} \quad (7.1.11)$$

An arbitrary matrix  $m_e$  would result in a completely unconstrained lepton mixing matrix. Similar considerations would apply to the neutrino mass matrix  $m_\nu$ .

The loss of predictability associated to the Kähler corrections may however be less severe than eq. (7.1.11) might suggest, for two reasons. First, note that the above solution requires a non-singular  $\mathcal{Y}^e(\tau)$ . A singular  $\mathcal{Y}^e(\tau)$  can only give rise to a singular  $m_e$ . Correspondingly, a hierarchical  $\mathcal{Y}^e(\tau)$  can only correspond to a hierarchical  $m_e$ , unless the eigenvalues of the matrix  $(z_{E^c}^{-1/2})^T$  in eq. (7.1.11) come in very large ratios. Although we cannot exclude the latter possibility, here we focus on the class of models where the corrections associated to the Kähler potential do not alter the “bare” limit by more than about one order of magnitude. Hence a singular or nearly singular  $\mathcal{Y}^e(\tau)$  will tame the loss of predictability associated with the Kähler potential. Needless to say, a hierarchical  $\mathcal{Y}^e(\tau)$  is needed to reproduce the mass spectrum in the charged lepton sector. Different considerations apply to the neutrino sector, where a singular  $\mathcal{C}^\nu(\tau)$  might not be a good first order approximation of the data.

A second constraint on the effect of the Kähler corrections arises in the vicinity of the fixed points of  $\Gamma$ ,  $\tau = i$ ,  $\tau = -1/2 + i\sqrt{3}/2$  and  $\tau = i\infty$ , invariant under the action of the elements  $S$ ,  $ST$  and  $T$ , respectively. In the following, we will assume the modulus to be in the vicinity of the point  $\tau = i$ , as suggested by several models to correctly reproduce the data. The invariance under  $S$  provides a constraint on the possible form of the Kähler potential at  $\tau = i$  and in its vicinity.

## 7.2. Residual symmetry near $\tau = i$

The residual symmetry of the theory at  $\tau = i$  is the cyclic group  $Z_4$  generated by the element  $S$ , whose action on the chiral multiplets  $\varphi_i$  in  $\tau = i$  can be read from eq. (7.1.1):

$$\varphi_i \rightarrow \sigma_{ij} \varphi_j, \quad \sigma_{ij} = i^{k_i} \rho(\tilde{S})_{ij} \quad (i, j > 0), \quad (7.2.1)$$

where  $\sigma$  is unitary,  $\sigma^2$  is a parity operator and  $\sigma^4 = 1$ . To analyse the neighbourhood of  $\tau = i$ , we expand both the Kähler potential and the superpotential in powers of the matter fields  $\varphi_i$  ( $i > 0$ ) <sup>7</sup>:

$$\begin{aligned} W &= \sum_{i_1, \dots, i_n} Y_{i_1, \dots, i_n}(\tau) \varphi_{i_1} \dots \varphi_{i_n} + \dots, \\ K &= \bar{\varphi}_i z_j^i(\tau, \bar{\tau}) \varphi_j + \dots \end{aligned} \quad (7.2.2)$$

---

<sup>7</sup>Electrically neutral multiplets whose scalar component acquires a VEV, like  $H_{u,d}$ , might mix in the kinetic term with the modulus  $\tau$ . The mixing is parametrically suppressed by  $v/\Lambda$  and will be ignored in the following.

In the vicinity of  $\tau = i$ , it is possible to cast the theory as an ordinary  $Z_4$  invariant theory, where the symmetry acts linearly on the fields, slightly broken by the spurion  $(\tau - i)$ . When we depart from  $\tau = i$ , the  $S$  elements acts on the fields as:

$$\tau \rightarrow -\frac{1}{\tau} \quad , \quad \varphi_i \rightarrow (-\tau)^{-k_i} \rho(\tilde{S})_{ij} \varphi_j \quad (i, j > 0). \quad (7.2.3)$$

We perform the field redefinition:

$$\begin{cases} \tau = i \frac{i+\frac{\epsilon}{2}}{i-\frac{\epsilon}{2}} \\ \tilde{\varphi}_j = (1 - i\frac{\epsilon}{2})^{-k_j} \varphi_j \end{cases} \quad (7.2.4)$$

mapping the upper-half complex plane into the disk  $|\epsilon| < 2$ . In the linear approximation:

$$\epsilon = (\tau - i) + O((\tau - i)^2). \quad (7.2.5)$$

Under the  $S$  transformation in (7.2.3), the new fields transform as:

$$\begin{cases} \epsilon \rightarrow -\epsilon \\ \tilde{\varphi}_i \rightarrow \sigma_{ij} \tilde{\varphi}_j \end{cases} . \quad (7.2.6)$$

We see that the action of the  $Z_4$  symmetry is linear in the new field basis, even when  $\tau \neq i$ . In particular  $\epsilon$  behaves as a spurion with  $Z_4$  charge  $+2$ . In the new field basis, the coefficients of the field expansion (7.2.2) read:

$$\begin{aligned} \tilde{Y}_{i_1, \dots, i_n} &= \left(1 - i\frac{\epsilon}{2}\right)^{k_{i_1} + \dots + k_{i_n}} Y_{i_1, \dots, i_n} \\ \tilde{z}^i_j &= \left(1 + i\frac{\bar{\epsilon}}{2}\right)^{k_i} z^i_j \left(1 - i\frac{\epsilon}{2}\right)^{k_j} . \end{aligned} \quad (7.2.7)$$

The invariance of the theory under  $Z_4$  requires  $\tilde{Y}_{i_1, \dots, i_n}(\epsilon)$  and  $\tilde{z}^i_j(\epsilon, \bar{\epsilon})$  to satisfy:

$$\begin{aligned} \tilde{Y}_{i_1, \dots, i_n}(\epsilon) &= \sigma_{j_1 i_1} \dots \sigma_{j_n i_n} \tilde{Y}_{j_1, \dots, j_n}(-\epsilon) \\ \tilde{z}^i_j(\epsilon, \bar{\epsilon}) &= \sigma^{\dagger ik} \tilde{z}^k_l(-\epsilon, -\bar{\epsilon}) \sigma_{lj} \end{aligned} . \quad (7.2.8)$$

In particular, setting  $\epsilon = 0$ , the above equations express the necessary conditions for the invariance of the theory at the symmetric point  $\tau = i$ . By expanding  $\tilde{z}^i_j(\epsilon, \bar{\epsilon})$  in powers of  $\epsilon$  we see that the terms of first order vanish, up to possible non-diagonal terms relating fields with opposite value of  $\sigma$ . We conclude that in a neighbourhood of the fixed point  $\tau = i$ , and in the absence of any information about the Kähler potential, the theory reduces to a linearly realised  $Z_4$  flavour symmetric theory, in the presence of a (small) spurion with charge  $+2$ .

### 7.3. Models

In this section, we present two models making use of the results of the previous section to account for the observed hierarchies in the lepton spectrum, namely the smallness of the charged lepton mass ratios,  $m_e/m_\tau$  and  $m_\mu/m_\tau$  and of the neutrino mass ratio  $r \equiv \delta m^2/|\Delta m^2|$ , where  $\delta m^2 \equiv m_2^2 - m_1^2$  and  $\Delta m^2 \equiv m_3^2 - (m_1^2 + m_2^2)/2$  (with the standard neutrino labeling). The hierarchies will be naturally accounted for by the small breaking of  $Z_4$ ,  $|\epsilon| \ll 1$ , i.e. by the closeness of the modulus  $\tau$  to the  $Z_4$  symmetric point

Observable	Best-fit value with $1\sigma$ error	
$m_e/m_\mu$	$0.0048^{+0.0002}_{-0.0002}$	
$m_\mu/m_\tau$	$0.0565^{+0.0045}_{-0.0045}$	
	NO	IO
$\delta m^2 [10^{-5} \text{ eV}^2]$	$7.42^{+0.21}_{-0.20}$	
$\Delta m^2 [10^{-3} \text{ eV}^2]$	$2.480^{+0.026}_{-0.028}$	$-2.461^{+0.028}_{-0.028}$
$r \equiv \delta m^2 /  \Delta m^2 $	$0.0299^{+0.0009}_{-0.0009}$	$0.0301^{+0.0009}_{-0.0009}$
$\sin^2 \theta_{12}$	$0.304^{+0.012}_{-0.012}$	$0.304^{+0.013}_{-0.012}$
$\sin^2 \theta_{13}$	$0.02219^{+0.00062}_{-0.00063}$	$0.02238^{+0.00063}_{-0.00062}$
$\sin^2 \theta_{23}$	$0.573^{+0.016}_{-0.020}$	$0.575^{+0.016}_{-0.019}$
$\delta/\pi$	$1.09^{+0.15}_{-0.13}$	$1.57^{+0.14}_{-0.17}$

TABLE 1. Best-fit values of the charged lepton mass ratios and the neutrino oscillation parameters with the corresponding  $1\sigma$  errors. For the charged lepton mass ratios we have used the values given in ref. [234], averaged over  $\tan\beta$  as described in the text, whereas for the neutrino parameters we have used the results obtained in refs. [41, 76] (with Super-Kamiokande atmospheric data).

$\tau = i$ , while the parameters in the superpotential will be  $\mathcal{O}(1)$ , and the corrections to the minimal Kähler will not be larger than  $\mathcal{O}(1)$ . In Table 1, we collect the best-fit values of the leptonic parameters with the corresponding  $1\sigma$  uncertainties.

For the charged lepton mass ratios we use the results of Ref. [234], where for  $m_\mu/m_\tau$  we take an average between the values obtained for  $\tan\beta = 10$  and  $\tan\beta = 38$ . For the neutrino oscillation parameters we employ the results of the global analysis performed in refs. [41, 76]. In what follows, when fitting models to the data, we use five dimensionless observables that have been measured with a good precision, i.e. two mass ratios<sup>8</sup>,  $m_\mu/m_\tau$  and  $r$ , and three leptonic mixing angles,  $\sin^2 \theta_{12}$ ,  $\sin^2 \theta_{13}$ ,  $\sin^2 \theta_{23}$ . Regarding the Dirac CPV phase,  $\delta$ , values between  $\pi$  and  $2\pi$  (approximately) are currently allowed at  $3\sigma$  for both neutrino mass spectrum with normal ordering (NO) and that with inverted ordering (IO). Moreover, in ref. [249], it has been shown that under the transformation  $\tau \rightarrow -\tau^*$  and complex conjugation of couplings present in the superpotential, CPV phases change their signs, whereas masses and mixing angles remain the same. In fact, this reflects CP properties of modular invariant models [250] (see also [265]). As a consequence, the Dirac phase  $\delta$  is not particularly constraining for our fits, and we do not include it in the list of input observables, regarding the obtained values as predictions.

**7.3.1. Model 1: Weinberg operator and inverted ordering.** We work at level 3, and the relevant finite modular group is  $\Gamma_3$ . In this subsection, we assume that neutrino masses are generated by the Weinberg operator. The field content of the model along with the assignment of  $\Gamma_3$  representations and modular weights  $k$  is shown in Table 2. The corresponding charges under  $Z_4$ , obtained using  $\sigma$ , are shown in Table 3. We work

<sup>8</sup>In the models presented below,  $m_e = 0$  by construction, so we do not include the ratio  $m_e/m_\mu$  here. See subsection 7.3.3 for possible ways of generating non-zero  $m_e$ .



	$L$	$E_1^c$	$E_2^c$	$E_3^c$	$H_u$	$H_d$
$SU(2)_L \times U(1)_Y$	$(\mathbf{2}, -1/2)$	$(\mathbf{1}, +1)$	$(\mathbf{1}, +1)$	$(\mathbf{1}, +1)$	$(\mathbf{2}, +1/2)$	$(\mathbf{2}, -1/2)$
$\Gamma_3$	$\mathbf{3}$	$\mathbf{1}$	$\mathbf{1}$	$\mathbf{1}'$	$\mathbf{1}$	$\mathbf{1}$
$k$	1	3	3	3	0	0

TABLE 2. Assignment of representations and modular weights in Model 1.

	$\tilde{L}_1$	$\tilde{L}_2$	$\tilde{L}_3$	$\tilde{E}_1^c$	$\tilde{E}_2^c$	$\tilde{E}_3^c$	$\tilde{H}_u$	$\tilde{H}_d$	$\epsilon$
$Z_4$	1	-1	-1	-1	-1	-1	0	0	2

TABLE 3.  $Z_4$  charges (mod 4) in Model 1.

in a real basis for the elements of  $\Gamma_3$  where  $\rho(\tilde{S}) = \text{diag}(+1, -1, -1)$  for the irreducible three-dimensional representation.

The quantum number assignments have immediate consequences for the charged lepton mass spectrum:

- (1) At  $\tau = i$ , the charged lepton mass matrix  $m_e$  has rank one. This follows from the  $Z_4$  charges in Table 3, forcing:

$$m_e = \begin{pmatrix} \alpha & 0 & 0 \\ \beta & 0 & 0 \\ \gamma & 0 & 0 \end{pmatrix}. \quad (7.3.1)$$

- (2) For a generic  $\tau \neq i$ ,  $m_e$  has rank two. While  $Z_4$  alone would allow  $m_e$  to have rank three, the underlying modular invariance forces the coefficients of the first and second rows of  $m_e$  to be proportional, thus reducing the rank. In fact, modular invariance requires the coupling of  $E_1^c$  and  $E_2^c$  to  $L$  to be proportional to the same modular form multiplet, namely, the triplet of weight four. The Kähler corrections cannot modify the rank condition. Thus, in the considered model, the electron has zero mass.

For  $\tau \approx i + \epsilon$ , with  $|\epsilon| \ll 1$ , we obtain the prediction

$$m_e : m_\mu : m_\tau = 0 : \mathcal{O}(\epsilon) : 1. \quad (7.3.2)$$

Concerning the neutrino mass spectrum, from the charges of the lepton doublets  $L_i$  in Table 3, we deduce that  $m_\nu$  in  $\tau = i$  takes the following general form:

$$m_\nu = \begin{pmatrix} 0 & a & b \\ a & 0 & 0 \\ b & 0 & 0 \end{pmatrix}. \quad (7.3.3)$$

This matrix has rank two and two degenerate non-zero eigenvalues. Notice that, while a generic  $Z_4$  model would not account for the values of the parameters  $a$  and  $b$ , here the underlying modular invariance fixes the relative values, before Kähler corrections. With the  $Z_4$  assignment of Table 3, we are implicitly using the basis where  $S$  is diagonal for the irreducible triplet of  $\Gamma_3$  and we find  $a/b = Y_3(i)/Y_2(i)$ , where  $Y^{(2)}(\tau) \equiv (Y_1(\tau), Y_2(\tau), Y_3(\tau))^T$  denotes the weight-two triplet of modular forms. On the other hand, generic Kähler corrections could mix  $L_2$  and  $L_3$ , as they have the same  $Z_4$  charge (see (7.2.8)), leading to

arbitrary  $a/b$ , as in generic  $Z_4$  models. For  $\tau \approx i + \epsilon$ , the rank of  $m_\nu$  becomes three, and we obtain the neutrino mass spectrum with inverted ordering of the form

$$m_1 : m_2 : m_3 = 1 : (1 + \mathcal{O}(\epsilon)) : \mathcal{O}(\epsilon), \quad (7.3.4)$$

and, in particular:

$$r = \mathcal{O}(\epsilon). \quad (7.3.5)$$

Clearly, both qualitative relations (7.3.2) and (7.3.5) are phenomenologically intriguing. They are consequences of modular invariance alone, and are thus independent from the parameters in the superpotential or the Kähler potential (provided these are non-hierarchical by themselves). In subsection 7.3.3, we discuss two possible mechanisms to generate a naturally small electron mass.

While this model successfully accounts for the observed mass hierarchies (with a non-vanishing electron mass still to be generated), it is not satisfactory when it comes to the mixing angles. The point is that in order for (7.3.3) to lead to a reasonable leading order approximation, the tau lepton should correspond to a linear combination of  $L_2$  and  $L_3$ , while eq. (7.3.1) forces the tau lepton to be mainly  $L_1$ . Indeed, the prediction for the mixing angles at  $\tau = i$  is

$$\sin^2 \theta_{13} = \cos^2 \theta_{12}^e, \quad \sin^2 \theta_{12} = \frac{1}{2}, \quad \sin^2 \theta_{23} = 1, \quad (7.3.6)$$

where  $\theta_{12}^e$  is an arbitrary angle related to the presence of two vanishing eigenvalues in  $m_e$ , to be fixed by the  $Z_4$  breaking. These predictions imply that in order to generate the correct mixing angles  $\sin^2 \theta_{23} \approx 0.6$  and  $\sin^2 \theta_{12} \approx 0.3$ , large hierarchical deviations from the minimal Kähler metrics are required<sup>9</sup>, as  $|\epsilon| \ll 1$  cannot give rise to such large corrections. This is clearly an unpleasant feature, since it introduces a source of hierarchy in the Lagrangian parameters. We carried out a full numerical study of the model, after adding a non-minimal Kähler potential depending on four new real parameters. The outcome confirms the above qualitative considerations. More precisely, we gauge the degree of hierarchy related to a non-canonical Kähler potential  $K$  by means of the condition number

$$\kappa(K) = \lambda_{\max}(z)/\lambda_{\min}(z), \quad (7.3.7)$$

the ratio between the maximum and minimum eigenvalues of  $z^i_j$  at the best-fit point. We find that all Kähler metrics providing a good fit near  $\tau = i$  turn out to have  $\kappa(K_{L,E^c})$  very large, typically in the range  $10^3 \div 10^4$ . We discuss in the next subsection a seesaw variant of the present model which allows to mitigate the need of hierarchical Kähler metrics.

**7.3.2. Model 2: seesaw mechanism and normal ordering.** The main phenomenological obstructions in the model discussed above are the leading order predictions for the mixing angles. In this subsection, we show how to evade them by introducing electroweak singlet neutrinos  $N^c$  and generating the Weinberg operator through the type I seesaw mechanism. This widens the class of possible neutrino mass matrices that can

---

<sup>9</sup>The need for non-minimal Kähler metrics stems not only from the leading order predictions for the mixing angles, but also from the mass spectrum of the model. In the vicinity of  $\tau = i$  we found, both numerically and through an approximate analytical study, that  $m_\mu/m_\tau$  is smaller than  $r$ , while data require the opposite.

be obtained, if the singlet neutrino mass matrix becomes singular in the limit  $\tau \rightarrow i$ . In this case, for the standard analysis of the seesaw mechanism to be valid, singlet neutrino masses are required to be large compared to the electroweak scale. In the example discussed below, this is easily achieved outside of a neighbourhood of  $\tau = i$ , provided the overall singlet neutrino mass scale is large enough.

To be concrete, we augment the field content of Table 2 with electroweak singlets  $N^c \sim \mathbf{3}$  under  $\Gamma_3$ , with weight  $k_{N^c} = 1$ . As before, we denote by  $Y^{(2)}$  the weight 2 modular form triplet, and by  $Y^{(4)} \equiv (Y^{(2)}Y^{(2)})_{\mathbf{3}_S}$  the weight 4 triplet of modular forms. We denote by  $\mathbf{3}_S$  and  $\mathbf{3}_A$  the symmetric and antisymmetric triplet contractions of two  $\Gamma_3$  triplets, respectively. The superpotential  $W = W_e + W_\nu$  of the lepton sector reads:

$$W_e = -[\alpha E_1^c (LY^{(4)})_{\mathbf{1}} + \beta E_2^c (LY^{(4)})_{\mathbf{1}} + \gamma E_3^c (LY^{(4)})_{\mathbf{1}''}] H_d, \quad (7.3.8)$$

$$W_\nu = -\kappa [(N^c L)_{\mathbf{3}_S} + g (N^c L)_{\mathbf{3}_A}] Y^{(2)}_{\mathbf{1}} H_u - \Lambda (N^c N^c Y^{(2)})_{\mathbf{1}}. \quad (7.3.9)$$

The parameters  $\kappa$  and  $\Lambda$  can be made real without loss of generality, whereas  $g$  is complex in general. In the real basis for  $\mathbf{3}$  of  $\Gamma_3$ , this superpotential leads to the following matrices  $\mathcal{Y}^e(\tau)$ ,  $\mathcal{Y}^\nu(\tau)$  and  $\mathcal{M}(\tau)$ :

$$\mathcal{Y}^e(\tau) = 2 \begin{pmatrix} \alpha Y_2 Y_3 & \alpha Y_1 Y_3 & \alpha Y_1 Y_2 \\ \beta Y_2 Y_3 & \beta Y_1 Y_3 & \beta Y_1 Y_2 \\ \gamma Y_2 Y_3 & \gamma \omega Y_1 Y_3 & \gamma \omega^2 Y_1 Y_2 \end{pmatrix}, \quad (7.3.10)$$

$$\mathcal{Y}^\nu(\tau) = \kappa \left[ \begin{pmatrix} 0 & Y_3 & Y_2 \\ Y_3 & 0 & Y_1 \\ Y_2 & Y_1 & 0 \end{pmatrix} + g \begin{pmatrix} 0 & Y_3 & -Y_2 \\ -Y_3 & 0 & Y_1 \\ Y_2 & -Y_1 & 0 \end{pmatrix} \right], \quad (7.3.11)$$

$$\mathcal{M}(\tau) = 2\Lambda \begin{pmatrix} 0 & Y_3 & Y_2 \\ Y_3 & 0 & Y_1 \\ Y_2 & Y_1 & 0 \end{pmatrix}. \quad (7.3.12)$$

The matrix  $\mathcal{C}^\nu(\tau)$  of eq. (7.1.8) is now given by the seesaw formula of eq. (7.1.10).

Some analytical considerations easily follow from the previous equations for the “bare” quantities, i.e. those corresponding to the minimal Kähler potential. We make use of the following  $\epsilon$ -expansion of  $Y^{(2)}$ <sup>10</sup>:

$$Y_1 = -ix\epsilon, \quad Y_2 = y(1 + i\epsilon), \quad Y_3 = y^*(1 + i\epsilon), \quad (7.3.13)$$

where, up to an overall constant,  $x \approx 1.49087$  and  $y = \sqrt{3}/2 + i(3/2 - \sqrt{3})$ . To first order in  $\epsilon$  we obtain:

$$\frac{\mathcal{Y}_\nu(\tau)}{\kappa} = \begin{pmatrix} 0 & (1+g)y^* & (1-g)y \\ (1-g)y^* & 0 & 0 \\ (1+g)y & 0 & 0 \end{pmatrix} + i\epsilon \begin{pmatrix} 0 & (1+g)y^* & (1-g)y \\ (1-g)y^* & 0 & -(1+g)x \\ (1+g)y & -(1-g)x & 0 \end{pmatrix}, \quad (7.3.14)$$

<sup>10</sup>One can prove, in general, that  $\frac{d}{d\tau}\big|_i Y_{2,3} = i Y_{2,3}(i)$ . Moreover, we can rephase  $Y^{(2)}$  in such a way that  $(Y_3(i))^* = Y_2(i) \equiv y$ . In this basis, we find that  $\frac{d}{d\tau}\big|_i Y_1 \in -i\mathbb{R}^+$ .

$$\frac{\mathcal{M}(\tau)}{2\Lambda} = \begin{pmatrix} 0 & y^* & y \\ y^* & 0 & 0 \\ y & 0 & 0 \end{pmatrix} + i\epsilon \begin{pmatrix} 0 & y^* & y \\ y^* & 0 & -x \\ y & -x & 0 \end{pmatrix}. \quad (7.3.15)$$

Notice that the bare Majorana mass matrix has one eigenvalue proportional to  $\epsilon$ , thus vanishing in the limit  $\tau \rightarrow i$ . This corresponds to the case of single right-handed neutrino dominance, in which one of the electroweak singlet neutrinos is massless in the symmetric limit<sup>11</sup>. Inverting the matrix in eq. (7.3.15) and using the seesaw relation for the bare light neutrino mass matrix  $m_\nu^{(0)}$  we find to  $\mathcal{O}(\epsilon)$ :

$$m_\nu^{(0)} = \begin{pmatrix} \frac{2ig^2|y|^2}{x} \frac{1}{\epsilon} - \frac{4g^2|y|^2}{x} & -(1+g^2)y^* & -(1+g^2)y \\ -(1+g^2)y^* & 0 & 0 \\ -(1+g^2)y & 0 & 0 \end{pmatrix} + \mathcal{O}(\epsilon). \quad (7.3.16)$$

The leading order form of the charged lepton mass matrix is as in eq. (7.3.1).

The leading order predictions for neutrino masses and mixing angles strongly depend upon the parameter  $g$ .

- A neutrino mass spectrum with IO can be realised when  $|g|^2 \ll |\epsilon|$ . Then,  $m_\nu^{(0)}$  has approximately the same form as in the model with the Weinberg operator considered in subsection 7.3.1. We get the neutrino mass spectrum with IO:

$$m_1 : m_2 : m_3 = 1 : \approx 1 : \mathcal{O}(\epsilon) \quad (7.3.17)$$

and the predictions for the mixing angles reported in eq. (7.3.6), in particular,  $\sin^2 \theta_{23} = 1$ .

- A neutrino mass spectrum with NO can be realised when  $|\epsilon| \ll |g|^2$ . In this case,

$$m_\nu^{(0)} = \begin{pmatrix} c(g^2/\epsilon) & a & b \\ a & 0 & 0 \\ b & 0 & 0 \end{pmatrix} + \mathcal{O}(\epsilon), \quad (7.3.18)$$

with  $|a|$ ,  $|b|$ ,  $|c|$  being  $\mathcal{O}(1)$  numbers. Therefore, we have the neutrino mass spectrum with NO:

$$m_1 : m_2 : m_3 = \mathcal{O}(\epsilon^2/g^2) : \mathcal{O}(\epsilon^2/g^4) : \mathcal{O}(1) \quad (7.3.19)$$

implying  $r = \mathcal{O}(\epsilon^4/g^4)$ . The mixing angles are:

$$\sin^2 \theta_{12} = \mathcal{O}(1), \quad \sin^2 \theta_{23} \approx \sin^2 \theta_{13} \approx r^{1/2}. \quad (7.3.20)$$

Again, the leading order prediction for  $\sin^2 \theta_{23}$  is far away from its measured value and requires significant corrections from the Kähler potential.

To verify the viability of the model we have performed a full numerical study, also allowing for a non-minimal form of the Kähler potential for the matter fields. In general, modular invariance allows many terms in the Kähler potential [43, 258]. In the considered bottom-up approach, there seems to be no way of reducing the number of these terms. However, this may change if modular symmetry is augmented by a traditional finite

<sup>11</sup>As already observed, in order for the standard seesaw analysis to be valid, we must require the product  $|\epsilon|\Lambda$  (that is the order of magnitude of the lightest right-handed neutrino mass) to be large with respect to the electroweak scale. For the present model this does not pose any practical restriction, since the best-fit region (see below) is achieved for values of  $|\epsilon| \sim 10^{-2} \div 10^{-1}$ .

flavour symmetry [266] or, perhaps, if some other top-down principle is in action. In what follows, to be concrete, we adopt three simplifying assumptions:

- The new terms in  $K$  are quadratic in  $Y^{(2)}$ . This is sufficient to illustrate our results.
- The minimal form (up to overall normalisation) is restored at  $\text{Im}\tau \rightarrow \infty$ . This assumption is inspired by the minimal form of the Kähler potential arising in certain string theory compactifications in the large volume limit, corresponding to  $\text{Im}\tau \rightarrow \infty$  (see, e.g. [258, 259] and references therein).
- The diagonal entries, already controlled by the minimal Kähler potential, are not affected by the new terms.

Under these assumptions and with the assignment of representations and weights given in Table 2, we find <sup>12</sup>:

$$K = L^\dagger K_L L + E^{c\dagger} K_{E^c} E^c, \quad (7.3.21)$$

where

$$K_L = \frac{1}{2\text{Im}\tau} \begin{pmatrix} 1 & 0 & 0 \\ 0 & 1 & 0 \\ 0 & 0 & 1 \end{pmatrix} + 2\text{Im}\tau \begin{pmatrix} 0 & (\alpha_5 + i\alpha_6) X_{12} & (\alpha_5 - i\alpha_6) X_{13} \\ (\alpha_5 - i\alpha_6) X_{12}^* & 0 & (\alpha_5 + i\alpha_6) X_{23} \\ (\alpha_5 + i\alpha_6) X_{13}^* & (\alpha_5 - i\alpha_6) X_{23}^* & 0 \end{pmatrix}. \quad (7.3.22)$$

Here  $\alpha_5$  and  $\alpha_6$  are real coefficients and

$$X_{12} = Y_1^* Y_2 - Y_1 Y_2^*, \quad X_{13} = Y_1^* Y_3 - Y_1 Y_3^*, \quad X_{23} = Y_2^* Y_3 - Y_2 Y_3^*. \quad (7.3.23)$$

In the  $E^c$  sector, we obtain:

$$K_{E^c} = \frac{1}{8(\text{Im}\tau)^3} \begin{pmatrix} 1 & 0 & 0 \\ 0 & 1 & 0 \\ 0 & 0 & 1 \end{pmatrix} + \frac{1}{2\text{Im}\tau} \begin{pmatrix} 0 & 0 & c_{13}X \\ 0 & 0 & c_{23}X \\ c_{13}^* X^* & c_{23}^* X^* & 0 \end{pmatrix}, \quad (7.3.24)$$

where  $c_{13}$  and  $c_{23}$  are complex coefficients and

$$X = Y_1^* Y_1 + \omega Y_2^* Y_2 + \omega^2 Y_3^* Y_3 \sim \mathbf{1}''. \quad (7.3.25)$$

Noteworthy, the seesaw formula (7.1.10) does not depend on the renormalisation factor  $z_{N^c}^{-1/2}$  of the heavy fields  $N^c$ , so that we will not need to specify the Kähler metric of  $N^c$  in what follows.

The inclusion of a non-minimal Kähler potential, even within the above restrictive assumptions, brings in several additional free parameters:  $\alpha_{5,6}$ ,  $\text{Re}(c_{13,23})$  and  $\text{Im}(c_{13,23})$  <sup>13</sup>. Adding them to  $\beta/\alpha$ ,  $\gamma/\alpha$ ,  $\text{Re}(g)$ ,  $\text{Im}(g)$ ,  $\text{Re}(\tau)$  and  $\text{Im}(\tau)$ , we have a total of 12 dimensionless input parameters, more than the number of observables. Thus the focus of our analysis cannot be on predictability. Rather, we are interested in accounting for the mass hierarchies in terms of the  $Z_4$  parameter  $\epsilon$ , in the context of a model reproducing all lepton masses and mixings. While the mass hierarchies alone can be easily accommodated without the need of hierarchical Lagrangian parameters, some degree of hierarchy turns out to be required by the need to fix the mixing parameters. Useful parameters to estimate such hierarchies in the Kähler potential are the condition numbers

<sup>12</sup>We present the full expressions for  $K_L$  and  $K_{E^c}$  quadratic in  $Y^{(2)}$  in Appendix 7.5.

<sup>13</sup>In our numerical analysis, we have set  $\text{Im}(c_{13,23}) = 0$ .

Input parameters		Observables		Predictions	
$\text{Re}\tau$	$\pm 0.0235$	$m_e/m_\mu$	0	$m_1$ [eV]	0.0062
$\text{Im}\tau$	1.080	$m_\mu/m_\tau$	0.0565	$m_2$ [eV]	0.0106
$\beta/\alpha$	0.1459	$r$	0.0299	$m_3$ [eV]	0.0506
$\gamma/\alpha$	5.955	$\sin^2 \theta_{12}$	0.304	$\delta/\pi$	$\pm 0.92$
$\text{Reg}$	-0.1494	$\sin^2 \theta_{13}$	0.02219	$\alpha_{21}/\pi$	$\pm 0.97$
$\text{Img}$	$\mp 0.3169$	$\sin^2 \theta_{23}$	0.573	$\alpha_{31}/\pi$	$\pm 0.93$
$\alpha_5$	-0.2071	$\delta m^2$ [ $10^{-5}$ eV <sup>2</sup> ]	7.42	$ m_{ee} $ [eV]	0
$\alpha_6$	-0.1437	$\Delta m^2$ [ $10^{-3}$ eV <sup>2</sup> ]	2.480	$\sum_i m_i$ [eV]	0.0673
$c_{13}$	-0.2656			Ordering	NO
$c_{23}$	0.0145			$M_1/\Lambda$	0.225
$v_u^2 \kappa^2/\Lambda$ [eV]	0.0189			$M_2/\Lambda$	2.298
$ \epsilon  \approx  \tau - i $	0.0830			$M_3/\Lambda$	2.524

TABLE 4. First pair of best-fit points in a vicinity of  $\tau = i$  found considering the Kähler potential in eqs. (7.3.22)–(7.3.25).

Input parameters		Observables		Predictions	
$\text{Re}\tau$	$\pm 0.0328$	$m_e/m_\mu$	0	$m_1$ [eV]	0.0063
$\text{Im}\tau$	1.137	$m_\mu/m_\tau$	0.0565	$m_2$ [eV]	0.0107
$\beta/\alpha$	0.2388	$r$	0.0299	$m_3$ [eV]	0.0506
$\gamma/\alpha$	7.854	$\sin^2 \theta_{12}$	0.304	$\delta/\pi$	$\pm 0.91$
$\text{Reg}$	-0.2234	$\sin^2 \theta_{13}$	0.02219	$\alpha_{21}/\pi$	$\pm 0.98$
$\text{Img}$	$\pm 0.4469$	$\sin^2 \theta_{23}$	0.573	$\alpha_{31}/\pi$	$\pm 0.88$
$\alpha_5$	-0.1865	$\delta m^2$ [ $10^{-5}$ eV <sup>2</sup> ]	7.42	$ m_{ee} $ [eV]	0
$\alpha_6$	-0.1116	$\Delta m^2$ [ $10^{-3}$ eV <sup>2</sup> ]	2.480	$\sum_i m_i$ [eV]	0.0675
$c_{13}$	-0.2405			Ordering	NO
$c_{23}$	-0.0959			$M_1/\Lambda$	0.353
$v_u^2 \kappa^2/\Lambda$ [eV]	0.0191			$M_2/\Lambda$	2.130
$ \epsilon  \approx  \tau - i $	0.1408			$M_3/\Lambda$	2.483

TABLE 5. Second pair of best-fit points in a vicinity of  $\tau = i$  found considering the Kähler potential in eqs. (7.3.22)–(7.3.25).

of eq. (7.3.7). To establish the possibility to reproduce all the relevant observables, and the role of  $Z_4$  breaking in setting the mass hierarchies, we have selected several benchmark points with slightly different features. We show the results of two (pairs) of the benchmark points in Tables 4 and 5. In all such benchmark points, all five dimensionless observables take exactly their experimental best-fit values (for the time being we set  $m_e = 0$ ). In addition, the model predicts a normal ordered neutrino mass spectrum and the values of the CPV phases. Interestingly, for both pairs of the benchmark points, the predicted value of  $\delta$  (the one with minus sign) matches its experimental best-fit value. Notice also the interesting result  $|m_{ee}| = 0$  which at the leading order can be seen as

a simple consequence of the matrix patterns (7.3.16) and (7.3.1) <sup>14</sup>. Finally, we report in the last column the masses  $M_i$ ,  $i = 1, 2, 3$ , of the heavy neutrinos in the units of  $\Lambda$ . Although the value of  $\Lambda$  cannot be uniquely fixed, it can be estimated as (see the first column of the tables)  $\Lambda \approx v_u^2 \kappa^2 / (0.02 \text{ eV}) \approx 10^{15} \sin^2 \beta \text{ GeV}$ , where we have used  $v_u = v \sin \beta$ , with  $v = 174 \text{ GeV}$ , and  $\kappa \sim \mathcal{O}(1)$ . This implies that for  $\tan \beta \gtrsim 1$ , the scale  $\Lambda \gtrsim 5 \times 10^{14} \text{ GeV}$ . Let us stress once again that in the considered model,  $M_1 \sim |\epsilon| \Lambda$ , and thus, it is generated by a small departure of  $\tau$  from  $i$ .

Our analysis shows that the mass hierarchies are indeed governed by  $Z_4$  breaking, whereas, in general, Kähler corrections reflect on the lepton mass spectrum through  $\mathcal{O}(1)$  changes. For example, in the first pair of benchmark points (see Table 4), we verified numerically that Kähler corrections only affect the mass ratios by about a factor of 2 <sup>15</sup>; on the other hand, at these points, the Kähler metrics are by themselves somewhat hierarchical, as shown by the condition numbers  $\kappa(K_L) \approx 12$  and  $\kappa(K_{E^c}) \approx 16$ . In the second pair of benchmark points shown in Table 5, the hierarchies in the Kähler metrics are both reduced (the condition numbers are  $\kappa(K_L) \approx 6$  and  $\kappa(K_{E^c}) \approx 12$ ), and points with even milder hierarchies may potentially be found. These observations lead us to conclude that the deviations from the canonical Kähler metric present in the best-fit points, have little to do with the mass spectrum hierarchies; rather, they are necessary in order to reproduce the correct PMNS mixing angles.

We have analysed more in detail the dependence of the fitted observables on the parameters of the Kähler potential. In Figs. 7.3.1 and 7.3.2, we plot the values of the five dimensionless observables versus  $\alpha_{5,6}$  and  $c_{13,23}$ , respectively <sup>16</sup>. All other input parameters are fixed to their best-fit values as in Table 4. We see that the parameters  $\alpha_5$  and  $\alpha_6$  strongly impact the predictions for the mixing angles and the two mass ratios,  $r$  and  $m_\mu/m_\tau$ , whereas  $c_{13}$  and  $c_{23}$  in  $K_{E^c}$  mainly affect the predictions for  $\sin^2 \theta_{23}$  and  $m_\mu/m_\tau$ .

In conclusion, we see that a mass matrix of reduced rank at the self-dual point  $\tau = i$  can explain the observed mass hierarchies in terms of  $\mathcal{O}(1)$  Lagrangian parameters. At the same time, at least in the model considered here, moderately hierarchical Kähler and superpotential parameters are needed to fix the mixing angle predictions. Whether or not this is a general feature of this class of models is a question which definitely requires further investigation, but is beyond the scope of the present Chapter. On the other hand, in order to get a fully realistic description of lepton masses we should still generate a non-vanishing electron mass, without perturbing too much the results achieved so far. We discuss this point in the next subsection.

**7.3.3. Generating  $m_e \neq 0$ .** Both the models discussed above yield, by construction,  $m_e = 0$ . One can easily concoct mechanisms to generate the small electron mass without

<sup>14</sup>Given the column ordering in eq. (7.3.1),  $|m_{ee}|$  is given at the leading order by  $(m_\nu^{(0)})_{33} = 0 + \mathcal{O}(\epsilon)$ .

<sup>15</sup>For the minimal Kähler potential, *i.e.* setting  $\alpha_5 = \alpha_6 = c_{13} = c_{23} = 0$ , we find  $m_\mu/m_\tau = 0.0520$  and  $r = 0.0637$ , whereas the angles  $\sin^2 \theta_{12} = 0.228$ ,  $\sin^2 \theta_{13} = 0.03751$  and  $\sin^2 \theta_{23} = 0.256$  are far away from their experimental values.

<sup>16</sup>For the values of  $\alpha_{5,6}$  ( $c_{13,23}$ ) beyond the range displayed in the  $x$ -axis, the matrix  $K_L$  ( $K_{E^c}$ ) is not positive definite, and thus, the corresponding Kähler metric is well-defined only for the displayed range of  $\alpha_{5,6}$  ( $c_{13,23}$ ).

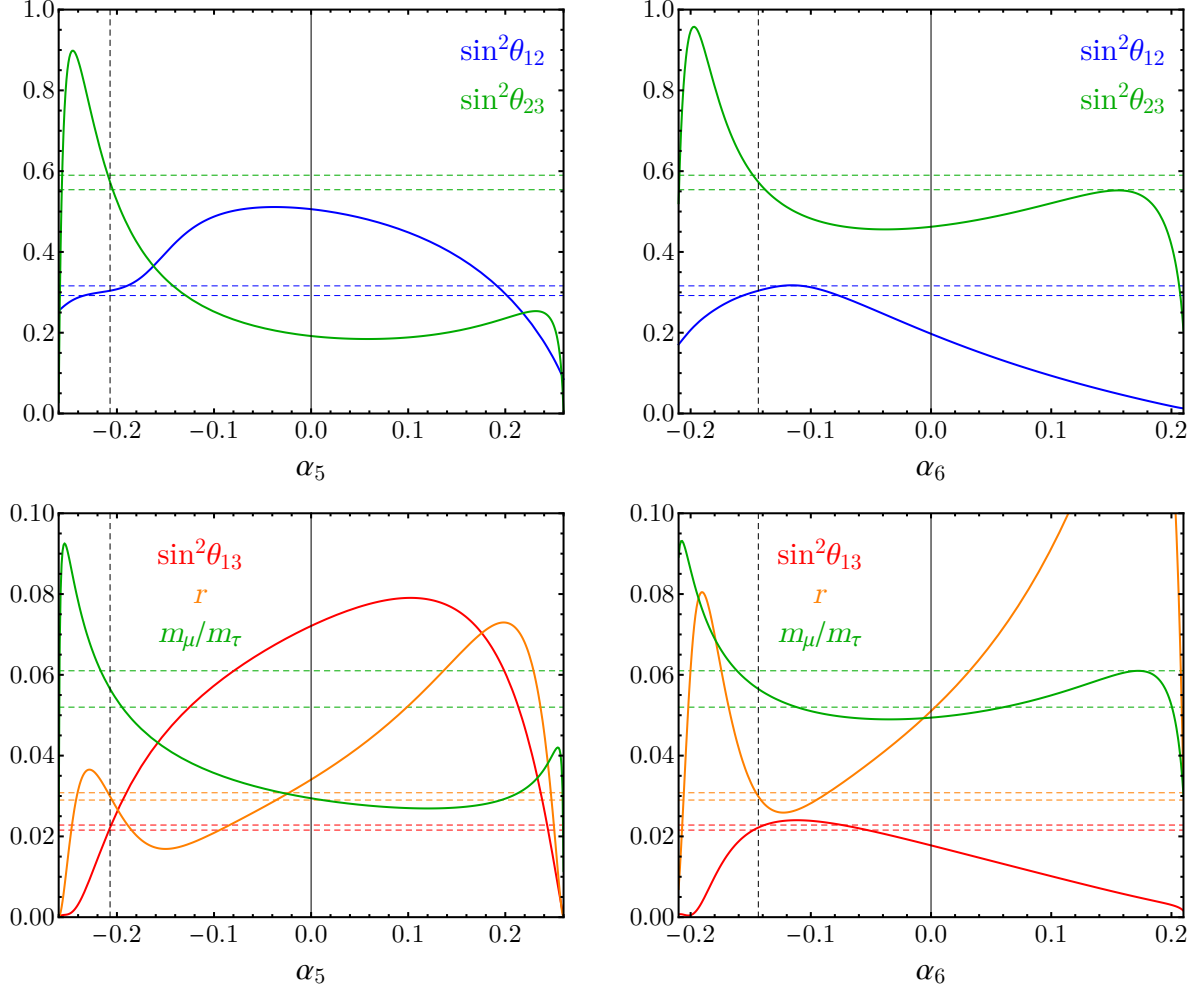


FIGURE 7.3.1. Dependence of the mixing angles and two mass ratios on  $\alpha_5$  (left) and  $\alpha_6$  (right), fixing all other input parameters to their best-fit values from Table 4. The *horizontal dashed lines* indicate the boundaries of the respective  $1\sigma$  ranges from Table 1. The *vertical dashed line* in the left (right) panels stands for the best-fit value of  $\alpha_5$  ( $\alpha_6$ ) from Table 4.

spoiling the other predictions. We give below two examples, where  $m_e$  is generated by supersymmetry breaking and by dimension six operators, respectively.

If supersymmetry is broken by some  $F$ -term, fermion masses get corrected by the second term of eq. (7.1.6), which, as discussed below the same equation, scales as  $m_{\text{SUSY}} v/M$  for SM fermion masses (where  $M$  is the SUSY breaking messenger scale). For instance, a Kähler interaction of the form:

$$K \supset \frac{1}{\Lambda^2} \chi^\dagger E_i^c \left[ a_i(\tau) H_d + b_i(\tau) \tilde{H}_u \right] L + \text{h.c.},$$

where the superfield  $\chi$  gets a supersymmetry breaking expectation value  $\langle \chi \rangle = F\theta^2$ , gives a contribution to the charged lepton Yukawa matrix proportional to  $F/\Lambda^2$ , which in turn generically induces an electron Yukawa coupling of the same order.



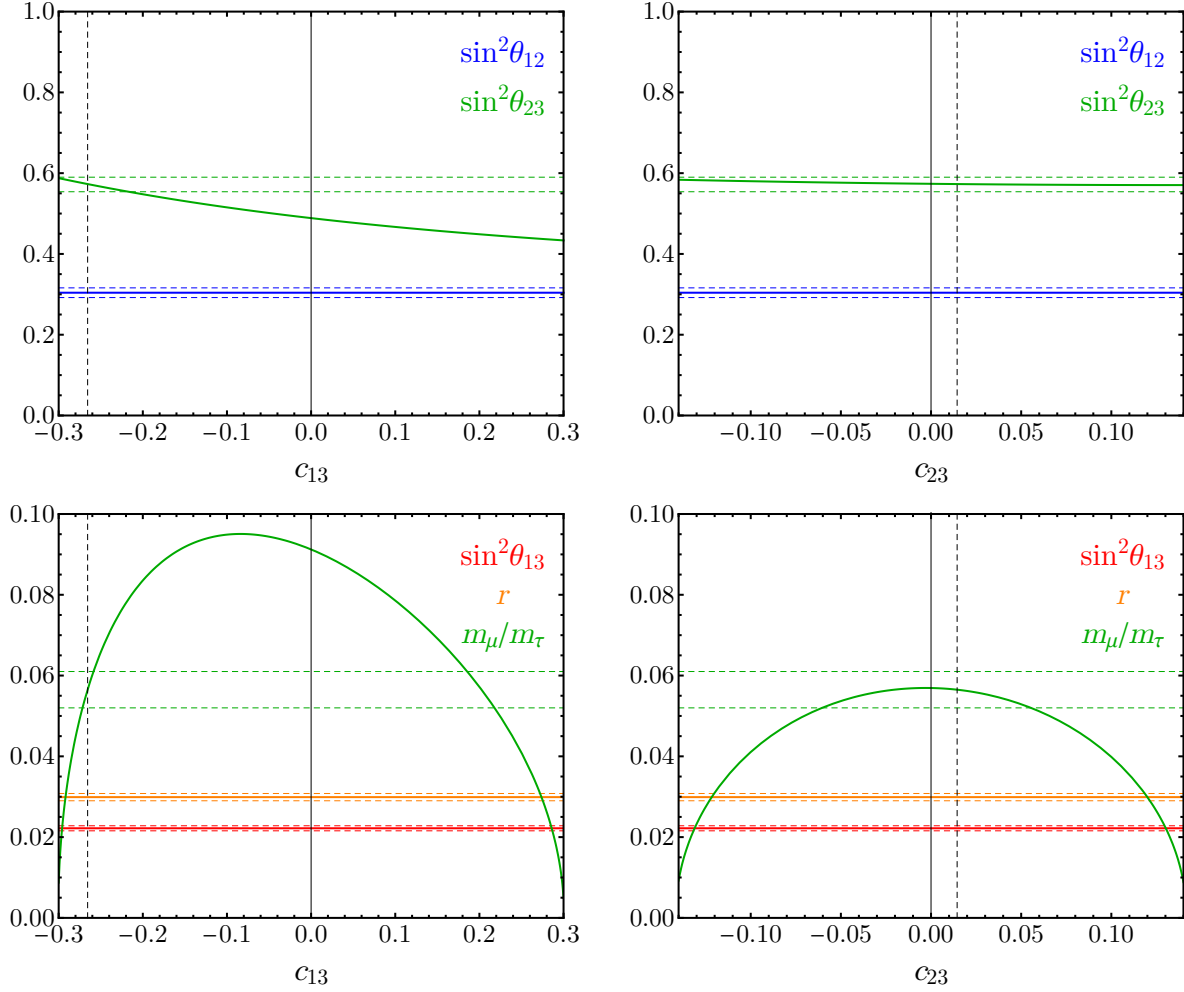


FIGURE 7.3.2. Dependence of the mixing angles and two mass ratios on  $c_{13}$  (left) and  $c_{23}$  (right), fixing all other input parameters to their best-fit values from Table 4. The *horizontal dashed lines* indicate the boundaries of the respective  $1\sigma$  ranges from Table 1. The *vertical dashed line* in the left (right) panels stands for the best-fit value of  $c_{13}$  ( $c_{23}$ ) from Table 4.

As a second possibility, one may generate  $m_e \neq 0$  through the dimension six operator:

$$(E_i^c L H_d)(H_u H_d), \quad (7.3.26)$$

whose Wilson coefficient should be a modular form of the appropriate weight. In order for this mechanism to work, we need to generalise the weight assignments in Table 2. We make the following requirements:

$$k_L = 1 - k_u, \quad (7.3.27)$$

$$k_{E^c} = 3 + k_u - k_d, \quad (7.3.28)$$

$$k_u + k_d \neq 0. \quad (7.3.29)$$

The first two conditions ensure that the superpotentials discussed in the previous subsections have weight zero; the last condition implies that the operator (7.3.26) has different weight from the corresponding renormalisable Yukawa term<sup>17</sup>, so that it couples to a functionally independent modular form multiplet (making the resulting charged lepton mass matrix of rank three). Such a mechanism thus generates  $m_e \sim v_u v_d^2 / \Lambda^2$ , where  $\Lambda$  is the scale at which the operator in eq. (7.3.26) is generated.

While in some flavour models, the ratios  $m_e/m_\tau$  and  $m_\mu/m_\tau$  are associated to different powers of the same expansion parameter, we note that here the two ratios are associated to independent parameters.

## 7.4. Conclusions

Supersymmetric modular invariant theories offer an attractive framework to address the flavour puzzle. The role of flavour symmetry is played by modular invariance, regarded as a discrete gauge symmetry, thus circumventing the obstruction concerning fundamental global symmetries. The arbitrary symmetry breaking sector of the conventional models based on flavour symmetries is replaced by the moduli space. Yukawa couplings become modular forms, severely restricted by the matter transformation properties. So far this framework has delivered interesting preliminary results especially in the lepton sector, where neutrino masses and lepton mixing parameters can be efficiently described in terms of a limited number of input parameters.

Weak points in most of the existing constructions are the need of independent hierarchical parameters to describe charged lepton masses, the reduced predictability caused by a general form of the Kähler potential, and the absence of a reliable dynamical mechanism to determine the value of  $\tau$  in the vacuum. As a matter of fact, in several models reproducing lepton masses and mixing parameters, the required value of  $\tau$  is close to  $i$ , the self-dual point where the generator  $S$  of the modular group and CP (if the Lagrangian is CP invariant) are unbroken. A small departure of  $\tau$  from  $i$  suffices to generate sizeable CP-violating effects in the lepton sector.

For these reasons, we were led to analyse more in detail the vicinity of  $\tau = i$ . Our goal was to show that a small deviation from the self-dual point can be responsible for the observed mass hierarchy  $m_e \ll m_\mu \ll m_\tau$  and  $\delta m^2 \ll \Delta m^2$ . At  $\tau = i$ , the theory has an exact  $Z_4$  symmetry, generated by the element  $S$  of the modular group. In the neighbourhood of  $\tau = i$ , the breaking of  $Z_4$  can be fully described by the (small) spurion  $\epsilon \approx \tau - i$ , that flips its sign under  $Z_4$ . We explained how to exploit this residual  $Z_4$  symmetry in order to obtain lepton mass matrices having reduced rank at  $\tau = i$ . This can be easily done with a suitable assignment of modular weights and representations for matter fields. There is a twofold advantage in this strategy. First, mass ratios that are forced to vanish at  $\tau = i$  by the  $Z_4$  symmetry are expected to acquire small values  $\propto |\epsilon|^n$  ( $n > 0$ ) near the self-dual point. Second, the reduced rank of the mass matrices can tame the contribution from a non-minimal Kähler potential, provided the metrics of the matter fields do not display large hierarchies.

---

<sup>17</sup>Curiously, the same condition can be exploited to make the Higgs  $\mu$ -term vanish at  $\tau = i$ . The Higgs  $\mu$ -term, being a  $\Gamma_3$  singlet modular form of weight  $k_u + k_d$ , vanishes by eq. (7.2.8) at  $\tau = i$  if  $k_u + k_d \neq 0 \pmod{4}$ , since all  $\Gamma_3$  singlets have  $\rho(\tilde{S}) = 1$ .

To see whether this strategy can be successfully realised or not, we built a concrete model at level 3, where neutrinos get masses through the type I seesaw mechanism. The model predicts a normal mass ordering. The number of parameters exceeds the number of fitted observables and we cannot claim predictability. However, with  $\tau$  being near  $i$ , mass ratios and mixing angles are reproduced with input parameters nearly of the same order of magnitude and matter kinetic terms display only a moderate hierarchy. We saw that the main contribution to the mass hierarchy can be induced by the singular mass matrix at the  $Z_4$  symmetric point. In the model we considered, the Kähler potential and the other Lagrangian parameters are crucial in order to correctly reproduce the values of the mixing angles. While the  $Z_4$  symmetry plays a fundamental role in all our discussion, we notice that our model could not have been realised in the context of a  $Z_4$  flavour symmetry alone. In particular, the electron mass vanishes in the models we have considered due to the correlations among generic  $Z_4$ -invariant operators provided by the underlying modular invariance. Also the leading order values of the mixing angles are dictated by  $Z_4$ . We have discussed possible sources of a non-vanishing electron mass. While the models we formulated have clearly room for improvement, we consider them as a good starting point to naturally accommodate the observed fermion mass hierarchies within a modular invariant framework.

### 7.5. Appendix: Kähler potential quadratic in $Y^{(2)}$

In the real basis for the  $\Gamma_3$  generators  $S$  and  $T$  in the 3-dimensional representation we employ in this Chapter,  $L^*$  and  $Y^{(2)*}$  transform as triplets, i.e.  $L^* \rightarrow \rho_3(\tilde{\gamma})L^*$  and  $Y^{(2)*} \rightarrow \rho_3(\tilde{\gamma})Y^{(2)*}$ . Thus, we can contract first  $L^*$  with  $L$  and  $Y^{(2)*}$  with  $Y^{(2)}$ , and after that perform contractions of the obtained multiplets. Proceeding in this way, we obtain:

$$(L^*L)_1 = L^\dagger L, \quad (L^*L)_{1'} = L^\dagger M_{1'} L, \quad (L^*L)_{1''} = L^\dagger M_{1''} L, \quad (7.5.1)$$

$$(L^*L)_{3_S} = \begin{pmatrix} L^\dagger M_{3_S}^{(1)} L \\ L^\dagger M_{3_S}^{(2)} L \\ L^\dagger M_{3_S}^{(3)} L \end{pmatrix}, \quad (L^*L)_{3_A} = \begin{pmatrix} L^\dagger M_{3_A}^{(1)} L \\ L^\dagger M_{3_A}^{(2)} L \\ L^\dagger M_{3_A}^{(3)} L \end{pmatrix}, \quad (7.5.2)$$

with the matrices  $M_\bullet$  being:

$$M_{1'} = \begin{pmatrix} 1 & 0 & 0 \\ 0 & \omega^2 & 0 \\ 0 & 0 & \omega \end{pmatrix}, \quad M_{1''} = \begin{pmatrix} 1 & 0 & 0 \\ 0 & \omega & 0 \\ 0 & 0 & \omega^2 \end{pmatrix}, \quad (7.5.3)$$

$$M_{3_S}^{(1)} = \begin{pmatrix} 0 & 0 & 0 \\ 0 & 0 & 1 \\ 0 & 1 & 0 \end{pmatrix}, \quad M_{3_S}^{(2)} = \begin{pmatrix} 0 & 0 & 1 \\ 0 & 0 & 0 \\ 1 & 0 & 0 \end{pmatrix}, \quad M_{3_S}^{(3)} = \begin{pmatrix} 0 & 1 & 0 \\ 1 & 0 & 0 \\ 0 & 0 & 0 \end{pmatrix}, \quad (7.5.4)$$

$$M_{3_A}^{(1)} = \begin{pmatrix} 0 & 0 & 0 \\ 0 & 0 & 1 \\ 0 & -1 & 0 \end{pmatrix}, \quad M_{3_A}^{(2)} = \begin{pmatrix} 0 & 0 & -1 \\ 0 & 0 & 0 \\ 1 & 0 & 0 \end{pmatrix}, \quad M_{3_A}^{(3)} = \begin{pmatrix} 0 & 1 & 0 \\ -1 & 0 & 0 \\ 0 & 0 & 0 \end{pmatrix}, \quad (7.5.5)$$

and  $\omega = e^{2\pi i/3}$ . The same equations hold for  $(Y^{(2)*}Y^{(2)})_{\bullet}$ . Taking further invariant contractions of the obtained multiplets, we find

$$\begin{aligned}
K_L = (2\text{Im}\tau)^{-k_L} + \\
+ (2\text{Im}\tau)^{k_Y - k_L} \left\{ \alpha_1 Y^{(2)\dagger} Y^{(2)} \mathbb{1} + \alpha_2 \left[ (Y^{(2)\dagger} M_{1''} Y^{(2)}) M_{1'} + (Y^{(2)\dagger} M_{1'} Y^{(2)}) M_{1''} \right] \right. \\
+ \alpha_3 i \left[ (Y^{(2)\dagger} M_{1''} Y^{(2)}) M_{1'} - (Y^{(2)\dagger} M_{1'} Y^{(2)}) M_{1''} \right] \\
+ \alpha_4 \sum_{n=1}^3 \left( Y^{(2)\dagger} M_{\mathbf{3}_S}^{(n)} Y^{(2)} \right) M_{\mathbf{3}_S}^{(n)} + \alpha_5 \sum_{n=1}^3 \left( Y^{(2)\dagger} M_{\mathbf{3}_A}^{(n)} Y^{(2)} \right) M_{\mathbf{3}_A}^{(n)} \\
\left. + \alpha_6 \sum_{n=1}^3 i \left( Y^{(2)\dagger} M_{\mathbf{3}_A}^{(n)} Y^{(2)} \right) M_{\mathbf{3}_S}^{(n)} + \alpha_7 \sum_{n=1}^3 i \left( Y^{(2)\dagger} M_{\mathbf{3}_S}^{(n)} Y^{(2)} \right) M_{\mathbf{3}_A}^{(n)} \right\}, \tag{7.5.6}
\end{aligned}$$

where  $\alpha_j$ ,  $j = 1, \dots, 7$ , are real coefficients, which accompany hermitian matrices. (We have used the fact that  $M_{1'}^\dagger = M_{1''}$ ,  $M_{\mathbf{3}_S}^{(n)\dagger} = M_{\mathbf{3}_S}^{(n)}$ , and  $M_{\mathbf{3}_A}^{(n)\dagger} = -M_{\mathbf{3}_A}^{(n)}$ .)

One of our assumptions is that the canonical form of  $K_L$  is restored at  $\text{Im}\tau \rightarrow \infty$ . The  $q$ -expansions of  $Y_i$  in the real basis read:

$$Y_1(\tau) = \frac{1}{\sqrt{3}} (1 - 6q^{1/3} - 18q^{2/3} + 12q + \dots), \tag{7.5.7}$$

$$Y_2(\tau) = \frac{1}{\sqrt{3}} (1 - 6\omega q^{1/3} - 18\omega^2 q^{2/3} + 12q + \dots), \tag{7.5.8}$$

$$Y_3(\tau) = \frac{1}{\sqrt{3}} (1 - 6\omega^2 q^{1/3} - 18\omega q^{2/3} + 12q + \dots), \tag{7.5.9}$$

where  $q = e^{2\pi i\tau}$ . Thus, at  $\text{Im}\tau \rightarrow \infty$

$$Y_1 = Y_2 = Y_3 \sim \frac{1}{\sqrt{3}}, \tag{7.5.10}$$

and  $K_L$  has the following form:

$$K_L \sim \frac{1}{2\text{Im}\tau} + \frac{2}{3} \text{Im}\tau \begin{pmatrix} \frac{3}{2}\alpha_1 & \alpha_4 + i\alpha_7 & \alpha_4 - i\alpha_7 \\ \alpha_4 - i\alpha_7 & \frac{3}{2}\alpha_1 & \alpha_4 + i\alpha_7 \\ \alpha_4 + i\alpha_7 & \alpha_4 - i\alpha_7 & \frac{3}{2}\alpha_1 \end{pmatrix}, \tag{7.5.11}$$

where we have used  $k_L = 1$  and  $k_Y = 2$ . To satisfy our assumption of the asymptotic behaviour of  $K_L$ , the coefficients  $\alpha_1 = \alpha_4 = \alpha_7 = 0$ . Thus, the number of free parameters

in  $K_L$  is reduced from seven to four. Then, the elements of  $K_L$  from eq. (7.5.6) read:

$$(K_L)_{11} = \frac{1}{2\text{Im}\tau} + 2\text{Im}\tau \left[ 2\alpha_2 |Y_1|^2 - (\alpha_2 + \sqrt{3}\alpha_3) |Y_2|^2 - (\alpha_2 - \sqrt{3}\alpha_3) |Y_3|^2 \right], \quad (7.5.12)$$

$$(K_L)_{22} = \frac{1}{2\text{Im}\tau} + 2\text{Im}\tau \left[ -(\alpha_2 - \sqrt{3}\alpha_3) |Y_1|^2 + 2\alpha_2 |Y_2|^2 - (\alpha_2 + \sqrt{3}\alpha_3) |Y_3|^2 \right], \quad (7.5.13)$$

$$(K_L)_{33} = \frac{1}{2\text{Im}\tau} + 2\text{Im}\tau \left[ -(\alpha_2 + \sqrt{3}\alpha_3) |Y_1|^2 - (\alpha_2 - \sqrt{3}\alpha_3) |Y_2|^2 + 2\alpha_2 |Y_3|^2 \right], \quad (7.5.14)$$

$$(K_L)_{12} = 2\text{Im}\tau (\alpha_5 + i\alpha_6) [Y_1^* Y_2 - Y_1 Y_2^*], \quad (7.5.15)$$

$$(K_L)_{13} = 2\text{Im}\tau (\alpha_5 - i\alpha_6) [Y_1^* Y_3 - Y_1 Y_3^*], \quad (7.5.16)$$

$$(K_L)_{23} = 2\text{Im}\tau (\alpha_5 + i\alpha_6) [Y_2^* Y_3 - Y_2 Y_3^*]. \quad (7.5.17)$$

For the sake of simplicity, we set further  $\alpha_2 = \alpha_3 = 0$ . In this case, the diagonal entries of  $K_L$  are not affected by the contributions containing modular forms, on the contrary to the off-diagonal elements. Thereby, we arrive at the form of  $K_L$  in eqs. (7.3.22) and (7.3.23).

What concerns  $K_{E^c}$ , with the assignment of representations and weights given in Table 2, the most general Kähler potential quadratic in  $Y^{(2)}$  reads

$$K_{E^c} = \frac{1}{8(\text{Im}\tau)^3} \begin{pmatrix} c_{11}^0 & c_{12}^0 & 0 \\ c_{12}^{0*} & c_{22}^0 & 0 \\ 0 & 0 & c_{33}^0 \end{pmatrix} + \frac{1}{2\text{Im}\tau} \begin{pmatrix} c_{11} Y^{(2)\dagger} Y^{(2)} & c_{12} Y^{(2)\dagger} Y^{(2)} & c_{13} Y^{(2)\dagger} M_{1''} Y^{(2)} \\ c_{12}^* Y^{(2)\dagger} Y^{(2)} & c_{22} Y^{(2)\dagger} Y^{(2)} & c_{23} Y^{(2)\dagger} M_{1''} Y^{(2)} \\ c_{13}^* Y^{(2)\dagger} M_{1'} Y^{(2)} & c_{23}^* Y^{(2)\dagger} M_{1'} Y^{(2)} & c_{33} Y^{(2)\dagger} Y^{(2)} \end{pmatrix}, \quad (7.5.18)$$

with  $c_{ii}^{(0)}$  being real and  $c_{ij}^{(0)}$ ,  $i \neq j$ , complex coefficients.

Taking into account that at  $\text{Im}\tau \rightarrow \infty$ , the invariant combination  $Y^{(2)\dagger} Y^{(2)} \sim 1$ , whereas  $X \equiv Y^{(2)\dagger} M_{1''} Y^{(2)}$  and  $X^* \equiv Y^{(2)\dagger} M_{1'} Y^{(2)}$  decay exponentially, we find

$$K_{E^c} \sim \frac{1}{8(\text{Im}\tau)^3} \begin{pmatrix} c_{11}^0 & c_{12}^0 & 0 \\ c_{12}^{0*} & c_{22}^0 & 0 \\ 0 & 0 & c_{33}^0 \end{pmatrix} + \frac{1}{2\text{Im}\tau} \begin{pmatrix} c_{11} & c_{12} & 0 \\ c_{12}^* & c_{22} & 0 \\ 0 & 0 & c_{33} \end{pmatrix}. \quad (7.5.19)$$

In order to restore the canonical form of  $K_{E^c}$  in the considered limit,  $c_{12}^0 = c_{12} = 0$ . Furthermore, we set  $c_{ii} = 0$  for simplicity. Finally, we can always make  $c_{ii}^0 = 1$  by independent rescalings of  $E_i^c$ ,  $i = 1, 2, 3$ . Thus, we recover  $K_{E^c}$  given by eqs. (7.3.24) and (7.3.25).

## Bibliography

- [1] S. L. Glashow, *Partial Symmetries of Weak Interactions*, *Nucl. Phys.* **22** (1961) 579–588.
- [2] S. Weinberg, *A Model of Leptons*, *Phys. Rev. Lett.* **19** (1967) 1264–1266.
- [3] A. Salam, *Weak and Electromagnetic Interactions*, *Conf. Proc. C* **680519** (1968) 367–377.
- [4] **ATLAS** Collaboration, G. Aad et al., *Observation of a new particle in the search for the Standard Model Higgs boson with the ATLAS detector at the LHC*, *Phys. Lett. B* **716** (2012) 1–29, [[arXiv:1207.7214](#)].
- [5] **CMS** Collaboration, S. Chatrchyan et al., *Observation of a New Boson at a Mass of 125 GeV with the CMS Experiment at the LHC*, *Phys. Lett. B* **716** (2012) 30–61, [[arXiv:1207.7235](#)].
- [6] P. W. Higgs, *Broken Symmetries and the Masses of Gauge Bosons*, *Phys. Rev. Lett.* **13** (1964) 508–509.
- [7] F. Englert and R. Brout, *Broken Symmetry and the Mass of Gauge Vector Mesons*, *Phys. Rev. Lett.* **13** (1964) 321–323.
- [8] G. S. Guralnik, C. R. Hagen, and T. W. B. Kibble, *Global Conservation Laws and Massless Particles*, *Phys. Rev. Lett.* **13** (1964) 585–587.
- [9] **Particle Data Group** Collaboration, P. Zyla et al., *Review of Particle Physics*, *PTEP* **2020** (2020), no. 8 083C01.
- [10] A. Romanino, *Naturalness After LHC run I*, *Frascati Phys. Ser.* **61** (2016) 26–34.
- [11] C. Gross, A. Polosa, A. Strumia, A. Urbano, and W. Xue, *Dark Matter in the Standard Model?*, *Phys. Rev. D* **98** (2018), no. 6 063005, [[arXiv:1803.10242](#)].
- [12] G. 't Hooft, *Naturalness, chiral symmetry, and spontaneous chiral symmetry breaking*, *NATO Sci. Ser. B* **59** (1980) 135–157.
- [13] G. F. Giudice, *Naturally Speaking: The Naturalness Criterion and Physics at the LHC*, [arXiv:0801.2562](#).
- [14] F. Feruglio, *Pieces of the Flavour Puzzle*, *Eur. Phys. J. C* **75** (2015), no. 8 373, [[arXiv:1503.04071](#)].
- [15] **BaBar** Collaboration, J. Lees et al., *Evidence for an excess of  $\bar{B} \rightarrow D^{(*)}\tau^-\bar{\nu}_\tau$  decays*, *Phys. Rev. Lett.* **109** (2012) 101802, [[arXiv:1205.5442](#)].
- [16] **BaBar** Collaboration, J. Lees et al., *Measurement of an Excess of  $\bar{B} \rightarrow D^{(*)}\tau^-\bar{\nu}_\tau$  Decays and Implications for Charged Higgs Bosons*, *Phys. Rev. D* **88** (2013), no. 7 072012, [[arXiv:1303.0571](#)].
- [17] **LHCb** Collaboration, R. Aaij et al., *Measurement of the ratio of branching fractions  $\mathcal{B}(\bar{B}^0 \rightarrow D^{*+}\tau^-\bar{\nu}_\tau)/\mathcal{B}(\bar{B}^0 \rightarrow D^{*+}\mu^-\bar{\nu}_\mu)$* , *Phys. Rev. Lett.* **115** (2015), no. 11 111803, [[arXiv:1506.08614](#)]. [Erratum: *Phys.Rev.Lett.* **115**, 159901 (2015)].
- [18] **Belle** Collaboration, M. Huschle et al., *Measurement of the branching ratio of  $\bar{B} \rightarrow D^{(*)}\tau^-\bar{\nu}_\tau$  relative to  $\bar{B} \rightarrow D^{(*)}\ell^-\bar{\nu}_\ell$  decays with hadronic tagging at Belle*, *Phys. Rev. D* **92** (2015), no. 7 072014, [[arXiv:1507.03233](#)].
- [19] **Belle** Collaboration, Y. Sato et al., *Measurement of the branching ratio of  $\bar{B}^0 \rightarrow D^{*+}\tau^-\bar{\nu}_\tau$  relative to  $\bar{B}^0 \rightarrow D^{*+}\ell^-\bar{\nu}_\ell$  decays with a semileptonic tagging method*, *Phys. Rev. D* **94** (2016), no. 7 072007, [[arXiv:1607.07923](#)].
- [20] **Belle** Collaboration, S. Hirose et al., *Measurement of the  $\tau$  lepton polarization and  $R(D^*)$  in the decay  $\bar{B} \rightarrow D^*\tau^-\bar{\nu}_\tau$* , *Phys. Rev. Lett.* **118** (2017), no. 21 211801, [[arXiv:1612.00529](#)].

- [21] Belle Collaboration, S. Hirose et al., *Measurement of the  $\tau$  lepton polarization and  $R(D^*)$  in the decay  $\bar{B} \rightarrow D^* \tau^- \bar{\nu}_\tau$  with one-prong hadronic  $\tau$  decays at Belle*, *Phys. Rev. D* **97** (2018), no. 1 012004, [arXiv:1709.00129].
- [22] LHCb Collaboration, R. Aaij et al., *Measurement of the ratio of the  $B^0 \rightarrow D^{*-} \tau^+ \nu_\tau$  and  $B^0 \rightarrow D^{*-} \mu^+ \nu_\mu$  branching fractions using three-prong  $\tau$ -lepton decays*, *Phys. Rev. Lett.* **120** (2018), no. 17 171802, [arXiv:1708.08856].
- [23] LHCb Collaboration, R. Aaij et al., *Test of Lepton Flavor Universality by the measurement of the  $B^0 \rightarrow D^{*-} \tau^+ \nu_\tau$  branching fraction using three-prong  $\tau$  decays*, *Phys. Rev. D* **97** (2018), no. 7 072013, [arXiv:1711.02505].
- [24] LHCb Collaboration, B. Siddi, *Measurement of  $R(D^*)$  with hadronic  $\tau$  decays*, *J. Phys. Conf. Ser.* **956** (2018), no. 1 012015.
- [25] Belle Collaboration, G. Caria et al., *Measurement of  $\mathcal{R}(D)$  and  $\mathcal{R}(D^*)$  with a semileptonic tagging method*, *Phys. Rev. Lett.* **124** (2020), no. 16 161803, [arXiv:1910.05864].
- [26] LHCb Collaboration, R. Aaij et al., *Measurement of Form-Factor-Independent Observables in the Decay  $B^0 \rightarrow K^{*0} \mu^+ \mu^-$* , *Phys. Rev. Lett.* **111** (2013) 191801, [arXiv:1308.1707].
- [27] LHCb Collaboration, R. Aaij et al., *Test of lepton universality using  $B^+ \rightarrow K^+ \ell^+ \ell^-$  decays*, *Phys. Rev. Lett.* **113** (2014) 151601, [arXiv:1406.6482].
- [28] LHCb Collaboration, R. Aaij et al., *Angular analysis of the  $B^0 \rightarrow K^{*0} \mu^+ \mu^-$  decay using  $3 \text{ fb}^{-1}$  of integrated luminosity*, *JHEP* **02** (2016) 104, [arXiv:1512.04442].
- [29] LHCb Collaboration, R. Aaij et al., *Angular analysis and differential branching fraction of the decay  $B_s^0 \rightarrow \phi \mu^+ \mu^-$* , *JHEP* **09** (2015) 179, [arXiv:1506.08777].
- [30] LHCb Collaboration, R. Aaij et al., *Measurement of the  $B_s^0 \rightarrow \mu^+ \mu^-$  branching fraction and effective lifetime and search for  $B^0 \rightarrow \mu^+ \mu^-$  decays*, *Phys. Rev. Lett.* **118** (2017), no. 19 191801, [arXiv:1703.05747].
- [31] LHCb Collaboration, R. Aaij et al., *Test of lepton universality with  $B^0 \rightarrow K^{*0} \ell^+ \ell^-$  decays*, *JHEP* **08** (2017) 055, [arXiv:1705.05802].
- [32] ATLAS Collaboration, M. Aaboud et al., *Study of the rare decays of  $B_s^0$  and  $B^0$  mesons into muon pairs using data collected during 2015 and 2016 with the ATLAS detector*, *JHEP* **04** (2019) 098, [arXiv:1812.03017].
- [33] LHCb Collaboration, R. Aaij et al., *Search for lepton-universality violation in  $B^+ \rightarrow K^+ \ell^+ \ell^-$  decays*, *Phys. Rev. Lett.* **122** (2019), no. 19 191801, [arXiv:1903.09252].
- [34] Belle Collaboration, A. Abdesselam et al., *Test of lepton flavor universality in  $B \rightarrow K^* \ell^+ \ell^-$  decays at Belle*, arXiv:1904.02440.
- [35] LHCb Collaboration, R. Aaij et al., *Measurement of CP-Averaged Observables in the  $B^0 \rightarrow K^{*0} \mu^+ \mu^-$  Decay*, *Phys. Rev. Lett.* **125** (2020), no. 1 011802, [arXiv:2003.04831].
- [36] LHCb Collaboration, R. Aaij et al., *Test of lepton universality in beauty-quark decays*, arXiv:2103.11769.
- [37] D. Lancierini, G. Isidori, P. Owen, and N. Serra, *On the significance of new physics in  $b \rightarrow s \ell^+ \ell^-$  decays*, arXiv:2104.05631.
- [38] S. Bifani, S. Descotes-Genon, A. Romero Vidal, and M.-H. Schune, *Review of Lepton Universality tests in B decays*, *J. Phys. G* **46** (2019), no. 2 023001, [arXiv:1809.06229].
- [39] L. Di Luzio and M. Nardecchia, *What is the scale of new physics behind the B-flavour anomalies?*, *Eur. Phys. J. C* **77** (2017), no. 8 536, [arXiv:1706.01868].
- [40] T. Nomura and T. Shimomura, *Search for  $Z'$  pair production from scalar boson decay in minimal  $U(1)_{L_\mu-L_\tau}$  model at the LHC*, *Eur. Phys. J. C* **81** (2021), no. 4 297, [arXiv:2012.13049].
- [41] I. Esteban, M. C. Gonzalez-Garcia, M. Maltoni, T. Schwetz, and A. Zhou, *The fate of hints: updated global analysis of three-flavor neutrino oscillations*, *JHEP* **09** (2020) 178, [arXiv:2007.14792].
- [42] KATRIN Collaboration, M. Aker et al., *Improved Upper Limit on the Neutrino Mass from a Direct Kinematic Method by KATRIN*, *Phys. Rev. Lett.* **123** (2019), no. 22 221802, [arXiv:1909.06048].
- [43] F. Feruglio, *Are neutrino masses modular forms?* 2019. arXiv:1706.08749.

- [44] V. Gherardi, D. Marzocca, and E. Venturini, *Matching scalar leptoquarks to the SMEFT at one loop*, *JHEP* **07** (2020) 225, [[arXiv:2003.12525](#)].
- [45] V. Gherardi, D. Marzocca, M. Nardecchia, and A. Romanino, *Rank-One Flavor Violation and B-meson anomalies*, *JHEP* **10** (2019) 112, [[arXiv:1903.10954](#)].
- [46] V. Gherardi, D. Marzocca, and E. Venturini, *Low-energy phenomenology of scalar leptoquarks at one-loop accuracy*, *JHEP* **01** (2021) 138, [[arXiv:2008.09548](#)].
- [47] F. Feruglio, V. Gherardi, A. Romanino, and A. Titov, *Modular invariant dynamics and fermion mass hierarchies around  $\tau = i$* , *JHEP* **05** (2021) 242, [[arXiv:2101.08718](#)].
- [48] G. Degrand, S. Di Vita, J. Elias-Miro, J. R. Espinosa, G. F. Giudice, G. Isidori, and A. Strumia, *Higgs mass and vacuum stability in the Standard Model at NNLO*, *JHEP* **08** (2012) 098, [[arXiv:1205.6497](#)].
- [49] M. Gell-Mann and F. E. Low, *Quantum electrodynamics at small distances*, *Phys. Rev.* **95** (1954) 1300–1312.
- [50] M. Gockeler, R. Horsley, V. Linke, P. E. L. Rakow, G. Schierholz, and H. Stuben, *Is there a Landau pole problem in QED?*, *Phys. Rev. Lett.* **80** (1998) 4119–4122, [[hep-th/9712244](#)].
- [51] W. Buchmüller and D. Wyler, *Effective Lagrangian Analysis of New Interactions and Flavor Conservation*, *Nucl. Phys. B* **268** (1986) 621–653.
- [52] B. Grzadkowski, M. Iskrzynski, M. Misiak, and J. Rosiek, *Dimension-Six Terms in the Standard Model Lagrangian*, *JHEP* **10** (2010) 085, [[arXiv:1008.4884](#)].
- [53] J. E. Kim and G. Carosi, *Axions and the Strong CP Problem*, *Rev. Mod. Phys.* **82** (2010) 557–602, [[arXiv:0807.3125](#)]. [Erratum: *Rev. Mod. Phys.* 91, 049902 (2019)].
- [54] S. Weinberg, *Baryon and Lepton Nonconserving Processes*, *Phys. Rev. Lett.* **43** (1979) 1566–1570.
- [55] S. Kamefuchi, L. O’Raifeartaigh, and A. Salam, *Change of variables and equivalence theorems in quantum field theories*, *Nucl. Phys.* **28** (1961) 529–549.
- [56] M. Bando, T. Kugo, and K. Yamawaki, *Nonlinear Realization and Hidden Local Symmetries*, *Phys. Rept.* **164** (1988) 217–314.
- [57] H. Georgi, *Effective field theory*, *Ann. Rev. Nucl. Part. Sci.* **43** (1993) 209–252.
- [58] A. J. Buras, *Weak Hamiltonian, CP violation and rare decays*, in *Les Houches Summer School in Theoretical Physics, Session 68: Probing the Standard Model of Particle Interactions*, pp. 281–539, 6, 1998. [hep-ph/9806471](#).
- [59] M. Jiang, N. Craig, Y.-Y. Li, and D. Sutherland, *Complete One-Loop Matching for a Singlet Scalar in the Standard Model EFT*, *JHEP* **02** (2019) 031, [[arXiv:1811.08878](#)].
- [60] J. de Blas, J. C. Criado, M. Perez-Victoria, and J. Santiago, *Effective description of general extensions of the Standard Model: the complete tree-level dictionary*, *JHEP* **03** (2018) 109, [[arXiv:1711.10391](#)].
- [61] U. Haisch, M. Ruhdorfer, E. Salvioni, E. Venturini, and A. Weiler, *Singlet night in Feynman-ville: one-loop matching of a real scalar*, *JHEP* **04** (2020) 164, [[arXiv:2003.05936](#)]. [Erratum: *JHEP* 07, 066 (2020)].
- [62] B. Henning, X. Lu, and H. Murayama, *How to use the Standard Model effective field theory*, *JHEP* **01** (2016) 023, [[arXiv:1412.1837](#)].
- [63] J. Aebischer, M. Fael, A. Lenz, M. Spannowsky, and J. Virto, eds., *Computing Tools for the SMEFT*, 10, 2019.
- [64] J. C. Criado, *MatchingTools: a Python library for symbolic effective field theory calculations*, *Comput. Phys. Commun.* **227** (2018) 42–50, [[arXiv:1710.06445](#)].
- [65] S. Das Bakshi, J. Chakraborty, and S. K. Patra, *CoDEX: Wilson coefficient calculator connecting SMEFT to UV theory*, *Eur. Phys. J. C* **79** (2019), no. 1 21, [[arXiv:1808.04403](#)].
- [66] R. Huo, *Effective Field Theory of Integrating out Sfermions in the MSSM: Complete One-Loop Analysis*, *Phys. Rev.* **D97** (2018), no. 7 075013, [[arXiv:1509.05942](#)].
- [67] J. D. Wells and Z. Zhang, *Effective field theory approach to trans-TeV supersymmetry: covariant matching, Yukawa unification and Higgs couplings*, *JHEP* **05** (2018) 182, [[arXiv:1711.04774](#)].
- [68] M. Boggia, R. Gomez-Ambrosio, and G. Passarino, *Low energy behaviour of standard model extensions*, *JHEP* **05** (2016) 162, [[arXiv:1603.03660](#)].



- [69] M. Chala and A. Titov, *One-loop matching in the SMEFT extended with a sterile neutrino*, [arXiv:2001.07732](#).
- [70] J. Davighi, M. Kirk, and M. Nardecchia, *Anomalies and accidental symmetries: charging the scalar leptoquark under  $L_\mu$ - $L_\tau$* , [arXiv:2007.15016](#).
- [71] L. Di Luzio, J. F. Kamenik, and M. Nardecchia, *Implications of perturbative unitarity for scalar di-boson resonance searches at LHC*, *Eur. Phys. J. C* **77** (2017), no. 1 30, [[arXiv:1604.05746](#)].
- [72] S. R. Coleman and E. J. Weinberg, *Radiative Corrections as the Origin of Spontaneous Symmetry Breaking*, *Phys. Rev. D* **7** (1973) 1888–1910.
- [73] S. Herrlich and U. Nierste, *Evanescent operators, scheme dependences and double insertions*, *Nucl. Phys. B* **455** (1995) 39–58, [[hep-ph/9412375](#)].
- [74] W. Dekens and P. Stoffer, *Low-energy effective field theory below the electroweak scale: matching at one loop*, *JHEP* **10** (2019) 197, [[arXiv:1908.05295](#)].
- [75] E. E. Jenkins, A. V. Manohar, and M. Trott, *Renormalization Group Evolution of the Standard Model Dimension Six Operators II: Yukawa Dependence*, *JHEP* **01** (2014) 035, [[arXiv:1310.4838](#)].
- [76] I. Esteban, M. C. Gonzalez-Garcia, M. Maltoni, T. Schwetz, and A. Zhou, “NuFIT 5.0: Three-neutrino fit based on data available in July 2020.” [www.nu-fit.org](#).
- [77] **UTfit** Collaboration, M. Bona et al., *Model-independent constraints on  $\Delta F = 2$  operators and the scale of new physics*, *JHEP* **03** (2008) 049, [[arXiv:0707.0636](#)].
- [78] **UTfit** Collaboration, M. Bona, *Latest results from Ufit*, *PoS CKM2016* (2017) 096, [[http://www.utfit.org/UTfit/](#)].
- [79] G. D’Ambrosio, G. F. Giudice, G. Isidori, and A. Strumia, *Minimal flavor violation: An Effective field theory approach*, *Nucl. Phys. B* **645** (2002) 155–187, [[hep-ph/0207036](#)].
- [80] R. Barbieri, G. Isidori, J. Jones-Perez, P. Lodone, and D. M. Straub,  *$U(2)$  and Minimal Flavour Violation in Supersymmetry*, *Eur. Phys. J. C* **71** (2011) 1725, [[arXiv:1105.2296](#)].
- [81] D. Buttazzo, A. Greljo, G. Isidori, and D. Marzocca, *B-physics anomalies: a guide to combined explanations*, *JHEP* **11** (2017) 044, [[arXiv:1706.07808](#)].
- [82] M. Bordone, G. Isidori, and A. Pattori, *On the Standard Model predictions for  $R_K$  and  $R_{K^*}$* , *Eur. Phys. J. C* **76** (2016), no. 8 440, [[arXiv:1605.07633](#)].
- [83] **HFLAV** Collaboration, Y. Amhis et al., *Averages of  $b$ -hadron,  $c$ -hadron, and  $\tau$ -lepton properties as of summer 2016*, *Eur. Phys. J. C* **77** (2017), no. 12 895, [[arXiv:1612.07233](#)].
- [84] M. Algueró, B. Capdevila, A. Crivellin, S. Descotes-Genon, P. Masjuan, J. Matias, M. Novoa Brunet, and J. Virto, *Emerging patterns of New Physics with and without Lepton Flavour Universal contributions*, *Eur. Phys. J. C* **79** (2019), no. 8 714, [[arXiv:1903.09578](#)]. [Addendum: *Eur.Phys.J.C* 80, 511 (2020)].
- [85] M. Algueró, B. Capdevila, A. Crivellin, S. Descotes-Genon, P. Masjuan, J. Matias, and J. Virto, *Addendum: "Patterns of New Physics in  $b \rightarrow s\ell^+\ell^-$  transitions in the light of recent data"*, [arXiv:1903.09578](#).
- [86] L.-S. Geng, B. Grinstein, S. Jäger, S.-Y. Li, J. Martin Camalich, and R.-X. Shi, *Implications of new evidence for lepton-universality violation in  $b \rightarrow s\ell^+\ell^-$  decays*, [arXiv:2103.12738](#).
- [87] W. Altmannshofer and P. Stangl, *New Physics in Rare B Decays after Moriond 2021*, [arXiv:2103.13370](#).
- [88] B. Gripaios, M. Nardecchia, and S. Renner, *Linear flavour violation and anomalies in B physics*, *JHEP* **06** (2016) 083, [[arXiv:1509.05020](#)].
- [89] R. Coy, M. Frigerio, F. Mescia, and O. Sumensari, *New physics in  $b \rightarrow s\ell\ell$  transitions at one loop*, *Eur. Phys. J. C* **80** (2020), no. 1 52, [[arXiv:1909.08567](#)].
- [90] **Muon g-2** Collaboration, G. W. Bennett et al., *Final Report of the Muon E821 Anomalous Magnetic Moment Measurement at BNL*, *Phys. Rev. D* **73** (2006) 072003, [[hep-ex/0602035](#)].
- [91] **Muon g-2** Collaboration, B. Abi et al., *Measurement of the Positive Muon Anomalous Magnetic Moment to 0.46 ppm*, *Phys. Rev. Lett.* **126** (2021), no. 14 141801, [[arXiv:2104.03281](#)].
- [92] T. Aoyama et al., *The anomalous magnetic moment of the muon in the Standard Model*, [arXiv:2006.04822](#).

- [93] E. E. Jenkins, A. V. Manohar, and M. Trott, *Renormalization Group Evolution of the Standard Model Dimension Six Operators I: Formalism and lambda Dependence*, *JHEP* **10** (2013) 087, [[arXiv:1308.2627](#)].
- [94] R. Alonso, E. E. Jenkins, A. V. Manohar, and M. Trott, *Renormalization Group Evolution of the Standard Model Dimension Six Operators III: Gauge Coupling Dependence and Phenomenology*, *JHEP* **04** (2014) 159, [[arXiv:1312.2014](#)].
- [95] E. E. Jenkins, A. V. Manohar, and P. Stoffer, *Low-Energy Effective Field Theory below the Electroweak Scale: Anomalous Dimensions*, *JHEP* **01** (2018) 084, [[arXiv:1711.05270](#)].
- [96] J. Aebischer, W. Altmannshofer, D. Guadagnoli, M. Reboud, P. Stangl, and D. M. Straub, *B-decay discrepancies after Moriond 2019*, *Eur. Phys. J. C* **80** (2020), no. 3 252, [[arXiv:1903.10434](#)].
- [97] M. Bordone, M. Jung, and D. van Dyk, *Theory determination of  $\bar{B} \rightarrow D^{(*)} \ell^- \bar{\nu}$  form factors at  $\mathcal{O}(1/m_c^2)$* , *Eur. Phys. J. C* **80** (2020), no. 2 74, [[arXiv:1908.09398](#)].
- [98] Belle Collaboration, A. Abdesselam et al., *Measurement of the  $D^{*-}$  polarization in the decay  $B^0 \rightarrow D^{*-} \tau^+ \nu_\tau$* , in *10th International Workshop on the CKM Unitarity Triangle*, 3, 2019, [[arXiv:1903.03102](#)].
- [99] A. Akeroyd and C.-H. Chen, *Constraint on the branching ratio of  $B_c \rightarrow \tau \bar{\nu}$  from LEP1 and consequences for  $R(D^{(*)})$  anomaly*, *Phys. Rev. D* **96** (2017), no. 7 075011, [[arXiv:1708.04072](#)].
- [100] BaBar Collaboration, B. Aubert et al., *Measurements of the Semileptonic Decays  $\text{anti-}B \rightarrow D l \text{ anti-}\nu$  and  $\text{anti-}B \rightarrow D^* l \text{ anti-}\nu$  Using a Global Fit to  $D X l \text{ anti-}\nu$  Final States*, *Phys. Rev. D* **79** (2009) 012002, [[arXiv:0809.0828](#)].
- [101] Belle Collaboration, R. Glattauer et al., *Measurement of the decay  $B \rightarrow D \ell \nu_\ell$  in fully reconstructed events and determination of the Cabibbo-Kobayashi-Maskawa matrix element  $|V_{cb}|$* , *Phys. Rev. D* **93** (2016), no. 3 032006, [[arXiv:1510.03657](#)].
- [102] S. Aoki et al., *Review of lattice results concerning low-energy particle physics*, *Eur. Phys. J. C* **77** (2017), no. 2 112, [[arXiv:1607.00299](#)].
- [103] Particle Data Group Collaboration, M. Tanabashi et al., *Review of Particle Physics*, *Phys. Rev. D* **98** (2018), no. 3 030001.
- [104] A. J. Buras, J. Girrbach-Noe, C. Niehoff, and D. M. Straub,  *$B \rightarrow K^{(*)} \nu \bar{\nu}$  decays in the Standard Model and beyond*, *JHEP* **02** (2015) 184, [[arXiv:1409.4557](#)].
- [105] Belle Collaboration, J. Grygier et al., *Search for  $B \rightarrow h \nu \bar{\nu}$  decays with semileptonic tagging at Belle*, *Phys. Rev. D* **96** (2017), no. 9 091101, [[arXiv:1702.03224](#)]. [Addendum: *Phys. Rev. D* 97, 099902 (2018)].
- [106] NA62 Collaboration, E. Cortina Gil et al., *An investigation of the very rare  $K^+ \rightarrow \pi^+ \nu \bar{\nu}$  decay*, [[arXiv:2007.08218](#)].
- [107] KOTO Collaboration, J. Ahn et al., *Search for the  $K_L \rightarrow \pi^0 \nu \bar{\nu}$  and  $K_L \rightarrow \pi^0 X^0$  decays at the J-PARC KOTO experiment*, *Phys. Rev. Lett.* **122** (2019), no. 2 021802, [[arXiv:1810.09655](#)].
- [108] LHCb Collaboration, R. Aaij et al., *Search for the lepton-flavour-violating decays  $B_s^0 \rightarrow \tau^\pm \mu^\mp$  and  $B^0 \rightarrow \tau^\pm \mu^\mp$* , *Phys. Rev. Lett.* **123** (2019), no. 21 211801, [[arXiv:1905.06614](#)].
- [109] BaBar Collaboration, J. Lees et al., *A search for the decay modes  $B^{+-} \rightarrow h^{+-} \tau^{+-} l$* , *Phys. Rev. D* **86** (2012) 012004, [[arXiv:1204.2852](#)].
- [110] LHCb Collaboration, R. Aaij et al., *Search for the lepton flavour violating decay  $B^+ \rightarrow K^+ \mu^- \tau^+$  using  $B_{s2}^{*0}$  decays*, *JHEP* **06** (2020) 129, [[arXiv:2003.04352](#)].
- [111] UTfit Collaboration, *Latest results from UTfit*, <http://www.utfit.org/UTfit/> 2016.
- [112] A. Pich, *Precision Tau Physics*, *Prog. Part. Nucl. Phys.* **75** (2014) 41–85, [[arXiv:1310.7922](#)].
- [113] Belle Collaboration, Y. Miyazaki et al., *Search for Lepton-Flavor-Violating tau Decays into a Lepton and a Vector Meson*, *Phys. Lett. B* **699** (2011) 251–257, [[arXiv:1101.0755](#)].
- [114] K. Hayasaka et al., *Search for Lepton Flavor Violating Tau Decays into Three Leptons with 719 Million Produced Tau+Tau- Pairs*, *Phys. Lett. B* **687** (2010) 139–143, [[arXiv:1001.3221](#)].
- [115] MEG Collaboration, A. Baldini et al., *Search for the lepton flavour violating decay  $\mu^+ \rightarrow e^+ \gamma$  with the full dataset of the MEG experiment*, *Eur. Phys. J. C* **76** (2016), no. 8 434, [[arXiv:1605.05081](#)].

- [116] **BaBar** Collaboration, B. Aubert et al., *Searches for Lepton Flavor Violation in the Decays  $\tau^{+-} \rightarrow e^{+-} \gamma$  and  $\tau^{+-} \rightarrow \mu^{+-} \gamma$* , *Phys. Rev. Lett.* **104** (2010) 021802, [[arXiv:0908.2381](#)].
- [117] M. Pospelov and A. Ritz, *CKM benchmarks for electron electric dipole moment experiments*, *Phys. Rev. D* **89** (2014), no. 5 056006, [[arXiv:1311.5537](#)].
- [118] C. Smith and S. Touati, *Electric dipole moments with and beyond flavor invariants*, *Nucl. Phys. B* **924** (2017) 417–452, [[arXiv:1707.06805](#)].
- [119] **ACME** Collaboration, V. Andreev et al., *Improved limit on the electric dipole moment of the electron*, *Nature* **562** (2018), no. 7727 355–360.
- [120] **Muon (g-2)** Collaboration, G. Bennett et al., *An Improved Limit on the Muon Electric Dipole Moment*, *Phys. Rev. D* **80** (2009) 052008, [[arXiv:0811.1207](#)].
- [121] **Belle** Collaboration, K. Inami et al., *Search for the electric dipole moment of the tau lepton*, *Phys. Lett. B* **551** (2003) 16–26, [[hep-ex/0210066](#)].
- [122] A. Keshavarzi, D. Nomura, and T. Teubner,  *$g - 2$  of charged leptons,  $\alpha(M_Z^2)$ , and the hyperfine splitting of muonium*, *Phys. Rev. D* **101** (2020), no. 1 014029, [[arXiv:1911.00367](#)].
- [123] R. H. Parker, C. Yu, W. Zhong, B. Estey, and H. Müller, *Measurement of the fine-structure constant as a test of the Standard Model*, *Science* **360** (2018) 191, [[arXiv:1812.04130](#)].
- [124] D. Hanneke, S. Fogwell, and G. Gabrielse, *New Measurement of the Electron Magnetic Moment and the Fine Structure Constant*, *Phys. Rev. Lett.* **100** (2008) 120801, [[arXiv:0801.1134](#)].
- [125] **Muon g-2** Collaboration, G. Bennett et al., *Final Report of the Muon E821 Anomalous Magnetic Moment Measurement at BNL*, *Phys. Rev. D* **73** (2006) 072003, [[hep-ex/0602035](#)].
- [126] **DELPHI** Collaboration, J. Abdallah et al., *Study of tau-pair production in photon-photon collisions at LEP and limits on the anomalous electromagnetic moments of the tau lepton*, *Eur. Phys. J. C* **35** (2004) 159–170, [[hep-ex/0406010](#)].
- [127] **ALEPH, DELPHI, L3, OPAL, SLD, LEP Electroweak Working Group, SLD Electroweak Group, SLD Heavy Flavour Group** Collaboration, S. Schael et al., *Precision electroweak measurements on the Z resonance*, *Phys. Rept.* **427** (2006) 257–454, [[hep-ex/0509008](#)].
- [128] P. Janot and S. Jadach, *Improved Bhabha cross section at LEP and the number of light neutrino species*, *Phys. Lett. B* **803** (2020) 135319, [[arXiv:1912.02067](#)].
- [129] I. Doršner and A. Greljo, *Leptoquark toolbox for precision collider studies*, *JHEP* **05** (2018) 126, [[arXiv:1801.07641](#)].
- [130] M. Schmaltz and Y.-M. Zhong, *The leptoquark Hunter’s guide: large coupling*, *JHEP* **01** (2019) 132, [[arXiv:1810.10017](#)].
- [131] D. Marzocca, *Addressing the B-physics anomalies in a fundamental Composite Higgs Model*, *JHEP* **07** (2018) 121, [[arXiv:1803.10972](#)].
- [132] A. Angelescu, D. Bečirević, D. Faroughy, and O. Sumensari, *Closing the window on single leptoquark solutions to the B-physics anomalies*, *JHEP* **10** (2018) 183, [[arXiv:1808.08179](#)].
- [133] S. Saad, *Combined explanations of  $(g - 2)_\mu$ ,  $R_{D^{(*)}}$ ,  $R_{K^{(*)}}$  anomalies in a two-loop radiative neutrino mass model*, *Phys. Rev. D* **102** (2020), no. 1 015019, [[arXiv:2005.04352](#)].
- [134] D. A. Faroughy, A. Greljo, and J. F. Kamenik, *Confronting lepton flavor universality violation in B decays with high- $p_T$  tau lepton searches at LHC*, *Phys. Lett. B* **764** (2017) 126–134, [[arXiv:1609.07138](#)].
- [135] A. Greljo and D. Marzocca, *High- $p_T$  dilepton tails and flavor physics*, *Eur. Phys. J. C* **77** (2017), no. 8 548, [[arXiv:1704.09015](#)].
- [136] Y. Afik, J. Cohen, E. Gozani, E. Kajomovitz, and Y. Rozen, *Establishing a Search for  $b \rightarrow s \ell^+ \ell^-$  Anomalies at the LHC*, *JHEP* **08** (2018) 056, [[arXiv:1805.11402](#)].
- [137] Y. Afik, S. Bar-Shalom, J. Cohen, and Y. Rozen, *Searching for New Physics with  $b\bar{b}\ell^+\ell^-$  contact interactions*, *Phys. Lett. B* **807** (2020) 135541, [[arXiv:1912.00425](#)].
- [138] A. Angelescu, D. A. Faroughy, and O. Sumensari, *Lepton Flavor Violation and Dilepton Tails at the LHC*, *Eur. Phys. J. C* **80** (2020), no. 7 641, [[arXiv:2002.05684](#)].

- [139] W. Altmannshofer, P. Bhupal Dev, and A. Soni,  $R_{D^{(*)}}$  anomaly: A possible hint for natural supersymmetry with  $R$ -parity violation, *Phys. Rev. D* **96** (2017), no. 9 095010, [arXiv:1704.06659].
- [140] A. Greljo, J. Martin Camalich, and J. D. Ruiz-Álvarez, *Mono- $\tau$  Signatures at the LHC Constrain Explanations of  $B$ -decay Anomalies*, *Phys. Rev. Lett.* **122** (2019), no. 13 131803, [arXiv:1811.07920].
- [141] M. Abdullah, J. Calle, B. Dutta, A. Flórez, and D. Restrepo, *Probing a simplified,  $W'$  model of  $R(D^{(*)})$  anomalies using  $b$ -tags,  $\tau$  leptons and missing energy*, *Phys. Rev. D* **98** (2018), no. 5 055016, [arXiv:1805.01869].
- [142] G. Brooijmans et al., *Les Houches 2019 Physics at TeV Colliders: New Physics Working Group Report*, in *11th Les Houches Workshop on Physics at TeV Colliders: PhysTeV Les Houches*, 2, 2020. arXiv:2002.12220.
- [143] J. Fuentes-Martin, A. Greljo, J. Martin Camalich, and J. D. Ruiz-Alvarez, *Charm Physics Confronts High- $p_T$  Lepton Tails*, arXiv:2003.12421.
- [144] D. Marzocca, U. Min, and M. Son, *Bottom-Flavored Mono-Tau Tails at the LHC*, arXiv:2008.07541.
- [145] A. Crivellin, D. Mueller, and F. Saturnino, *Leptoquarks in Oblique Corrections and Higgs Signal Strength: Status and Prospects*, arXiv:2006.10758.
- [146] D. Marzocca, S. Trifinopoulos, and E. Venturini, *From  $B$ -meson anomalies to Kaon physics with scalar leptoquarks*, arXiv:2106.15630.
- [147] M. Bauer and M. Neubert, *Minimal Leptoquark Explanation for the  $R_{D^{(*)}}$ ,  $R_K$ , and  $(g-2)_g$  Anomalies*, *Phys. Rev. Lett.* **116** (2016), no. 14 141802, [arXiv:1511.01900].
- [148] Y. Cai, J. Gargalionis, M. A. Schmidt, and R. R. Volkas, *Reconsidering the One Leptoquark solution: flavor anomalies and neutrino mass*, *JHEP* **10** (2017) 047, [arXiv:1704.05849].
- [149] A. Azatov, D. Barducci, D. Ghosh, D. Marzocca, and L. Ubaldi, *Combined explanations of  $B$ -physics anomalies: the sterile neutrino solution*, *JHEP* **10** (2018) 092, [arXiv:1807.10745].
- [150] A. Crivellin, M. Hoferichter, and P. Schmidt-Wellenburg, *Combined explanations of  $(g-2)_{\mu,e}$  and implications for a large muon EDM*, *Phys. Rev. D* **98** (2018), no. 11 113002, [arXiv:1807.11484].
- [151] I. Bigaran and R. R. Volkas, *Getting chirality right: single scalar leptoquark solution/s to the  $(g-2)_{e,\mu}$  puzzle*, *Phys. Rev. D* **102** (2020), no. 7 075037, [arXiv:2002.12544].
- [152] I. Doršner, S. Fajfer, and S. Saad,  $\mu \rightarrow e\gamma$  selecting scalar leptoquark solutions for the  $(g-2)_{e,\mu}$  puzzles, *Phys. Rev. D* **102** (2020), no. 7 075007, [arXiv:2006.11624].
- [153] A. Crivellin, D. Müller, and T. Ota, *Simultaneous explanation of  $R(D^{(*)})$  and  $b \rightarrow s\mu^+\mu^-$ : the last scalar leptoquarks standing*, *JHEP* **09** (2017) 040, [arXiv:1703.09226].
- [154] J. Haller, A. Hoecker, R. Kogler, K. Mönig, T. Peiffer, and J. Stelzer, *Update of the global electroweak fit and constraints on two-Higgs-doublet models*, *Eur. Phys. J. C* **78** (2018), no. 8 675, [arXiv:1803.01853].
- [155] ATLAS Collaboration, G. Aad et al., *Combined measurements of Higgs boson production and decay using up to  $80\text{ fb}^{-1}$  of proton-proton collision data at  $\sqrt{s} = 13\text{ TeV}$  collected with the ATLAS experiment*, *Phys. Rev. D* **101** (2020), no. 1 012002, [arXiv:1909.02845].
- [156] ATLAS Collaboration, G. Aad et al., *A search for the  $Z\gamma$  decay mode of the Higgs boson in  $pp$  collisions at  $\sqrt{s} = 13\text{ TeV}$  with the ATLAS detector*, *Phys. Lett. B* **809** (2020) 135754, [arXiv:2005.05382].
- [157] CMS Collaboration, A. M. Sirunyan et al., *Search for the decay of a Higgs boson in the  $\ell\ell\gamma$  channel in proton-proton collisions at  $\sqrt{s} = 13\text{ TeV}$* , *JHEP* **11** (2018) 152, [arXiv:1806.05996].
- [158] R. Barbieri, A. Pomarol, R. Rattazzi, and A. Strumia, *Electroweak symmetry breaking after LEP-1 and LEP-2*, *Nucl. Phys. B* **703** (2004) 127–146, [hep-ph/0405040].
- [159] J. D. Wells and Z. Zhang, *Effective theories of universal theories*, *JHEP* **01** (2016) 123, [arXiv:1510.08462].
- [160] I. Doršner, S. Fajfer, and O. Sumensari, *Muon  $g-2$  and scalar leptoquark mixing*, *JHEP* **06** (2020) 089, [arXiv:1910.03877].

- [161] M. Cepeda et al., *Report from Working Group 2: Higgs Physics at the HL-LHC and HE-LHC*, *CERN Yellow Rep. Monogr.* **7** (2019) 221–584, [[arXiv:1902.00134](#)].
- [162] **Belle-II** Collaboration, W. Altmannshofer et al., *The Belle II Physics Book*, *PTEP* **2019** (2019), no. 12 123C01, [[arXiv:1808.10567](#)]. [Erratum: *PTEP* 2020, 029201 (2020)].
- [163] R. Aaij et al., *Physics case for an LHCb Upgrade II - Opportunities in flavour physics, and beyond, in the HL-LHC era*, other thesis, 2016.
- [164] **BaBar** Collaboration, J. Lees et al., *Search for  $B^+ \rightarrow K^+ \tau^+ \tau^-$  at the BaBar experiment*, *Phys. Rev. Lett.* **118** (2017), no. 3 031802, [[arXiv:1605.09637](#)].
- [165] **LHCb** Collaboration, R. Aaij et al., *Search for the decays  $B_s^0 \rightarrow \tau^+ \tau^-$  and  $B^0 \rightarrow \tau^+ \tau^-$* , *Phys. Rev. Lett.* **118** (2017), no. 25 251802, [[arXiv:1703.02508](#)].
- [166] **COMET** Collaboration, M. Moritsu, *The COMET Experiment: Search for Muon-to-Electron Conversion*, *JPS Conf. Proc.* **33** (2021) 011111.
- [167] C. Ankenbrandt, D. Bogert, F. DeJongh, S. Geer, D. McGinnis, D. Neuffer, M. Popovic, and E. Prebys, *Using the Fermilab proton source for a muon to electron conversion experiment*, [physics/0611124](#).
- [168] **mu2e** Collaboration, K. Knoepfel et al., *Feasibility Study for a Next-Generation Mu2e Experiment*, in *Community Summer Study 2013: Snowmass on the Mississippi*, 7, 2013. [arXiv:1307.1168](#).
- [169] **Mu2e** Collaboration, L. Bartoszek et al., *Mu2e Technical Design Report*, [arXiv:1501.05241](#).
- [170] **Mu3e** Collaboration, K. Arndt et al., *Technical design of the phase I Mu3e experiment*, [arXiv:2009.11690](#).
- [171] G. D’Amico, M. Nardecchia, P. Panci, F. Sannino, A. Strumia, R. Torre, and A. Urbano, *Flavour anomalies after the  $R_{K^*}$  measurement*, [arXiv:1704.05438](#).
- [172] G. Hiller and M. Schmaltz,  *$R_K$  and future  $b \rightarrow s\ell\ell$  physics beyond the standard model opportunities*, *Phys. Rev.* **D90** (2014) 054014, [[arXiv:1408.1627](#)].
- [173] S. Descotes-Genon, L. Hofer, J. Matias, and J. Virto, *Global analysis of  $b \rightarrow s\ell\ell$  anomalies*, *JHEP* **06** (2016) 092, [[arXiv:1510.04239](#)].
- [174] W. Altmannshofer, C. Niehoff, P. Stangl, and D. M. Straub, *Status of the  $B \rightarrow K^* \mu^+ \mu^-$  anomaly after Moriond 2017*, *Eur. Phys. J.* **C77** (2017), no. 6 377, [[arXiv:1703.09189](#)].
- [175] B. Capdevila, A. Crivellin, S. Descotes-Genon, J. Matias, and J. Virto, *Patterns of New Physics in  $b \rightarrow s\ell^+ \ell^-$  transitions in the light of recent data*, [arXiv:1704.05340](#).
- [176] W. Altmannshofer, P. Stangl, and D. M. Straub, *Interpreting Hints for Lepton Flavor Universality Violation*, [arXiv:1704.05435](#).
- [177] L.-S. Geng, B. Grinstein, S. Jäger, J. Martin Camalich, X.-L. Ren, and R.-X. Shi, *Towards the discovery of new physics with lepton-universality ratios of  $b \rightarrow s\ell\ell$  decays*, [arXiv:1704.05446](#).
- [178] M. Ciuchini, A. M. Coutinho, M. Fedele, E. Franco, A. Paul, L. Silvestrini, and M. Valli, *On Flavourful Easter eggs for New Physics hunger and Lepton Flavour Universality violation*, *Eur. Phys. J.* **C77** (2017), no. 10 688, [[arXiv:1704.05447](#)].
- [179] G. Hiller and I. Nisandzic,  *$R_K$  and  $R_{K^*}$  beyond the standard model*, *Phys. Rev.* **D96** (2017), no. 3 035003, [[arXiv:1704.05444](#)].
- [180] A. K. Alok, B. Bhattacharya, A. Datta, D. Kumar, J. Kumar, and D. London, *New Physics in  $b \rightarrow s\mu^+ \mu^-$  after the Measurement of  $R_{K^*}$* , *Phys. Rev.* **D96** (2017), no. 9 095009, [[arXiv:1704.07397](#)].
- [181] T. Hurth, F. Mahmoudi, D. Martinez Santos, and S. Neshatpour, *Update on lepton non-universality in exclusive  $b \rightarrow s\ell\ell$  decays*, [arXiv:1705.06274](#).
- [182] A. K. Alok, A. Dighe, S. Gangal, and D. Kumar, *Continuing search for new physics in  $b \rightarrow s\mu\mu$  decays: two operators at a time*, [arXiv:1903.09617](#).
- [183] M. Ciuchini, A. M. Coutinho, M. Fedele, E. Franco, A. Paul, L. Silvestrini, and M. Valli, *New Physics in  $b \rightarrow s\ell^+ \ell^-$  confronts new data on Lepton Universality*, [arXiv:1903.09632](#).
- [184] M. Algueró, B. Capdevila, S. Descotes-Genon, P. Masjuan, and J. Matias, *Are we overlooking Lepton Flavour Universal New Physics in  $b \rightarrow s\ell\ell$  ?*, [arXiv:1809.08447](#).

- [185] M. Algueró, B. Capdevila, S. Descotes-Genon, P. Masjuan, and J. Matias, *What  $R_K$  and  $Q_5$  can tell us about New Physics in  $b \rightarrow s\ell\ell$  transitions?*, [arXiv:1902.04900](#).
- [186] A. Datta, J. Kumar, and D. London, *The  $B$  Anomalies and New Physics in  $b \rightarrow se^+e^-$* , [arXiv:1903.10086](#).
- [187] **LHCb** Collaboration, R. Aaij et al., *Search for lepton-universality violation in  $B^+ \rightarrow K^+\ell^+\ell^-$  decays*, [arXiv:1903.09252](#).
- [188] **Belle** Collaboration, *Seminar at rencontres de moriond ew*, 2019.
- [189] S. L. Glashow, D. Guadagnoli, and K. Lane, *Lepton Flavor Violation in  $B$  Decays?*, *Phys. Rev. Lett.* **114** (2015) 091801, [[arXiv:1411.0565](#)].
- [190] B. Bhattacharya, A. Datta, D. London, and S. Shivashankara, *Simultaneous Explanation of the  $R_K$  and  $R(D^{(*)})$  Puzzles*, *Phys. Lett.* **B742** (2015) 370–374, [[arXiv:1412.7164](#)].
- [191] J. M. Cline,  *$B$  decay anomalies and dark matter from vectorlike confinement*, *Phys. Rev.* **D97** (2018), no. 1 015013, [[arXiv:1710.02140](#)].
- [192] J. M. Cline and J. M. Cornell,  *$R(K^{(*)})$  from dark matter exchange*, *Phys. Lett.* **B782** (2018) 232–237, [[arXiv:1711.10770](#)].
- [193] C. Bobeth, M. Gorbahn, T. Hermann, M. Misiak, E. Stamou, and M. Steinhauser,  *$B_{s,d} \rightarrow l^+l^-$  in the Standard Model with Reduced Theoretical Uncertainty*, *Phys. Rev. Lett.* **112** (2014) 101801, [[arXiv:1311.0903](#)].
- [194] **LHCb** Collaboration, R. Aaij et al., *First measurement of the differential branching fraction and  $CP$  asymmetry of the  $B^\pm \rightarrow \pi^\pm\mu^+\mu^-$  decay*, *JHEP* **10** (2015) 034, [[arXiv:1509.00414](#)].
- [195] D. Du, A. El-Khadra, S. Gottlieb, A. Kronfeld, J. Laiho, E. Lunghi, R. Van de Water, and R. Zhou, *Phenomenology of semileptonic  $B$ -meson decays with form factors from lattice QCD*, *Phys. Rev. D* **93** (2016), no. 3 034005, [[arXiv:1510.02349](#)].
- [196] A. Khodjamirian and A. V. Rusov,  *$B_s \rightarrow K\ell\nu_\ell$  and  $B_{(s)} \rightarrow \pi(K)\ell^+\ell^-$  decays at large recoil and  $CKM$  matrix elements*, *JHEP* **08** (2017) 112, [[arXiv:1703.04765](#)].
- [197] **LHCb** Collaboration, R. Aaij et al., *Improved limit on the branching fraction of the rare decay  $K_S^0 \rightarrow \mu^+\mu^-$* , *Eur. Phys. J.* **C77** (2017), no. 10 678, [[arXiv:1706.00758](#)].
- [198] **E871** Collaboration, D. Ambrose et al., *Improved branching ratio measurement for the decay  $K^0(L) \rightarrow \mu^+\mu^-$* , *Phys. Rev. Lett.* **84** (2000) 1389–1392.
- [199] G. Isidori and R. Unterdorfer, *On the short distance constraints from  $K(L,S) \rightarrow \mu^+\mu^-$* , *JHEP* **01** (2004) 009, [[hep-ph/0311084](#)].
- [200] **KTEV** Collaboration, A. Alavi-Harati et al., *Search for the Decay  $K_L \rightarrow \pi^0\mu^+\mu^-$* , *Phys. Rev. Lett.* **84** (2000) 5279–5282, [[hep-ex/0001006](#)].
- [201] G. D’Ambrosio, G. Ecker, G. Isidori, and J. Portoles, *The Decays  $K \rightarrow \pi l^+l^-$  beyond leading order in the chiral expansion*, *JHEP* **08** (1998) 004, [[hep-ph/9808289](#)].
- [202] G. Buchalla, G. D’Ambrosio, and G. Isidori, *Extracting short distance physics from  $K(L,S) \rightarrow \pi^0 e^+e^-$  decays*, *Nucl. Phys.* **B672** (2003) 387–408, [[hep-ph/0308008](#)].
- [203] G. Isidori, C. Smith, and R. Unterdorfer, *The Rare decay  $K_L \rightarrow \pi^0\mu^+\mu^-$  within the SM*, *Eur. Phys. J.* **C36** (2004) 57–66, [[hep-ph/0404127](#)].
- [204] F. Mescia, C. Smith, and S. Trine,  *$K(L) \rightarrow \pi^0 e^+e^-$  and  $K(L) \rightarrow \pi^0 \mu^+\mu^-$ : A Binary star on the stage of flavor physics*, *JHEP* **08** (2006) 088, [[hep-ph/0606081](#)].
- [205] **LHCb** Collaboration, R. Aaij et al., *Search for the rare decay  $K_S \rightarrow \mu^+\mu^-$* , *JHEP* **01** (2013) 090, [[arXiv:1209.4029](#)].
- [206] M. Bordone, D. Buttazzo, G. Isidori, and J. Monnard, *Probing Lepton Flavour Universality with  $K \rightarrow \pi\nu\bar{\nu}$  decays*, [arXiv:1705.10729](#).
- [207] C. Bobeth and A. J. Buras, *Leptoquarks meet  $\varepsilon'/\varepsilon$  and rare Kaon processes*, *JHEP* **02** (2018) 101, [[arXiv:1712.01295](#)].
- [208] **E949** Collaboration, A. V. Artamonov et al., *New measurement of the  $K^+ \rightarrow \pi^+\nu\bar{\nu}$  branching ratio*, *Phys. Rev. Lett.* **101** (2008) 191802, [[arXiv:0808.2459](#)].
- [209] A. J. Buras, D. Buttazzo, J. Girrbach-Noe, and R. Knegjens,  *$K^+ \rightarrow \pi^+\nu\bar{\nu}$  and  $K_L \rightarrow \pi^0\nu\bar{\nu}$  in the Standard Model: status and perspectives*, *JHEP* **11** (2015) 033, [[arXiv:1503.02693](#)].

- [210] **ATLAS** Collaboration, M. Aaboud et al., *Search for new high-mass phenomena in the dilepton final state using  $36\text{ fb}^{-1}$  of proton-proton collision data at  $\sqrt{s} = 13\text{ TeV}$  with the ATLAS detector*, *JHEP* **10** (2017) 182, [[arXiv:1707.02424](#)].
- [211] B. Gripaios, M. Nardecchia, and S. Renner, *Composite leptoquarks and anomalies in  $B$ -meson decays*, *JHEP* **05** (2015) 006, [[arXiv:1412.1791](#)].
- [212] I. de Medeiros Varzielas and G. Hiller, *Clues for flavor from rare lepton and quark decays*, *JHEP* **06** (2015) 072, [[arXiv:1503.01084](#)].
- [213] I. Doršner, S. Fajfer, D. A. Faroughy, and N. Košnik, *The role of the  $S_3$  GUT leptoquark in flavor universality and collider searches*, *JHEP* **10** (2017) 188, [[arXiv:1706.07779](#)].
- [214] R. Barbieri, G. Isidori, A. Pattori, and F. Senia, *Anomalies in  $B$ -decays and  $U(2)$  flavour symmetry*, *Eur. Phys. J.* **C76** (2016), no. 2 67, [[arXiv:1512.01560](#)].
- [215] R. Alonso, B. Grinstein, and J. Martin Camalich, *Lepton universality violation and lepton flavor conservation in  $B$ -meson decays*, *JHEP* **10** (2015) 184, [[arXiv:1505.05164](#)].
- [216] R. Barbieri, C. W. Murphy, and F. Senia,  *$B$ -decay Anomalies in a Composite Leptoquark Model*, *Eur. Phys. J.* **C77** (2017), no. 1 8, [[arXiv:1611.04930](#)].
- [217] L. Di Luzio, A. Greljo, and M. Nardecchia, *Gauge leptoquark as the origin of  $B$ -physics anomalies*, *Phys. Rev. D* **96** (2017), no. 11 115011, [[arXiv:1708.08450](#)].
- [218] R. Barbieri and A. Tesi,  *$B$ -decay anomalies in Pati-Salam  $SU(4)$* , *Eur. Phys. J.* **C78** (2018), no. 3 193, [[arXiv:1712.06844](#)].
- [219] M. Bordone, C. Cornella, J. Fuentes-Martin, and G. Isidori, *A three-site gauge model for flavor hierarchies and flavor anomalies*, *Phys. Lett.* **B779** (2018) 317–323, [[arXiv:1712.01368](#)].
- [220] L. Di Luzio, J. Fuentes-Martin, A. Greljo, M. Nardecchia, and S. Renner, *Maximal Flavour Violation: a Cabibbo mechanism for leptoquarks*, *JHEP* **11** (2018) 081, [[arXiv:1808.00942](#)].
- [221] M. Bordone, C. Cornella, J. Fuentes-Martin, and G. Isidori, *Low-energy signatures of the  $PS^3$  model: from  $B$ -physics anomalies to LFV*, *JHEP* **10** (2018) 148, [[arXiv:1805.09328](#)].
- [222] A. Crivellin, C. Greub, D. Müller, and F. Saturnino, *Importance of Loop Effects in Explaining the Accumulated Evidence for New Physics in  $B$  Decays with a Vector Leptoquark*, *Phys. Rev. Lett.* **122** (2019), no. 1 011805, [[arXiv:1807.02068](#)].
- [223] M. J. Baker, J. Fuentes-Martin, G. Isidori, and M. König, *High- $p_T$  Signatures in Vector-Leptoquark Models*, [arXiv:1901.10480](#).
- [224] W. Altmannshofer, S. Gori, M. Pospelov, and I. Yavin, *Quark flavor transitions in  $L_\mu - L_\tau$  models*, *Phys. Rev.* **D89** (2014) 095033, [[arXiv:1403.1269](#)].
- [225] A. Crivellin, G. D’Ambrosio, and J. Heeck, *Explaining  $h \rightarrow \mu^\pm \tau^\mp$ ,  $B \rightarrow K^* \mu^+ \mu^-$  and  $B \rightarrow K \mu^+ \mu^- / B \rightarrow K e^+ e^-$  in a two-Higgs-doublet model with gauged  $L_\mu - L_\tau$* , *Phys. Rev. Lett.* **114** (2015) 151801, [[arXiv:1501.00993](#)].
- [226] C. Bonilla, T. Modak, R. Srivastava, and J. W. F. Valle,  *$U(1)_{B_3-3L_\mu}$  gauge symmetry as a simple description of  $b \rightarrow s$  anomalies*, *Phys. Rev.* **D98** (2018), no. 9 095002, [[arXiv:1705.00915](#)].
- [227] A. Biswas and A. Shaw, *Reconciling dark matter,  $R_{K^{(*)}}$  anomalies and  $(g-2)_\mu$  in an  $L_\mu - L_\tau$  scenario*, [arXiv:1903.08745](#).
- [228] A. Cerri et al., *Opportunities in Flavour Physics at the HL-LHC and HE-LHC*, [arXiv:1812.07638](#).
- [229] **KLEVER Project** Collaboration, F. Ambrosino et al., *KLEVER: An experiment to measure  $BR(K_L \rightarrow \pi^0 \nu \bar{\nu})$  at the CERN SPS*, [arXiv:1901.03099](#).
- [230] **NA62** Collaboration, G. Ruggiero, *Status of the CERN NA62 Experiment*, *J. Phys. Conf. Ser.* **800** (2017), no. 1 012023.
- [231] R. Gatto, G. Sartori, and M. Tonin, *Weak Selfmasses, Cabibbo Angle, and Broken  $SU(2) \times SU(2)$* , *Phys. Lett. B* **28** (1968) 128–130.
- [232] F. Feruglio and A. Romanino, *Lepton flavor symmetries*, *Rev. Mod. Phys.* **93** (Mar, 2021) 015007, [[arXiv:1912.06028](#)].
- [233] C. Giunti, *No Effect of Majorana Phases in Neutrino Oscillations*, *Phys. Lett. B* **686** (2010) 41–43, [[arXiv:1001.0760](#)].

- [234] G. Ross and M. Serna, *Unification and fermion mass structure*, *Phys. Lett. B* **664** (2008) 97–102, [[arXiv:0704.1248](#)].
- [235] P. Langacker, *Grand Unified Theories and Proton Decay*, *Phys. Rept.* **72** (1981) 185.
- [236] C. D. Froggatt and H. B. Nielsen, *Hierarchy of Quark Masses, Cabibbo Angles and CP Violation*, *Nucl. Phys. B* **147** (1979) 277–298.
- [237] R. N. Mohapatra, *Seesaw mechanism and its implications*, in *SEESAW25: International Conference on the Seesaw Mechanism and the Neutrino Mass*, 12, 2004. [hep-ph/0412379](#).
- [238] M. Farina, D. Pappadopulo, and A. Strumia, *A modified naturalness principle and its experimental tests*, *JHEP* **08** (2013) 022, [[arXiv:1303.7244](#)].
- [239] L. Ferretti, S. F. King, and A. Romanino, *Flavour from accidental symmetries*, *JHEP* **11** (2006) 078, [[hep-ph/0609047](#)].
- [240] G. Panico and A. Wulzer, *The Composite Nambu-Goldstone Higgs*, vol. 913. Springer, 2016.
- [241] L. J. Hall, H. Murayama, and N. Weiner, *Neutrino mass anarchy*, *Phys. Rev. Lett.* **84** (2000) 2572–2575, [[hep-ph/9911341](#)].
- [242] N. Haba and H. Murayama, *Anarchy and hierarchy*, *Phys. Rev. D* **63** (2001) 053010, [[hep-ph/0009174](#)].
- [243] A. de Gouvea and H. Murayama, *Statistical test of anarchy*, *Phys. Lett. B* **573** (2003) 94–100, [[hep-ph/0301050](#)].
- [244] J. R. Espinosa, *Anarchy in the neutrino sector?*, [hep-ph/0306019](#).
- [245] A. de Gouvea and H. Murayama, *Neutrino Mixing Anarchy: Alive and Kicking*, *Phys. Lett. B* **747** (2015) 479–483, [[arXiv:1204.1249](#)].
- [246] S. Weinberg, *Nonrenormalization theorems in nonrenormalizable theories*, *Phys. Rev. Lett.* **80** (1998) 3702–3705, [[hep-th/9803099](#)].
- [247] T. Kobayashi, N. Omoto, Y. Shimizu, K. Takagi, M. Tanimoto, and T. H. Tatsuishi, *Modular  $A_4$  invariance and neutrino mixing*, *JHEP* **11** (2018) 196, [[arXiv:1808.03012](#)].
- [248] J. C. Criado and F. Feruglio, *Modular Invariance Faces Precision Neutrino Data*, *SciPost Phys.* **5** (2018), no. 5 042, [[arXiv:1807.01125](#)].
- [249] P. Novichkov, J. Penedo, S. Petcov, and A. Titov, *Modular  $S_4$  models of lepton masses and mixing*, *JHEP* **04** (2019) 005, [[arXiv:1811.04933](#)].
- [250] P. Novichkov, J. Penedo, S. Petcov, and A. Titov, *Generalised CP Symmetry in Modular-Invariant Models of Flavour*, *JHEP* **07** (2019) 165, [[arXiv:1905.11970](#)].
- [251] H. Okada and M. Tanimoto, *Towards unification of quark and lepton flavors in  $A_4$  modular invariance*, [arXiv:1905.13421](#).
- [252] J. C. Criado, F. Feruglio, and S. J. King, *Modular Invariant Models of Lepton Masses at Levels 4 and 5*, *JHEP* **02** (2020) 001, [[arXiv:1908.11867](#)].
- [253] T. Kobayashi, T. Nomura, and T. Shimomura, *Type II seesaw models with modular  $A_4$  symmetry*, *Phys. Rev. D* **102** (2020), no. 3 035019, [[arXiv:1912.00637](#)].
- [254] H. Okada and M. Tanimoto, *Quark and lepton flavors with common modulus  $\tau$  in  $A_4$  modular symmetry*, [arXiv:2005.00775](#).
- [255] P. Novichkov, J. Penedo, and S. Petcov, *Double Cover of Modular  $S_4$  for Flavour Model Building*, *Nucl. Phys. B* **963** (2021) 115301, [[arXiv:2006.03058](#)].
- [256] X. Wang, *Dirac neutrino mass models with a modular  $S_4$  symmetry*, *Nucl. Phys. B* **962** (2021) 115247, [[arXiv:2007.05913](#)].
- [257] H. Okada and M. Tanimoto, *Spontaneous CP violation by modulus  $\tau$  in  $A_4$  model of lepton flavors*, [arXiv:2012.01688](#).
- [258] M.-C. Chen, S. Ramos-Sánchez, and M. Ratz, *A note on the predictions of models with modular flavor symmetries*, *Phys. Lett. B* **801** (2020) 135153, [[arXiv:1909.06910](#)].
- [259] T. Asaka, Y. Heo, and T. Yoshida, *Lepton flavor model with modular  $A_4$  symmetry in large volume limit*, *Phys. Lett. B* **811** (2020) 135956, [[arXiv:2009.12120](#)].
- [260] S. Ferrara, D. Lust, A. D. Shapere, and S. Theisen, *Modular Invariance in Supersymmetric Field Theories*, *Phys. Lett. B* **225** (1989) 363.



- [261] S. Ferrara, D. Lust, and S. Theisen, *Target Space Modular Invariance and Low-Energy Couplings in Orbifold Compactifications*, *Phys. Lett. B* **233** (1989) 147–152.
- [262] X.-G. Liu, C.-Y. Yao, B.-Y. Qu, and G.-J. Ding, *Half-integral weight modular forms and application to neutrino mass models*, *Phys. Rev. D* **102** (2020), no. 11 115035, [[arXiv:2007.13706](#)].
- [263] H. P. Nilles, S. Ramos-Sánchez, and P. K. Vaudrevange, *Eclectic Flavor Groups*, *JHEP* **02** (2020) 045, [[arXiv:2001.01736](#)].
- [264] A. Brignole, F. Feruglio, and F. Zwirner, *Aspects of spontaneously broken  $N=1$  global supersymmetry in the presence of gauge interactions*, *Nucl. Phys. B* **501** (1997) 332–374, [[hep-ph/9703286](#)].
- [265] T. Kobayashi, Y. Shimizu, K. Takagi, M. Tanimoto, T. H. Tatsuishi, and H. Uchida,  *$CP$  violation in modular invariant flavor models*, *Phys. Rev. D* **101** (2020), no. 5 055046, [[arXiv:1910.11553](#)].
- [266] H. P. Nilles, S. Ramos-Sanchez, and P. K. Vaudrevange, *Lessons from eclectic flavor symmetries*, *Nucl. Phys. B* **957** (2020) 115098, [[arXiv:2004.05200](#)].